Heft 70
Neubiberg, 2001

U. Roßbach

Positioning and Navigation Using the Russian Satellite System GLONASS

SCHRIFTENREIHE

STUDIENGANG GEODÄSIE UND GEOINFORMATION
UNIVERSITÄT DER BUNDESWEHR MÜNCHEN

Heft 70
Neubiberg, 2001

U. Roßbach

Positioning and Navigation Using the Russian Satellite System GLONASS

SCHRIFTENREIHE

STUDIENGANG GEODÄSIE UND GEOINFORMATION
UNIVERSITÄT DER BUNDESWEHR MÜNCHEN

Der Druck dieses Heftes wurde aus Haushaltsmitteln der Universität der Bundeswehr München gefördert.

Auflagenhöhe: 150

Herausgeber der Schriftenreihe:

Der Prodekan des Studiengang Geodäsie und Geoinformation der Universität der Bundeswehr München

Bezugsnachweis:

Universität der Bundeswehr München
Fakultät für Bauingenieur- und Vermessungswesen
Studiengang Geodäsie und Geoinformation
Werner-Heisenberg-Weg 39
D - 85577 Neubiberg

ISSN 0173 - 1009

Positioning and Navigation Using the Russian Satellite System GLONASS

von

Udo Roßbach

Vollständiger Abdruck der von der Fakultät für Bauingenieur- und Vermessungswesen der Universität der Bundeswehr München zur Erlangung des akademischen Grades eines Doktor-Ingenieurs (Dr.-Ing.) genehmigten Dissertation.

Vorsitzender:	Univ.-Prof. Dr.-Ing. W. Reinhardt
1. Berichterstatter:	Univ.-Prof. Dr.-Ing. G. W. Hein
2. Berichterstatter:	Univ.-Prof. Dr.-Ing. E. Groten
3. Berichterstatter:	Univ.-Prof. Dr.-Ing. B. Eissfeller

Die Dissertation wurde am 2. März 2000 bei der Universität der Bundeswehr München, Werner-Heisenberg-Weg 39, D-85577 Neubiberg eingereicht.

Tag der mündlichen Prüfung: 20. Juni 2000

Abstract

Satellite navigation systems have not only revolutionized navigation, but also geodetic positioning. By means of satellite range measurements, positioning accuracies became available that were previously unknown, especially for long baselines. This has long been documented for applications of GPS, the American Global Positioning System. Besides this, there is the Russian Global Navigation Satellite System GLONASS. Comparable to GPS from the technical point of view, it is suffering under the economic decline of the Russian Federation, which prevents it from drawing the attention it deserves.

Due to the similarities of GPS and GLONASS, both systems may also be used in combined applications. However, since both systems are not entirely compatible to each other, first a number of inter-operability issues have to be solved. Besides receiver hardware issues, these are mainly the differences in coordinate and time reference frames. For both issues, proposed solutions are provided. For the elimination of differences in coordinate reference frames, possible coordinate transformations are introduced, determined using both a conventional and an innovative approach.

Another important topic in the usage of GLONASS for high-precision applications is the fact that GLONASS satellites are distinguished by slightly different carrier frequencies instead of different PRN codes. This results in complications, when applying double difference carrier phase measurements to position determination the way it is often done with GPS. To overcome these difficulties and make use of GLONASS double difference carrier phase measurements for positioning, a new mathematical model for double difference carrier phase observations has been developed.

These solutions have been implemented in a GLONASS and combined GPS/GLONASS processing software package.

Zusammenfassung

Satelliten-Navigationssysteme haben nicht nur die Navigation, sondern auch die geodätische Positionsbestimmung revolutioniert. Mit Hilfe von Entfernungsmessungen zu Satelliten wurden vorher nicht gekannte Genauigkeiten in der Positionierung verfügbar. Für Anwendungen des amerikanischen GPS Global Positioning System ist dies schon lange dokumentiert. Daneben gibt es das russische Global Navigation Satellite System GLONASS. Vom technischen Standpunkt her vergleichbar zu GPS, leidet es unter dem wirtschaftlichen Niedergang der Russischen Föderation und erhält deswegen nicht die Aufmerksamkeit, die es verdient.

Aufgrund der Ähnlichkeiten zwischen GPS und GLONASS können beide System auch gemeinsam in kombinierten Anwendungen genutzt werden. Da beide System jedoch nicht vollständig zueinander kompatibel sind, müssen vorher noch einige Fragen der gemeinsamen Nutzung geklärt werden. Neben Fragen der Empfänger-Hardware sind dies hauptsächlich die Unterschiede in den Koordinaten- und Zeit-Bezugssystemen. Für beide Punkte wurden Lösungen vorgeschlagen. Um die Unterschiede in den Koordinaten-Bezugssystemen auszuräumen, werden mögliche Koordinatentransformationen vorgestellt. Diese wurden sowohl über einen konventionellen als auch mit einem innovativen Ansatz bestimmt.

Ein anderer wichtiger Punkt in der Nutzung von GLONASS für hochpräzise Anwendungen ist die Tatsache, daß sich GLONASS-Satelliten durch die leicht unterschiedlichen Trägerfrequenzen ihrer Signale unterscheiden, und nicht durch unterschiedliche PRN-Codes. Dies bringt Komplikationen mit sich bei der Anwendung doppelt-differenzierter Trägerphasenmessungen, wie sie bei GPS häufig verwendet werden. Um diese Schwierigkeiten zu überwinden und auch doppelt differenzierte GLONASS-Trägerphasenmessungen für die Positionsbestimmung verwenden zu können, wurde ein neues mathematisches Modell der Doppeldifferenz-Phasenbeobachtungen hergeleitet.

Die gewonnenen Erkenntnisse wurden in einem Software-Paket zur Prozessierung von GLONASS und kombinierten GPS/GLONASS Beobachtungen implementiert.

Contents

List of Figures

List of Tables

1 Introduction

Parallel to the American NAVSTAR-GPS, the former Soviet Union also worked on developing and putting up a satellite navigation system based on one-way range measurements. This system, called GLONASS (ГЛОНАСС – Глобальная Навигационная Спутниковая Система, Global'naya Navigatsionnaya Sputnikowaya Sistema, Global Navigation Satellite System), today is continued by the Commonwealth of Independent States (CIS) and especially the Russian Federation as the successor of the Soviet Union.

Like its American counter-piece, GLONASS is intended to provide an unlimited number of users at any time on any place on Earth in any weather with highly precise position and velocity fixes. The principle of GLONASS is equivalent to that of its American counter-piece. Each satellite carries an atomic clock and transmits radio signals, which contain clock readings as well as information on the satellite orbit and the satellite clock offset from system time. The user receives these satellite signals and compares the time of signal transmission with the time of signal reception, as read on the receiver's own clock. The difference of these two clock readings, multiplied by the speed of light, equals the distance between the satellite and the user. Four such one-way distance measurements to four different satellites simultaneously, together with the satellite position and clock offsets known from the orbit data, yield the three coordinates of the user's position and the user's clock offset with respect to system time as the fourth unknown.

Equivalent to the Standard Positioning Service (SPS) and the Precise Positioning Service (PPS) of GPS, GLONASS provides a standard precision (SP) navigation signal and a high precision (HP) navigation signal. These signals are sometimes also referred to as Channel of Standard Accuracy (CSA) and Channel of High Accuracy (CHA), respectively. The SP signal is available to all civil users world-wide on a continuous basis. Accuracy of GLONASS navigation using the SP signal is specified to be 50 - 70 m (99.7 %) in the horizontal plane and 70 m (99.7 %) in height. Accuracy of estimated velocity vectors is 15 cm/s (99.7 %). Timing accuracy is 1 μs (99.7 %) (*CSIC, 1998*). These accuracies can be increased using dual-frequency P-code measurements of the HP signal. A further increase is possible in differential operation.

Applications of GLONASS are equivalent to those of GPS and can be seen mostly in highly precise navigation of land, sea, air and low orbiting spacecraft (*CSIC, 1994*). Besides this, GLONASS is also suitable for the dissemination of highly precise global and local time scales as well as for establishing global geodetic coordinate systems and local geodetic networks. The system can also be used for providing precise coordinates for cadastre works. Further usage could contain the support of research work in geology, geophysics, geodynamics, oceanography and others by providing position and time information. Similar uses are possible for large scale construction projects.

With this range of applications and the achievable accuracy, GLONASS has become an attractive tool for navigational and geodetic purposes. But not only GLONASS as a stand-alone system draws the interest of scientists around the world. The fact that there are two independent, but generally very similar satellite navigation systems also draws attention to the combined use of both systems. This combined use brings up a number of advantages. At first, the number of available (observable) satellites is increased with respect to one single system. This will provide a user with a better satellite geometry and more redundant information, allowing him to compute a more accurate position fix. In cases with obstructed visibility of the sky, such as mountainous or urban areas, a position fix might not be possible at all without these additional satellites. Besides that, the more satellite measurements are available, the earlier and more reliably a user can detect and isolate measurement outliers or even malfunctioning satellites. Thus, the combined use of GPS and GLONASS may aid in Receiver Autonomous Integrity Monitoring (RAIM), providing better integrity of the position fix than a single system alone (*Hein et al., 1997*).

In a similar way, an increased number of observed satellites improves and accelerates the determination of integer ambiguities in high-precision (surveying) applications. Therefore, the combination of GPS and

GLONASS is expected to provide better performance in RTK surveying than GPS (or GLONASS) alone (*Landau and Vollath, 1996*).

This doctoral thesis deals with the use of GLONASS for positioning determination in geodesy and navigation, especially in combination with GPS. To do so, after a brief history of the GLONASS system in Chapter 2, the system is explained in detail in Chapter 3. The differences to GPS in terms of time frame (Chapter 4) and coordinate frame (Chapter 5) are worked out and ways are shown, how these differences can be overcome in combined GPS/GLONASS applications. Chapter 6 provides details on a measurement campaign carried out by IfEN in cooperation with other institutions to determine a transformation between the GLONASS and GPS coordinate reference frames and presents results of this transformation. The algorithms used for GLONASS satellite position and clock offset determination – cornerstones in GLONASS positioning – are described and analyzed in Chapter 7. Afterwards, the different formulations of the GLONASS and combined GPS/GLONASS observation equations are introduced and assessed in Chapter 8. The implications on GLONASS carrier phase processing caused by the different signal frequencies are identified and possible solutions are shown, as well as the effects of combined GPS/GLONASS observations on the DOP values. Finally, in Chapter 9 an overview is given on different GPS/GLONASS software tools created in connection with this work and used to compute the results presented in this thesis.

2 History of the GLONASS System

Development of the GLONASS system started in the mid-1970s, parallel to the American GPS (*Bartenev et al., 1994*). The first GLONASS satellite was put into orbit October 12, 1982 (*CSIC, 1998*). By the end of 1985, ten satellites were operational. This marked the end of the so-called pre-operational phase. In the operational phase, beginning 1986, the planned constellation was successively completed. These efforts faced a setback in May 1989, when satellite launches were halted for one year because of recent satellite failures.

The Soviet air and naval forces were considered to be the primary users of GLONASS. But as with GPS, though a military system, the possibilities of civil usage soon were recognized, at first in the areas of geodesy and geodynamics. Since May 1987, GLONASS was used for the determination of Earth Rotation Parameters (ERP). One year later, in May 1988, at the ICAO conference on Future Air Navigation Systems (FANS) in Montreal/Canada, the system was presented to the civil public (*Anodina, 1988*). The system was offered to be used by the civil aviation community. In the same year, a similar presentation and offer was made at a conference of the IMO.

In 1989/1990, interest in GLONASS grew steadily in the United States and other Western countries. Although at that time only around ten satellites were operational, the capabilities of GLONASS and especially of the GPS/GLONASS combination were beginning to be seen. In part this may have been spurred by the US DoD activating Selective Availability on GPS in March 1990 (*N.N., 1990a*). Except for a brief time during the Gulf War (to allow US and Allied troops to use "civilian" GPS receivers to compensate for military P-code receivers not yet being available in sufficient numbers), S/A then was left active, leaving the GPS signal intentionally degraded. During that time some initial work on assessing the value of GLONASS for civil air navigation were started. FAA awarded a contract to Honeywell and Northwest Airlines to evaluate GLONASS performance on-board a commercial airliner (*N.N., 1990d*; *Hartmann, 1992*). This project was mainly aimed at collecting data for the purpose of certification of future GPS/GLONASS navigation equipment. The Massachusetts Institute of Technology, Lincoln Laboratories, started tracking GLONASS satellites and evaluating system performance, availability and integrity, also on behalf of the FAA (*N.N., 1990c*; *N.N., 1990b*).

Also in Europe, interest in GLONASS and combined use of GPS and GLONASS emerged. Especially here, scientists and officials felt uncomfortable with the current state of GPS and GLONASS both being systems controlled by one foreign country's military forces. So tendencies to use GPS and GLONASS as the basis for a future Civil Navigation Satellite System or a Global Navigation Satellite System (GNSS) under civil control rose strongly in the early 1990s (*N.N., 1993a*; *N.N., 1993b*). But before being able to plan for and design such a system, one had to get to know the existing systems very well.

The collapse of the Soviet Union and its successor, the Russian Federation, at first affected the efforts to complete the system. But Russian officials clung to the system. After all, GLONASS was also intended to replace ground based navigation systems, which are expensive in the vastness of the Russian territory. GLONASS thus was officially commissioned and placed under the auspices of the Russian Military Space Forces (Voenno Kosmicheski Sily, VKS) September 24, 1993, with 16 satellites operational. In the months to follow, however, some of the older spacecraft had to be withdrawn, bringing the number of operational satellites down to ten in August 1994. At that point, GLONASS was granted highest priority, when President Yeltsin issued a decree, ordering to have the system completed by the end of 1995 (*GPNN, 1994*). When launched from Baikonur/Kazakhstan, the Proton launch vehicle can simultaneously carry three GLONASS satellites into orbit. Thus, five more launches were necessary at that time.

On March 7, 1995, the Russian government issued a decree, ordering the Ministry of Defense, the Ministry of Transportation, the Russian Space Agency and the State Committee on the Defense-oriented Industry to cooperate in completing and further developing GLONASS (including differential reference stations and user equipment) and fostering its civil use (*Government, 1995*).

To underline this commitment to civil use of GLONASS, the Russian Space Forces had set up a GLONASS Coordinational Scientific Information Center (CSIC) already in early 1995. This is a literal

but rather bulky translation of the original Russian name Koordinatsionnyj Nauchno-Informatsionnyj Tsentr (KNITs) – Координационный Научно-Информационный Центр (КНИЦ). The more elegant translation "Coordination Center of Scientific Information (CCSI)" is hardly used. The mission of the CSIC is to continuously provide the civil community with accurate information on the status of the system.

The last of the five remaining launches (as of August 1994) took place in December 1995, and on January 18, 1996, the 24^{th} satellite was put into operation. Appendix B shows the launch history of GLONASS satellites, depicting these continuing advances in the construction of the system.

In February 1996, the Russian Ministry of Transport offered to use the GLONASS SP signal for civil aviation for a period of at least 15 years without direct user fees. At an ICAO meeting in March, this offer was discussed. An enhanced Russian offer was presented in July and finally accepted on July 29, 1996, by the ICAO (*ICAO, 1996*).

Since then, however, the continuing decline of the Russian Federation and especially its industries more and more affects the maintenance of the GLONASS system. Older satellites had to be withdrawn, after their design life time had been exceeded. They were not replaced, although replacement satellites had already been built, and the launch in December 1995 already carried a spare satellite into orbit. Thus, in June 1997 only nineteen satellites were usable, in December 1997 only fourteen (operational and healthy). From then on, the number of available satellites remained relatively stable at twelve to fourteen. This may partly be due to a November 1997 decree of the government of the Russian Federation, which was issued with the intention to ensure funding of the program and again fostering its civil and in particular its geodetic use (*Government, 1997*). Figure 2.1 shows this decline in satellite availability. In December 1998, the number of satellites had dropped to eleven, before on December 30 finally another triplet of GLONASS SVs was launched. This constituted the first GLONASS launch in three years. This launch is not immediately visible in Figure 2.1, since GLONASS satellites are not commissioned directly after launch. First, they undergo a series of orbital manoeuvering and various post-launch tests. These usually may last up to five or six weeks. The satellites launched in December 1998 thus went operational in late January and in February 1999. In April 1999, GLONASS 778 finally went operational. This satellite was kept as an orbiting spare after its launch in December 1995. After the withdrawal of GLONASS 780 from slot no. 15 on April 6, GLONASS 778 was manoeuvered from its original position in slot no. 9 to this free slot and put into operation on April 26. However, in late 1999 a number of satellites had to be withdrawn from the constellation, bringing down the number of usable satellites to around ten. Figure 2.2 illustrates the current status of the GLONASS space segment.

Due to the relatively short design life time (three years) of the GLONASS satellites, maintaining GLONASS requires frequent satellite launches. GLONASS satellites are most effectively launched by the Proton carriers. The only launch site capable of handling this powerful rocket is Baikonur in the former Soviet Republic of Kazakhstan. Although the Russian Federation and the Republic of Kazakhstan in March 1994 signed an agreement on the long-term lease of the Baikonur cosmodrome, Russia started planning to extend its own launch site in Plesetsk (*Kowalski, 1995*). This site in northern Russia is exclusively used by the Military Space Forces (VKS). Being located at 62.8° North, it is perfectly suited for high inclination (such as GLONASS), polar, and highly elliptical orbits (*RAG, 1998*; *NASA, 1998*). But funding for this project was stopped. Alternatively, the smaller Molniya booster, which operates regularly from Plesetsk, could place one GLONASS satellite at a time into orbit. This option was already taken into consideration at the beginning of the GLONASS program, but discarded at that time, because reaching the GLONASS orbit would require two major burns of the Molniya upper stage instead of one as is the case with Molniya's regular payloads (*Johnson, 1994*). As a second alternative, the new Zenit launcher could put two GLONASS satellites at a time into orbit, either from Baikonur or from Plesetsk.

Funding problems due to the constant decline in Russian economy also affects the proposed successor of GLONASS, called GLONASS-M. The advantages of GLONASS-M, compared to GLONASS, should be more stable satellite clocks (hydrogen masers instead of cesium clocks), an autonomous spacecraft

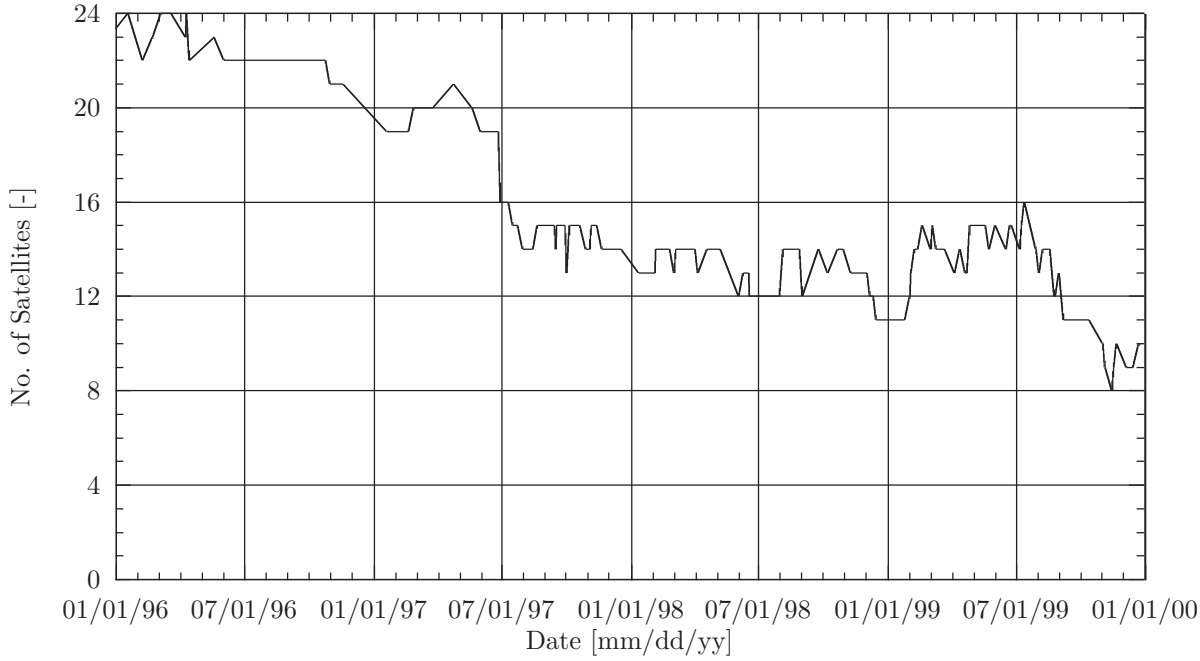

Figure 2.1: Number of available (operational and healthy) satellites in 1996 through 1999.

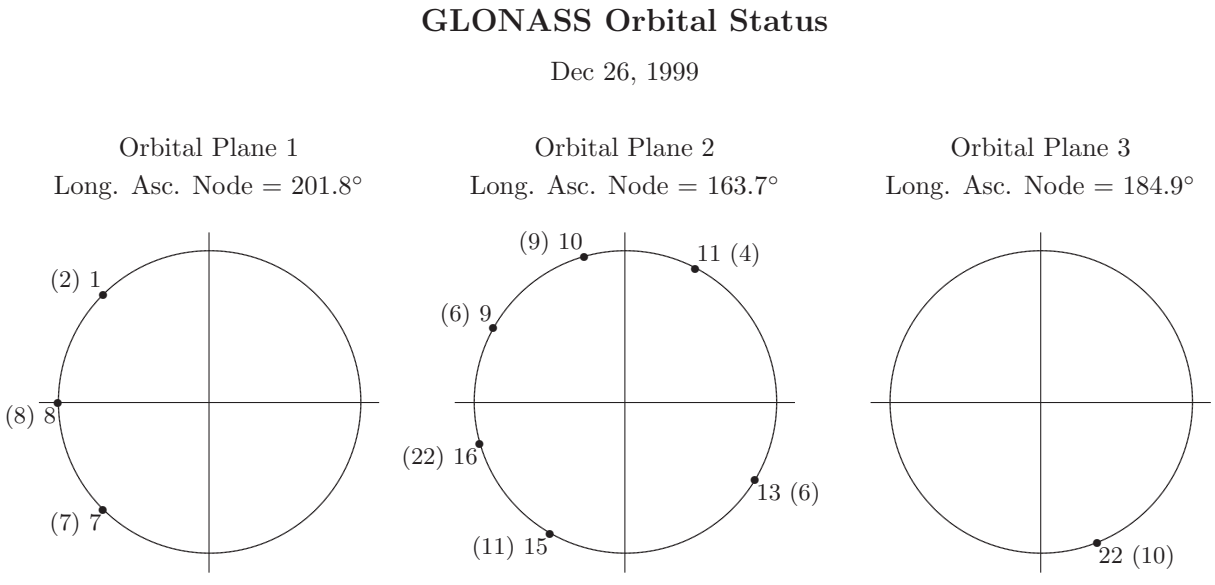

Figure 2.2: Current status of the GLONASS space segment; distribution of available (operational and healthy) satellites by orbital plane and argument of latitude.

operation mode and an extended design life time of five to seven years, enabling a less expensive maintenance of the satellite constellation by the system operators. GLONASS-M spacecraft originally were scheduled to be launched beginning in 1996 to replace the older GLONASS satellites (*Bartenev et al., 1994*; *Ivanov et al., 1995*; *Kazantsev, 1995*).

Thus, the future of GLONASS seems uncertain for financial reasons. From the technical point of view, however, GLONASS is at least comparable to the American GPS and deserves continuous upkeep and development.

3 GLONASS System Description

This section describes the GLONASS system and its major components. Since most of its future applications tend to be combined applications of GPS and GLONASS, GLONASS is compared to GPS, where appropriate.

3.1 Reference Systems

Just as GPS, GLONASS employs its own reference systems for time and coordinates. In the following, these are briefly described and compared to those of GPS. A more thorough discussion of these reference systems will follow later on in separate chapters.

3.1.1 Time Systems

GLONASS, just like GPS, defines its own system time. But whereas GPS system time represents a uniform time scale that started on January 6, 1980 (*ICD-GPS, 1991*), GLONASS system time is closely coupled to Moscow time $\mathrm{UTC_{SU}}$ (*ICD-GLONASS, 1995*). GLONASS system time is permanently monitored and adjusted in a way that the difference to $\mathrm{UTC_{SU}}$ not exceed approximately 100 ns. Therefore, GLONASS introduces leap seconds, contrary to GPS. Thus, the difference between GLONASS and GPS system times amounted to 13 seconds in January 2000, for example. These are the 13 leap seconds that had been introduced into UTC since the start of GPS system time.

As with GPS, the time scale of each individual satellite is regularly compared to system time. GLONASS navigational information contains parameters necessary to calculate the system time from satellite time as well as $\mathrm{UTC_{SU}}$ from GLONASS system time. Thus the user is enabled to adjust his own time scale to $\mathrm{UTC_{SU}}$ to within ± 1 ms.

3.1.2 Coordinate Systems

GLONASS satellite coordinates (and thus user coordinates) originally were expressed using the Soviet Geodetic System 1985 (SGS-85), whereas GPS employs the World Geodetic System 1984 (WGS84). In 1994, the GLONASS coordinate reference system changed to SGS-90, the definition of which was equal to that of SGS-85. After the collapse of the Soviet Union, SGS for a short time stood for **S**pecial **G**eodetic **S**ystem. Later the name was changed to Parametry Zemli 1990 Goda (Parameters of the Earth Year 1990), abbreviated PZ-90 or PE-90 (from the Russian and the English name, respectively). SGS-85 and its successors are defined as follows (*ICD-GLONASS, 1995*):

- Origin is Earth's center of mass.
- The z-axis is parallel to the direction of the mean North pole according to the mean epoch 1900 - 1905 as defined by the International Astronomical Union and the International Association of Geodesy.
- The x-axis is parallel to the direction of the Earth's equator for the epoch 1900 - 1905, with the XOZ plane being parallel to the average Greenwich meridian, defining the position of the origin of the adopted longitude system.
- The y-axis completes the geocentric rectangular coordinate system as a right-handed system.

The definition of WGS84 is (*ICD-GPS, 1991*):

- Origin is Earth's center of mass.
- z-axis is parallel to the direction of the Conventional International Origin (CIO) for polar motion, as defined by the Bureau International de l'Heure (BIH) on the basis of the latitudes adopted for the BIH stations.

Parameter	Abbr.	Value PZ-90	Value WGS84
Earth's gravitational constant	μ	$3.9860044 \cdot 10^{14}$ m^3/s^2	$3.986005 \cdot 10^{14}$ m^3/s^2
Earth's equatorial radius	a_E	$6.378136 \cdot 10^6$ m	$6.378137 \cdot 10^6$ m
Earth's flattening	f	1/298.257839303	1/298.257223563
Earth's rotational velocity	ω_E	$7.292115 \cdot 10^{-5}$ rad/s	$7.292115 \cdot 10^{-5}$ rad/s
2^{nd} zonal coefficient	c_{20} J_2	-1.08263 $\cdot 10^{-3}$	 $1.08263 \cdot 10^{-3}$
Speed of light	c	$2.99792458 \cdot 10^8$ m/s	$2.99792458 \cdot 10^8$ m/s

Table 3.1: Parameters of the reference systems PZ-90 and WGS84 (*Jansche, 1993*; *CSIC, 1998*; *ICD-GPS, 1991*; *NIMA, 1997*).

- x-axis is the intersection of the WGS84 reference meridian plane and the plane of the mean astronomic equator, the reference meridian being parallel to the zero meridian defined by the BIH on the basis of the longitudes adopted for the BIH stations.
- y-axis completes a right-handed Earth-centered, Earth-fixed orthogonal system.

Although these definitions are very similar, there are deviations in origin and direction parameters of the realizations of these systems. These differences and possible transformations between the reference systems are described in detail in one of the following chapters.

Further parameters of both systems are summarized in Table 3.1. They also show the similarities of the two systems.

3.2 Ground Segment

It is the task of the GLONASS ground segment to ensure operation and coordination of the entire system. To accomplish this, satellite orbits as well as time and frequency parameters are determined regularly. In addition, the health of all satellites is monitored continuously. Collected data are regularly transmitted to the satellites to be included in the broadcast navigational information.

The ground segment consists of the System Control Center, the Central Synchronizer and the Phase Control Center, which are all situated in Moscow. Seven additional ground stations are maintained in the territory of the former Soviet Union, serving for orbit determination and satellite monitoring. These stations are equipped with radar, laser distance meters and/or telemetry. They are situated near the following towns (see Figure 3.1):

St. Petersburg	TT&C
Ternopol	TT&C, laser ranging, monitoring
Jenisejsk	TT&C
Komsomol'sk-na-Amure	TT&C, laser ranging, monitoring
Balchas	Laser ranging
Jevpatoria	Laser ranging
Kitab	Laser ranging

Only satellites over the northern hemisphere, exclusive large parts of North America, are visible from these stations. (*Jansche, 1993*). This lacking of a global coverage is a large handicap of the GLONASS system, since it may cause delays in the discovery of satellite anomalies and updating of satellite data. Therefore, during the development phase of GLONASS, ground stations were planned to be set up in fellow socialist countries Cuba and Angola. But after the collapse of the Soviet Union, these plans were not realized.

In order to determine the satellite orbits, satellites are tracked by radar 3 – 5 times for 10 – 15 minutes each every 10 – 14 revolutions (*Bartenev et al., 1994*). By these means, the determination of the

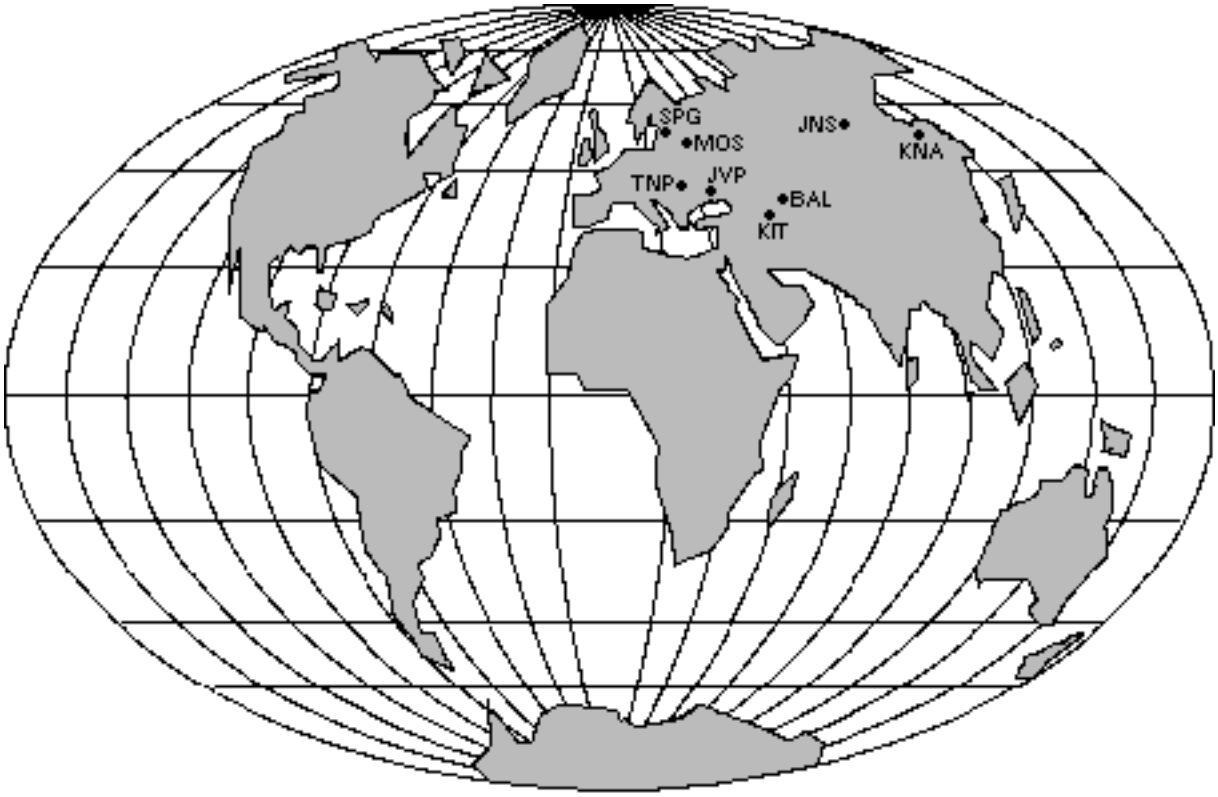

Figure 3.1: Locations of GLONASS ground stations.

satellite positions is accomplished with an accuracy of approximately 2 – 3 m at the times of tracking. The radar data are regularly compared to the results of laser tracking of the satellites to calibrate the radar facilities. These laser range measurements yield accuracies near 1.5 – 2 cm in distance and 2 – 3" in angular coordinates. The equations of motion of the satellites are numerically integrated, considering the Earth's gravitational potential as well as gravitational and non-gravitational disturbances, with the measured satellite positions as initial values. Obtained solutions are extrapolated for up to 30 days and uploaded to the satellites, where they are stored. Error specifications for the GLONASS broadcast orbits are given in Table 3.2.

3.3 Space Segment

The GLONASS space segment consists of 24 satellites, distributed over three orbital planes. The longitude of ascending node differs by 120° from plane to plane. Each plane comprises eight satellites, staggered

	Mean square error	
Satellite position vector	Along track	20 m
	Cross track	10 m
	Radial	5 m
Satellite velocity vector	Along track	0.05 cm/s
	Cross track	0.1 cm/s
	Radial	0.3 cm/s
Time scale synchronization		20 ns

Table 3.2: Mean square errors of GLONASS broadcast ephemerides (*ICD-GLONASS, 1995*).

Parameter	GLONASS	GPS
Semi-major axis	25510 km	26580 km
Orbital height	19130 km	20200 km
Orbital period	11 h 15.8 min	11 h 58 min
Inclination	64.8°	55°
Eccentricity	≤0.01	≤0.1
Distinguishing between satellites	FDMA (1 code, multiple frequencies)	CDMA (1 frequency, multiple codes)
Frequencies L_1 L_2	1602 - 1615.5 MHz 1246 - 1256.5 MHz	1575.42 MHz 1227.60 MHz
Signal polarization	RHCP	RHCP

Table 3.3: Parameters of the GLONASS and GPS space segments (*ICD-GLONASS, 1995*; *ICD-GPS, 1991*).

by 45° in argument of latitude. The arguments of latitude of satellites in equivalent slots in two different orbital planes differ by 15°.

The GPS space segment also consists of nominally 24 satellites, which are, however, distributed over six orbital planes, differing from plane to plane by 60° in longitude of the ascending node. Orbital and other parameters of the spacecraft are summarized in Table 3.3.

The orbital period of 11 h 15.8 min for GLONASS satellites means that for a stationary observer the same satellite is visible at the same point in the sky every eight sidereal days. Since there are eight satellites in each orbital plane, each day a different satellite appears at the same point in the sky. With the 11 h 58 min orbital period for GPS satellites, the same GPS satellite is visible at the same point in the sky every (sidereal) day.

Besides its atomic clock and the equipment for receiving, processing, storing and transmitting navigational data, GLONASS satellites carry an extensive propulsion system, enabling the satellite to keep its orbital position, to control its attitude and even to manoeuvre to a different orbital position. The attitude control system obtains its information from a number of different sensors, including an earth sensor and a magnetometer. Reflectors on the satellite body near the transmission antennae serve for purposes of laser ranging from ground stations. The cylindrical body measures 2.35 m in diameter and more than 3 m in length; overall length (with magnetometer boom unfolded) is 7.84 m. The solar arrays span 7.23 m and include an area of 17.5 m^2. They supply a total of 1.6 kW of electrical power. The mass of a GLONASS satellite is approximately 1300 kg. The satellites launched in 1995 were second generation spacecraft (not to be confounded with GLONASS-M). They are already designed for a longer life time of five years and incorporate more stable frequency standards. Their mass is approximately 1410 kg, with 23.6 m^2 of solar panels for improved power supply (*Johnson, 1994*; *Revnivykh and Mitrikas, 1998*; *CSIC, 1998*; *Bartenev et al., 1994*; *Kazantsev, 1995*; *Gouzhva et al., 1995*). A GLONASS satellite is depicted in Figure 3.2.

3.4 GLONASS Frequency Plan

To distinguish between individual satellites GLONASS satellites employ different frequencies to broadcast their navigational information. Satellite frequencies are determined by the equation

$$\begin{aligned} f_{L_1} &= 1602 + k \cdot 0.5625 \text{ MHz} \quad L_1 \text{ frequency and} \\ f_{L_2} &= 1246 + k \cdot 0.4375 \text{ MHz} \quad L_2 \text{ frequency.} \end{aligned}$$

In this equation, k means the frequency number of the satellite. The frequency domain as specified in Table 3.3 is equivalent to the frequency numbers 0 – 24. Frequency number 0 is the so-called technical

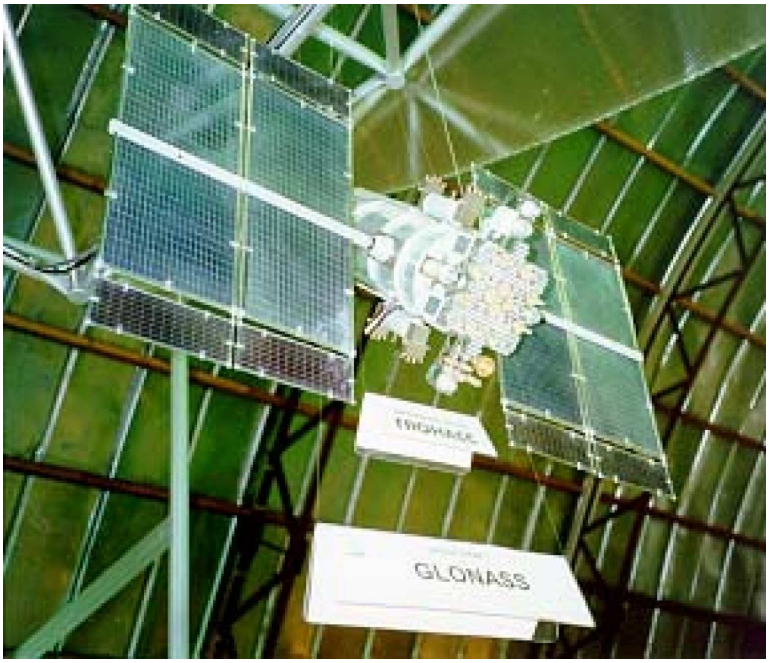

Figure 3.2: GLONASS satellite (model displayed at 1997 Moscow Air Show, taken from (*CDISS, 1998*)).

frequency. It is reserved for testing purposes during the commissioning phase of a satellite. Numbers 1 – 24 are assigned to operational satellites. The frequency ratio f_{L_2}/f_{L_1} equals 7/9 for GLONASS. The corresponding frequency ratio for GPS is 60/77.

Originally, each of the 24 satellites was scheduled to have its own unique frequency number. But part of this GLONASS frequency spectrum also is important for radio astronomy. 1612 MHz (equalling GLONASS frequency number 18 in the L_1 sub-band) is the frequency for radiation emitted by the $1 \rightarrow 2$ transition in the quartet of ${}^2\Pi_{\frac{3}{2}}$, $J = \frac{3}{2}$ state of hydroxyl (OH), a molecule common in interstellar clouds. The 1612 MHz line of hydroxyl in particular seems always to arise in the atmosphere of cool IR stars. Observation of hydroxyl molecules may provide vital clues about the evolution of our galaxy (*Cook, 1977*; *Litvak, 1969*; *Verschuur and Kellermann, 1974*). In addition, some providers of satellite communications services (especially Motorola, Inc. for their Iridium system) started claiming other parts of the GLONASS frequency band. At the World Administrative Radio Conference 1992, these satellite communications providers were granted the right to share use of the upper portion of the GLONASS frequency band (from 1610 MHz onwards) (*N.N., 1992*). (Meanwhile another agreement has been reached between Motorola and radio astronomers regarding usage of the 1612 MHz.)

Therefore, beginning in 1993 the GLONASS frequency plan was re-organized in such a way that antipodal satellites – i.e. satellites in opposing slots within the same orbital plane – share the same frequency numbers, thus cutting to half the number of required frequencies. This sharing of frequencies by antipodal satellites avoids unintentional mutual jamming of satellites at least for land, sea and airborne users of the system. Spaceborne users above an orbital height of approximately 200 km, however, may see both satellites transmitting on the same frequency at least during part of their orbits – cf. (*Werner, 1998*).

This re-organization of the frequency plan is scheduled to take place in three stages. The first stage was implemented from 1993 to 1998. It called for frequency sharing by antipodal satellites to avoid usage of frequency numbers 16 – 20 (1611.0 – 1613.25 MHz), thus clearing the 1612 MHz for radio astronomy. Frequency numbers 13, 14, 15 and 21 were to be used only under exceptional circumstances, frequency number 0 remained as technical frequency. This left frequency numbers 1 ... 12, 22, 23 and 24 to be used for normal operation.

Plane 1				Plane 2				Plane 3			
Slot	Freq.	Slot	Freq.	Slot	Freq.	Slot	Freq.	Slot	Freq.	Slot	Freq.
1	–	5	–	9	6	13	6	17	24	21	–
2	–	6	13	10	9	14	9	18	10	22	10
3	21	7	–	11	4	15	4	19	3	23	–
4	12	8	–	12	22	16	22	20	1	24	–

Table 3.4: Usage of GLONASS frequency numbers in January of 1998.

Table 3.4 shows the usage of frequency numbers by GLONASS satellites (identified by their almanac slot number) as of January 1998. The assignment of identical frequency numbers to opposing satellites can be clearly seen, especially in orbital plane 2. However, it must also be noticed that frequency numbers 13 and 21 are still in use by satellites launched in 1994, even though these channels should be used only under exceptional circumstances.

The second stage, from 1998 to 2005, further limits usage of frequency numbers to numbers 1 ... 12, with frequency number 13 to be used only under extreme circumstances and frequency number 0 as technical frequency.

Beyond 2005, GLONASS frequencies will be shifted to frequency numbers -7 ... +4, with +5 and +6 as technical frequencies. This equals a frequency domain of 1598.0625 – 1605.375 MHz in the L_1 sub-band and 1242.9375 – 1248.625 MHz in the L_2 sub-band.

Figure 3.3 illustrates the scheduled usage of frequency numbers.

GLONASS satellites generally provide the possibility to switch their carrier frequency between three frequency numbers – the technical frequency and two operational frequencies. Satellites launched after 1995 will already be equipped to transmit on one of the frequency numbers -7 ... -1. This way, shifting the entire GLONASS frequency band beyond 2005 will not require replacement of satellites.

3.5 Signal Structure

Just like GPS, GLONASS employs the spread spectrum technique for its satellite transmissions.

The GLONASS signal consists of two components, the PRN (Pseudo-Random Noise) code and the navigational information, which are modulo 2 added. The navigational information itself consists of the digital information and a time code. The digital information is created by modulo 2 addition of the characters of digital information and a meander signal. The resulting signal is modulated onto the carrier signal by means of Binary Phase Shift Keying (BPSK). All signal components are derived from the 5 MHz fundamental signal of the satellite's onboard frequency normal (*ICD-GLONASS, 1995*).

Exactly as GPS, GLONASS uses a Coarse Acquisition (C/A-)Code and a Precision (P-)Code. The L_1 carrier signal is modulated by both C/A- and P-code, whereas the L_2 signal carries the P-code only.

3.5.1 C/A-Code

The C/A-code as employed by GLONASS is an unshortened pseudo-stochastic sequence of binary digits, derived from the seventh bit of a nine bit shift register. The code is described by the irreducible polynomial $1 + x^5 + x^9$. This code is 511 characters long. At a clock frequency of 511 kHz, this equals a duration of 1 ms. The initial state is defined as each bit containing the value '1'. Figure 3.4 shows a simplified scheme of the PRN code generation.

The GPS C/A-code is 1023 bits long at a clock frequency of 1023 kHZ, also equalling a code duration of 1 ms (*ICD-GPS, 1991*).

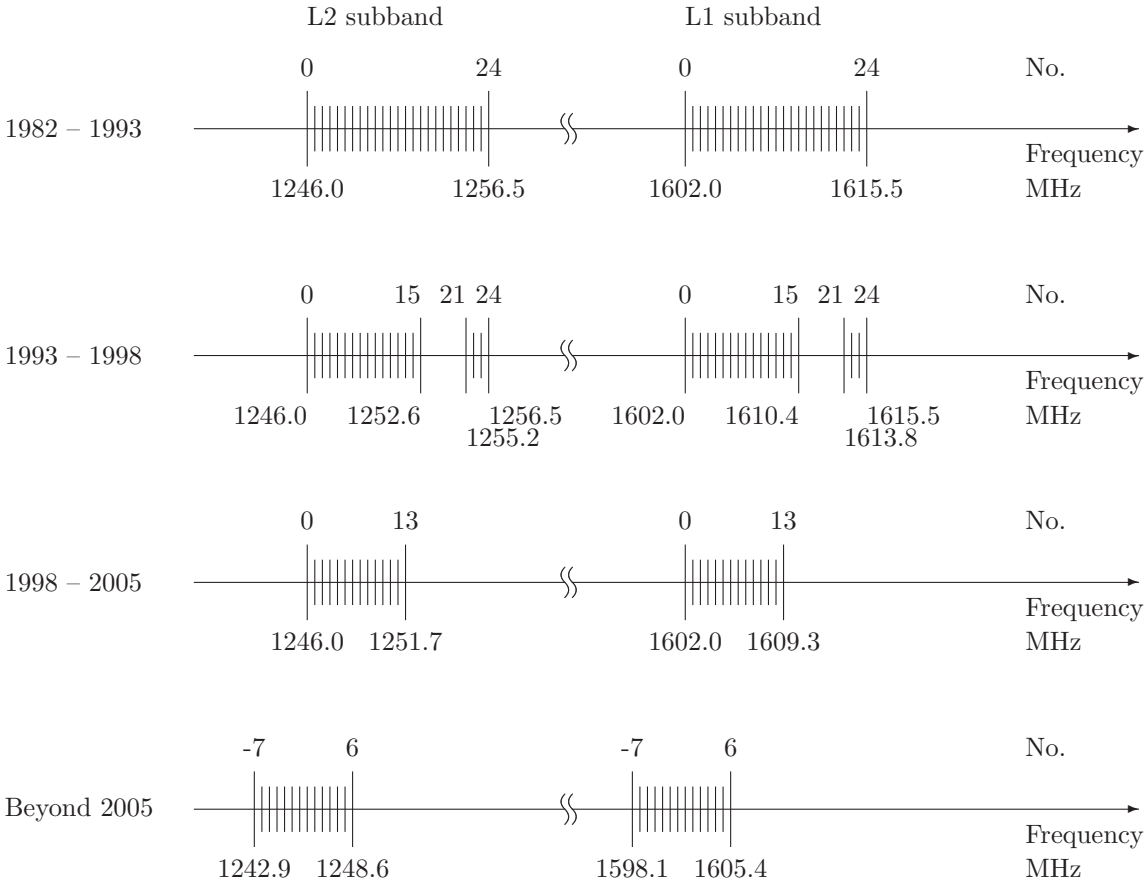

Figure 3.3: GLONASS frequency plan.

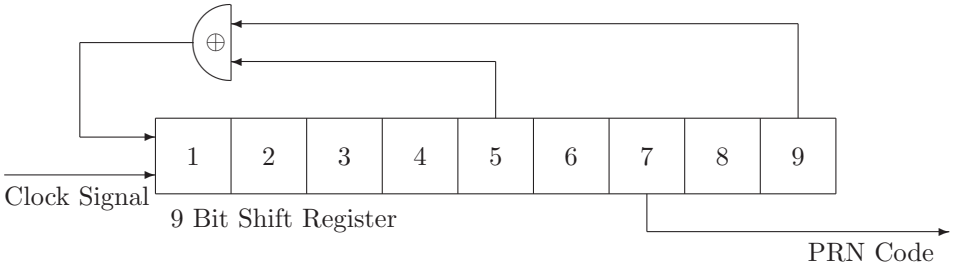

Figure 3.4: GLONASS C/A-code generation (schematic).

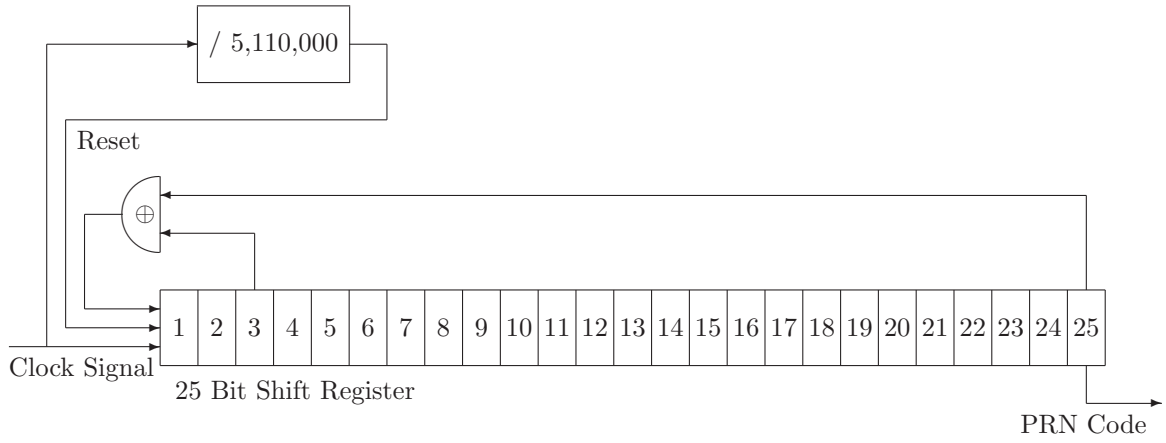

Figure 3.5: GLONASS P-code generation (schematic).

3.5.2 P-Code

The P-code as employed by GLONASS is a shortened pseudo-stochastic sequence of binary digits, derived from the last bit of a 25-bit shift register (*Lennen, 1989*). The code is described by the irreducible polynomial $1 + x^3 + x^{25}$. This code is 33554431 characters long. At a clock frequency of 5.11 MHz, this equals a duration of 6.566 s. The initial state is defined as each bit containing the value '1'. The P-code is truncated by resetting the shift register to its initial state at each second epoch. Thus, the GLONASS P-code effectively is only 1 s long. Figure 3.5 shows a simplified scheme of the PRN code generation.

The GPS P-code is $2.3547 \cdot 10^{14}$ bits long at a clock frequency of 10.23 MHZ, equalling a code duration of approximately 266.4 days. The GPS P-code is truncated at each weekly epoch, bringing down the effective length of the P-code to one week (*Hofmann-Wellenhof et al., 1993*).

3.5.3 C/A-Code Data Sequence

The GLONASS C/A-code data sequence consists of so-called superframes, each lasting 2 1/2 minutes. Each superframe is divided into five frames of 30 s duration. Each of these frames contains 15 lines of 2 s duration. One line is made of a sequence of digital information lasting for 1.7 s, followed by a 0.3 s time code. The sequence of digital information is obtained by modulo 2 addition of 85 bits of digital information and a 100 bit/s meander signal. 77 out of these 85 characters of digital information contain the navigational information of the respective line. The remaining 8 bits contain a Hamming code for purposes of error detection and removal. This structure is shown in Figure 3.6.

Russian officials have not published any information on the GLONASS P-code data message. However, it is known that the complete message repeats itself after 12 minutes, in contrast to the C/A-code, which repeats itself after 2 1/2 minutes. Ephemeris and clock parameters in the P-code navigation message repeat every 10 s, whereas in the C/A-code these parameters repeat every 30 s (*Langley, 1997*).

3.5.4 Time Code

The time code broadcast at the end of each line is 0.3 s long and consists of 30 bits. This equals a bit rate of 100 bit/s, the same as the meander signal. The time code is a fixed but shortened pseudo-stochastic sequence, described by the generating polynomial $1 + x^3 + x^5$ and consisting of the characters:

111110001101110101000010010110

The first bit of the digital information of each line always is a '0' to complete the shortened sequence of the time code of the previous line.

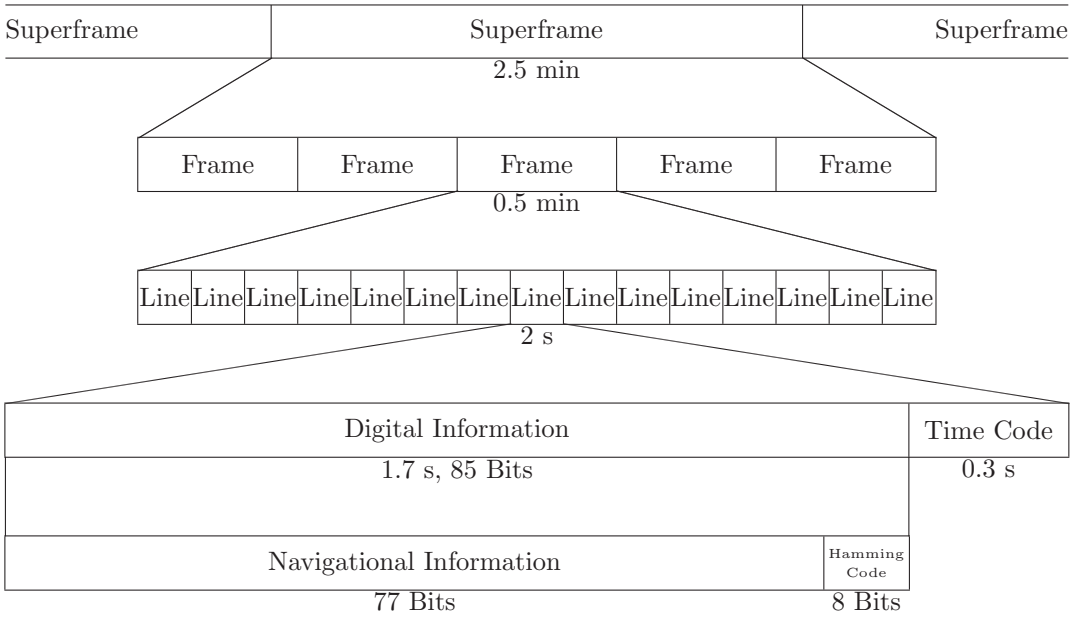

Figure 3.6: Structure of the C/A-code data sequence.

3.5.5 Bit Synchronization

The boundaries of lines, characters of digital information, bits of the meander signal, characters of the time code and bits of the PRN code are all synchronized to each other. The boundaries of the meander signal and the boundaries of the boundaries of the characters of digital information coincide with the beginning of the first bit of the PRN code. The ending of the last bit of the time code coincides with that moment in time that, in the satellite time scale, differs from the beginning of the day (Moscow time) by an integer, even number of seconds.

3.5.6 Structure of Navigation Data

Lines 1 – 4 of a frame contain operative information regarding the transmitting satellite (ephemeris data). Line 5 contains non-operative information for the entire system. These lines are repeated in each frame of a superframe as long as their data contents is valid. Lines 6 – 15 contain non-operative information regarding specified satellites (almanac data). The almanac data of one satellite require two full lines. Thus, the almanac data of five satellites can be transmitted within one frame. The almanac data of the entire system (24 satellites) therefore require five frames, which is one superframe. Complete GLONASS almanac data can be downloaded from one satellite within the time span of 2 1/2 minutes. In contrast, downloading the complete GPS almanac using data from only one satellite would require 12 1/2 minutes.

The GLONASS almanac data are organized that way that the first four frames of a superframe each contain the almanac data of five succeeding satellites (1 – 5, 6 – 10, etc.), while the data of satellites 21 – 24 occupy lines 6 – 13 of frame 5. Lines 14 and 15 of frame 5 are not used for the transmission of data.

The data structures of the individual lines are shown in Figures 3.7 and 3.8 as well as Tables 3.5 and 3.6. Some of the data require more thorough remarks:

- Change of operative information:

  Length of the time interval between t_b of the current and of the previous frames. Valid values: ’00’ – 0 min, ’01’ – 30 min, ’10’ – 45 min, ’11’ – 60 min

Attribute	Meaning	Bits	Scale	Unit
0	First bit always 0	1	1	–
m	Line number	4	1	–
Π_1	Change of operative information	2	see remarks	
Π_2	Change of t_b flag	1	see remarks	
Π_3	Number of satellites in almanac	1	see remarks	
B	Satellite health	3	see remarks	
t_k	Time of frame start	12	see remarks	
t_b	Reference time of ephemeris data	7	15	min
γ	Relative frequency offset	11	2^{-40}	–
x, y, z	Satellite position	27	2^{-11}	km
$\dot{x}$, $\dot{y}$, $\dot{z}$	Satellite velocity	24	2^{-20}	km/s
$\ddot{x}$, $\ddot{y}$, $\ddot{z}$	Satellite acceleration due to lunar-solar attraction	5	2^{-30}	km/s^2
$\tau\,(t_b)$	Satellite clock offset	22	2^{-30}	s
E	Age of data	5	1	days
N_A	Reference day for almanac data	11	1	days
τ_c	Time system correction with respect to UTC_{SU}	28	2^{-27}	s

Table 3.5: Structure of lines 1 – 5.

- Change of t_b flag:

  Indicates even ('0') or odd ('1') serial number of the current validity period.

- Number of satellites in almanac:

  Indicates whether the almanac contains data of five ('1') or four ('0') satellites.

- Satellite health:

  If the first bit is set, the satellite is unhealthy. The remaining bits are not analyzed by the user equipment.

- Time of frame start:

  5 most significant bits: Hours since start of current day
  6 median bits: Minutes since start of current hour
  1 least significant bit: Half minutes since start of current minute

- Reference day for almanac data:

  Day number within the four year period starting with a leap year.

In all values that can bear a negative sign the most significant bit always identifies the sign ('0' for positive, '1' for negative), whereas the remaining bits represent the absolute value. GLONASS does not employ the otherwise wide-spread formulation in twos complements.

3.5.7 GLONASS-M Navigation Data

Improvements of the proposed GLONASS-M satellites include transmission of the difference between GLONASS and GPS time scales (see Chapter 4) and other useful information currently not transmitted by the GLONASS satellites. To accomplish this without interfering with the traditional GLONASS navigation data structure, some of the spare bits in the navigation message have been assigned a meaning. In addition, line numbers 14 and 15 of the fifth frame within a superframe are now also used to broadcast navigation data.

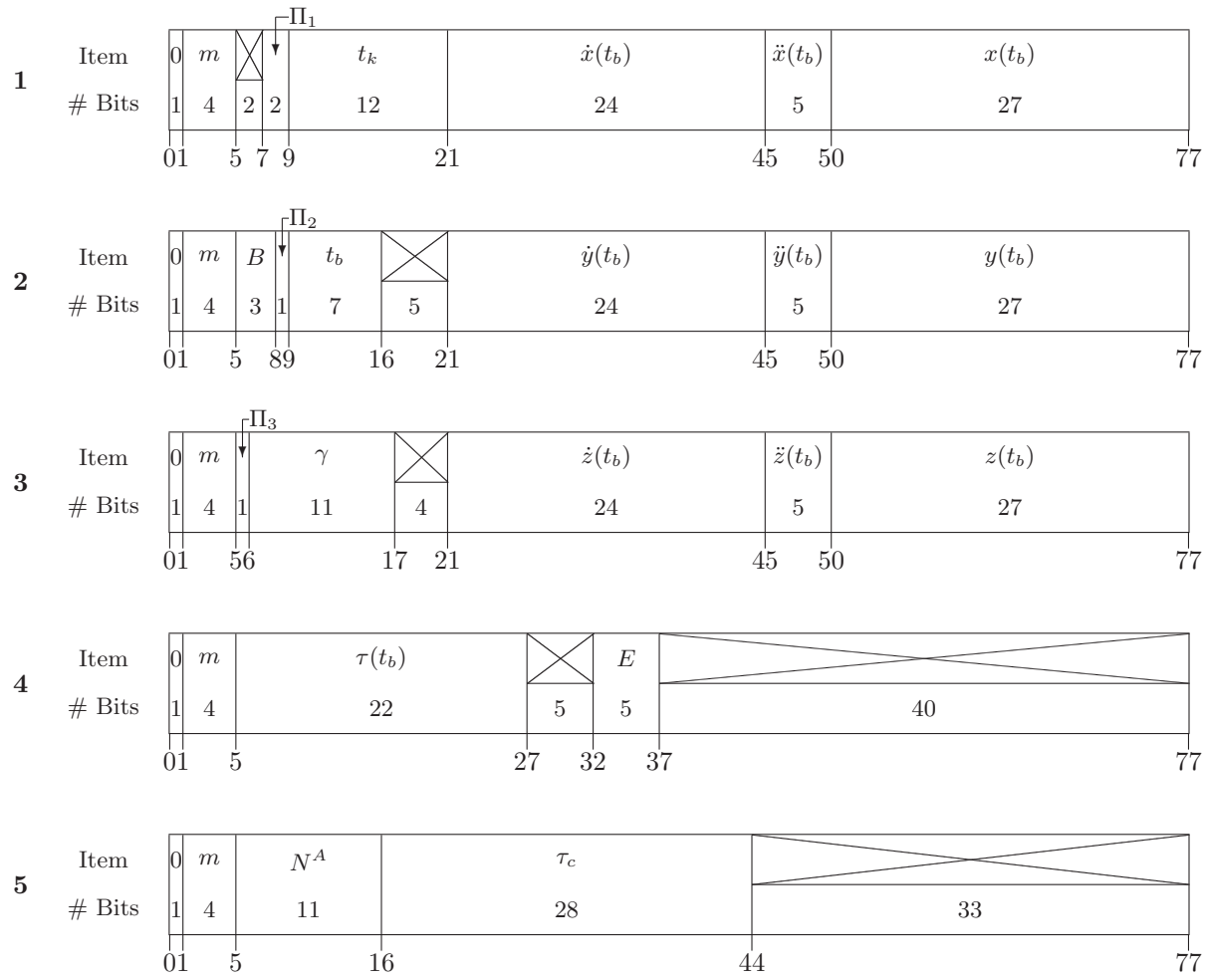

Figure 3.7: Structure of ephemeris data (lines 1 – 4) and general data (line 5). Crossed out areas represent spare bits, which are not used for transmission of data.

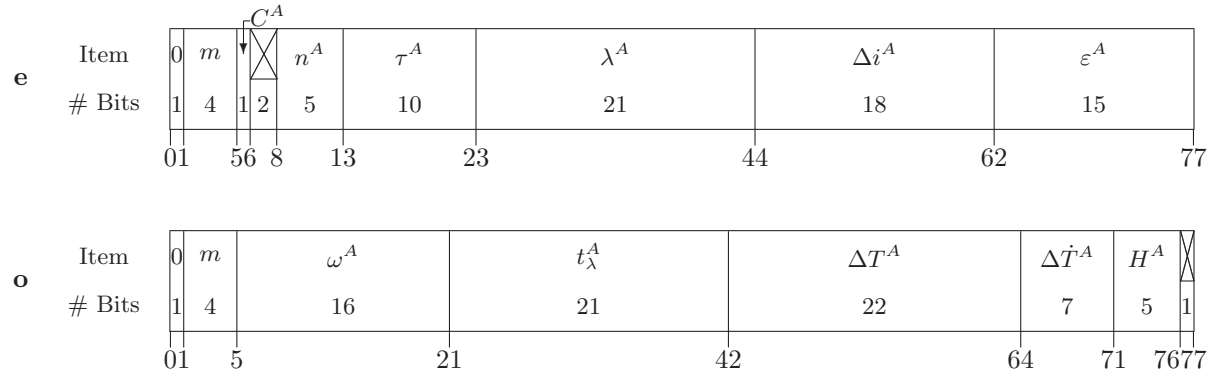

Figure 3.8: Structure of almanac data (lines 6 – 15) (e - even lines, o - odd lines). Crossed out areas represent spare bits, which are not used for transmission of data.

Attribute	Meaning	Bits	Scale	Unit
0	First bit always 0	1	1	–
m	Line number	4	1	–
n^A	Satellite slot number	5	1	–
C^A	Satellite health	1	0 = no, 1 = yes	
τ^A	Satellite clock offset	10	2^{-18}	s
λ^A	Greenwich longitude of first equator crossing	21	2^{-20}	semi-circles
Δi^A	Correction to nominal inclination	18	2^{-20}	semi-circles
ε^A	Eccentricity	15	2^{-20}	–
ω^A	Argument of perigee	16	2^{-15}	semi-circles
t_λ^A	Time of first equator crossing	21	2^{-5}	s
ΔT^A	Correction to nominal orbital period	22	2^{-9}	s
$\Delta \dot{T}^A$	Rate of change of orbital period	7	2^{-14}	s/orbit
H^A	Satellite frequency number	5	1	–

Table 3.6: Structure of lines 6 – 15.

Figures 3.9 and 3.10 show the modified data structure. Newly introduced data fields are highlighted in Tables 3.7 and 3.9. See also the modified GLONASS ICD (*ICD-GLONASS, 1998*).

Some of these newly introduced parameters require more thorough remarks:

- Indicator for frequency/time data computation mode:

  Indicates whether the frequency and time correction parameters were computed and uploaded by the control segment ('0') or computed onboard the satellite ('1').

- Indicator for update of data:

  Indicates whether updated ephemeris and frequency/time parameters are being transmitted within the given frame. '1' means transmission of updated data.

- Current date:

  Calendar number of day within current four-year interval starting with a leap year.

- Satellite modification flag:

  Indicates the modification state of the satellite: '00' – conventional GLONASS satellite, '01' – GLONASS-M satellite, other values are reserved for further use.

- Notification of forthcoming leap second correction:

  Indicates whether a leap second correction is to take place at the end of the current quarter: '00' – no leap second correction planned for end of current quarter, '01' – leap second correction (+1 s) planned for end of current quarter, '11' – leap second correction (−1 s) planned for end of current quarter, '10' – no decision on leap second correction at the end of current quarter has been made yet. A decision on a leap second correction is made at latest eight weeks before the end of the quarter, but may be made earlier. As soon as it is made, the transmitted '10' will be replaced by the proper value.

The data field τ_c for the time system correction with respect to $\mathrm{UTC_{SU}}$ has been extended from 28 to 32 bits in the GLONASS-M data structure. This was achieved by re-assigning four immediately following spare bits to this data field. Simultaneously, the resolution of the time system correction was increased by a factor of 2^{-4}. The additional bits therefore contribute to an improved resolution of the value.

Attribute	Meaning	Bits	Scale	Unit
P	Frequency/time data computation mode indicator	1	see remarks	
l	Satellite health indicator	1	0 = yes, 1 = no	
$\Delta\tau$	Time difference between transmission in L_2 and L_1	5	2^{-30}	s
Π_4	Indicator for update of broadcast data	1	see remarks	
F_T	Accuracy of measurements indicator	4	see Table 3.8	
N_T	Current date	11	see remarks	
n	Almanac slot number of transmitting satellite	5	1	–
M	Satellite modification flag	2	see remarks	
τ_c	Time system correction with respect to UTC_{SU}	32	2^{-31}	s
N_4	Four-year interval number, starting with 1996	5	1	–
τ_{GPS}	Time difference to GPS system time	22	2^{-30}	s

Table 3.7: New or modified GLONASS-M data fields in lines 1 – 5.

Value of F_T	1 σ accuracy of measurements [m]	Value of F_T	1 σ accuracy of measurements [m]
0	1	8	14
1	2	9	16
2	2.5	10	32
3	4	11	64
4	5	12	128
5	7	13	256
6	10	14	512
7	12	15	Not used

Table 3.8: Accuracy of measurements indicator F_T.

This modification does not result in an interference with the traditional data structure. An old receiver – not knowing about the difference between GLONASS and GLONASS-M – will evaluate the first 28 bits of the τ_c data field of a GLONASS-M satellite and obtain a less precise, but not a wrong value. A new receiver may evaluate the data field correctly, depending on the modification state of the satellite. It is, however, not required for the receiver to evaluate the first 28 bits only for a traditional GLONASS satellite. Since the spare bits are transmitted as zeroes, the full 32 bits may be evaluated without obtaining a different value.

The negative frequency numbers to be used by GLONASS beyond 2005 will be encoded in the H^A data word as follows:

Frequency number	-1	-2	-3	-4	-5	-6	-7
Value of H^A	31	30	29	28	27	26	25

That is, the negative frequency numbers are offset by a value of 32, thus making use of the range 25 ... 31 currently not used.

3.6 System Assurance Techniques

GPS has its signal intentionally degraded by so-called system assurance techniques to deny the full system accuracy to the "unauthorized" user. These techniques are Selective Availability (S/A) and Anti-Spoofing (A-S).

S/A is the intentional degradation of the satellite orbit ("epsilon process") and clock ("clock dither") parameters. For the user, this results in a horizontal positioning error of 100 m and a vertical error of

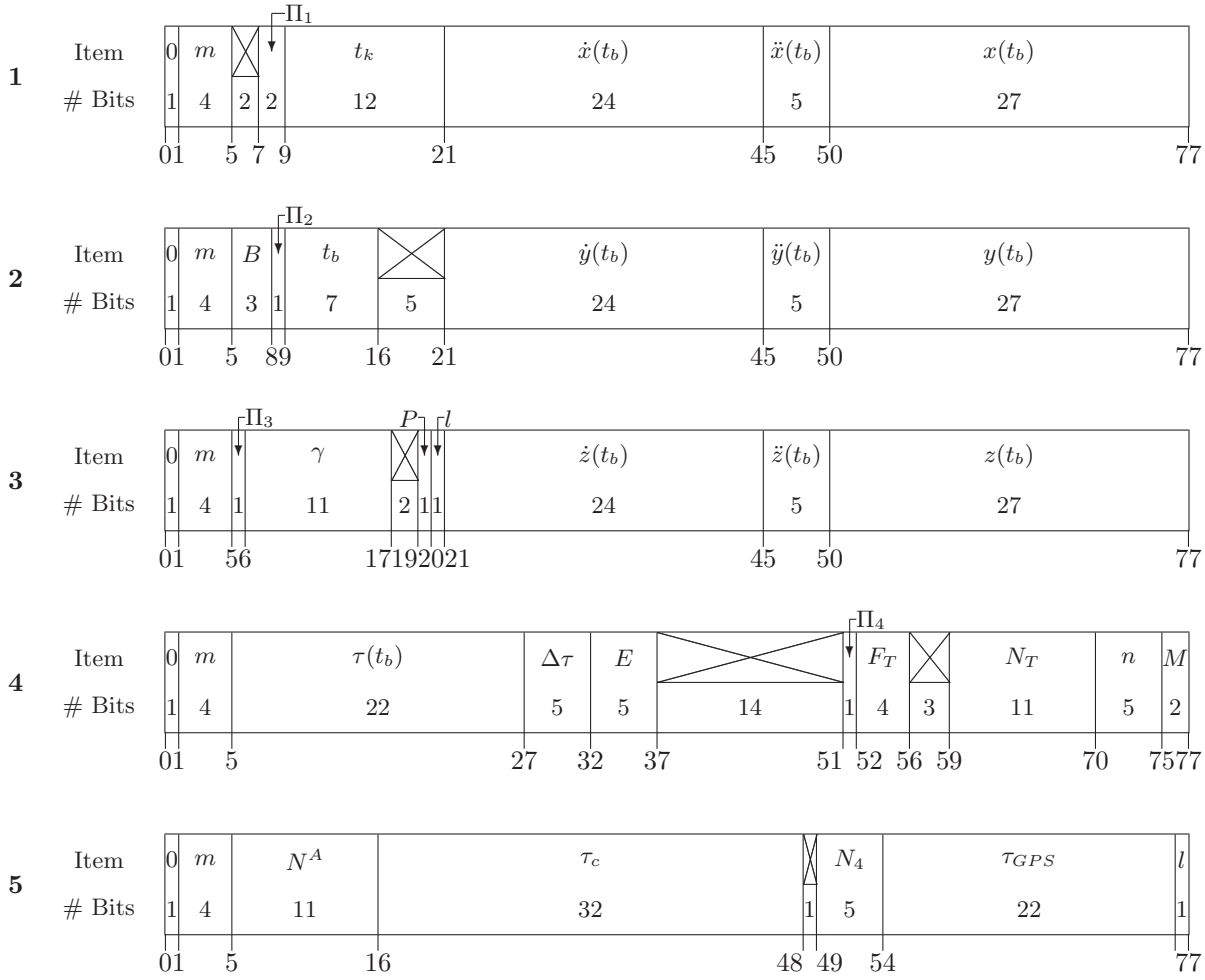

Figure 3.9: Structure of ephemeris data (lines 1 – 4) and general data (line 5) for GLONASS-M satellites. Crossed out areas represent spare bits, which are not used for transmission of data.

Attribute	Meaning	Bits	Scale	Unit
M^A	Satellite modification flag	2	see remarks	
B_1	Time difference between UT1 and UTC	11	2^{-10}	s
B_2	Drift in difference between UT1 and UTC	10	2^{-16}	s/day
KP	Notification of forthcoming leap second change	2	see remarks	
l	Health indicator for transmitting satellite	1	0 = yes, 1 = no	

Table 3.9: New or modified GLONASS-M data fields in lines 6 – 15.

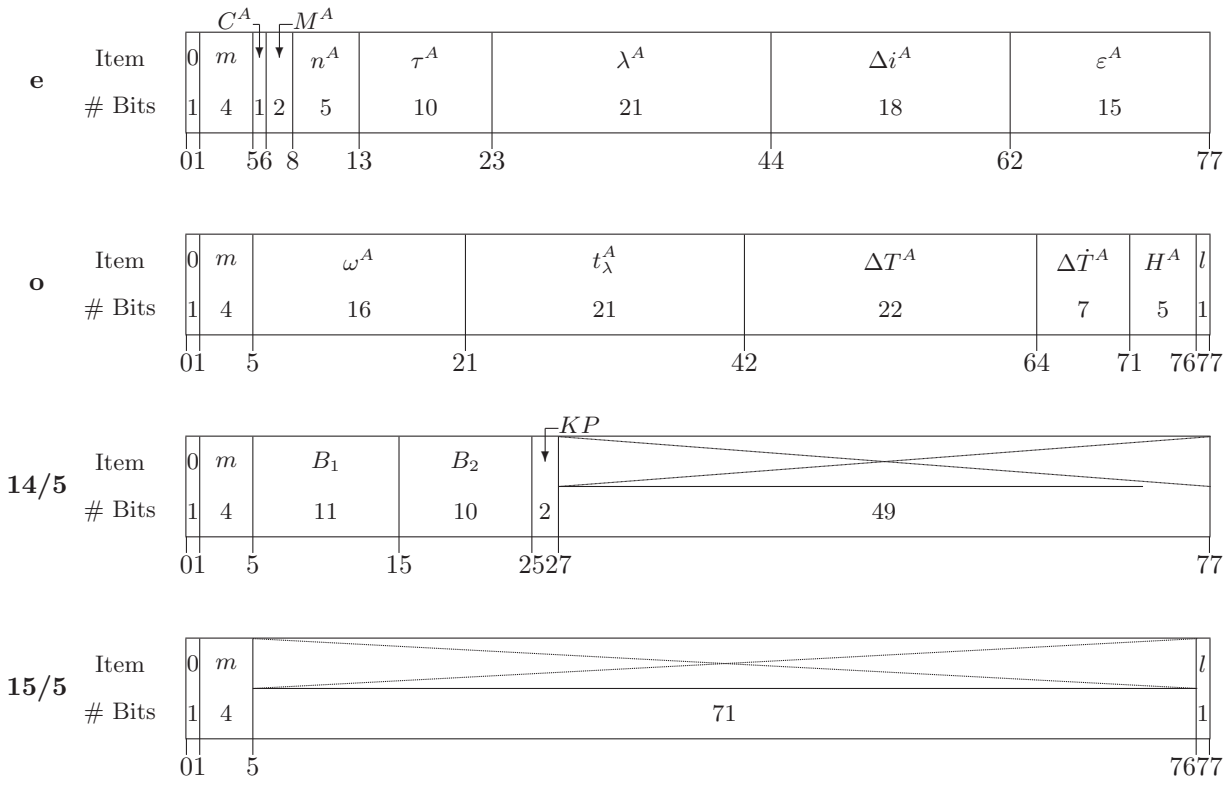

Figure 3.10: Structure of almanac data (lines 6 – 15) for GLONASS-M satellites. (14/5 - line no. 14 of fifth frame, 15/5 - line no. 15 of fifth frame, e - all other even lines, o - all other odd lines). Crossed out areas represent spare bits, which are not used for transmission of data.

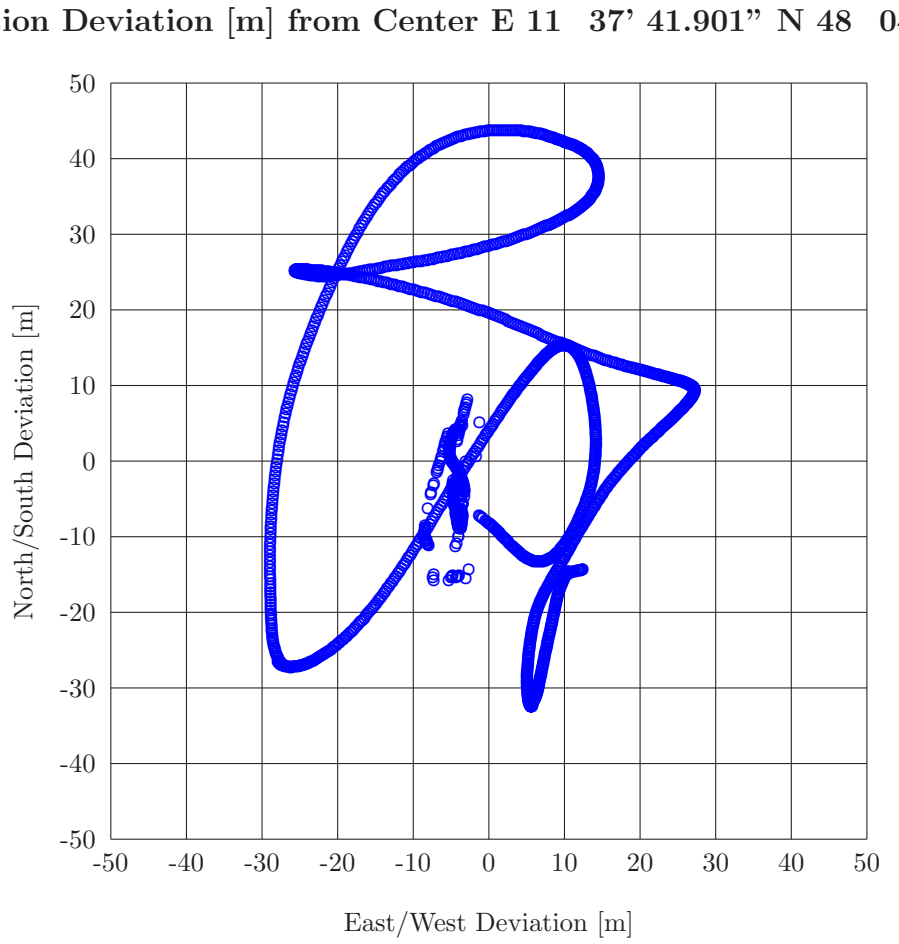

Figure 3.11: Single point positioning using GPS (example).

140 m, each 95% of the time, compared to 20 m and 30 m, respectively, that are achievable when S/A is turned off (*Graas and Braasch, 1996*). Due to this affection by Selective Availability, results of single point positioning from GPS measurements scatter very much. Figure 3.11 shows a typical example of GPS positioning under the influence of S/A.

Contrary to GPS, GLONASS is not degraded artificially by the system operators. Neither there are plans to introduce such measures in future. The large scattering of the positioning solution thus cannot be observed with GLONASS, see Figure 3.12. The positioning accuracy of GLONASS approximately equals that of GPS with S/A turned off. To illustrate the relation between the positioning accuracies achievable with GPS (S/A on) and GLONASS (no S/A), the scale of both Figures 3.11 and 3.12 was chosen identical.

A-S is the additional encrypting of the P-code, thus denying the non-military user access to this source of precise range measurements. Like with S/A, there is no such technique employed by GLONASS, nor is it planned to introduce anything like it in future. The GLONASS P-code never was published by the system operators, but it was made known to the scientific community by e.g. (*Lennen, 1989*). This means, the GLONASS P-code is fully available. This enables the user to employ dual-frequency measurements for correction of ionospheric effects. This provides a further improvement in obtainable positioning accuracy. However, along with the P-code not being published by the system operators, it neither was officially released for use outside the Russian Armed Forces. Instead, they reserve the right to alter the code in future. This keeps a number of potential users and receiver manufacturers from actually implementing the GLONASS P-code.

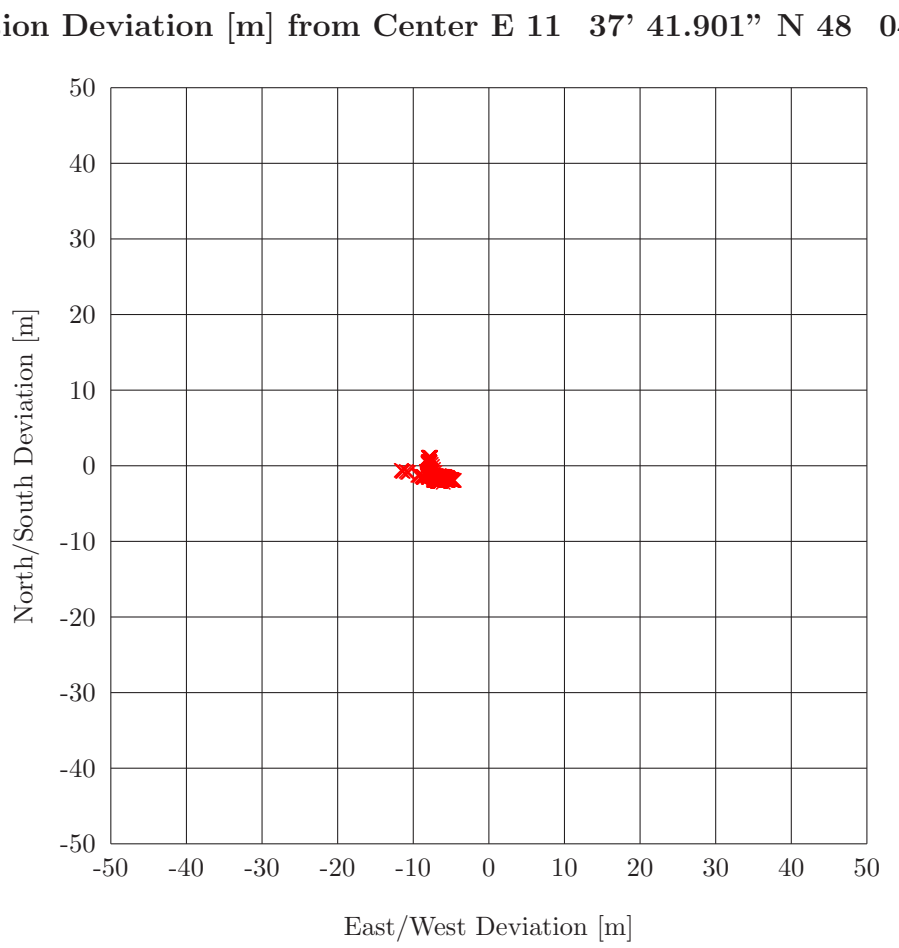

Figure 3.12: Single point positioning using GLONASS (example).

3.7 User Segment and Receiver Development

The user segment consists of the entirety of GLONASS receivers. These receive and evaluate the signals transmitted by the satellites. Evaluation of the signals comprises the computation of the user's position, velocity and acceleration. The necessary computational steps will be presented in one of the following chapters. Furthermore, the results of these computations are to be made available to the user. Additional tasks of the user equipment may include storage of data (raw data, computational results) for later use (e.g. post-mission analysis).

Strictly speaking, the user segment must be divided into military and civilian receivers, the latter being subdivided into navigational and geodetic receivers. However, since the GLONASS P-Code is publicly available and not scrambled, as it is the case with GPS, the division between military and civilian receivers is not as sharp as it is for GPS. In addition, outside the armed forces of the Russian Federation and some CIS countries, military use of GLONASS is negligible. This leaves the discrimination between navigational and geodetic receivers. For GPS, the latter classification comprises those receivers capable of measuring the carrier phase observables on both L_1 and L_2, thus enabling the user to compute a much more precise position, especially with differential methods. Navigational receivers originally only measured the code phase observable on L_1 C/A-Code. With advantages in microelectronics and growing accuracy demands also in navigation, GPS navigational receivers started also to measure the L_1 carrier phase observable, leaving only small hand-held receivers to measure only the code phase observable. Due to the fact that GLONASS receiver development outside Russia started relatively late, GLONASS receivers, at least those developed outside Russia, were able to measure the carrier phase observable from the beginning. So for GLONASS, navigational receivers can be classified as capable of measuring L_1 C/A-Code and carrier phase only, whereas geodetic receivers are capable of measuring both L_1 and L_2 code (C/A and P) and carrier phases. However, geodetic quality GLONASS receivers are not very frequent.

Until around 1993, receivers for GLONASS signals were almost exclusively made in Russia. The Russian Institute of Radionavigation and Time (RIRT) in St. Petersburg runs one of the two Russian time standards and is one of the principle designers of the GLONASS system. From the beginning, they provided key components such as the satellite clocks and the ground synchronization network. They were also responsible for the first GLONASS receivers. Another receiver manufacturer is the Institute of Space Device Engineering (ISDE) in Moscow.

Among the receivers developed in Russia were models "Reper" (*ISDE, 1991b*), a GLONASS receiver for geodetic and navigational use, "Gnom" (*ISDE, 1991a*), a six-channel L_1 GPS/GLONASS navigational receiver, "Skipper" (*Kayser-Threde, 1991b*) and ASN-16 (*Kayser-Threde, 1991a*). The two latter receivers were one-channel sequential C/A-Code GLONASS navigational receivers. "Skipper" was intended for marine navigation, whereas the ASN-16 was built for aviation purposes. In 1991, these receivers became the first Russian-built GLONASS receivers available world-wide, when RIRT started a joint venture with Munich-based aerospace company Kayser-Threde GmbH to distribute these receivers. Kayser-Threde also performed research work in comparisons of GPS and GLONASS receivers, together with the Institute of Astronomical and Physical Geodesy (IAPG, now Institute of Geodesy and Navigation, IfEN) of the University of the Federal Armed Forces Munich.

At the University of Leeds in England, however, an experimental device had been developed. With this receiver, Prof. Peter Daly conducted the first research works on GLONASS in the Western hemisphere (*Dale et al., 1988*; *Dale et al., 1989*; *Lennen, 1989*; *Riley, 1992*). The Leeds receiver eventually was developed into a full-scale 20 channel GPS/GLONASS receiver (*Riley and Daly, 1995*) and was chosen by the European Space Agency (ESA) as the basic design for developing a space-qualified GNSS receiver (*Riley et al., 1995*).

In 1991, Prof. Misra at the Massachusetts Institute of Technology (MIT) on behalf of the US Federal Aviation Administration (FAA) started tracking GLONASS satellites and analyzing measurements (*Misra et al., 1992*). For that purpose, he used two GLONASS receivers specially built by Magnavox. These

Figure 3.13: IfEN's 3S Navigation R-100/R-101 GPS/GLONASS receiver, mounted in a 19" rack.

were 8 channel L_1 C/A-code receivers (*Eastwood, 1990*). These two Magnavox prototypes never were succeeded by a production stage receiver.

In 1992, California-based company 3S Navigation produced the first combined GPS/GLONASS receiver, their R-100 (*Beser and Danaher, 1993*; *Balendra et al., 1994*). This receiver was available in different versions, depending on the number and capabilities of its hardware channels. The Institute of Geodesy and Navigation (Institut für Erdmessung und Navigation – IfEN) of the University of the Federal Armed Forces Munich in 1994 purchased a couple of these receivers in the version R-100/R-101. This receiver provides 20 hardware channels in total. 8 of these channels are able to track GLONASS signals on either L_1 C/A-Code, L_1 P-Code or L_2 P-Code; they are called the P-channels. The remaining twelve channels can be employed to receive GPS or GLONASS signals on L_1 C/A-Code; these are the so-called C/A-channels (*3S Navigation, 1994*). There are, however, some constraints regarding the distribution of satellites on these channels:

- When tracking merely GLONASS satellites, each of the twelve C/A-channels can track the signal of one GLONASS satellite.
- When tracking merely GPS satellites, the signals of seven satellites can be received.
- In combined operation, any combination of GLONASS and GPS satellites can be tracked that fulfills the equations $a + b \leq 12$ and $a + 2b \leq 15$, where a means the number of GLONASS satellites tracked and b means the number of GPS satellites tracked.

Therefore, at IfEN these receivers in most cases are utilized in that manner that signals of up to eight GLONASS satellites are tracked using the P-channels, whereas the C/A-channels are employed to track up to seven GPS satellites.

These devices represented the first generation of combined GPS/GLONASS receivers. They were relatively large and bulky (see Figure 3.13). The antenna fed the satellite signals to an external HF/IF

Figure 3.14: MAN / 3S Navigation GNSS-200 GPS/GLONASS receiver.

unit, which in turn fed the receiver. The receiver itself was realized as a number of plug-in boards for an IBM compatible industrial PC. In particular, there were two boards for the twelve C/A-channels and one board for each P-channel, ten boards in total. With one of their two receivers, IfEN replaced the standard CRT display by an LCD monitor to increase the mobility of the receiver to at least some extent.

Also in 1993, renowned GPS receiver manufacturer Trimble Navigation, Ltd. also started developing a combined GPS/GLONASS receiver. The Trimble 4000SGL was a 9 channel dual-frequency receiver that was able to track either GPS or GLONASS satellites, but not GPS and GLONASS at the same time (*CSIC, 1994*). It never reached the production stage.

Neither did a GLONASS receiver developed by Navstar Systems. This receiver was a GLONASS adaptation of the company's XR5 fast sequencing L_1 C/A-code GPS receiver (*Leisten et al., 1995*).

In 1995, 3S Navigation teamed up with MAN Technologie AG from Karlsfeld, Germany, to develop a miniaturized version of the R-100. This receiver, the GNSS-200, was merely the basic R-100 version (with only the twelve C/A-channels), fitted into a specially modified industrial computer, which provided just enough slots for the two C/A-channel plug-in boards and a graphics adapter. This mini computer did not feature a hard disk or comparable mass storage for the satellite measurements. So data had to be sent to a serial communications port and logged by an external device. The casing further provided connectors for a VGA display and a keyboard (*Heinrichs and Götz, 1996*; *3S Navigation, 1996a*). One year later, its successor, the GNSS-300, was introduced. It provided the same features as the GNSS-200, but was again shrunk (*3S Navigation, 1996b*).

In 1995, when GLONASS made rapid progress towards the completion of the space segment, other receiver manufacturers also started to trust in GLONASS and began developing combined GPS/GLONASS receivers.

In 1996, the Navigation and Flight Guidance Systems branch of (then) Daimler-Benz Aerospace (DASA-NFS) introduced a combined GPS/GLONASS receiver, which they had developed in a joint venture together with RIRT. This receiver, called ASN-22, provided 18 channels, 12 for tracking GPS satellites on L_1 C/A-Code and 6 for GLONASS satellites on L_1 C/A-Code. The receiver was designed as a single board OEM module, measuring 18.2 × 16.0 cm (later versions were reshaped to approximately 22 × 12 cm) (*DASA, 1996*; *Felhauer et al., 1997*). Due to NFS's attempts to have this receiver certified for aviation use from the beginning, market availability of this receiver was postponed time after time. In fact, it never reached its production stage.

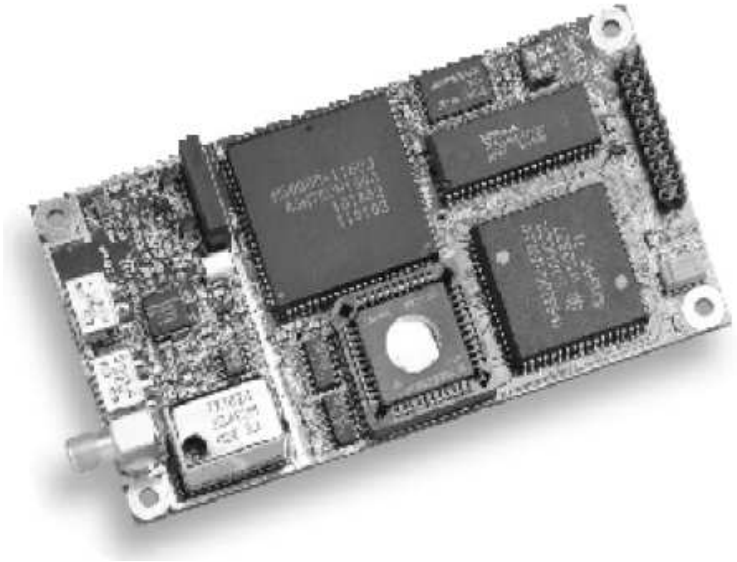

Figure 3.15: Ashtech GG24 GPS/GLONASS receiver OEM board (taken from (*Ashtech, 1998a*)).

At the same time, Ashtech Inc., too, came out with a combined GPS/GLONASS receiver. The GG24 receiver provides 24 channels, 12 of which can be used for tracking GPS satellites and 12 for GLONASS satellites. In contrast to the R-100/R-101, however, this receiver can only track L_1 C/A-Code. On the other hand, the receiver is much smaller than the older 3S receivers. The Ashtech GG24 is distributed as a single board OEM module in the size of a Euro plug-in board (16.7 × 10 cm) (*Gourevitch et al., 1996*; *Ashtech, 1996*).

Based on this OEM module, MAN Technologie AG introduced a family of navigational receivers, the NR Series, in late 1997. This family comprises the NR-N124 receiver for marine navigation and the NR-R124 reference station receiver. A surveying receiver, the NR-S124, is also foreseen by MAN. All these receivers feature the GG24 board plus a control and display unit (*Heinrichs et al., 1997*).

Spectra Precision AB of Danderyd, Sweden, also offers a combined GPS/GLONASS receiver, the GPS-GLONASS 3320, based on this OEM module (*Spectra Precision, 1998*).

In 1998, Ashtech – meanwhile Ashtech Division of the Magellan Corp. – introduced the Z-18 receiver, a combined GPS/GLONASS receiver capable of tracking L_1 and L_2 C/A- and P-Code of up to 18 satellites (*Ashtech, 1998b*). Like the GG24, this receiver is designed as a single board OEM module in the size of a Euro plug-in board. After having produced a limited number of these receivers for participants of the IGEX-98 campaign, Ashtech halted production to watch the market for these receivers.

Also in 1998, the newly founded company Javad Positioning Systems – directed by Mr. Javad Ashjaee, former founder and chairman of Ashtech, Inc. – introduced a series of GPS receivers, which are prepared for a GLONASS option. A total of forty channels provide dual-frequency measurements to GPS and GLONASS satellites. These receivers differ by the degree of integration with control unit and antenna and the type of the integrated antenna. The "Odyssey" features a detachable control unit and an integrated antenna, the "Regency" provides an integrated choke ring antenna, but no control unit, whereas the "Legacy" has neither an integrated antenna nor a control unit (*Javad, 1998*).

At the ION GPS-98 meeting in Nashville, NovAtel Inc. of Calgary, Canada, for the first time presented their MiLLenium–GLONASS card, a version of the well introduced MiLLenium GPS card capable of receiving both GPS and GLONASS L_1 signals. It is also designed as a Eurocard, 17.4 × 10 cm in size (*NovAtel, 1998a*; *NovAtel, 1998b*).

Of course this brief listing of GLONASS and combined GPS/GLONASS receivers does not claim to be complete.

Figure 3.16: Javad Positioning Systems GPS/GLONASS receivers, from left to right: Odyssey, Regency, Legacy (taken from (*Javad, 1998*)).

Figure 3.17: NovAtel MiLLenium–GLONASS GPS/GLONASS receiver OEM board (taken from (*NovAtel, 1998a*)).

The user segment also comprises Differential GLONASS (DGLONASS) and Differential GPS/GLONASS (DGPS/DGLONASS) systems. Research work on differential GLONASS systems in the Russian Federation started as early as the development of GLONASS itself, in the late seventies. However, since the accuracy of the GLONASS Standard Precision (SP) signal (a few ten meters due to the lack of S/A or similar degradation) was believed to be sufficient to meet the requirements of the common user, research and especially implementation went slowly (*CSIC, 1998*; *Ganin, 1995*). In the early nineties, with foreign DGPS networks already partially overlapping Russian territory and coastal waters and Western DGPS service providers pushing into the Russian market, implementation of DGLONASS systems was enforced. But due to the sheer size of the Russian territory, departmental specializations and the economic breakdown, DGLONASS coverage in Russia remains inconsistent and incomplete. Research work therefore is directed towards regional and wide area differential systems (RADS / WADS) rather than local area differential systems (LADS).

A conceived United Differential System (UDS) is to be built on a hierarchic structure, consisting of three levels of service and accuracy. First level will be a WADS to provide 5 - 10 m accuracy within an area of 1500 - 2000 km. Regional area differential systems providing 3 - 10 m accuracy within an area of 500 km will form the second level. In areas of particular interest, LADS will provide accuracies down to decimeter level over distances in the range of some tens of kilometers.

On international level, Russian scientists and officials in 1993 proposed to modify the well-established RTCM SC-104 standards for Differential GPS services to also include Differential GLONASS messages (*Zeglov et al., 1993*). These proposals were too late to be included in version 2.1 in the RTCM standards being under discussion at that time and published in January 1994 (*RTCM, 1994*). But DGLONASS messages finally were encompassed in version 2.2 of these standards, published as draft in 1996 (*RTCM, 1996*) and finalized in 1998 (*RTCM, 1998*).

3.8 GLONASS Performance

The accuracy of GLONASS navigation using the SP signal is specified to be 50 - 70 m (99.7 %) in the horizontal plane and 70 m (99.7 %) in height. Accuracy of estimated velocity vectors is 15 cm/s (99.7 %). Timing accuracy is 1 μs (99.7 %) (*ICD-GLONASS, 1995*; *CSIC, 1998*).

Extensive analysis of GLONASS performance is done by Dr. Pratap Misra of the MIT Lincoln Laboratory and his group. Among others, they are monitoring positioning accuracy and User Range Error (URE) to GLONASS satellites. The User Range Error is defined as the difference between the measured range to a satellite, corrected for receiver clock offset, and the geometric range to that satellite, based on satellite position from broadcast ephemerides and known user location. This encompasses errors in predicted ephemeris, instabilities in SV and system clocks, unmodeled ionospheric and tropospheric delays, multipath and receiver noise.

For satellites at elevation angles $> 7.5°$, the MIT group noticed near zero-mean UREs with a standard deviation of 8 - 10 m (*Misra et al., 1993*; *Misra et al., 1996b*) for GLONASS L_1 C/A-code measurements. The URE standard deviation for comparable GPS measurements was found to be about 7 m (S/A off). Taking into account that GLONASS does not employ an ionospheric correction model, GLONASS performance may well be called comparable to GPS in the absence of S/A. With S/A turned on, UREs for GPS show standard deviations around 25 - 40 m. For GLONASS P-code (*Riley and Daly, 1994*) found a URE standard deviation of 9.4 m for satellites at elevation angles $> 10°$, which is almost identical to that of the C/A-code. They explain this by most errors contributing to the URE, such as orbital errors, SV clock instabilites and atmospheric effects being common to the C/A-code and the P-code observations. Only multipath effects and receiver noise are different. Considering this, the URE depends on the observation site and the receiver type.

Besides the range error, positioning accuracy also depends on the satellite geometry, represented by the DOP values. For favorable satellite geometries ($HDOP < 2$), most of the horizontal positions measured by Dr. Misra appear to be within a circle of 30 m radius. For $HDOP < 4$, 95% of the horizontal position

estimates lie within a circle of 30 m radius (*Misra et al., 1993*). With a complete GLONASS constellation, 93% of the users are expected to have an $HDOP < 2$. Therefore it can be said that GLONASS should easily meet its specifications. For satellite geometries with an $HDOP < 5$, (*Riley and Daly, 1994*) found the horizontal positioning error using GLONASS P-code to be approximately 40 m (2drms).

On the other hand, (*Misra et al., 1993*) also revealed some glitches in system operations and upkeep. Due to the ground monitoring and upload stations being distributed over the territory of the former USSR only, satellite failures may go undetected for some hours, until that satellite again reaches the visibility area of the monitoring stations. Even more time will pass, until updated almanac data could be uploaded to all satellites.

The fact that GLONASS time is tightly coupled to UTC and thus introduces leap seconds whenever UTC introduces leap seconds also is a source of potential system anomalies. (*Misra et al., 1993*) reports User Range Errors with magnitudes of some hundred meters occurring between 0:00:00h and around 1:00:00h on July 1, 1992, when a leap second was introduced. Later introductions of leap seconds on June 30, 1993, and December 31, 1995, caused GLONASS to trip for about three minutes each (*Misra et al., 1996b*). According to the ICD (*ICD-GLONASS, 1995*), the two-second lines of the GLONASS navigation message are to begin at an even number of seconds within the day in the satellite time frame. By introducing a leap second, the number of seconds within a day suddenly becomes uneven, with two succeeding even second epochs. Half-way through the first line of the first frame of a superframe, this line has to be aborted and restarted. Obviously this process, along with the re-adjustment of the satellite clocks, causes problems to the data generation on-board the satellites.

When introducing a leap second in the night of June 30 to July 1, 1997, the whole GLONASS system went down for one day. However, as will be explained later, on that occasion not only a leap second was introduced, but also the GLONASS time frame was corrected to be closer to UTC. The system being down that day was announced eleven days in advance (*CSIC, 1997*). But shutting down the system for an entire day or only for a few minutes is not suitable to support the possible use of GLONASS as a sole means of navigation.

4 Time Systems

GPS and GLONASS both use their own time scales, which, in addition, are connected to different realizations of UTC. Therefore, GPS time and GLONASS time cannot easily be transformed from one time scale into the other.

In combined GPS/GLONASS data processing the differences between these time scales must be accounted for. Otherwise, systematic errors are introduced that will affect the combined positioning solution.

4.1 GLONASS Time

GLONASS system time is maintained by the GLONASS Central Synchronizer by means of a set of hydrogen masers (*Gouzhva et al., 1995*). It is closely coupled to UTC, but with a constant offset of three hours (corresponding to the offset of Moscow time to Greenwich time). Therefore, GLONASS system time also considers leap seconds. Further differences between GLONASS time and UTC arise from the keeping of the time scales by two different master clocks. These differences are in the order of microseconds. In October / November 1996, for example, this difference was around $(t_{UTC} - t_{GLONASS}) \bmod 1\text{ h} = -25\ \mu\text{s}$ (*RNTFS, 1996a*).

The GLONASS user is informed about the difference to UTC as maintained by the National Etalon of Time and Frequency in Moscow (UTC_{SU}). This information is obtained from the UTC parameter τ_c in frame 5 of the GLONASS ephemerides message (*ICD-GLONASS, 1995*).

UTC then can be computed from GLONASS time according to the simple relation

$$t_{UTC} = t_{GLONASS} + \tau_c - 3\text{ h} \tag{4.1.1}$$

The accuracy of this computed t_{UTC} is specified to be less than 1 μs (*ICD-GLONASS, 1995*).

On-board the GLONASS satellites, Cesium frequency standards are used. These clocks are specified to have a frequency instability of less than 5×10^{-13} (the satellites launched in 1995 have cesium clocks with frequency instabilities less than 1×10^{-13}) (*Gouzhva et al., 1995*). With time and frequency uploads to the satellite twice a day, this stability provides an accuracy of satellite time synchronization to system time of about 15 ns (1 σ). Accuracy of the uploaded corrections is specified to be less than 35 ns (1 σ).

4.2 GPS Time

GPS system time is maintained by the GPS Master Control Station. It was started on January 6, 1980. Since it is a uniform time scale, it differs from UTC by the leap seconds introduced into the latter time scale. Currently (February 2000) this difference is 13 seconds. In addition to the leap seconds, further differences between GPS system time and UTC arise from the fact that GPS system time and UTC are kept by different master clocks. These additional differences are in the order of nanoseconds. In fact, GPS operators usually keep GPS system time to within 100 ns of UTC as maintained by the US Naval Observatory (UTC_{USNO}). In December 1994, however, due to a malfunction, GPS system time made an excursion of about 270 ns from UTC for a period of about two weeks (*Lewandowski et al., 1997*) .

The GPS user is informed about the difference to UTC_{USNO}. This information is obtained from the UTC parameters in page 18 of subframe 4 of the GPS ephemerides message. This set of parameters consists of the following values (*ICD-GPS, 1991*):

WN_t	Reference time of UTC parameters (week number)
t_{ot}	Reference time of UTC parameters (s into week)
Δt_{LS}	Number of leap seconds
$A_0,\ A_1$	Polynomial coefficients
WN_{LSF}	Time of next scheduled change of leap seconds (week number)
DN	Number of day in WN_{LSF}, at the end of which leap seconds will change
Δt_{LSF}	Future value of leap seconds

For the computation of UTC from GPS time, three cases must be distinguished:

1. The time given by WN_{LSF} and DN is not in the past and the present time is not in the interval $[DN + 3/4, DN + 5/4]$.

   In this case UTC computes to:

   $$t_{UTC} = (t_{GPS} - \Delta t_{UTC}) \bmod 86400 \tag{4.2.1}$$

   with

   $$\Delta t_{UTC} = \Delta t_{LS} + A_0 + A_1 \left(t_{GPS} - t_{ot} + (WN - WN_t) \cdot 604800\right) \tag{4.2.2}$$

2. The present time is in the interval $[DN + 3/4, DN + 5/4]$.

   In this case UTC computes to:

   $$t_{UTC} = W \bmod (86400 + \Delta t_{LSF} - \Delta t_{LS}) \tag{4.2.3}$$

   with

   $$W = (t_{GPS} - \Delta t_{UTC} - 43200) \bmod 86400 + 43200 \tag{4.2.4}$$

   and Δt_{UTC} as given in Eq. (4.2.2).

3. The time given by WN_{LSF} and DN is in the past.

   In this case UTC is computed analogously to case 1, but Δt_{LSF} has to be substituted for Δt_{LS} in Eq. (4.2.2).

In these equations, t_{GPS} is always given in seconds into the week, whereas t_{UTC} is given in seconds into day. Therefore the modulo operations are performed. The accuracy of this computed t_{UTC} is specified to be less than 90 ns (1 σ) (*ICD-GPS, 1991*).

4.3 UTC, UTC_{USNO}, UTC_{SU} and GLONASS System Time

UTC is obtained from a combination of data from about 230 atomic clocks in 60 laboratories world-wide (*BIPM, 1995*). 47 timing centers are maintaining a local UTC. UTC_{USNO} and UTC_{SU} are two of these local UTCs. UTC_{USNO} is kept by an ensemble of cesium standards and hydrogen masers. Its difference to UTC is in the order of some ns. It generally remains within 20 ns. UTC_{SU} is kept by an ensemble of hydrogen masers and is regarded as one of the most stable atomic time scales in the world (*Lewandowski et al., 1996*). Its difference to UTC is in the order of some μs. Hence the difference between UTC_{USNO} and UTC_{SU} also is in the order of some μs. In October / November 1996, for example, this difference was around $UTC_{\text{SU}} - UTC = 7.95$ μs (*RNTFS, 1996a*). The difference $UTC_{\text{SU}} - t_{GPS}$ was around 8 μs.

Following Recommendation S4 (1996) of the Comité Consultatif pour la Définition de la Seconde (CCDS), which recommends that the reference times of satellite navigation systems with global coverage be synchronized as closely as possible to UTC (*CCDS, 1996*), on November 27, 1996, 0h 0m 0s UT, UTC_{SU} was corrected by 9 μs, yielding the difference $UTC_{\text{SU } old} - UTC_{\text{SU } new} = 9$ μs (*MMC, 1996*). Thus, after November 27, 1996 the difference $UTC_{\text{SU}} - UTC$ was around -1 μs, the difference $UTC_{\text{SU}} - t_{GPS}$ was around -0.9 μs. The difference between UTC_{SU} and GLONASS system time became $(t_{UTC} - t_{GLONASS}) \bmod 1\text{ h} = -35$ μs (*RNTFS, 1996b*).

After this change, UTC_{SU} slowly drifted towards UTC, and in May 1997 the offsets $UTC_{\text{SU}} - UTC$ and $UTC_{\text{SU}} - t_{GPS}$ both were approximately -0.7 μs (*RNTFS, 1997*).

In a next step to comply with CCDS Recommendation S4 (1996), on January 10, 1997, the frequency of the GLONASS Central Synchronizer clocks was slightly changed, bringing it closer to that

of $\mathrm{UTC_{SU}}$ and thus stabilizing the difference between GLONASS system time and UTC at around $(t_{UTC} - t_{GLONASS})$ mod 1 h $= -35.9$ μs. Subsequently, at midnight of July 1, 1997, GLONASS system time received a time step of approximately 35.3 μs (*Langley, 1997*). This moved both $\mathrm{UTC_{SU}}$ and GLONASS system time to within a few hundred nanoseconds of UTC (*Lewandowski and Azoubib, 1998*). Date and time for this operation were set to coincide with a leap second step in UTC. Further adjustments of these two time scales ($\mathrm{UTC_{SU}}$ and GLONASS system time) are expected.

Since the data from the local timing centers are not compared and combined to UTC in real-time, the difference between $\mathrm{UTC_{USNO}}$ and $\mathrm{UTC_{SU}}$ and therefore the difference between GPS and GLONASS system time neither is directly (a-priori) available in real-time. This is the crucial problem to be solved when combining GPS and GLONASS data in navigation or in other near real-time operation.

4.4 Resolving the Time Reference Difference

To determine this difference in the time reference systems, a number of procedures are possible. A selection of these procedures will be described and discussed in the following.

4.4.1 Introducing a Second Receiver Clock Offset

In this method, different receiver clock offsets are introduced with respect to GPS and GLONASS system time. These two clock offsets are instantaneously determined at each observation epoch together with the three unknowns of the receiver position.

Starting with a simplified non-linear observation equation (for the complete observation equations see Chapter 8) for a pseudorange observation to a satellite S of an arbitrary system (GPS or GLONASS) at an observer R,

$$PR_R^S = \varrho_R^S + c \cdot \delta t_R - c \cdot \delta t^S \tag{4.4.1}$$

and by introducing a Taylor series expansion around an approximate position P_0, we obtain the linearized equation

$$PR_R^S = \varrho_0^S + \frac{x_0 - x^S}{\varrho_0^S} \cdot (x_R - x_0) + \frac{y_0 - y^S}{\varrho_0^S} \cdot (y_R - y_0) + \frac{z_0 - z^S}{\varrho_0^S} \cdot (z_R - z_0) + c \cdot \delta t_R - c \cdot \delta t^S \tag{4.4.2}$$

with x_0, y_0, z_0 being the coordinates of the approximate position and

$$\varrho_0^S = \sqrt{(x_0 - x^S)^2 + (y_0 - y^S)^2 + (z_0 - z^S)^2}$$

being the geometric distance between the approximate position and the satellite position.

With the receiver clock error $\delta t_R = t_R - t_{Sys}$ (t_{Sys} being the GPS or GLONASS system time t_{GPS} or $t_{GLONASS}$, respectively) as one of the unknowns being a function of the system time t_{Sys}, it becomes clear that in mixed GPS/GLONASS processing two receiver clock errors will have to be introduced, one for the receiver clock offset with respect to GPS time and one for the receiver clock offset with respect to GLONASS time. We then obtain two different observation equations for a GPS satellite i and a GLONASS satellite j:

$$\begin{aligned} PR_R^{GPS\,i} &= \varrho_0^{GPS\,i} + \frac{x_0 - x^{GPS\,i}}{\varrho_0^{GPS\,i}} \cdot (x_R - x_0) + \frac{y_0 - y^{GPS\,i}}{\varrho_0^{GPS\,i}} \cdot (y_R - y_0) + \\ &\quad \frac{z_0 - z^{GPS\,i}}{\varrho_0^{GPS\,i}} \cdot (z_R - z_0) + c \cdot \delta t_{R,GPS} - c \cdot \delta t^{GPS\,i} \end{aligned} \tag{4.4.3}$$

$$\begin{aligned} PR_R^{GLO\,j} &= \varrho_0^{GLO\,j} + \frac{x_0 - x^{GLO\,j}}{\varrho_0^{GLO\,j}} \cdot (x_R - x_0) + \frac{y_0 - y^{GLO\,j}}{\varrho_0^{GLO\,j}} \cdot (y_R - y_0) + \\ &\quad \frac{z_0 - z^{GLO\,j}}{\varrho_0^{GLO\,j}} \cdot (z_R - z_0) + c \cdot \delta t_{R,GLONASS} - c \cdot \delta t^{GLO\,j} \end{aligned} \tag{4.4.4}$$

Due to the additional unknown, an additional (fifth) observation is necessary to obtain a positioning solution. Since the combined use of GPS and GLONASS approximately doubles the number of observations with respect to GLONASS or GPS alone (at least for the full GLONASS constellation), this sacrificing of one observation can easily be accepted. Generally, as long as at least two satellites of one system (GPS or GLONASS) are added to observations of the other system, this sacrificing of one measurement is acceptable.

Having a sufficient number of observations to both GPS and GLONASS satellites, the set of observation equations can be written in matrix notation:

$$\vec{l} = \mathbf{A} \cdot \vec{x} \tag{4.4.5}$$

with

$$\vec{l} = \begin{pmatrix} PR_R^i - \varrho_0^i + c \cdot \delta t^i \\ PR_R^j - \varrho_0^j + c \cdot \delta t^j \\ PR_R^k - \varrho_0^k + c \cdot \delta t^k \\ \vdots \end{pmatrix} \tag{4.4.6}$$

the vector of the known values,

$$\mathbf{A} = \begin{pmatrix} \frac{x_0 - x^i}{\varrho_0^i} & \frac{y_0 - y^i}{\varrho_0^i} & \frac{z_0 - z^i}{\varrho_0^i} & 1 & 0 \\ \frac{x_0 - x^j}{\varrho_0^j} & \frac{y_0 - y^j}{\varrho_0^j} & \frac{z_0 - z^j}{\varrho_0^j} & 0 & 1 \\ \frac{x_0 - x^k}{\varrho_0^k} & \frac{y_0 - y^k}{\varrho_0^k} & \frac{z_0 - z^k}{\varrho_0^k} & 1 & 0 \\ \vdots & \vdots & \vdots & \vdots & \vdots \end{pmatrix} \tag{4.4.7}$$

the design matrix (k being a GPS satellite), and

$$\vec{x} = \begin{pmatrix} (x_R - x_0) \\ (y_R - y_0) \\ (z_R - z_0) \\ c \cdot \delta t_{R,GPS} \\ c \cdot \delta t_{R,GLONASS} \end{pmatrix} = \begin{pmatrix} (x_R - x_0) \\ (y_R - y_0) \\ (z_R - z_0) \\ c \cdot (t_R - t_{GPS}) \\ c \cdot (t_R - t_{GLONASS}) \end{pmatrix} \tag{4.4.8}$$

the vector of the unknowns.

This system of equations can then be solved using the conventional methods, e.g. a least squares adjustment or Kalman filtering.

It should be noted that a solution of these equations is only possible, if indeed there are observations to satellites of both GPS and GLONASS. For observations to GPS or GLONASS satellites only, however, only one receiver clock offset is required. Furthermore, if all but one observed satellites are from one system, with only one satellite from the second system, this additional observation contributes only to the second receiver clock offset, but does not influence the computed position.

4.4.2 Introducing the Difference in System Time Scales

Starting with the pair of Eqs. (4.4.3) and (4.4.4), we can rewrite the receiver clock offset to GLONASS system time:

$$\delta t_{R,GLONASS} = t_R - t_{GLONASS} = t_R - t_{GPS} + t_{GPS} - t_{GLONASS} \tag{4.4.9}$$

Eq. (4.4.4) then transforms to

$$\begin{aligned} PR_R^{GLO\,j} \;=\; & \varrho_0^{GLO\,j} + \frac{x_0 - x^{GLO\,j}}{\varrho_0^{GLO\,j}} \cdot (x_R - x_0) + \frac{y_0 - y^{GLO\,j}}{\varrho_0^{GLO\,j}} \cdot (y_R - y_0) + \\ & \frac{z_0 - z^{GLO\,j}}{\varrho_0^{GLO\,j}} \cdot (z_R - z_0) + c \cdot \delta t_{R,GPS} + c \cdot (t_{GPS} - t_{GLONASS}) - c \cdot \delta t^{GLO\,j} \end{aligned} \tag{4.4.10}$$

Together with Eq. (4.4.3) we can now set up a new system of observation equations in matrix notation, identical to Eq. (4.4.5), but with modified design matrix and vector of unknowns:

$$\mathbf{A} = \begin{pmatrix} \frac{x_0 - x^i}{\varrho_0^i} & \frac{y_0 - y^i}{\varrho_0^i} & \frac{z_0 - z^i}{\varrho_0^i} & 1 & 0 \\ \frac{x_0 - x^j}{\varrho_0^j} & \frac{y_0 - y^j}{\varrho_0^j} & \frac{z_0 - z^j}{\varrho_0^j} & 1 & 1 \\ \frac{x_0 - x^k}{\varrho_0^k} & \frac{y_0 - y^k}{\varrho_0^k} & \frac{z_0 - z^k}{\varrho_0^k} & 1 & 0 \\ \vdots & \vdots & \vdots & \vdots & \vdots \end{pmatrix} \tag{4.4.11}$$

$$\vec{x} = \begin{pmatrix} (x_R - x_0) \\ (y_R - y_0) \\ (z_R - z_0) \\ c \cdot (t_R - t_{GPS}) \\ c \cdot (t_{GPS} - t_{GLONASS}) \end{pmatrix} \tag{4.4.12}$$

This method principally is equivalent to the one described in Section 4.4.1 (Eqs. (4.4.6) - (4.4.8)), but it is more elegant. The additional unknown $(t_{GPS} - t_{GLONASS})$ as the difference in system time scales is now independent of the receiver. Thus, when forming differences of the same kind between two receivers (receiver-receiver single differences), this unknown cancels out.

Similar to the case of two separate receiver clock offsets, a solution of these equations is only possible, if indeed there are observations to satellites of both GPS and GLONASS. For observations to GPS or GLONASS satellites only, however, only the receiver clock offset is required. Furthermore, if all but one observed satellites are from one system, with only one satellite from the second system, this additional observation contributes only to the difference in system time frames, but does not influence the computed position.

4.4.3 Application of A-priori Known Time Offsets

In this method, the difference in system time between GPS and GLONASS (or the difference between $\mathrm{UTC_{USNO}}$ and $\mathrm{UTC_{SU}}$, respectively) is considered to be known a-priori from some external knowledge. This is a very effective method in the sense of one unknown being eliminated.

Having a-priori knowledge of the difference between GPS and GLONASS time $(t_{GPS} - t_{GLONASS})$, the respective term in Eq. (4.4.10) is shifted to the left-hand side of the equation, when writing the matrix notation according to Eq. (4.4.5). The result is a system of observation equations with modified vectors and design matrix:

$$\vec{l} = \mathbf{A} \cdot \vec{x} \tag{4.4.13}$$

with

$$\vec{l} = \begin{pmatrix} PR_R^i - \varrho_0^i + c \cdot \delta t^i \\ PR_R^j - \varrho_0^j + c \cdot \delta t^j - c \cdot (t_{GPS} - t_{GLONASS}) \\ PR_R^k - \varrho_0^k + c \cdot \delta t^k \\ \vdots \end{pmatrix} \tag{4.4.14}$$

$$\mathbf{A} = \begin{pmatrix} \frac{x_0 - x^i}{\varrho_0^i} & \frac{y_0 - y^i}{\varrho_0^i} & \frac{z_0 - z^i}{\varrho_0^i} & 1 \\ \frac{x_0 - x^j}{\varrho_0^j} & \frac{y_0 - y^j}{\varrho_0^j} & \frac{z_0 - z^j}{\varrho_0^j} & 1 \\ \frac{x_0 - x^k}{\varrho_0^k} & \frac{y_0 - y^k}{\varrho_0^k} & \frac{z_0 - z^k}{\varrho_0^k} & 1 \\ \vdots & \vdots & \vdots & \vdots \end{pmatrix} \tag{4.4.15}$$

$$\vec{x} = \begin{pmatrix} (x_R - x_0) \\ (y_R - y_0) \\ (z_R - z_0) \\ c \cdot \delta t_{R,GPS} \end{pmatrix} = \begin{pmatrix} (x_R - x_0) \\ (y_R - y_0) \\ (z_R - z_0) \\ c \cdot (t_R - t_{GPS}) \end{pmatrix} \tag{4.4.16}$$

As stated above, however, the exact difference between $\mathrm{UTC_{USNO}}$ and $\mathrm{UTC_{SU}}$ and therefore the difference between GPS and GLONASS system times definitely is not available in real-time as external knowledge. Thus, this method is only applicable in a post-mission analysis software for geodetic applications, but not in real-time GPS/GLONASS navigation or other (near) real-time applications. In the latter case, a time series of these differences could be used to extrapolate the instantaneous time difference, with all the uncertainties that come along with extrapolations.

4.4.4 Dissemination of Difference in Time Reference

The Russian Military Space Forces as the operator of the GLONASS system are planning to include the time difference between GLONASS system time and GPS system time in the navigation message of the next generation of GLONASS satellites, the so-called GLONASS-M spacecraft (*Ivanov et al., 1995*; *Kazantsev, 1995*). In principle, this will be equivalent to the use of a-priori known time offsets, as described in Section 4.4.3, but it will drop the need for determining this time offset during processing. The problem of possible loss of accuracy in the extrapolated time offsets, however, will remain. It will only shift from the user to the GLONASS Control Center. But given their experience in monitoring the GLONASS system clock and forecasting clock offsets, the broadcast time difference between GLONASS time and GPS time can be expected to be sufficiently accurate.

As stated above, the dissemination of this time difference in the broadcast navigation message is planned for the GLONASS-M satellites. According to the latest version of the GLONASS ICD (*ICD-GLONASS, 1998*), GLONASS-M satellites will broadcast a τ_{GPS} data word. This will specify the fractional part (as expressed in seconds) of the difference between GPS and GLONASS system time scales. The difference between these two time scales can then be obtained as

$$t_{GPS} - t_{GLONASS} = \Delta t_{LS} + \tau_{GPS} \tag{4.4.17}$$

with Δt_{LS} being the number of leap seconds between GPS time and UTC. This value is broadcast in the GPS navigation message.

The first launch of a GLONASS-M satellite originally was scheduled for 1996, but was delayed due to the economic problems in Russia. Up to now (February 2000), not a single GLONASS-M satellite has in fact been launched. And it seems uncertain, if the GLONASS-M program will ever be realized at all. Thus, for the time being one of the methods described in the previous sections will have to be applied.

4.5 Conclusions

A number of possible methods to resolve the difference in reference time between GPS and GLONASS have been described in the previous sections. For a decision, which of them is best to be implemented in combined GPS/GLONASS data processing, two cases must be considered:

- **There is no GLONASS-M satellite among the tracked satellites.**

  In this case, the time difference between GPS time and GLONASS system time is not known at processing time. Therefore, a measure of the difference in reference time must be determined as an additional unknown during processing. The most promising way to do so is to estimate the time difference between GPS time and GLONASS time itself rather than introducing a separate receiver clock error with respect to GLONASS time. Thus, the five unknowns to be solved for are the three coordinates of the receiver position, the receiver clock offset to GPS system time plus the time difference between GPS time and GLONASS time. The implementation of this method was described in Section 4.4.2.

- **There is at least one GLONASS-M satellite among the tracked satellites.**

  In this case, the time difference between GPS time and GLONASS system time is disseminated as part of the satellite navigation message and can be considered to be known. This reduces the number of unknowns to be determined during processing to four, namely the three coordinates of the receiver position plus the receiver clock offset to GPS or GLONASS system time. These are the same unknowns that are already solved for in GPS or GLONASS only processing. The implementation of this method was described in Section 4.4.4.

  However, as long as no GLONASS-M satellites have been launched, considering this case is merely of academic interest.

Even in the latter case, an additional determination of the difference between GPS time and GLONASS time still could be performed, e.g. for purposes of integrity monitoring in safety-critical applications (air navigation) or for enhancing the accuracy of the broadcast value of this difference in high precision applications.

5 Coordinate Systems

5.1 PZ-90 (GLONASS)

GLONASS originally used a coordinate system called SGS-85 to express the coordinates of its satellites and thus the coordinates of a receiver that used these satellites for a position fix. The abbreviation SGS-85 stood for **S**oviet **G**eodetic **S**ystem 19**85**. In 1994, the GLONASS coordinate reference system changed to SGS-90, the definition of which was equal to that of SGS-85, but the realization was slightly different. After the collapse of the Soviet Union, SGS for a short time was said to be **S**pecial **G**eodetic **S**ystem. Later the name was changed to Parametry Zemli 1990 Goda (Параметры Земли 1990 Года – Parameters of the Earth Year 1990), abbreviated PZ-90 (ПЗ-90) or PE-90 (from the Russian and the English name, respectively).

The definition of these coordinate frames as used by GLONASS is defined as follows (*ICD-GLONASS, 1995*):

- Origin is Earth's center of mass.
- The z-axis is parallel to the direction of the mean North pole according to the mean epoch 1900 - 1905 as defined by the International Astronomical Union and the International Association of Geodesy.
- The x-axis is parallel to the direction of the Earth's equator for the epoch 1900 - 1905, with the XOZ plane being parallel to the average Greenwich meridian, defining the position of the origin of the adopted longitude system.
- The y-axis completes the geocentric rectangular coordinate system as a right-handed system.

Besides this, (*ICD-GLONASS, 1995*) and (*CSIC, 1998*) also define the parameters of the associated terrestrial ellipsoid and other geodetic constants:

Semi-major axis	$6.378136 \cdot 10^6$ m
Flattening	1/298.257839303
Gravitational constant	$3.9860044 \cdot 10^{14}$ m^3/s^2
Earth's rotation rate	$7.292115 \cdot 10^{-5}$ rad/s
2^{nd} zonal coefficient	$-1.08263 \cdot 10^{-3}$

5.2 WGS84 (GPS)

Likewise, GPS originally employed a coordinate frame known as World Geodetic System 1972 (WGS72), which it inherited from its predecessor, the US Navy TRANSIT system. Later the reference frame changed to the World Geodetic System 1984 (WGS84). Again, this system does not differ in its definition, but in a more refined realization.

These reference frames as used by GPS are defined as follows (*ICD-GPS, 1991*):

- Origin is Earth's center of mass.
- z-axis is parallel to the direction of the Conventional International Origin (CIO) for polar motion, as defined by the Bureau International de l'Heure (BIH) on the basis of the latitudes adopted for the BIH stations.
- x-axis is the intersection of the WGS84 reference meridian plane and the plane of the mean astronomic equator, the reference meridian being parallel to the zero meridian defined by the BIH on the basis of the longitudes adopted for the BIH stations.
- y-axis completes a right-handed Earth-centered, Earth-fixed orthogonal system.

Besides this, (*NIMA, 1997*) and (*ICD-GPS, 1991*) name four defining parameters of the associated terrestrial ellipsoid and one value derived from them:

Semi-major axis	$6.378137 \cdot 10^6$ m
Flattening	1/298.257223563
Gravitational constant	$3.986004418 \cdot 10^{14}$ m^3/s^2
Earth's rotation rate	$7.292115 \cdot 10^{-5}$ rad/s
Normalized 2^{nd} zonal coefficient	$-0.484166774985 \cdot 10^{-3}$

Before the fall of 1994, WGS84 was defined with a gravitational constant of $3.986005 \cdot 10^{14}$ m^3/s^2. This value is also used by the GPS control center for purposes of orbit propagation. In orbit determination, a GPS receiver should apply the same value as the control center does to avoid errors. So to avoid costly software changes in all GPS receivers, the GPS operators decided to retain this value for the gravitational constant for purposes of orbit propagation.

So-called *secondary parameters* are the coefficients of an Earth gravity field model (EGM) of degree and order $n = m = 180$.

5.3 Realizations

The WGS84 coordinate frame is realized by means of a consistent set of stations with defined coordinates. These stations originally were surveyed by means of Doppler observations to US Navy TRANSIT satellites. Coordinates of these stations later were refined gradually. The accuracy (one sigma) of WGS84 coordinates directly determined in WGS84 by GPS satellite point positioning, their respective precise ephemerides and ground-based satellite tracking acquired in static mode, in terms of geodetic latitude φ, geodetic longitude λ, and geodetic height h are:

Horizontal $s_\varphi = s_\lambda = \pm 1$ m $(1\ \sigma)$
Vertical $s_h = \pm 1 \ldots 2$ m $(1\ \sigma)$

These errors do not incorporate the observational errors, but the errors associated with placing the origin of the WGS84 coordinate system at the Earth's center of mass and determining the correct scale. These absolute values should not be confused with the centimeter precision of GPS differential positioning. In fact, WGS84 is very close to the International Terrestrial Reference Frame (ITRF) (*Abusali et al., 1995*). The WGS84 coordinates of a point are within decimeter range from the point position in ITRF.

It should, however, be noted that WGS84 cannot be realized by GPS (single point positioning) itself with meter accuracy. Differential positioning rather uses as absolute stations those ones with precise ITRF coordinates and interpolates within this frame with WGS84 derived baseline vectors. Thus, the resulting coordinates are theoretically in a mixed ITRF/WGS84 coordinate system. For the sake of simplicity, it is commonly only described as WGS84 system.

In a similar way, the PZ-90 reference frame is also realized by a set of stations with defined coordinates. Its internal accuracy also is in the range of 1 - 2 meters. The set of stations used to define PZ-90 differs from that used for the realization of WGS84. Thus, although the definitions of WGS84 and PZ-90 sound similar, due to the different realizations, there may very likely be differences in origin, orientation and scale. The WGS84 coordinates of an arbitrary point therefore generally are not identical to its coordinates in PZ-90.

5.4 Combining Coordinate Frames

In GLONASS only solutions, satellite positions in PZ-90 are obtained from the ephemeris data, thus the user position is in PZ-90. In GPS only positioning solutions, the satellite positions are given in WGS84 and thus the user position is in WGS84. But due to the differences in reference frame realizations, in a combined positioning solution, with some of the satellite coordinates in WGS84 and some of them in PZ-90, the coordinate frame of the calculated user position is undefined. This holds true at least for

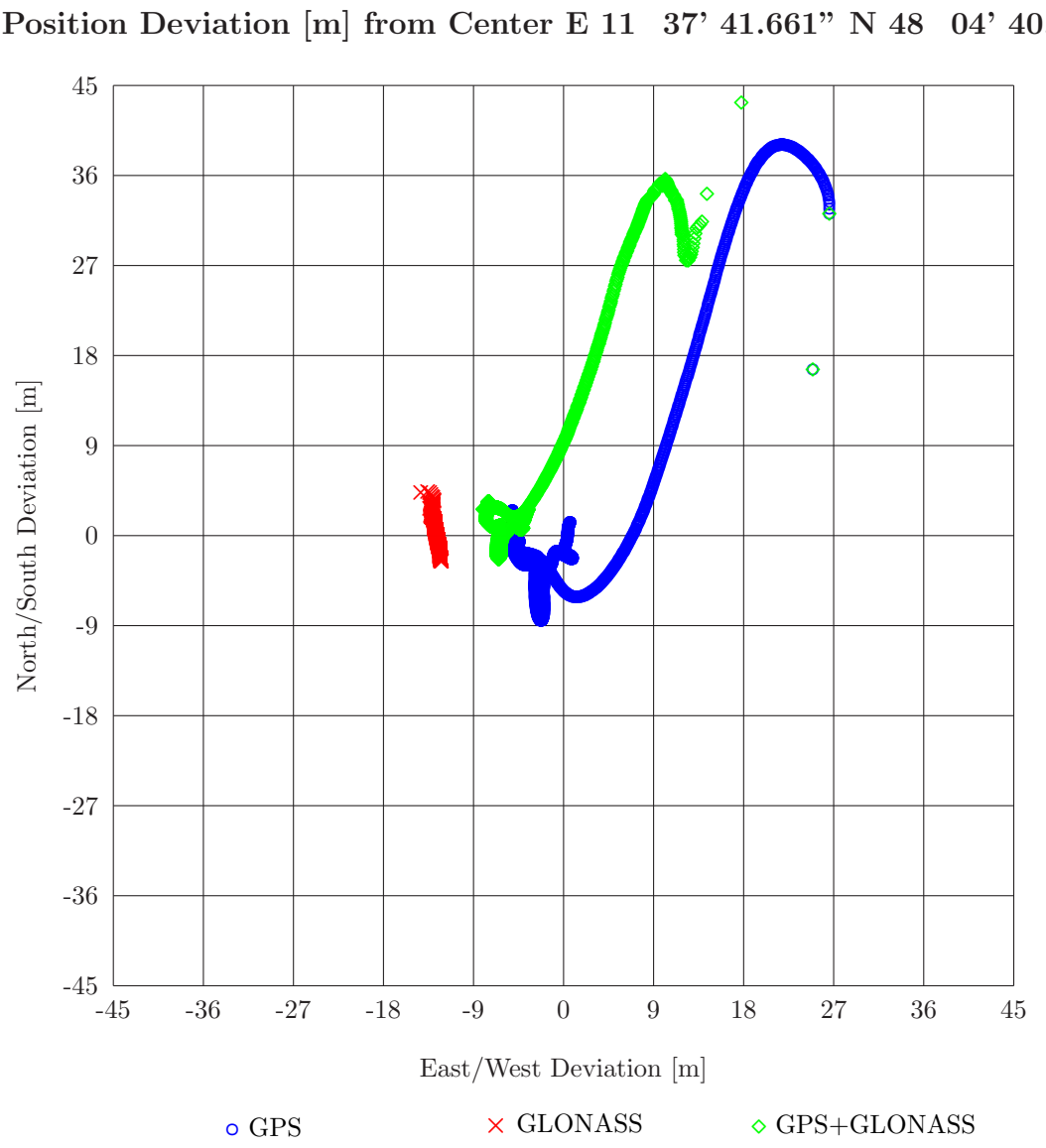

Figure 5.1: Example of combined GPS/GLONASS positioning without coordinate transformation.

single point positioning. The influence of the different coordinate frames on the results of differential processing will be investigated later.

Figure 5.1 shows an example of such processing. GPS and GLONASS range measurements of one receiver were processed in single point mode without regard of different coordinate frames. Receiver position was determined in a Kalman-filtered epoch-by-epoch solution of carrier smoothed pseudoranges. Time span of the data was approximately one hour at a data interval of 1 s. For both GPS and GPS/GLONASS solutions there are about 3600 epoch solutions, and nearly 2300 epoch solutions for GLONASS only, due to limited satellite availability. On display are the deviations in the local plane of the computed coordinates with respect to the last computed GPS only receiver position. It can be clearly seen that the centers of the GPS, GLONASS and combined GPS/GLONASS position distributions, where the Kalman filter eventually converges, differ by more than 10 meters. They are aligned roughly along a line from East (GPS) to West (GLONASS).

Therefore, in order to get meaningful results when combining GPS and GLONASS measurements, those coordinate differences must be accounted for. A straight-forward way to accomplish this is to transform the obtained satellite coordinates at the time of signal transmission from one coordinate frame to another, before forming the design matrix and calculating the user position.

Since GPS navigation has become the standard in Western countries and WGS84 therefore is more widely spread and better known than PZ-90, it is considered best to transform GLONASS satellite positions from PZ-90 to WGS84, thus obtaining the user position also in WGS84.

5.5 7-Parameter Coordinate Transformation

Given the three-dimensional coordinates of a point P in a Cartesian coordinate frame (u, v, w), the coordinates of this point in a different, but nearly parallel coordinate frame (x, y, z) can be computed using the relation (*Soler and Hothem, 1988*):

$$\begin{pmatrix} x \\ y \\ z \end{pmatrix}_P = \begin{pmatrix} \Delta x \\ \Delta y \\ \Delta z \end{pmatrix} + (1 + \delta s) \cdot \begin{pmatrix} 1 & \delta\omega & -\delta\psi \\ -\delta\omega & 1 & \delta\varepsilon \\ \delta\psi & -\delta\varepsilon & 1 \end{pmatrix} \cdot \begin{pmatrix} u \\ v \\ w \end{pmatrix}_P \tag{5.5.1}$$

with

$\Delta x,\ \Delta y,\ \Delta z$	coordinates of the origin of frame (u, v, w) in frame (x, y, z)
$\delta\varepsilon,\ \delta\psi,\ \delta\omega$	differential rotations around the axes (u, v, w), respectively, to establish parallelism with frame (x, y, z)
δs	differential scale change

This transformation is also known as the 7 Parameter Helmert Transformation.

Considering PZ-90 to be the (u, v, w) frame in Eq. (5.5.1) and WGS84 to be the (x, y, z) frame, PZ-90 coordinates of a GLONASS satellite can be transformed to WGS84 coordinates, once these seven transformation parameters are known.

5.6 Transformation Parameters

Since there are no official publications by the Russian Military Space Forces on PZ-90 and its transformation to WGS84, these transformation parameters for a long time were unknown in the GLONASS user community. Interested groups of scientists thus independently determined their own sets of transformation parameters that differ as much as their methods to obtain the parameters.

5.6.1 Methods for Determination of Transformation Parameters

There are several possible methods to determine the transformation parameters from PZ-90 to WGS84. Common to all these methods is the necessity to measure or otherwise obtain the coordinates of a given set of points. Coordinates of these points must be determined in both coordinate frames, PZ-90 and WGS84. Afterwards, a set of transformation parameters is calculated that brings the coordinates into coincidence when applied to the coordinates in one of the coordinate frames.

To determine the seven parameters of the coordinate transformation as introduced above, at least seven point coordinates must be known in both frames to obtain seven equations for solving seven unknowns. Since each point in space supplies three coordinates (one each for the x-, y- and z-axes), measuring three points is mathematically sufficient to calculate the desired transformation parameters. However, to have a good quality of the obtained parameters, one is desired to have coordinates of as much points as possible for reasons of redundancy in the equations. In addition, these points should be globally distributed to extend the validity area of the derived parameters. With only a regional distribution of these points, translational and rotational parameters cannot be sufficiently separated from each other. This will likely result in a set of transformation parameters that is only valid in a specific area of the earth (where the measured points were located).

Possible methods of parameter determination can be distinguished by the location of the points the coordinates of which are obtained in both systems:

- Ground-based techniques: Coordinates of points on the surface of the earth are made known in both coordinate frames. Usually, either a set of points known in WGS84 is occupied and measured in PZ-90 or the other way round.

- Space-based techniques: Coordinates of satellites at a specified epoch in time are made known in both coordinate frames. Usually, coordinates of GLONASS satellites are obtained from their ephemerides (in PZ-90) and from ground tracking from sites known in WGS84.

Each of the ground-based techniques suffers from a disadvantage with respect to the space-based techniques: There are no known points with coordinates known in PZ-90 outside the territory of the former Soviet Union, making it nearly impossible to occupy these points with GPS receivers, determine their coordinates in WGS84 and derive a globally valid set of transformation parameters. On the other hand, there is plenty of points with coordinates known in WGS84 all around the world. But until recently, there was only a few geodetic quality GLONASS receivers. These were too few to occupy these points, determine their coordinates in PZ-90 and derive a globally valid set of transformation parameters. Only in 1998, a considerable number of Ashtech Z-18 receivers became available to be used in a global observation campaign, IGEX-98. One objective of this campaign is the determination of a set of globally valid transformation parameters (*Willis et al., 1998*; *IGN, 1998*).

Regarding this, the space-based techniques have one major advantage: With only a few GLONASS navigational receivers, broadcast ephemeris data (in the PZ-90 frame) of all GLONASS satellites all around the world can be received, providing global coverage. However, getting GLONASS orbit data in the WGS84 frame can be expensive. These can only be obtained by radar and/or SLR tracking of the satellites, both requiring a large infrastructure, if global coverage is to be obtained. Therefore, each group of scientists that determined transformation parameters using a space-based technique cooperated closely or was sponsored by an organization that can provide such an infrastructure, e.g. NASA.

A different possibility to determine orbits of GLONASS satellites in the WGS84 frame is to track the satellites using a network of receivers located at sites surveyed in WGS84 and then compute the satellite orbits from the range measurements, like IGS does to obtain precise ephemerides of GPS satellites. This approach was chosen by some of the analysis centers involved in the IGEX-98 campaign. But again, this requires a sufficient number of globally distributed GLONASS receivers.

5.6.2 Russian Estimations

One of the first estimations of the transformation parameters between the geodetic reference frames used for GPS and for GLONASS was performed by Russian scientists (*Boykov et al., 1993*). They determined the following set of transformation parameters for the transformation from PZ-90 to WGS84:

Parameter	Δx	Δy	Δz	$\delta\varepsilon$	$\delta\psi$	$\delta\omega$	δs
Value	0 m	0 m	1.5 m	0”	0”	-0.076”	0

In 1998, another group of Russian scientists presented a different estimation of the transformation parameters (*Mitrikas et al., 1998*). They derived their estimation of the parameters by comparing the orbits of GLONASS satellites obtained from the GLONASS control center (given in PZ-90) with orbits determined by means of SLR tracking of these satellites from stations given in WGS84. In their work they included twenty months of orbital data, but to two satellites only. From these data, they determined the following set of transformation parameters from PZ-90 to WGS84:

Parameter	Δx	Δy	Δz	$\delta\varepsilon$	$\delta\psi$	$\delta\omega$	δs
Value	-0.47 m	-0.51 m	-2.00 m	-0.002”	-0.001”	-0.356”	$22 \cdot 10^{-9}$

(*Mitrikas et al., 1998*) stated also that the definition of the PZ-90 frame did not take into account Earth's polar motion, contrary to the WGS84 frame, and that therefore transformation parameters between these two coordinate frames will be time dependent.

Another estimation was presented by scientists of the 29^{th} Research Institute of the Russian Ministry of Defense Topographic Service (*Bazlov et al., 1999*). They based their set of transformation parameters on approximately one year of observation data from eight sites in Russia. These sites were surveyed in

both PZ-90 and WGS84 by means of measurements from combined GPS/GLONASS receivers. Two of the observation sites used (Irkutsk and Krasnoye Selo) are regularly recording data for the IGS network.

Parameter	Δx	Δy	Δz	$\delta\varepsilon$	$\delta\psi$	$\delta\omega$	δs
Value	-1.10 m	-0.30 m	-0.90 m	0”	0”	-0.169”	$-12{\cdot}10^{-8}$

5.6.3 American Estimations

Extensive work on the determination of transformation parameters between geodetic reference frames used for GLONASS (PZ-90 and its predecessor SGS-85) and WGS84 was conducted at the Massachusetts Institute of Technology (*Misra and Abbot, 1994*; *Misra et al., 1996a*). They estimated these parameters by comparing the coordinates of GLONASS satellites in PZ-90 and in WGS84. The satellite position in PZ-90 were obtained from the broadcast satellite ephemerides, whereas the coordinates in WGS84 were obtained from radar and laser tracking of the satellites. Parameters for the transformation of both SGS-85 and PZ-90 coordinates to WGS84 were published in 1994 and 1996, respectively.

The transformation parameters for a transformation from SGS-85 to WGS84 were determined to be the following (*Misra and Abbot, 1994*):

Parameter	Δx	Δy	Δz	$\delta\varepsilon$	$\delta\psi$	$\delta\omega$	δs
Value	0 m	0 m	4 m	0”	0”	-0.6”	0

When applied to the GLONASS satellite coordinates, this transformation yielded a residual of 30 – 40 m rms in the coordinates.

For the transformation of PZ-90 coordinates to WGS84, the following set of parameters was estimated (*Misra et al., 1996a*):

Parameter	Δx	Δy	Δz	$\delta\varepsilon$	$\delta\psi$	$\delta\omega$	δs
Value	0 m	2.5 m	0 m	0”	0”	-0.4”	0

When applied to the GLONASS satellite coordinates, this transformation yielded a residual of 12 – 14 m rms in the coordinates.

Another estimation of the transformation parameters was published in (*Cook, 1997*). They used long-term observations of GLONASS satellites to one site on the West coast of the United States to determine the coordinates of that point in PZ-90. By comparing these coordinates to the known coordinates in WGS84, they derived the following transformation parameters:

Parameter	Δx	Δy	Δz	$\delta\varepsilon$	$\delta\psi$	$\delta\omega$	δs
Value	0 m	0 m	0 m	0”	0”	-0.33”	0

Since these parameters were derived from measurements at one observation site only, their validity is questionable. They are, however, in perfect agreement with the transformation parameters from (*Roßbach et al., 1996*).

5.6.4 German Estimations

A terrestrial observation campaign to determine transformation parameters between PZ-90 and WGS84 was carried out by three German institutes in May 1996. Participants in this campaign were the Institute of Geodesy and Navigation of the University FAF Munich, the Institute of Applied Geodesy in Frankfurt on Main and the German Aerospace Research Establishment, Remote Sensing Ground Station Neustrelitz.

Six GLONASS P-Code receivers were set up at IGS stations, at known coordinates in the WGS84 frame. By means of GLONASS satellite observations, the coordinates of these stations were determined

in the PZ-90 frame. Transformation parameters were derived from these two sets of coordinates. The following set of parameters were obtained from these data:

Parameter	Δx	Δy	Δz	$\delta\varepsilon$	$\delta\psi$	$\delta\omega$	δs
Value	0 m	0 m	0 m	0”	0”	-0.33”	0

When applied to the station coordinates, this transformation yielded a residual of 30 – 40 cm rms in the coordinates.

A more detailed description of this measurement campaign and the data analysis is given in (*Roßbach et al., 1996*) and in Chapter 6.

In another attempt to estimate a set of transformation parameters between PZ-90 and WGS84, an alternative way of estimation was developed that does not depend on the determination of positions in both coordinate frames. Instead, transformation parameters are determined directly from range measurements to GLONASS satellites, taken at observation sites whose WGS84 coordinates are known. This method is also described in detail in Section 6.3. Applied on a set of data from the IGEX-98 experiment, the following parameters were estimated:

Parameter	Δx	Δy	Δz	$\delta\varepsilon$	$\delta\psi$	$\delta\omega$	δs
Value	0.404 m	0.357 m	-0.476 m	0.024”	-0.012”	-0.343”	$-2.6\cdot10^{-9}$

Taking into account the standard deviations of these transformation parameters (see Section 6.3), the rotation around the z-axis again must be regarded as the most significant parameter. The value of this parameter shows good coincidence with the value from (*Roßbach et al., 1996*).

5.6.5 IGEX-98 Estimations

Transformation parameters from PZ-90 to WGS84 were also estimated by analysis centers involved in the International GLONASS Experiment 1998 (IGEX-98). This global observation campaign started in October 1998 and officially lasted until April 1999. However, recording and analysis of data continued on a best effort basis, and during the IGEX-98 workshop in September 1999 it was decided to transform the experiment into some kind of regular service, similar to the IGS (International GPS Service for Geodynamics).

The determination of transformation parameters between PZ-90 and WGS84 was and still is one of the objectives of this experiment. Some of the analysis centers, like e.g. the BKG in Frankfurt, Germany (the former IfAG), compute precise orbits for GLONASS satellites from the range measurements to these satellites. Since coordinates of the observation sites are known in the ITRF-96 frame, these precise ephemerides are also given in this frame. By comparing the precise ephemerides to the broadcast orbits, transformation parameters between PZ-90 and ITRF-96 can be derived. The latter can be regarded as coinciding with the WGS84 frame to decimeter level. Therefore, these parameters are also valid for the transformation from PZ-90 to WGS84.

Results for the transformation parameters from BKG are computed on a daily basis and published weekly through the IGEXMail facility. For days 291 through 346 of 1998, results can also be found in (*Habrich, 1999*). According to these results, the translations along the x- and z-axes can be considered as zero, when their RMS errors are taken into consideration. However, the translation along the y-axis and the rotations show a significant drift in time. This confirms the change of parameters in time that was also reported by (*Mitrikas et al., 1998*). Average values for the time span in question were:

Parameter	Δx	Δy	Δz	$\delta\varepsilon$	$\delta\psi$	$\delta\omega$	δs
Value	0.06 m	0.07 m	-0.57 m	0.035”	-0.021”	-0.358”	$-1.0\cdot10^{-8}$

Not accounting for drift in the parameters, when applied to the satellite positions this transformation yields an RMS error of around 5 m. This error mostly indicates the quality of the GLONASS broadcast

orbits. This may also lead to the conclusion that the GLONASS broadcast orbits in general are much more accurate than specified in Table 3.2.

5.7 Applying the Coordinate Transformation

A number of known transformations between the geodetic reference frames used for GPS and for GLONASS have described in the previous sections. The two most reliable sets of transformation parameters between PZ-90 and WGS84 – judged more or less on the availability of details and background information as well as the time span available to collect experience with these transformations – seem to be the ones from (*Misra et al., 1996a*) and (*Roßbach et al., 1996*). These two sets of parameters differ by 0.07" in the rotation around the z-axis and by 2.5 m in the offset of the origin. Thus, the maximum difference in WGS84 coordinates obtained from applying these two transformations to a point at the Earth's equator will be 4.6 m. For a point near Munich (48° North, 11.5° East), the difference in obtained WGS84 coordinates will be around 30 cm in x-coordinate and around 4 m in y-coordinate. Compared to an expected positioning error of 30 m for single point positioning, the difference in these two coordinate transformations is relatively insignificant.

Applied to the coordinates of a GLONASS satellite position (with a semi-major axis of 25500 km), the maximum difference between these transformations is about 11 m. (*ICD-GLONASS, 1995*) specifies the rms error in satellite position prediction to be 20 m along track, 10 m cross track and 5 m radially, see Table 3.2. These values yield an rms position error of approximately 23 m. This is about double the value of the maximum difference between these two coordinate transformations. So these two sets of transformation parameters can equivalently be used for the conversion of satellite positions in a combined GPS/GLONASS navigation solution, where meter-level positioning is sufficient.

However, residuals of the transformed coordinates showed to be much better when using the transformation from (*Roßbach et al., 1996*). Applied to coordinates of observation stations, the residuals were in the range of 30 – 40 cm rms. The transformation according to (*Misra et al., 1996a*) yielded rms residuals of 12 – 14 m in satellite coordinates. Reduced to the Earth's surface (at about a quarter of the satellite's distance from the geocenter), the residuals would be around 3 – 3.5 m rms, which is ten times the residuals of the transformation according to (*Roßbach et al., 1996*).

Comparing the transformation according to (*Mitrikas et al., 1998*) to the transformations (*Roßbach et al., 1996*) and (*Misra et al., 1996a*), the case of a point near Munich yields a difference in converted coordinates of approximately 50 cm in x-coordinate, 10 cm in y-coordinate and 2 m in z-coordinate between (*Mitrikas et al., 1998*) and (*Roßbach et al., 1996*). The difference between (*Mitrikas et al., 1998*) and (*Misra et al., 1996a*) for that case is about 20 cm in x-coordinate, 4 m in y-coordinate and 2 m in z-coordinate. These differences also allow for the transformation (*Misra et al., 1996a*) to be used in navigation applications, when meter-level positioning is sufficient.

Figures 5.2 to 5.4 show examples of a GPS/GLONASS positioning solution with the transformations according to (*Misra et al., 1996a*), (*Roßbach et al., 1996*) and (*Mitrikas et al., 1998*), respectively, applied. The data used in Figure 5.1 were processed in the same way, but now the calculated coordinates of the GLONASS satellites at the time of signal transmission were transformed to WGS84, before the user position was calculated. To convert PZ-90 coordinates to WGS84, the transformation parameters as proposed in (*Misra et al., 1996a*), (*Roßbach et al., 1996*) and (*Mitrikas et al., 1998*), respectively, were employed.

It can be clearly seen that now the centers of the GPS, GLONASS and combined GPS/GLONASS position distributions, where the Kalman filter finally converges, are much closer together than without the coordinate transformation. In fact, these positions now coincide to within a few meters. Especially the differences between (*Roßbach et al., 1996*) and (*Mitrikas et al., 1998*) (Figures 5.3 and 5.4) are hardly recognizable. So any of these coordinate transformations may be used for navigational applications, where meter-level accuracy is sufficient.

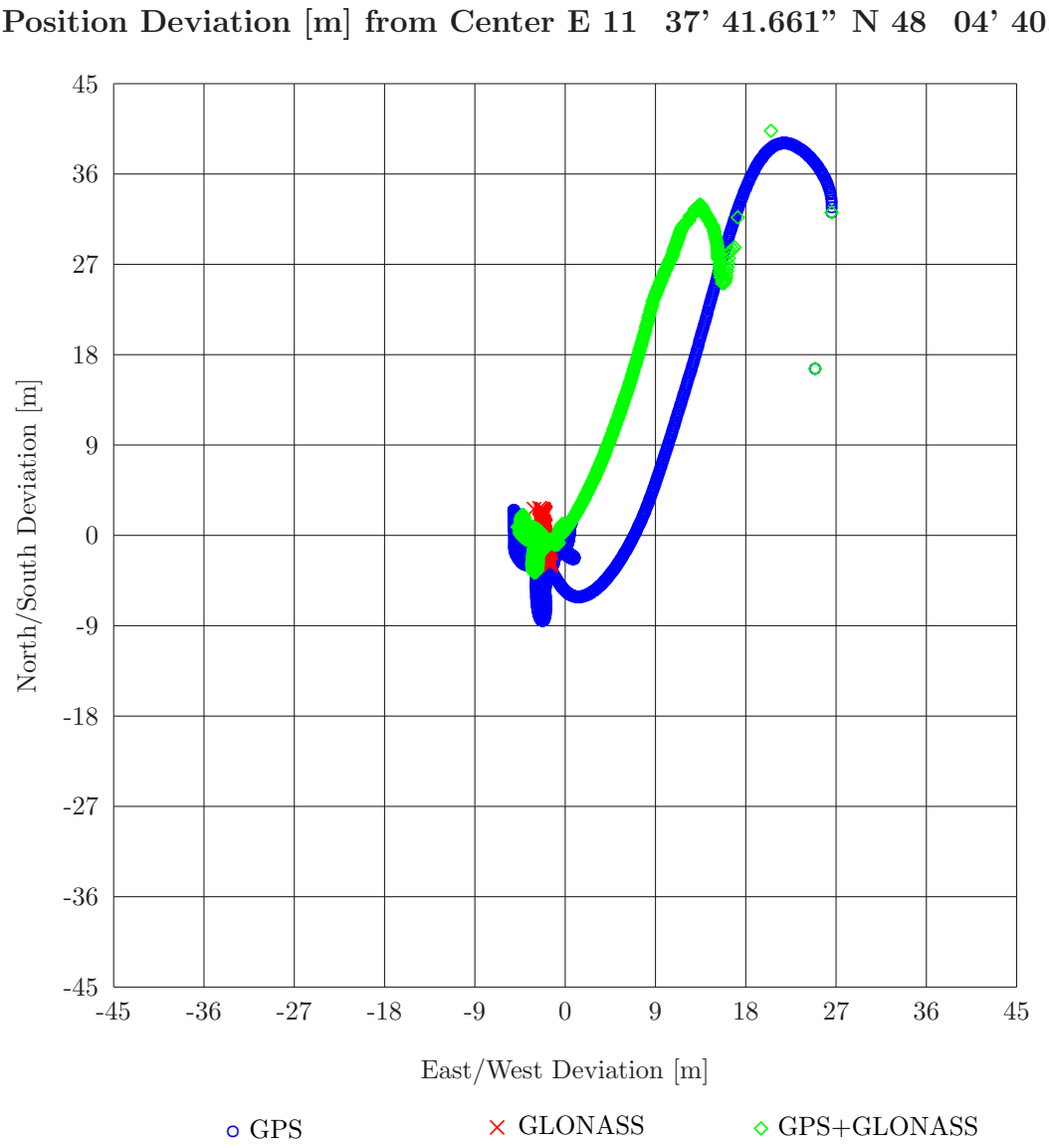

Figure 5.2: Example of combined GPS/GLONASS positioning with coordinate transformation according to (*Misra et al., 1996a*).

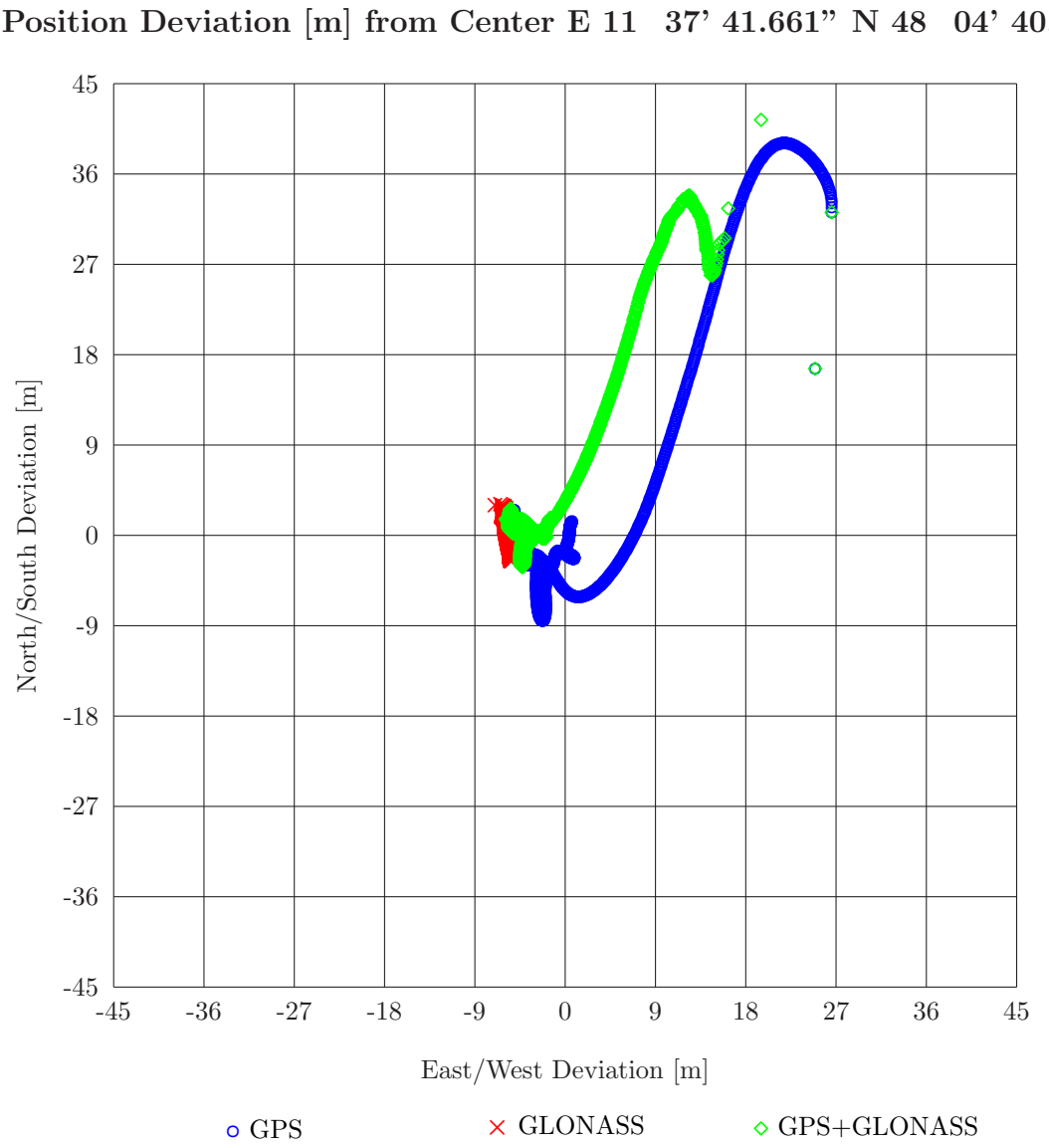

Figure 5.3: Example of combined GPS/GLONASS positioning with coordinate transformation according to (*Roßbach et al., 1996*).

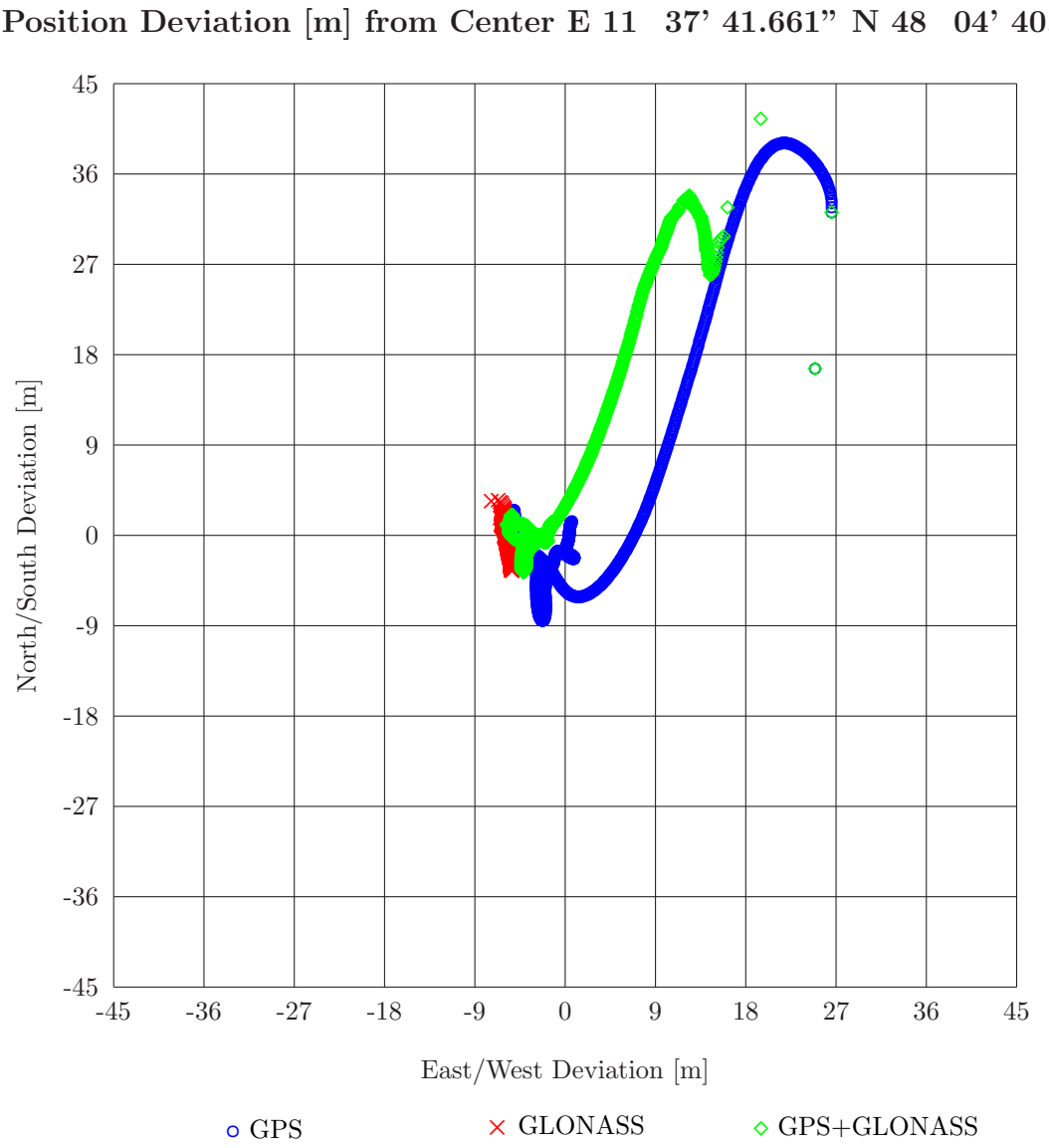

Figure 5.4: Example of combined GPS/GLONASS positioning with coordinate transformation according to (*Mitrikas et al., 1998*).

5.8 Coordinate Frames in Differential Processing

Where better accuracy is required, e.g. in surveying and geodesy, positioning will usually be done in differential mode. In this case, differences in the coordinate frame of the satellite positions can be regarded as orbital errors, which cancel out in differential processing, at least over short baselines.

According to (*Beutler et al., 1987*; *Landau and Vollath, 1996*), a radial error of 4 m will lead to an error of approximately 0.03 ppm in the baseline. Orbital errors of 75 m along track or cross track (which would correspond to the coordinate transformation (*Misra and Abbot, 1994*)) may cause a rotation of the baseline of around 0.6" and a maximum baseline error of 2.8 ppm.

Writing a simplified pseudorange observation equation from receiver R to satellite S, considering the error in orbit determination e^{orb}:

$$PR_R^S = \varrho_R^S + c \cdot \delta t_R - c \cdot \delta t^S + e_R^{S,orb} \tag{5.8.1}$$

and linearizing this equation with

$$\varrho_R^S = \sqrt{(x_R - x^S)^2 + (y_R - y^S)^2 + (z_R - z^S)^2} \tag{5.8.2}$$

the position vectors of receiver $\vec{x}_R$ and satellite $\vec{x}^S$ must be given in the same coordinate frame.

In case the satellite position vector is given in a different coordinate frame $\hat{\vec{x}}^S$ with a locally valid transformation $\vec{x}^S = \hat{\vec{x}}^S + \delta\vec{x}$, Eq. (5.8.1) rewrites to

$$PR_R^S = \sqrt{(x_R - \hat{x}^S - \delta x)^2 + (y_R - \hat{y}^S - \delta y)^2 + (z_R - \hat{z}^S - \delta z)^2} + c \cdot \delta t_R - c \cdot \delta t^S + e_R^{S,orb} \tag{5.8.3}$$

Linearizing the geometric range in terms of components of the transformation around zero:

$$\begin{aligned} \varrho_R^S(\delta x, \delta y, \delta z) &= \varrho_R^S(\delta x = 0, \delta y = 0, \delta z = 0) + \left.\frac{\partial \varrho_R^S(\delta x, \delta y, \delta z)}{\partial \delta x}\right|_{\substack{\delta x = 0 \\ \delta y = 0 \\ \delta z = 0}} \cdot \delta x + \\ &\quad \left.\frac{\partial \varrho_R^S(\delta x, \delta y, \delta z)}{\partial \delta y}\right|_{\substack{\delta x = 0 \\ \delta y = 0 \\ \delta z = 0}} \cdot \delta y + \left.\frac{\partial \varrho_R^S(\delta x, \delta y, \delta z)}{\partial \delta z}\right|_{\substack{\delta x = 0 \\ \delta y = 0 \\ \delta z = 0}} \cdot \delta z \end{aligned} \tag{5.8.4}$$

$$= \hat{\varrho}_R^S - \frac{x_R - \hat{x}^S}{\hat{\varrho}_R^S} \cdot \delta x - \frac{y_R - \hat{y}^S}{\hat{\varrho}_R^S} \cdot \delta y - \frac{z_R - \hat{z}^S}{\hat{\varrho}_R^S} \cdot \delta z \tag{5.8.5}$$

$$= \hat{\varrho}_R^S + f(\vec{x}_R, \hat{\vec{x}}^S, \delta\vec{x}) \tag{5.8.6}$$

with the range in different coordinate frames

$$\hat{\varrho}_R^S = \sqrt{(x_R - \hat{x}^S)^2 + (y_R - \hat{y}^S)^2 + (z_R - \hat{z}^S)^2} \tag{5.8.7}$$

Thus, we can write for the pseudorange observation equation

$$PR_R^S = \hat{\varrho}_R^S + f(\vec{x}_R, \hat{\vec{x}}^S, \delta\vec{x}) + c \cdot \delta t_R - c \cdot \delta t^S + e_R^{S,orb} \tag{5.8.8}$$

Doing the same for a second user receiver U:

$$PR_U^S = \hat{\varrho}_U^S + f(\vec{x}_U, \hat{\vec{x}}^S, \delta\vec{x}) + c \cdot \delta t_U - c \cdot \delta t^S + e_U^{S,orb} \tag{5.8.9}$$

and forming the receiver-to-receiver single difference, we obtain:

$$\Delta PR_{UR}^S = \Delta\hat{\varrho}_{UR}^S + c \cdot \Delta\delta t_{UR} + f(\vec{x}_U, \hat{\vec{x}}^S, \delta\vec{x}) - f(\vec{x}_R, \hat{\vec{x}}^S, \delta\vec{x}) + \Delta e_{UR}^{S,orb} \tag{5.8.10}$$

For short baselines between user and reference receivers, the orbital errors will be very similar: $\Delta e_{UR}^{S,orb} \to 0$ for $\vec{x}_U \to \vec{x}_R$.

From Eqs. (5.8.5) and (5.8.6), we can write for the single difference of the first-order terms

$$
\begin{aligned}
& f(\vec{x}_U, \hat{\vec{x}}^S, \delta\vec{x}) - f(\vec{x}_R, \hat{\vec{x}}^S, \delta\vec{x}) \\
&= \frac{x_R - \hat{x}^S}{\hat{\varrho}_R^S} \cdot \delta x + \frac{y_R - \hat{y}^S}{\hat{\varrho}_R^S} \cdot \delta y + \frac{z_R - \hat{z}^S}{\hat{\varrho}_R^S} \cdot \delta z - && (5.8.11) \\
&\quad \frac{x_U - \hat{x}^S}{\hat{\varrho}_U^S} \cdot \delta x - \frac{y_U - \hat{y}^S}{\hat{\varrho}_U^S} \cdot \delta y - \frac{z_U - \hat{z}^S}{\hat{\varrho}_U^S} \cdot \delta z \\
&= \left(\frac{x_R - \hat{x}^S}{\hat{\varrho}_R^S} - \frac{x_U - \hat{x}^S}{\hat{\varrho}_U^S} \right) \cdot \delta x + \left(\frac{y_R - \hat{y}^S}{\hat{\varrho}_R^S} - \frac{y_U - \hat{y}^S}{\hat{\varrho}_U^S} \right) \cdot \delta y + && (5.8.12) \\
&\quad \left(\frac{z_R - \hat{z}^S}{\hat{\varrho}_R^S} - \frac{z_U - \hat{z}^S}{\hat{\varrho}_U^S} \right) \cdot \delta z \\
&= \frac{1}{\hat{\varrho}_R^S} \left(x_R \delta x + y_R \delta y + z_R \delta z \right) - \frac{1}{\hat{\varrho}_U^S} \left(x_U \delta x + y_U \delta y + z_U \delta z \right) - && (5.8.13) \\
&\quad \frac{1}{\hat{\varrho}_R^S} \left(\hat{x}^S \delta x + \hat{y}^S \delta y + \hat{z}^S \delta z \right) + \frac{1}{\hat{\varrho}_U^S} \left(\hat{x}^S \delta x + \hat{y}^S \delta y + \hat{z}^S \delta z \right) \\
&= \frac{1}{\hat{\varrho}_R^S} \vec{x}_R \cdot \delta\vec{x} - \frac{1}{\hat{\varrho}_U^S} \vec{x}_U \cdot \delta\vec{x} - \frac{\hat{\varrho}_U^S - \hat{\varrho}_R^S}{\hat{\varrho}_R^S \hat{\varrho}_U^S} \hat{\vec{x}}^S \cdot \delta\vec{x} && (5.8.14) \\
&= \frac{1}{\hat{\varrho}_R^S \hat{\varrho}_U^S} \left[\hat{\varrho}_U^S \vec{x}_R - \hat{\varrho}_R^S \vec{x}_U - \left(\hat{\varrho}_U^S - \hat{\varrho}_R^S \right) \hat{\vec{x}}^S \right] \cdot \delta\vec{x} && (5.8.15)
\end{aligned}
$$

For the two observers U and R located close together, the position vectors approach each other ($\vec{x}_U \to \vec{x}_R$), and so do the geometric ranges to the satellite ($\hat{\varrho}_U^S \to \hat{\varrho}_R^S$). Thus, the single difference of the first-order terms in Eq. (5.8.10) will approach zero: $f(\vec{x}_U, \hat{\vec{x}}^S, \delta\vec{x}) - f(\vec{x}_R, \hat{\vec{x}}^S, \delta\vec{x}) \to 0$. In other words, these terms will disappear for short baselines.

Small differences in the coordinate frames of given (reference) receiver position and satellite position therefore can be treated equal to orbital errors, which cancel out on differencing over short baselines. Therefore, any of the proposed coordinate transformations from PZ-90 to WGS84 introduced above will suffice, even if sub-meter level positioning is required, as long as user positions are calculated using differential processing.

Of course, the single difference of the first-order terms $f(\vec{x}_U, \hat{\vec{x}}^S, \delta\vec{x}) - f(\vec{x}_R, \hat{\vec{x}}^S, \delta\vec{x})$ in Eq. (5.8.10) will not only disappear for short baselines, but also for small local transformation vectors $\delta\vec{x}$. Therefore, it must also be stated that the more precise a coordinate transformation is applied the longer baselines between reference station and user are allowed in order to keep the errors due to different coordinate frames small. In other words, a coordinate transformation from PZ-90 to WGS84 as precise as possible is desirable for differential operation, too. But the knowledge of accurate transformation parameters is not quite as vital for differential positioning as it is for single point positioning.

Figure 5.5 shows the average differences in calculated point positions between different coordinate transformations for a number of sample baselines. Positions of a static rover receiver were computed from carrier-smoothed pseudorange measurements to GLONASS satellites. Position of the reference receiver was given in WGS84 coordinates. To obtain the user positions in WGS84 also, two different coordinate transformations were employed, the transformations according to (*Roßbach et al., 1996*) and (*Misra et al., 1996a*). In a third computation run, no coordinate transformation was applied to the positions of the GLONASS satellites at the time of signal transmission. Illustrated are the average deviations of the computed user positions. Positioning results with the transformation (*Roßbach et al., 1996*) applied are taken as reference results. Deviations are measured in one case from the positions with no transformation applied to the positions with the reference transformation applied, in the other case from positions with transformation (*Misra et al., 1996a*) to the positions with the reference transformation applied.

It can be clearly seen that these deviations rise with increasing baseline length. However, the deviations between the two coordinate transformations rise more slowly than the deviations between coordinate transformation and no coordinate transformation. This is due to the fact that with a coordinate trans-

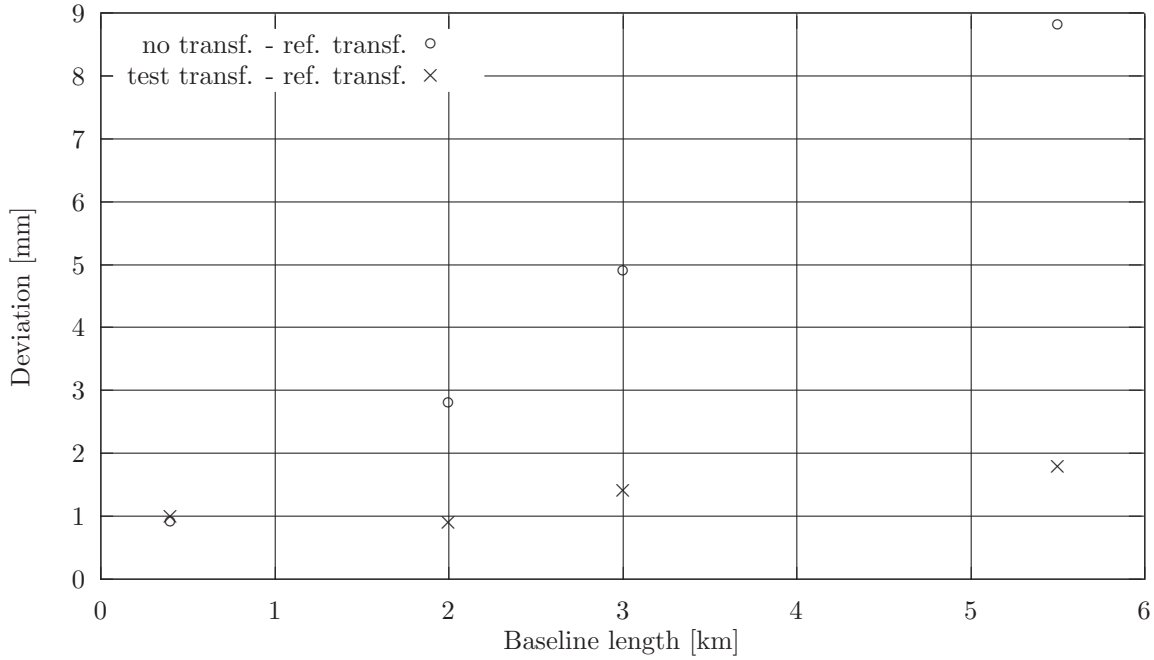

Figure 5.5: Average deviations of differentially computed user positions (static tests).
Curve marked with ○: Differences between positions computed with no transformation applied and with reference transformation (*Roßbach et al., 1996*) applied.
Curve marked with ×: Differences between positions computed with transformation (*Misra et al., 1996a*) and with reference transformation (*Roßbach et al., 1996*) applied.

formation applied, the magnitude of the local transformation vector $\delta\vec{x}$ in Eq. (5.8.15) decreases, thus allowing larger differences between the position vectors $\vec{x}_R$ of reference receiver and $\vec{x}_U$ of user receiver, equal to longer baselines.

Whereas the deviations from reference for the 'no transformation' case already approach the centimeter level for baselines longer than 5 km, the deviations between the two cases with a coordinate transformation applied remain smaller than 2 mm for these baselines. It can be concluded that for high-precision applications, where centimeter-level accuracies are required, a proper coordinate transformation should be applied to GLONASS satellite positions, if the reference coordinates are given in WGS84.

Figure 5.6 shows similar results for a kinematic test drive. The rover receiver was set up in a vehicle, which drove away from the reference station, went North about 60 km and then returned to the reference station on a partly different route. Unfortunately, a GLONASS only positioning solution for the roving receiver could not always be computed in this case, especially at the greater distances. However, the results of the static tests are confirmed. The deviations between the two computations with a coordinate transformation applied to GLONASS satellite positions before calculating the user position are much smaller than those between positioning solutions with and without application of a coordinate transformation. In the latter case, the deviations reach the centimeter level already at a distance of approximately 5 to 8 km, whereas the deviations between the two coordinate transformations approach the centimeter mark only at a distance of about 35 km. At a distance of about 60 km, the deviations between positioning solutions with and without application of a coordinate transformation nearly reach one decimeter, while the deviations between the two coordinate transformations are still well below 3 cm.

In both cases, the deviations seem to increase linearly with the distance from the reference station. So it can be concluded that differential GLONASS positioning with the reference coordinates given in the WGS84 frame introduces an error of approximately 1.5 ppm, when no coordinate transformation is

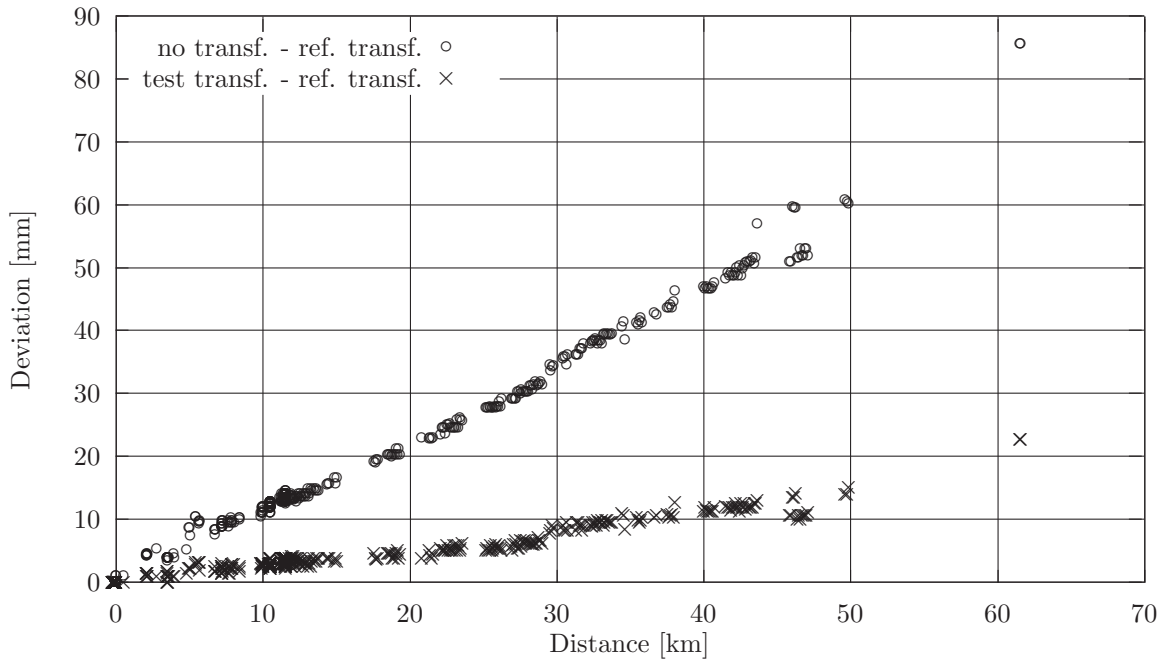

Figure 5.6: Deviations of differentially computed user positions (kinematic tests).
Curve marked with ○: Differences between positions computed with no transformation applied and with reference transformation (*Roßbach et al., 1996*) applied.
Curve marked with ×: Differences between positions computed with transformation (*Misra et al., 1996a*) and with reference transformation (*Roßbach et al., 1996*) applied.

applied to the GLONASS satellite positions. With a proper coordinate transformation applied, these errors can be reduced considerably to around 0.5 ppm.

These were examples of GLONASS only processing. In combined GPS/GLONASS processing, the deviations will be smaller, due to the influence of the GPS satellites, which do not require a coordinate transformation. The exact amount will depend on how many GPS and GLONASS satellites contribute to the solution. But still, a proper coordinate transformation should be applied to GLONASS satellite positions in order to keep errors caused by the different coordinate frames small.

In differential navigation, when meter-level accuracy is sufficient, doing without a coordinate transformation may not contribute significantly to the error level even for baselines of 50 km and more.

5.9 GLONASS Ephemerides in WGS84

Part of the data products of the IGEX-98 campaign were and still are precise ephemerides of GLONASS satellites, given in the WGS84 frame. When using these ephemeris data, the need for converting GLONASS satellite coordinates from PZ-90 to WGS84 drops.

However, as with the precise GPS ephemerides, these data are not available in real-time. Therefore, these ephemerides can only be applied when post-processing observation data. They cannot be used in real-time navigation.

6 Determination of Transformation Parameters

6.1 Preparations and Realization of IfEN's Measurement Campaign

The precise coordinate transformation from PZ-90 to WGS84 is one of the major issues in GPS/GLONASS inter-operability. Therefore, attempts to determine a set of transformation parameters started very early. The terrestrial determination of these parameters, however, suffered from the lack of sites that were accurately surveyed in both systems. This, in turn, was due to the facts that GLONASS was not yet fully operational and that there were few geodetic quality GLONASS or GPS/GLONASS receivers available.

Early attempts by American researchers (*Misra and Abbot, 1994*; *Misra et al., 1996a*) evaded these difficulties by using the GLONASS satellites themselves as observation sites, determining their positions in both WGS84 and SGS-85, respectively its successor PZ-90. SGS-85 (or PZ-90) coordinates were obtained directly from the broadcast ephemerides, whereas WGS84 positions were derived from radar and optical satellite tracking data. By comparing these coordinates, they derived sets of transformation parameters (cf. Section 5.6.3).

With the GLONASS constellation complete by the beginning of 1996 and accurate GLONASS P-code receivers at least in some number available, the main obstructions for the terrestrial determination of the transformation parameters had been overcome. Thus, known points in the WGS84 (ITRF) system could now also be surveyed precisely in PZ-90 to determine the parameters of a Helmert transformation between these two coordinate frames.

The Institute of Geodesy and Navigation (IfEN) of the University FAF Munich, together with the Institute of Applied Geodesy (IfAG), Geodetic Research Division, and the DLR-DFD Remote Sensing Ground Station Neustrelitz, planned and carried out an observation campaign, in which known ITRF sites distributed over Europe were surveyed in PZ-90 by means of GLONASS observations. In a first approximation, ITRF-94 can be considered to be nearly identical to WGS84. According to (*Abusali et al., 1995*), referred to GPS week 500 (August 1989), WGS84 and ITRF-90 were compatible at the one-meter-level, with only the differential scale change of 0.21 ppm being larger than the 1σ uncertainties of 0.1 ppm estimated by DMA for the WGS84. Subsequently, the WGS84 frame was revised twice (in 1994 and in 1996) (*NIMA, 1997*), to eliminate this scale bias. Today, WGS84 coordinates of a point are within decimeter range of the coordinates in ITRF-94. This is below the uncertainties of ± 1 m in latitude and longitude and ± 2 m in height, specified for the WGS84. (*NIMA, 1997*) thus considers WGS84 and ITRF to be identical for mapping and charting purposes. In this observation campaign, the transformation parameters between PZ-90 and ITRF-94 were derived from the measured positions and baselines (cf. (*Roßbach et al., 1996*)).

IfEN, IfAG and DLR-DFD started planning this observation campaign in November 1995. The idea of the campaign was to occupy stations with known coordinates in WGS84 or ITRF with GLONASS P-code receivers to determine the coordinates of the observation sites in PZ-90. By comparing these sets of coordinates, transformation parameters between the two reference frames were to be derived.

The three institutes together have five 3S Navigation R-100/R-101 GPS/GLONASS receivers available. To have WGS84 coordinates as precisely as possible, permanently occupied stations of the IGS network would be preferred. In order to have the resulting parameters valid in as large an area as possible, the observation sites should be well-distributed over Europe.

Since March 1996, IfAG has been permanently operating one of their R-100/R-101 receivers at the Wettzell IGS station. The remaining four stations chosen were Maspalomas (Canary Islands), Herstmonceux (England), Zvenigorod (Russia) and Simeiz (Ukraine). Due to administrative problems, Simeiz had to be dropped shortly before the scheduled start of the campaign. As a short-term substitution, Metsahovi (Finland) was selected as the fifth observation site. However, this meant a considerable disadvantage for the station geometry.

During the final stage of the preparations we learned that in Madrid another 3S R-100/R-101 receiver was set up at Grupo de Mecanica de Vuelo (GMV) S.A. for a different campaign. This receiver was

Station	x-Coordinate [m]	y-Coordinate [m]	z-Coordinate [m]
Herstmonceux	4033459.2240	23626.3949	4924303.3794
Madrid[a]	4840708.7400	−313614.9000	4128586.9400
Maspalomas	5439190.6340	−1522055.2014	2953458.3141
Metsahovi	2892570.0625	1311843.5601	5512634.5644
Wettzell	4075580.1234	931855.2459	4801568.2600
Zvenigorod	2886328.2440	2155996.8210	5245817.5600

[a]The coordinates of Madrid are only approximate and are not given in ITRF-94.

Table 6.1: Known station coordinates in ITRF-94 at the time of the campaign, epoch 1996.4.

Figure 6.1: Participating observation sites.

available during our scheduled observation period. On request, GMV offered us to operate the receiver during that time and provide us with the measurement data. The campaign was finally observed in this configuration (see Figure 6.1). The coordinates of these stations in the ITRF frame, referred to the location of the antenna phase centers of the receivers, are given in Table 6.1.

The R-100/R-101 receivers employed in the campaign are 20 channel dual-frequency receivers (see Section 3.7). Eight of these 20 channels are capable of tracking GLONASS satellites on L_1 C/A-code, L_1 P-code or L_2 P-code. (P-channels). The remaining twelve channels are capable of tracking GPS and GLONASS satellites on L_1 C/A-code (C/A-channels). To make use of the possibility of obtaining ionospheric corrections from dual-frequency measurements, the receivers were configured to track four satellites on L_1 P-code and L_2 P-code simultaneously on the eight P-channels. Furthermore, whenever possible these four satellites observed were chosen to be satellites that were visible at all participating stations simultaneously. This considerably improved the chances of computing baseline solutions. On the other hand, these four satellites visible at all stations not necessarily provided the optimum geometry at all stations. The receivers were configured to output raw pseudorange and carrier phase measurements at a 1 Hz rate, with the exception of the receiver in Madrid, which recorded at 10 s intervals. Utilizing the C/A-channels and tracking eight satellites on L_2 P-code and L_1 C/A-code would have provided a much better geometry, but the C/A-code measurements are also much more noisy, and the combined load on the receivers at the 1 Hz rate was found unbearable during pre-campaign tests.

Even with only the eight P-channels, the amount of data written to the hard disk of the host PC was of about 5 MB per hour or 120 MB per day, so a daily break was scheduled in the observation plan to download the measurement data to a different device.

Station	**May 14/15 (135/136)**	**May 15/16 (136/137)**	**May 16/17 (137/138)**	**May 17/18 (138/139)**
Herstmonceux		x	x	x
Madrid	x	x	x	
Maspalomas		x	x	x
Metsahovi	x	x	x	x
Wettzell	x	x	x	
Zvenigorod		x	x	x
Station	**May 18/19 (139/140)**	**May 19/20 (140/141)**	**May 20/21 (141/142)**	
Herstmonceux	x	x		
Madrid			x	
Maspalomas		x		
Metsahovi	x	x	x	
Wettzell				
Zvenigorod	x	x		

Table 6.2: Summary of available observations at stations by campaign day.

The campaign officially started May 15 at 14 h UTC and lasted until May 20 14 h UTC, but some stations slightly extended the observation period.

Despite all efforts to obtain simultaneous measurements to the same set of satellites from all stations, a couple of setbacks were experienced in this respect. The receiver at Wettzell shut down on Saturday morning, May 18, and could not be restarted until Monday morning. But after that data quality remained very poor.

Something similar happened to the receiver at Maspalomas, which shut down Saturday afternoon. Due to security reasons at the station, this receiver could not be attended on Sunday so it could be restarted only on Monday morning. At least this shut-down may be caused by GLONASS satellite 24, frequency letter 1 turning unhealthy on May 18, when it was on the observation schedule.

Table 6.2 summarizes the days, for which data were available.

A quality check of the observation data was performed at DLR with their GLONASS quality control software (*Zarraoa et al., 1996*). Disregarding the poor data from Wettzell mentioned above, noise of the raw P-code observations was found to be 30 – 40 cm rms. Noise of the carrier phase measurements was about 5 mm rms for Maspalomas and 2 – 3 mm rms for the other sites.

At Maspalomas an extra long antenna cable had to be used, which exceeded the maximum length specified by the receiver manufacturer. An additional pre-amplifier was not available. Therefore, the signal-to-noise ratio was quite low, yielding the high noise of the carrier phase measurements. The noise of the P-code observations, however, was comparable to that at the other stations.

At Madrid, carrier smoothed pseudorange measurements were recorded. Their noise was only a few cm rms. But most of the time there were only three satellites available.

At all stations, except for Metsahovi, there were occasional problems, when there was a jump of 100 m or more in either the L_1 or L_2 P-code measurements.

6.2 Data Analysis

Recorded observation data were exchanged between the participating agencies IfEN, IfAG and DLR and analyzed separately. Two different analysis methods were employed. The original intention was to compute accurate baselines between the observation sites from double difference carrier phase measurements. From these baselines, three rotation parameters and a scale factor can be derived. As precise coordinates

Station		x-Coordinate [m]	y-Coordinate [m]	z-Coordinate [m]
Herstmonceux	IfEN	4033460.361	23618.212	4924304.424
	IfAG	4033460.738	23619.197	4924301.617
	DLR	4033460.136	23617.881	4924304.882
Madrid	IfEN	———	———	———
	IfAG	4840703.738	−313628.333	4128580.061
	DLR	4840704.653	−313626.237	4128584.737
Maspalomas	IfEN	5439188.557	−1522065.338	2953458.471
	IfAG	5439189.389	−1522064.805	2953456.011
	DLR	5439187.648	−1522065.822	2953457.737
Metsahovi	IfEN	2892574.615	1311837.469	5512637.581
	IfAG	2892573.414	1311838.102	5512633.539
	DLR	2892572.551	1311838.105	5512635.774
Wettzell	IfEN	4075580.636	931848.121	4801568.404
	IfAG	4075581.778	931848.137	4801566.415
	DLR	4075580.656	931848.335	4801568.577
Zvenigorod	IfEN	2886333.317	2155990.304	5245818.258
	IfAG	2886333.377	2155991.329	5245815.635
	DLR	2886331.972	2155992.484	5245818.135

Table 6.3: Computed station coordinates in the PZ-90 frame (single point positioning).

in PZ-90 for any of the observing stations (including Zvenigorod, which is situated on Russian territory) were not available to estimate also the translation offset between both systems, a single point positioning using code measurements was performed in addition. This single point positioning was expected to be less accurate than the double difference baseline solutions due to the increased noise in the code measurements and the often unfavorable satellite geometry, but it was the only way of enabling the computation of all seven parameters of a Helmert transformation.

To analyze the data, IfAG used a modification of the Bernese software (*Rothacher et al., 1993*), modified at IfAG to include GLONASS satellite measurements. Both IfEN and DLR employed their own analysis software. IfEN's software package is partly described in (*Roßbach and Hein, 1996a*; *Roßbach and Hein, 1996b*) and in Chapter 9.

The single point positioning was done using an ionosphere free linear combination of unsmoothed L_1 and L_2 P-code pseudoranges. Positions were computed on the basis of daily solutions. These daily solutions were averaged to form a campaign solution.

Additionally, double difference baseline solutions have also been computed by each analysis center.

6.2.1 Single Point Positioning

Single point solutions for the PZ-90 coordinates of the observation sites were computed separately at IfEN, IfAG and DLR with different software. The computed positions are shown in Table 6.3. Observations from Madrid were not included in the computations at IfEN due to the uncertainties in the receiver coordinates in the ITRF-94 reference frame and the fact that there were almost exclusively only three satellites available. For the same reason, IfAG and DLR computed positions for Madrid, but did not include these positions in the estimation of transformation parameters. The station coordinates resulting from the separate computations partially show significant discrepancies of up to 1 – 2 m and even 4 m for the z-coordinate of Madrid. In topocentric coordinates, deviations from a mean position reach up to 1.5 m in East/West and North/South direction and up to 2 m in the vertical.

Institute		IfEN	IfAG	DLR
Translation x	[m]	3.461	0.933 ±1.720	2.006 ±1.018
Translation y	[m]	3.658	2.372 ±2.375	−0.449 ±1.186
Translation z	[m]	−4.815	0.268 ±1.726	1.318 ±1.522
Rotation x	[”]	−0.0561 ±0.0856	−0.0340 ±0.0610	0.0266 ±0.0250
Rotation y	[”]	0.1970 ±0.1109	0.0880 ±0.0780	0.0023 ±0.0394
Rotation z	[”]	−0.2792 ±0.0773	−0.2880 ±0.0580	−0.3863 ±0.0528
Scale	[-]	$-9.8 \cdot 10^{-9} \pm 2.33 \cdot 10^{-7}$	$-5.2 \cdot 10^{-8} \pm 1.17 \cdot 10^{-7}$	$-3.2 \cdot 10^{-7} \pm 2.17 \cdot 10^{-7}$

Table 6.4: Estimated transformation parameters from single point solutions, 7 parameter transformation.

Considering the fact that during a large part of the observation time there was an unfortunate satellite geometry, these deviations are not far beyond what is regarded as the usual daily repeatability of pseudorange measurements, namely 1 m in the horizontal and 4 m in the vertical.

Of course, these discrepancies lead to different estimations of the transformation parameters, especially in the less significant values, as can be seen from Table 6.4. In average, the following values can be estimated:

- Translation x: 2.133 [m]
- Translation y: 1.860 [m]
- Translation z: -1.076 [m]
- Rotation x: -0.021 [”]
- Rotation y: 0.096 [”]
- Rotation z: -0.318 [”]
- Scale: $-1.27 \cdot 10^{-7}$ [-]

At IfEN, transformation parameters were computed in two steps, first rotation and scale parameters, then origin parameters. Thus, standard deviations for the translation parameters would not be very meaningful.

The residuals for this 7 parameter transformation are given in Table 6.5.

Looking at the transformation parameters and their standard deviations in Table 6.4, rotations around the x- and y-axes and the scale factor do not seem to be significant. This is consistent with the results in (*Misra and Abbot, 1994*). So the parameters of a transformation including a three-dimensional translation and a rotation around the z-axis were computed. These parameters are given in Table 6.6. Residuals of this transformation are slightly higher than for the full 7 parameter transformation.

The averaged values are:

- Translation x: -0.401 [m]
- Translation y: 0.283 [m]
- Translation z: 0.100 [m]
- Rotation z: -0.374 [”]

The resulting translation parameters differ significantly from these of the 7 parameter similarity transformation, only the rotation angle around the z-axis is comparable to that of the full 7 parameter Helmert transformation. Obviously this rotation really is the most significant parameter of the transformation from PZ-90 to ITRF and thus WGS84.

Station		**Residual x-coordinate [m]**	**Residual y-coordinate [m]**	**Residual z-coordinate [m]**
Herstmonceux	IfEN	0.177	0.404	−0.039
	IfAG	−0.100	0.001	0.022
	DLR	−1.361	0.782	−1.080
Madrid	IfEN	———	———	———
	IfAG	5.647	4.961	4.808
	DLR	———	———	———
Maspalomas	IfEN	−0.570	−0.097	−0.093
	IfAG	−0.269	0.040	0.113
	DLR	0.128	−0.050	0.072
Metsahovi	IfEN	−0.944	0.029	−1.266
	IfAG	0.054	0.018	−0.408
	DLR	−0.931	0.251	−0.396
Wettzell	IfEN	1.914	−0.736	0.573
	IfAG	0.978	−0.120	−0.069
	DLR	0.733	−0.556	0.177
Zvenigorod	IfEN	−0.577	0.399	0.826
	IfAG	−0.663	0.061	0.342
	DLR	−0.594	−0.516	0.250

Table 6.5: Residuals of 7 parameter transformation.

Institute		**IfEN**	**IfAG**	**DLR**
Translation x	[m]	−0.838	−1.139±0.218	0.774±0.534
Translation y	[m]	0.938	0.692±0.543	−0.782±1.063
Translation z	[m]	−1.012	1.772±0.205	−0.459±0.283
Rotation z	["]	−0.356±0.055	−0.335±0.027	−0.431±0.045

Table 6.6: Estimated transformation parameters from single point solutions, 4 parameter transformation.

Baseline	x-Component [m]	y-Component [m]	z-Component [m]
Herstmonceux → Maspalomas	1405731.4100	−1545681.5963	−1970845.0653
Herstmonceux → Metsahovi	−1140889.1615	1288217.1652	588331.1850
Herstmonceux → Wettzell	42120.8994	908228.8510	−122735.1194
Herstmonceux → Zvenigorod	−1147130.9800	2132370.4261	321514.1806

Table 6.7: Known baselines between stations in ITRF-94 at the time of the campaign, epoch 1996.4.

Baseline		x-Component [m]	y-Component [m]	z-Component [m]
Herstmonceux	IfEN	1405730.311	−1545682.835	−1970846.874
→ Maspalomas	IfAG	1405727.564	−1545683.962	−1970846.814
	DLR	1405728.000	−1545684.624	−1970846.437
Herstmonceux	IfEN	−1140888.762	1288219.515	588331.479
→ Metsahovi	IfAG	−1140886.881	1288219.262	588331.498
	DLR	−1140887.249	1288220.125	588331.812
Herstmonceux	IfEN	42122.310	908229.815	−122735.373
→ Wettzell	IfAG	42122.239	908228.892	−122735.242
	DLR	42122.500	908229.968	−122735.375
Herstmonceux	IfEN	−1147129.006	2132373.110	321514.283
→ Zvenigorod	IfAG	−1147127.402	2132372.510	321514.263
	DLR	−1147127.599	2132373.375	321514.343

Table 6.8: Computed baselines between stations in the PZ-90 frame (double difference baseline solution).

6.2.2 Double Difference Baselines

In addition to the single point solutions, the transformation parameters have also been computed from a baseline solution. Baselines from Herstmonceux to the other observation sites were calculated from double difference dual-frequency carrier phase measurements. These baselines were compared to the respective baselines in the ITRF frame (see Table 6.7). From this, three rotation and one scale parameter could be estimated.

At IfEN, the PZ-90 baselines were computed in three-hourly solutions, with one hour overlap. All these solutions were averaged to determine the campaign solution for the baselines. At DLR and IfAG, 24-hour data sets were used to compute the baseline solution, and then averaged for the entire observation period. The computed baselines are shown in Table 6.8. Deviations of these baseline solutions partially are much larger than one would expect the repeatability of double difference carrier phase solutions to be. This may be caused by the mostly unfavorable satellite geometry, which of course does not only affect single point solutions, but also double differences. In addition, at Maspalomas the noise of the carrier phase measurements was rather high, as explained earlier. Different results at IfEN may also be due to the slightly different analysis procedure. Singular inconsistencies in the data, such as undetected cycle slips or the above mentioned jumps in the P-code measurements of one frequency, may play a more significant role in the three-hourly solutions than in a daily solution.

Considering an orbital error of some ten meters in the broadcast ephemerides, the baselines may still be affected by a 1 ppm error. The baseline from Herstmonceux to Maspalomas for example, nearly 3000 km long, therefore may contain an error of 3 m.

The estimations of the four transformation parameters (three rotations and the scale factor) from each group, are presented in Table 6.9.

The average results yield:

- Rotation x: -0.002 [”]

Institute		IfEN	IfAG	DLR
Rotation x	["]	0.0583 ±0.0856	0.0010 ±0.0300	−0.0639 ±0.0388
Rotation y	["]	−0.0249 ±0.1109	0.1330 ±0.0390	0.1469 ±0.0381
Rotation z	["]	−0.2468 ±0.0773	−0.3420 ±0.0280	−0.2981 ±0.0324
Scale	[-]	$-9.8 \cdot 10^{-7} \pm 2.33 \cdot 10^{-7}$	$-1.0 \cdot 10^{-7} \pm 0.58 \cdot 10^{-7}$	$-5.1 \cdot 10^{-7} \pm 0.97 \cdot 10^{-7}$

Table 6.9: Estimated transformation parameters from baseline solutions, 4 parameter transformation.

- Rotation y: 0.085 ["]
- Rotation z: -0.296 ["]
- Scale: $-5.308 \cdot 10^{-7}$

As already observed with the above 4 parameter transformation from the single point solutions, the rotation around the z-axis remains comparable to the value derived from the full 7 parameter similarity transformation, but the other parameters differ significantly.

The residuals of the baseline transformation using these parameters are in the range of 30 – 40 cm for the different groups.

Considering the fact that the rotation around the z-axis seems to be the most significant parameter, only this rotation was estimated from the measured and known baselines. The results of the different analysis centers were:

- IfEN: -0.2232 ±0.0551 ["]
- IfAG: -0.3960 ±0.0320 ["]
- DLR: -0.3843 ±0.0425 ["]
- Average: -0.3345 ["]

The parameters of a similarity transformation between the PZ-90 and WGS84 (ITRF) reference frames have been determined terrestrially by measuring the PZ-90 coordinates of sites known in ITRF by means of GLONASS observations.

The preliminarily estimated transformation parameters revealed only one significant parameter, the rotation around the z-axis. The value of this parameter can be estimated to about -0.33" or $-1.6 \cdot 10^{-6}$ rad. Transformation from PZ-90 coordinates (u,v,w) to ITRF-94 (x,y,z) thus can be written as:

$$\begin{pmatrix} x \\ y \\ z \end{pmatrix}_{ITRF} = \begin{pmatrix} 1 & -1.6 \cdot 10^{-6} & 0 \\ 1.6 \cdot 10^{-6} & 1 & 0 \\ 0 & 0 & 1 \end{pmatrix} \cdot \begin{pmatrix} u \\ v \\ w \end{pmatrix}_{PZ} \tag{6.2.1}$$

6.3 Direct Estimation of Transformation Parameters

The different methods of determination of transformation parameters as described above and in Chapter 5 all have in common that coordinates in PZ-90 were calculated for points known in WGS84 (or ITRF) or vice versa. The transformation parameters then were derived from comparing these coordinates in PZ-90 and WGS84. The points used for comparison could be located on the surface of the Earth or in space (satellites).

However, for observation sites given in WGS84 (or any other ECEF coordinate frame) tracking GLONASS satellites, transformation parameters can also be determined directly from the range measurements themselves, skipping the necessity for determination of the coordinates of the sample point in the PZ-90 frame. The following section introduces this method of parameter determination and shows the results of this procedure being applied to the data of the IGEX-98 observation campaign; cf. also (*Roßbach,*

1999). Originally, a set of transformation parameters was to be derived from data of the measurement campaign described above using this method. However, the much better geometry of the IGEX sites provided significantly better results.

The principle of direct determination of the transformation parameters is shown for station coordinates given in WGS84. It can, however, be applied to any other ECEF coordinate frame as well. In the IGEX-98 campaign, coordinates of the observation sites were given in ITRF-96. Thus, the results of this process will be a set of transformation parameters from PZ-90 to ITRF-96. However, ITRF-96 and WGS84 can be regarded as identical.

The (simplified) pseudorange observation equation from receiver R to satellite S is given by

$$PR_R^S = \varrho_R^S + c \cdot \delta t_R - c \cdot \delta t^S + c \cdot \delta t_R^{S,Trop} + c \cdot \delta t_R^{S,Iono} \tag{6.3.1}$$

with

$$\varrho_R^S = \sqrt{(x_R - x^S)^2 + (y_R - y^S)^2 + (z_R - z^S)^2} \tag{6.3.2}$$

The position vectors of receiver $\vec{x}_R$ and satellite $\vec{x}^S$ in Eq. (6.3.2) must be given in the same coordinate frame.

In the given case of direct determination of transformation parameters between PZ-90 and WGS84 from range measurements to GLONASS satellites, the known coordinates of the observation sites are given in WGS84, whereas the coordinates of the GLONASS satellites are determined from ephemeris data and are given in PZ-90. Since both WGS84 and PZ-90 are Earth-centered Earth-fixed (ECEF) coordinate frames, they rotate along with the Earth. Their orientation therefore is a function of time. More precise, thus, the coordinates of the observation sites are given in WGS84, as valid at the time of signal reception t_{RX}, and the coordinates of the satellites are given in PZ-90, as valid at the time of signal transmission t_{TX}.

$$\begin{aligned} \vec{x}_R &= \vec{x}_{R,WGS(t_{RX})} \\ \vec{x}^S &= \vec{x}^S_{PZ(t_{TX})} \end{aligned}$$

To obtain the actual geometrical distance from receiver to satellite, one of these two sets of coordinates must be transformed to the coordinate frame of the other set. Here it is chosen to transform the satellite coordinates to the coordinate frame of the observer. This requires two steps of transformation:

- Transformation from PZ-90 to WGS84: $\vec{x}^S_{PZ(t_{TX})} \rightarrow \vec{x}^S_{WGS(t_{TX})}$
- Correction of Earth rotation: $\vec{x}^S_{WGS(t_{TX})} \rightarrow \vec{x}^S_{WGS(t_{RX})}$

Correction of Earth rotation

While the satellite signal is travelling towards the observer, the Earth – and along with it the Earth-fixed coordinate frame – keeps rotating. During this signal travel time, it rotates by an angle of $\alpha = \varrho_R^S / c \cdot \omega_E$. This is a positive rotation around the z-axis. Thus, the satellite coordinates transform by

$$\vec{x}^S_{PZ(t_{RX})} = \begin{pmatrix} 1 & \alpha & 0 \\ -\alpha & 1 & 0 \\ 0 & 0 & 1 \end{pmatrix} \cdot \vec{x}^S_{PZ(t_{TX})} \tag{6.3.3}$$

for small angles α.

The geometrical distance therefore becomes

$$\varrho_R^S = \sqrt{\left(x_{R,PZ(t_{RX})} - x^S_{PZ(t_{RX})}\right)^2 + \left(y_{R,PZ(t_{RX})} - y^S_{PZ(t_{RX})}\right)^2 + \left(z_{R,PZ(t_{RX})} - z^S_{PZ(t_{RX})}\right)^2} \tag{6.3.4}$$

or

$$\begin{aligned}
{\varrho_R^S}^2 &= \left(x_{R,PZ(t_{RX})} - x^S_{PZ(t_{TX})} - \frac{\omega_E}{c}\varrho_R^S \cdot y^S_{PZ(t_{TX})}\right)^2 + \qquad (6.3.5)\\
&\quad \left(y_{R,PZ(t_{RX})} - y^S_{PZ(t_{TX})} + \frac{\omega_E}{c}\varrho_R^S \cdot x^S_{PZ(t_{TX})}\right)^2 + \left(z_{R,PZ(t_{RX})} - z^S_{PZ(t_{TX})}\right)^2\\
&= \left(x_{R,PZ(t_{RX})} - x^S_{PZ(t_{TX})}\right)^2 - 2\left(x_{R,PZ(t_{RX})} - x^S_{PZ(t_{TX})}\right)\frac{\omega_E}{c}\varrho_R^S y^S_{PZ(t_{TX})} + \frac{\omega_E^2}{c^2}{\varrho_R^S}^2 {y^S_{PZ(t_{TX})}}^2 +\\
&\quad \left(y_{R,PZ(t_{RX})} - y^S_{PZ(t_{TX})}\right)^2 + 2\left(y_{R,PZ(t_{RX})} - y^S_{PZ(t_{TX})}\right)\frac{\omega_E}{c}\varrho_R^S x^S_{PZ(t_{TX})} + \frac{\omega_E^2}{c^2}{\varrho_R^S}^2 {x^S_{PZ(t_{TX})}}^2 +\\
&\quad \left(z_{R,PZ(t_{RX})} - z^S_{PZ(t_{TX})}\right)^2 \qquad (6.3.6)\\
&= \left(x_{R,PZ(t_{RX})} - x^S_{PZ(t_{TX})}\right)^2 + \left(y_{R,PZ(t_{RX})} - y^S_{PZ(t_{TX})}\right)^2 + \left(z_{R,PZ(t_{RX})} - z^S_{PZ(t_{TX})}\right)^2 + \qquad (6.3.7)\\
&\quad \frac{\omega_E^2}{c^2}{\varrho_R^S}^2 \cdot \left({x^S_{PZ(t_{TX})}}^2 + {y^S_{PZ(t_{TX})}}^2\right) - 2\frac{\omega_E}{c}\varrho_R^S \cdot \left(x_{R,PZ(t_{RX})} y^S_{PZ(t_{TX})} - y_{R,PZ(t_{RX})} x^S_{PZ(t_{TX})}\right)
\end{aligned}$$

This transforms into

$$\begin{aligned}
0 &= {\varrho_R^S}^2 \cdot \left[1 - \left(\frac{\omega_E}{c}\right)^2 \left({x^S_{PZ(t_{TX})}}^2 + {y^S_{PZ(t_{TX})}}^2\right)\right] +\\
&\quad 2\frac{\omega_E}{c}\varrho_R^S \cdot \left(x_{R,PZ(t_{RX})} y^S_{PZ(t_{TX})} - y_{R,PZ(t_{RX})} x^S_{PZ(t_{TX})}\right) - \qquad (6.3.8)\\
&\quad \left(x_{R,PZ(t_{RX})} - x^S_{PZ(t_{TX})}\right)^2 - \left(y_{R,PZ(t_{RX})} - y^S_{PZ(t_{TX})}\right)^2 - \left(z_{R,PZ(t_{RX})} - z^S_{PZ(t_{TX})}\right)^2
\end{aligned}$$

The term $\left(\frac{\omega_E}{c}\right)^2 \cdot \left({x^S_{PZ(t_{TX})}}^2 + {y^S_{PZ(t_{TX})}}^2\right)$ in Eq. (6.3.8) is of the order of magnitude 10^{-12} and can be neglected with respect to the 1:

$$\begin{aligned}
0 &= {\varrho_R^S}^2 + 2\frac{\omega_E}{c}\varrho_R^S \cdot \left(x_{R,PZ(t_{RX})} y^S_{PZ(t_{TX})} - y_{R,PZ(t_{RX})} x^S_{PZ(t_{TX})}\right) - \qquad (6.3.9)\\
&\quad \left(x_{R,PZ(t_{RX})} - x^S_{PZ(t_{TX})}\right)^2 - \left(y_{R,PZ(t_{RX})} - y^S_{PZ(t_{TX})}\right)^2 - \left(z_{R,PZ(t_{RX})} - z^S_{PZ(t_{TX})}\right)^2
\end{aligned}$$

This quadratic equation has two possible solutions:

$$\begin{aligned}
\varrho^S_{R1,2} &= -\frac{\omega_E}{c} \cdot \left(x_{R,PZ(t_{RX})} y^S_{PZ(t_{TX})} - y_{R,PZ(t_{RX})} x^S_{PZ(t_{TX})}\right) \pm\\
&\quad \left[\left(\frac{\omega_E}{c}\right)^2 \cdot \left(x_{R,PZ(t_{RX})} y^S_{PZ(t_{TX})} - y_{R,PZ(t_{RX})} x^S_{PZ(t_{TX})}\right)^2 + \qquad (6.3.10)\right.\\
&\quad \left.\left(x_{R,PZ(t_{RX})} - x^S_{PZ(t_{TX})}\right)^2 + \left(y_{R,PZ(t_{RX})} - y^S_{PZ(t_{TX})}\right)^2 + \left(z_{R,PZ(t_{RX})} - z^S_{PZ(t_{TX})}\right)^2\right]^{1/2}
\end{aligned}$$

Since the square root is always positive and of larger magnitude than the term in front of it, the negative sign in front of the square root does not provide a physically meaningful solution. Therefore the distance between satellite and observer, corrected for Earth rotation during the signal travel time, can be written as:

$$\begin{aligned}
\varrho^S_R &= -\frac{\omega_E}{c} \cdot \left(x_{R,PZ(t_{RX})} y^S_{PZ(t_{TX})} - y_{R,PZ(t_{RX})} x^S_{PZ(t_{TX})}\right) +\\
&\quad \left[\left(\frac{\omega_E}{c}\right)^2 \cdot \left(x_{R,PZ(t_{RX})} y^S_{PZ(t_{TX})} - y_{R,PZ(t_{RX})} x^S_{PZ(t_{TX})}\right)^2 + \qquad (6.3.11)\right.\\
&\quad \left.\left(x_{R,PZ(t_{RX})} - x^S_{PZ(t_{TX})}\right)^2 + \left(y_{R,PZ(t_{RX})} - y^S_{PZ(t_{TX})}\right)^2 + \left(z_{R,PZ(t_{RX})} - z^S_{PZ(t_{TX})}\right)^2\right]^{1/2}
\end{aligned}$$

For deriving Eq. (6.3.11), the PZ-90 coordinate frame was used. Of course, Eq. (6.3.11) is also valid in the WGS84 coordinate frame:

$$\begin{aligned}
\varrho^S_R &= -\frac{\omega_E}{c} \cdot \left(x_{R,WGS(t_{RX})} y^S_{WGS(t_{TX})} - y_{R,WGS(t_{RX})} x^S_{WGS(t_{TX})}\right) +\\
&\quad \left[\left(\frac{\omega_E}{c}\right)^2 \cdot \left(x_{R,WGS(t_{RX})} y^S_{WGS(t_{TX})} - y_{R,WGS(t_{RX})} x^S_{WGS(t_{TX})}\right)^2 + \qquad (6.3.12)\right.\\
&\quad \left.\left(x_{R,WGS(t_{RX})} - x^S_{WGS(t_{TX})}\right)^2 + \left(y_{R,WGS(t_{RX})} - y^S_{WGS(t_{TX})}\right)^2 + \left(z_{R,WGS(t_{RX})} - z^S_{WGS(t_{TX})}\right)^2\right]^{1/2}
\end{aligned}$$

Transformation from PZ-90 to WGS84

The transformation of a position vector given in PZ-90 to WGS84 can be written as (cf. Section 5.5):

$$\begin{pmatrix} x \\ y \\ z \end{pmatrix}_{WGS} = \begin{pmatrix} \Delta x \\ \Delta y \\ \Delta z \end{pmatrix} + (1+\delta s) \cdot \begin{pmatrix} 1 & \delta\omega & -\delta\psi \\ -\delta\omega & 1 & \delta\varepsilon \\ \delta\psi & -\delta\varepsilon & 1 \end{pmatrix} \cdot \begin{pmatrix} x \\ y \\ z \end{pmatrix}_{PZ} \tag{6.3.13}$$

or in individual coordinates, valid at time t_{TX}:

$$\begin{aligned} x^S_{WGS(t_{TX})} &= \Delta x + (1+\delta s) \cdot \left(x^S_{PZ(t_{TX})} + \delta\omega \cdot y^S_{PZ(t_{TX})} - \delta\psi \cdot z^S_{PZ(t_{TX})} \right) \\ y^S_{WGS(t_{TX})} &= \Delta y + (1+\delta s) \cdot \left(-\delta\omega \cdot x^S_{PZ(t_{TX})} + y^S_{PZ(t_{TX})} + \delta\varepsilon \cdot z^S_{PZ(t_{TX})} \right) \\ z^S_{WGS(t_{TX})} &= \Delta z + (1+\delta s) \cdot \left(\delta\psi \cdot x^S_{PZ(t_{TX})} - \delta\varepsilon \cdot y^S_{PZ(t_{TX})} + z^S_{PZ(t_{TX})} \right) \end{aligned} \tag{6.3.14}$$

Inserting this into Eq. (6.3.12) yields

$$\begin{aligned} \varrho^S_R = & -\frac{\omega_E}{c} \left\{ x_{R,WGS(t_{RX})} \left[\Delta y + (1+\delta s) \cdot \left(-\delta\omega \cdot x^S_{PZ(t_{TX})} + y^S_{PZ(t_{TX})} + \delta\varepsilon \cdot z^S_{PZ(t_{TX})} \right) \right] - \right. \\ & \left. y_{R,WGS(t_{RX})} \left[\Delta x + (1+\delta s) \cdot \left(x^S_{PZ(t_{TX})} + \delta\omega \cdot y^S_{PZ(t_{TX})} - \delta\psi \cdot z^S_{PZ(t_{TX})} \right) \right] \right\} + \\ & \left[\left(\frac{\omega_E}{c} \right)^2 \left\{ x_{R,WGS(t_{RX})} \left[\Delta y + (1+\delta s) \cdot \left(-\delta\omega \cdot x^S_{PZ(t_{TX})} + y^S_{PZ(t_{TX})} + \delta\varepsilon \cdot z^S_{PZ(t_{TX})} \right) \right] - \right. \right. \\ & \left. \left. y_{R,WGS(t_{RX})} \left[\Delta x + (1+\delta s) \cdot \left(x^S_{PZ(t_{TX})} + \delta\omega \cdot y^S_{PZ(t_{TX})} - \delta\psi \cdot z^S_{PZ(t_{TX})} \right) \right] \right\}^2 + \right. \\ & \left\{ x_{R,WGS(t_{RX})} - \left[\Delta x + (1+\delta s) \cdot \left(x^S_{PZ(t_{TX})} + \delta\omega \cdot y^S_{PZ(t_{TX})} - \delta\psi \cdot z^S_{PZ(t_{TX})} \right) \right] \right\}^2 + \\ & \left\{ y_{R,WGS(t_{RX})} - \left[\Delta y + (1+\delta s) \cdot \left(-\delta\omega \cdot x^S_{PZ(t_{TX})} + y^S_{PZ(t_{TX})} + \delta\varepsilon \cdot z^S_{PZ(t_{TX})} \right) \right] \right\}^2 + \\ & \left. \left\{ z_{R,WGS(t_{RX})} - \left[\Delta z + (1+\delta s) \cdot \left(\delta\psi \cdot x^S_{PZ(t_{TX})} - \delta\varepsilon \cdot y^S_{PZ(t_{TX})} + z^S_{PZ(t_{TX})} \right) \right] \right\}^2 \right]^{1/2} \end{aligned} \tag{6.3.15}$$

Here, the coordinates $\vec{x}_{R,WGS(t_{RX})}$ are the known station coordinates, given in WGS84, valid at the time of signal reception. $\vec{x}^S_{PZ(t_{TX})}$ are the satellite coordinates at the time of signal transmission as obtained from ephemeris data. They are given in the PZ-90 frame, valid at the time of signal transmission. The transformation parameters Δx, Δy, Δz, δs, $\delta\varepsilon$, $\delta\psi$, $\delta\omega$ are unknown in this geometrical range in different coordinate frames Eq. (6.3.15). Inserting this geometrical range into the observation equation Eq. (6.3.1), these unknowns can be solved for, provided there is a sufficient number of observations. However, the receiver clock error δt_R in Eq. (6.3.1) is also unknown. The satellite clock error δt^S can be determined from ephemeris data, whereas tropospheric and ionospheric path delays $\delta t^{S,Trop}_R$ and $\delta t^{S,Iono}_R$ can be modelled. Since GLONASS offers free and unobstructed access to the second frequency, dual-frequency ionospheric corrections can be applied alternatively.

This leaves seven unknown transformation parameters and one unknown receiver clock error to solve for. Thus, with range measurements to eight GLONASS satellites at one observation site, a complete set of transformation parameters could be determined. Besides having eight GLONASS satellites in view is rather unlikely in times of depleted GLONASS constellation, this one observation site will provide a poor geometry to separate origin and orientation parameters. As discussed in Section 5.6.1, this will lead to a set of parameters that are only valid at a small area around the observation site. More stations will add more strength to the geometry. However, each additional observation site does also mean an additional receiver and thus one more receiver clock error as a further unknown. For simultaneous observations at five stations, as was the case during the IfEN/IfAG/DLR measurement campaign, this totals in twelve unknowns. Thus, with two to three observations at each station, it was possible to determine the transformation parameters directly from pseudorange observations. With seven or more observation sites, which can easily be reached with data from the IGEX campaign, only two satellites in view per site are required. This is another bonus of this method for determining the transformation

parameters: For the conventional method of determining point coordinates in PZ-90 from GLONASS satellite observations and then comparing these coordinates to known coordinates in WGS84, requires at least four satellites visible at a station to calculate station coordinates. This approach of direct estimation of the transformation parameters may work with as little as two observations per site. Depending on the number of stations involved, at some sites only one observation may mathematically be sufficient to get a solution, but this one measurement contributes only to the station clock error.

The geometrical range Eq. (6.3.15) and with it the observation equation Eq. (6.3.1) is non-linear in the unknown transformation parameters. Before trying to solve a system of observation equations, the Eq. (6.3.15) has to be linearized. Therefore, this equation is expanded in a Taylor series around the approximate values $\Delta x_0,\ \Delta y_0,\ \Delta z_0,\ \delta s_0,\ \delta\varepsilon_0,\ \delta\psi_0,\ \delta\omega_0$:

$$\begin{aligned}\varrho_R^S(\Delta x,\Delta y,\Delta z,\delta s,\delta\varepsilon,\delta\psi,\delta\omega) = \varrho_{R,0}^S &+ \left.\frac{\partial\varrho_R^S}{\partial\Delta x}\right|_0\cdot(\Delta x-\Delta x_0) + \left.\frac{\partial\varrho_R^S}{\partial\Delta y}\right|_0\cdot(\Delta y-\Delta y_0)+\\ &\left.\frac{\partial\varrho_R^S}{\partial\Delta z}\right|_0\cdot(\Delta z-\Delta z_0) + \left.\frac{\partial\varrho_R^S}{\partial\delta s}\right|_0\cdot(\delta s-\delta s_0) + \left.\frac{\partial\varrho_R^S}{\partial\delta\varepsilon}\right|_0\cdot(\delta\varepsilon-\delta\varepsilon_0) +\\ &\left.\frac{\partial\varrho_R^S}{\partial\delta\psi}\right|_0\cdot(\delta\psi-\delta\psi_0) + \left.\frac{\partial\varrho_R^S}{\partial\delta\omega}\right|_0\cdot(\delta\omega-\delta\omega_0)\end{aligned} \tag{6.3.16}$$

with

$$\begin{aligned}\varrho_{R,0}^S &= \varrho_R^S(\Delta x_0,\Delta y_0,\Delta z_0,\delta s_0,\delta\varepsilon_0,\delta\psi_0,\delta\omega_0)\\ \left.\frac{\partial\varrho_R^S}{\partial d}\right|_0 &= \frac{\partial\varrho_R^S}{\partial d}(\Delta x_0,\Delta y_0,\Delta z_0,\delta s_0,\delta\varepsilon_0,\delta\psi_0,\delta\omega_0),\qquad d\in\{\Delta x,\ \Delta y,\ \Delta z,\delta s,\ \delta\varepsilon,\ \delta\psi,\ \delta\omega\}\end{aligned}$$

For reasons of simplicity, Eq. (6.3.15) is not differentiated directly. Rather it is preferred to differentiate Eq. (6.3.14) and then insert the results into the differentiated Eq. (6.3.12).

Differentiating Eq. (6.3.12) by any of the unknown transformation parameters d, $d\in\{\Delta x,\ \Delta y,\ \Delta z,\ \delta s,\ \delta\varepsilon,\ \delta\psi,\ \delta\omega\}$ yields:

$$\begin{aligned}\left.\frac{\partial\varrho_R^S}{\partial d}\right|_0 = &-\frac{\omega_E}{c}\cdot\left(x_{R,WGS(t_{RX})}\cdot\left.\frac{\partial y_{WGS(t_{TX})}^S}{\partial d}\right|_0 - y_{R,WGS(t_{RX})}\cdot\left.\frac{\partial x_{WGS(t_{TX})}^S}{\partial d}\right|_0\right)+\\ &\frac{1}{S_0}\cdot\left[\left(\frac{\omega_E}{c}\right)^2 s_0\cdot\left(x_{R,WGS(t_{RX})}\cdot\left.\frac{\partial y_{WGS(t_{TX})}^S}{\partial d}\right|_0 - y_{R,WGS(t_{RX})}\cdot\left.\frac{\partial x_{WGS(t_{TX})}^S}{\partial d}\right|_0\right) -\right.\\ &\left.\xi_0\cdot\left.\frac{\partial x_{WGS(t_{TX})}^S}{\partial d}\right|_0 - \upsilon_0\cdot\left.\frac{\partial y_{WGS(t_{TX})}^S}{\partial d}\right|_0 - \zeta_0\cdot\left.\frac{\partial z_{WGS(t_{TX})}^S}{\partial d}\right|_0\right]\end{aligned} \tag{6.3.17}$$

with

$$\begin{aligned}S_0 &= \sqrt{\left(\frac{\omega_E}{c}\right)^2\cdot s_0^2+\xi_0^2+\upsilon_0^2+\zeta_0^2}\\ s_0 &= x_{R,WGS(t_{RX})}\cdot y_{WGS(t_{TX}),0}^S - y_{R,WGS(t_{RX})}\cdot x_{WGS(t_{TX}),0}^S\\ &= x_{R,WGS(t_{RX})}\cdot\left[\Delta y_0+(1+\delta s_0)\cdot\left(-\delta\omega_0\cdot x_{PZ(t_{TX})}^S + y_{PZ(t_{TX})}^S + \delta\varepsilon_0\cdot z_{PZ(t_{TX})}^S\right)\right] -\\ &\quad y_{R,WGS(t_{RX})}\cdot\left[\Delta x_0+(1+\delta s_0)\cdot\left(x_{PZ(t_{TX})}^S + \delta\omega_0\cdot y_{PZ(t_{TX})}^S - \delta\psi_0\cdot z_{PZ(t_{TX})}^S\right)\right]\\ \xi_0 &= x_{R,WGS(t_{RX})} - x_{WGS(t_{TX}),0}^S\\ &= x_{R,WGS(t_{RX})} - \Delta x_0 - (1+\delta s_0)\cdot\left(x_{PZ(t_{TX})}^S + \delta\omega_0\cdot y_{PZ(t_{TX})}^S - \delta\psi_0\cdot z_{PZ(t_{TX})}^S\right)\\ \upsilon_0 &= y_{R,WGS(t_{RX})} - y_{WGS(t_{TX}),0}^S\\ &= y_{R,WGS(t_{RX})} - \Delta y_0 - (1+\delta s_0)\cdot\left(-\delta\omega_0\cdot x_{PZ(t_{TX})}^S + y_{PZ(t_{TX})}^S + \delta\varepsilon_0\cdot z_{PZ(t_{TX})}^S\right)\\ \zeta_0 &= z_{R,WGS(t_{RX})} - z_{WGS(t_{TX}),0}^S\\ &= z_{R,WGS(t_{RX})} - \Delta z_0 - (1+\delta s_0)\cdot\left(\delta\psi_0\cdot x_{PZ(t_{TX})}^S - \delta\varepsilon_0\cdot y_{PZ(t_{TX})}^S + z_{PZ(t_{TX})}^S\right)\end{aligned}$$

$$
\begin{aligned}
x^S_{WGS(t_{TX}),0} &= x^S_{WGS(t_{TX})}(\Delta x_0, \Delta y_0, \Delta z_0, \delta s_0, \delta\varepsilon_0, \delta\psi_0, \delta\omega_0) \\
y^S_{WGS(t_{TX}),0} &= y^S_{WGS(t_{TX})}(\Delta x_0, \Delta y_0, \Delta z_0, \delta s_0, \delta\varepsilon_0, \delta\psi_0, \delta\omega_0) \\
z^S_{WGS(t_{TX}),0} &= z^S_{WGS(t_{TX})}(\Delta x_0, \Delta y_0, \Delta z_0, \delta s_0, \delta\varepsilon_0, \delta\psi_0, \delta\omega_0)
\end{aligned}
$$

$$
\begin{aligned}
\left.\frac{\partial x^S_{WGS(t_{TX})}}{\partial d}\right|_0 &= \frac{\partial x^S_{WGS(t_{TX})}}{\partial d}(\Delta x_0, \Delta y_0, \Delta z_0, \delta s_0, \delta\varepsilon_0, \delta\psi_0, \delta\omega_0) \\
\left.\frac{\partial y^S_{WGS(t_{TX})}}{\partial d}\right|_0 &= \frac{\partial y^S_{WGS(t_{TX})}}{\partial d}(\Delta x_0, \Delta y_0, \Delta z_0, \delta s_0, \delta\varepsilon_0, \delta\psi_0, \delta\omega_0) \\
\left.\frac{\partial z^S_{WGS(t_{TX})}}{\partial d}\right|_0 &= \frac{\partial z^S_{WGS(t_{TX})}}{\partial d}(\Delta x_0, \Delta y_0, \Delta z_0, \delta s_0, \delta\varepsilon_0, \delta\psi_0, \delta\omega_0)
\end{aligned}
$$

From Eq. (6.3.14) one obtains the following partial derivatives:

$$
\begin{aligned}
\frac{\partial x^S_{WGS(t_{TX})}}{\partial \Delta x}(\Delta x_0, \Delta y_0, \Delta z_0, \delta s_0, \delta\varepsilon_0, \delta\psi_0, \delta\omega_0) &= 1 \\
\frac{\partial x^S_{WGS(t_{TX})}}{\partial \Delta y}(\Delta x_0, \Delta y_0, \Delta z_0, \delta s_0, \delta\varepsilon_0, \delta\psi_0, \delta\omega_0) &= 0 \\
\frac{\partial x^S_{WGS(t_{TX})}}{\partial \Delta z}(\Delta x_0, \Delta y_0, \Delta z_0, \delta s_0, \delta\varepsilon_0, \delta\psi_0, \delta\omega_0) &= 0 \\
\frac{\partial x^S_{WGS(t_{TX})}}{\partial \delta s}(\Delta x_0, \Delta y_0, \Delta z_0, \delta s_0, \delta\varepsilon_0, \delta\psi_0, \delta\omega_0) &= x^S_{PZ(t_{TX})} + \delta\omega_0 \cdot y^S_{PZ(t_{TX})} - \delta\psi_0 \cdot z^S_{PZ(t_{TX})} \\
\frac{\partial x^S_{WGS(t_{TX})}}{\partial \delta\varepsilon}(\Delta x_0, \Delta y_0, \Delta z_0, \delta s_0, \delta\varepsilon_0, \delta\psi_0, \delta\omega_0) &= 0 \\
\frac{\partial x^S_{WGS(t_{TX})}}{\partial \delta\psi}(\Delta x_0, \Delta y_0, \Delta z_0, \delta s_0, \delta\varepsilon_0, \delta\psi_0, \delta\omega_0) &= -(1+\delta s_0) \cdot z^S_{PZ(t_{TX})} \\
\frac{\partial x^S_{WGS(t_{TX})}}{\partial \delta\omega}(\Delta x_0, \Delta y_0, \Delta z_0, \delta s_0, \delta\varepsilon_0, \delta\psi_0, \delta\omega_0) &= (1+\delta s_0) \cdot y^S_{PZ(t_{TX})}
\end{aligned}
\tag{6.3.18}
$$

$$
\begin{aligned}
\frac{\partial y^S_{WGS(t_{TX})}}{\partial \Delta x}(\Delta x_0, \Delta y_0, \Delta z_0, \delta s_0, \delta\varepsilon_0, \delta\psi_0, \delta\omega_0) &= 0 \\
\frac{\partial y^S_{WGS(t_{TX})}}{\partial \Delta y}(\Delta x_0, \Delta y_0, \Delta z_0, \delta s_0, \delta\varepsilon_0, \delta\psi_0, \delta\omega_0) &= 1 \\
\frac{\partial y^S_{WGS(t_{TX})}}{\partial \Delta z}(\Delta x_0, \Delta y_0, \Delta z_0, \delta s_0, \delta\varepsilon_0, \delta\psi_0, \delta\omega_0) &= 0 \\
\frac{\partial y^S_{WGS(t_{TX})}}{\partial \delta s}(\Delta x_0, \Delta y_0, \Delta z_0, \delta s_0, \delta\varepsilon_0, \delta\psi_0, \delta\omega_0) &= -\delta\omega_0 \cdot x^S_{PZ(t_{TX})} + y^S_{PZ(t_{TX})} + \delta\varepsilon_0 \cdot z^S_{PZ(t_{TX})} \\
\frac{\partial y^S_{WGS(t_{TX})}}{\partial \delta\varepsilon}(\Delta x_0, \Delta y_0, \Delta z_0, \delta s_0, \delta\varepsilon_0, \delta\psi_0, \delta\omega_0) &= (1+\delta s_0) \cdot z^S_{PZ(t_{TX})} \\
\frac{\partial y^S_{WGS(t_{TX})}}{\partial \delta\psi}(\Delta x_0, \Delta y_0, \Delta z_0, \delta s_0, \delta\varepsilon_0, \delta\psi_0, \delta\omega_0) &= 0 \\
\frac{\partial y^S_{WGS(t_{TX})}}{\partial \delta\omega}(\Delta x_0, \Delta y_0, \Delta z_0, \delta s_0, \delta\varepsilon_0, \delta\psi_0, \delta\omega_0) &= -(1+\delta s_0) \cdot x^S_{PZ(t_{TX})}
\end{aligned}
\tag{6.3.19}
$$

$$
\begin{aligned}
\frac{\partial z^S_{WGS(t_{TX})}}{\partial \Delta x}(\Delta x_0, \Delta y_0, \Delta z_0, \delta s_0, \delta\varepsilon_0, \delta\psi_0, \delta\omega_0) &= 0 \\
\frac{\partial z^S_{WGS(t_{TX})}}{\partial \Delta y}(\Delta x_0, \Delta y_0, \Delta z_0, \delta s_0, \delta\varepsilon_0, \delta\psi_0, \delta\omega_0) &= 0 \\
\frac{\partial z^S_{WGS(t_{TX})}}{\partial \Delta z}(\Delta x_0, \Delta y_0, \Delta z_0, \delta s_0, \delta\varepsilon_0, \delta\psi_0, \delta\omega_0) &= 1 \\
\frac{\partial z^S_{WGS(t_{TX})}}{\partial \delta s}(\Delta x_0, \Delta y_0, \Delta z_0, \delta s_0, \delta\varepsilon_0, \delta\psi_0, \delta\omega_0) &= \delta\psi_0 \cdot x^S_{PZ(t_{TX})} - \delta\varepsilon_0 \cdot y^S_{PZ(t_{TX})} + z^S_{PZ(t_{TX})} \\
\frac{\partial z^S_{WGS(t_{TX})}}{\partial \delta\varepsilon}(\Delta x_0, \Delta y_0, \Delta z_0, \delta s_0, \delta\varepsilon_0, \delta\psi_0, \delta\omega_0) &= -(1+\delta s_0) \cdot y^S_{PZ(t_{TX})} \\
\frac{\partial z^S_{WGS(t_{TX})}}{\partial \delta\psi}(\Delta x_0, \Delta y_0, \Delta z_0, \delta s_0, \delta\varepsilon_0, \delta\psi_0, \delta\omega_0) &= (1+\delta s_0) \cdot x^S_{PZ(t_{TX})} \\
\frac{\partial z^S_{WGS(t_{TX})}}{\partial \delta\omega}(\Delta x_0, \Delta y_0, \Delta z_0, \delta s_0, \delta\varepsilon_0, \delta\psi_0, \delta\omega_0) &= 0
\end{aligned}
\tag{6.3.20}
$$

Inserting these partial derivatives into Eq. (6.3.17), one obtains for the partial derivatives of the geometrical distance:

$$
\left.\frac{\partial \varrho^S_R}{\partial \Delta x}\right|_0 = \frac{\omega_E}{c} \cdot y_{R,WGS(t_{RX})} - \frac{1}{S_0} \cdot \left[\left(\frac{\omega_E}{c}\right)^2 s_0 \cdot y_{R,WGS(t_{RX})} + \xi_0\right] \tag{6.3.21}
$$

$$
\left.\frac{\partial \varrho^S_R}{\partial \Delta y}\right|_0 = -\frac{\omega_E}{c} \cdot x_{R,WGS(t_{RX})} + \frac{1}{S_0} \cdot \left[\left(\frac{\omega_E}{c}\right)^2 s_0 \cdot x_{R,WGS(t_{RX})} - \upsilon_0\right] \tag{6.3.22}
$$

$$
\left.\frac{\partial \varrho^S_R}{\partial \Delta z}\right|_0 = -\frac{1}{S_0} \cdot \zeta_0 \tag{6.3.23}
$$

$$
\begin{aligned}
\left.\frac{\partial \varrho^S_R}{\partial \delta s}\right|_0 = -\frac{\omega_E}{c} \cdot \Big(& x_{R,WGS(t_{RX})} \cdot \left(-\delta\omega_0 \cdot x^S_{PZ(t_{TX})} + y^S_{PZ(t_{TX})} + \delta\varepsilon_0 \cdot z^S_{PZ(t_{TX})}\right) - \\
& y_{R,WGS(t_{RX})} \cdot \left(x^S_{PZ(t_{TX})} + \delta\omega_0 \cdot y^S_{PZ(t_{TX})} - \delta\psi_0 \cdot z^S_{PZ(t_{TX})}\right)\Big) + \\
& \frac{1}{S_0} \cdot \left[\left(\frac{\omega_E}{c}\right)^2 s_0 \cdot \left(x_{R,WGS(t_{RX})} \cdot \left(-\delta\omega_0 \cdot x^S_{PZ(t_{TX})} + y^S_{PZ(t_{TX})} + \delta\varepsilon_0 \cdot z^S_{PZ(t_{TX})}\right) - \right.\right. \\
& \left. y_{R,WGS(t_{RX})} \cdot \left(x^S_{PZ(t_{TX})} + \delta\omega_0 \cdot y^S_{PZ(t_{TX})} - \delta\psi_0 \cdot z^S_{PZ(t_{TX})}\right)\right) - \\
& \xi_0 \cdot \left(x^S_{PZ(t_{TX})} + \delta\omega_0 \cdot y^S_{PZ(t_{TX})} - \delta\psi_0 \cdot z^S_{PZ(t_{TX})}\right) - \\
& \upsilon_0 \cdot \left(-\delta\omega_0 \cdot x^S_{PZ(t_{TX})} + y^S_{PZ(t_{TX})} + \delta\varepsilon_0 \cdot z^S_{PZ(t_{TX})}\right) - \\
& \left. \zeta_0 \cdot \left(\delta\psi_0 \cdot x^S_{PZ(t_{TX})} - \delta\varepsilon_0 \cdot y^S_{PZ(t_{TX})} + z^S_{PZ(t_{TX})}\right)\right]
\end{aligned}
\tag{6.3.24}
$$

$$
\begin{aligned}
\left.\frac{\partial \varrho^S_R}{\partial \delta\varepsilon}\right|_0 = (1+\delta s_0) \cdot \Big\{ & -\frac{\omega_E}{c} \cdot x_{R,WGS(t_{RX})} \cdot z^S_{PZ(t_{TX})} + \\
& \frac{1}{S_0} \cdot \left[\left(\frac{\omega_E}{c}\right)^2 s_0 \cdot x_{R,WGS(t_{RX})} \cdot z^S_{PZ(t_{TX})} - \upsilon_0 \cdot z^S_{PZ(t_{TX})} + \zeta_0 \cdot y^S_{PZ(t_{TX})}\right]\Big\}
\end{aligned}
\tag{6.3.25}
$$

$$
\begin{aligned}
\left.\frac{\partial \varrho^S_R}{\partial \delta\psi}\right|_0 = (1+\delta s_0) \cdot \Big\{ & -\frac{\omega_E}{c} \cdot y_{R,WGS(t_{RX})} \cdot z^S_{PZ(t_{TX})} + \\
& \frac{1}{S_0} \cdot \left[\left(\frac{\omega_E}{c}\right)^2 s_0 \cdot y_{R,WGS(t_{RX})} \cdot z^S_{PZ(t_{TX})} + \xi_0 \cdot z^S_{PZ(t_{TX})} - \zeta_0 \cdot x^S_{PZ(t_{TX})}\right]\Big\}
\end{aligned}
\tag{6.3.26}
$$

$$
\begin{aligned}
\left.\frac{\partial \varrho^S_R}{\partial \delta\omega}\right|_0 = (1+\delta s_0) \cdot \Big\{ & \frac{\omega_E}{c} \cdot \left(x_{R,WGS(t_{RX})} \cdot x^S_{PZ(t_{TX})} + y_{R,WGS(t_{RX})} \cdot y^S_{PZ(t_{TX})}\right) - \\
& \frac{1}{S_0} \cdot \left[\left(\frac{\omega_E}{c}\right)^2 s_0 \cdot \left(x_{R,WGS(t_{RX})} \cdot x^S_{PZ(t_{TX})} + y_{R,WGS(t_{RX})} \cdot y^S_{PZ(t_{TX})}\right) + \right. \\
& \left. \xi_0 \cdot y^S_{PZ(t_{TX})} + \upsilon_0 \cdot x^S_{PZ(t_{TX})}\right]\Big\}
\end{aligned}
\tag{6.3.27}
$$

Having linearized Eq. (6.3.1) this way, it can be written in matrix form. With n stations contributing to the solution, each of which with observations to $m(i)$ satellites $i = 1, \ldots, n$, the resulting system of equations reads:

$$\vec{l} = \mathbf{A} \cdot \vec{x} \tag{6.3.28}$$

with

$$\vec{l} = \begin{pmatrix} PR_1^{1(1)} - \varrho_{1,0}^{1(1)} - c \cdot \delta t_{1,0} + c \cdot \delta t^{1(1)} - c \cdot \delta t_1^{1(1),Trop} - c \cdot \delta t_1^{1(1),Iono} \\ \vdots \\ PR_1^{m(1)} - \varrho_{1,0}^{m(1)} - c \cdot \delta t_{1,0} + c \cdot \delta t^{m(1)} - c \cdot \delta t_1^{m(1),Trop} - c \cdot \delta t_1^{m(1),Iono} \\ PR_2^{1(2)} - \varrho_{2,0}^{1(2)} - c \cdot \delta t_{2,0} + c \cdot \delta t^{1(2)} - c \cdot \delta t_2^{1(2),Trop} - c \cdot \delta t_2^{1(2),Iono} \\ \vdots \\ PR_\nu^{m(\nu)} - \varrho_{\nu,0}^{m(\nu)} - c \cdot \delta t_{\nu,0} + c \cdot \delta t^{m(\nu)} - c \cdot \delta t_\nu^{m(\nu),Trop} - c \cdot \delta t_\nu^{m(\nu),Iono} \\ PR_n^{1(n)} - \varrho_{n,0}^{1(n)} - c \cdot \delta t_{n,0} + c \cdot \delta t^{1(n)} - c \cdot \delta t_n^{1(n),Trop} - c \cdot \delta t_n^{1(n),Iono} \\ \vdots \\ PR_n^{m(n)} - \varrho_{n,0}^{m(n)} - c \cdot \delta t_{n,0} + c \cdot \delta t^{m(n)} - c \cdot \delta t_n^{m(n),Trop} - c \cdot \delta t_n^{m(n),Iono} \end{pmatrix}$$

the vector of known values, including the approximations for transformation parameters and receiver clock offsets,

$$\mathbf{A} = \begin{pmatrix} \left.\frac{\partial \varrho_1^{1(1)}}{\partial \Delta x}\right|_0 & \left.\frac{\partial \varrho_1^{1(1)}}{\partial \Delta y}\right|_0 & \left.\frac{\partial \varrho_1^{1(1)}}{\partial \Delta z}\right|_0 & \left.\frac{\partial \varrho_1^{1(1)}}{\partial \delta s}\right|_0 & \left.\frac{\partial \varrho_1^{1(1)}}{\partial \delta \varepsilon}\right|_0 & \left.\frac{\partial \varrho_1^{1(1)}}{\partial \delta \psi}\right|_0 & \left.\frac{\partial \varrho_1^{1(1)}}{\partial \delta \omega}\right|_0 & 1 & 0 & \ldots & 0 & 0 \\ \vdots & \vdots & \vdots & \vdots & \vdots & \vdots & \vdots & \vdots & \vdots & \vdots & \vdots & \vdots \\ \left.\frac{\partial \varrho_1^{m(1)}}{\partial \Delta x}\right|_0 & \left.\frac{\partial \varrho_1^{m(1)}}{\partial \Delta y}\right|_0 & \left.\frac{\partial \varrho_1^{m(1)}}{\partial \Delta z}\right|_0 & \left.\frac{\partial \varrho_1^{m(1)}}{\partial \delta s}\right|_0 & \left.\frac{\partial \varrho_1^{m(1)}}{\partial \delta \varepsilon}\right|_0 & \left.\frac{\partial \varrho_1^{m(1)}}{\partial \delta \psi}\right|_0 & \left.\frac{\partial \varrho_1^{m(1)}}{\partial \delta \omega}\right|_0 & 1 & 0 & \ldots & 0 & 0 \\ \left.\frac{\partial \varrho_2^{1(2)}}{\partial \Delta x}\right|_0 & \left.\frac{\partial \varrho_2^{1(2)}}{\partial \Delta y}\right|_0 & \left.\frac{\partial \varrho_2^{1(2)}}{\partial \Delta z}\right|_0 & \left.\frac{\partial \varrho_2^{1(2)}}{\partial \delta s}\right|_0 & \left.\frac{\partial \varrho_2^{1(2)}}{\partial \delta \varepsilon}\right|_0 & \left.\frac{\partial \varrho_2^{1(2)}}{\partial \delta \psi}\right|_0 & \left.\frac{\partial \varrho_2^{1(2)}}{\partial \delta \omega}\right|_0 & 0 & 1 & \ldots & 0 & 0 \\ \vdots & \vdots & \vdots & \vdots & \vdots & \vdots & \vdots & \vdots & \vdots & \vdots & \vdots & \vdots \\ \left.\frac{\partial \varrho_\nu^{m(\nu)}}{\partial \Delta x}\right|_0 & \left.\frac{\partial \varrho_\nu^{m(\nu)}}{\partial \Delta y}\right|_0 & \left.\frac{\partial \varrho_\nu^{m(\nu)}}{\partial \Delta z}\right|_0 & \left.\frac{\partial \varrho_\nu^{m(\nu)}}{\partial \delta s}\right|_0 & \left.\frac{\partial \varrho_\nu^{m(\nu)}}{\partial \delta \varepsilon}\right|_0 & \left.\frac{\partial \varrho_\nu^{m(\nu)}}{\partial \delta \psi}\right|_0 & \left.\frac{\partial \varrho_\nu^{m(\nu)}}{\partial \delta \omega}\right|_0 & 0 & 0 & \ldots & 1 & 0 \\ \left.\frac{\partial \varrho_n^{1(n)}}{\partial \Delta x}\right|_0 & \left.\frac{\partial \varrho_n^{1(n)}}{\partial \Delta y}\right|_0 & \left.\frac{\partial \varrho_n^{1(n)}}{\partial \Delta z}\right|_0 & \left.\frac{\partial \varrho_n^{1(n)}}{\partial \delta s}\right|_0 & \left.\frac{\partial \varrho_n^{1(n)}}{\partial \delta \varepsilon}\right|_0 & \left.\frac{\partial \varrho_n^{1(n)}}{\partial \delta \psi}\right|_0 & \left.\frac{\partial \varrho_n^{1(n)}}{\partial \delta \omega}\right|_0 & 0 & 0 & \ldots & 0 & 1 \\ \vdots & \vdots & \vdots & \vdots & \vdots & \vdots & \vdots & \vdots & \vdots & \vdots & \vdots & \vdots \\ \left.\frac{\partial \varrho_n^{m(n)}}{\partial \Delta x}\right|_0 & \left.\frac{\partial \varrho_n^{m(n)}}{\partial \Delta y}\right|_0 & \left.\frac{\partial \varrho_n^{m(n)}}{\partial \Delta z}\right|_0 & \left.\frac{\partial \varrho_n^{m(n)}}{\partial \delta s}\right|_0 & \left.\frac{\partial \varrho_n^{m(n)}}{\partial \delta \varepsilon}\right|_0 & \left.\frac{\partial \varrho_n^{m(n)}}{\partial \delta \psi}\right|_0 & \left.\frac{\partial \varrho_n^{m(n)}}{\partial \delta \omega}\right|_0 & 0 & 0 & \ldots & 0 & 1 \end{pmatrix}$$

the design matrix with the partial derivatives from Eqs. (6.3.21) to (6.3.27), and

$$\vec{l} = \begin{pmatrix} \Delta x - \Delta x_0 \\ \Delta y - \Delta y_0 \\ \Delta z - \Delta z_0 \\ \delta s - \delta s_0 \\ \delta \varepsilon - \delta \varepsilon_0 \\ \delta \psi - \delta \psi_0 \\ \delta \omega - \delta \omega_0 \\ c \cdot (\delta t_1 - \delta t_{1,0}) \\ c \cdot (\delta t_2 - \delta t_{2,0}) \\ \vdots \\ c \cdot (\delta t_\nu - \delta t_{\nu,0}) \\ c \cdot (\delta t_n - \delta t_{n,0}) \end{pmatrix}$$

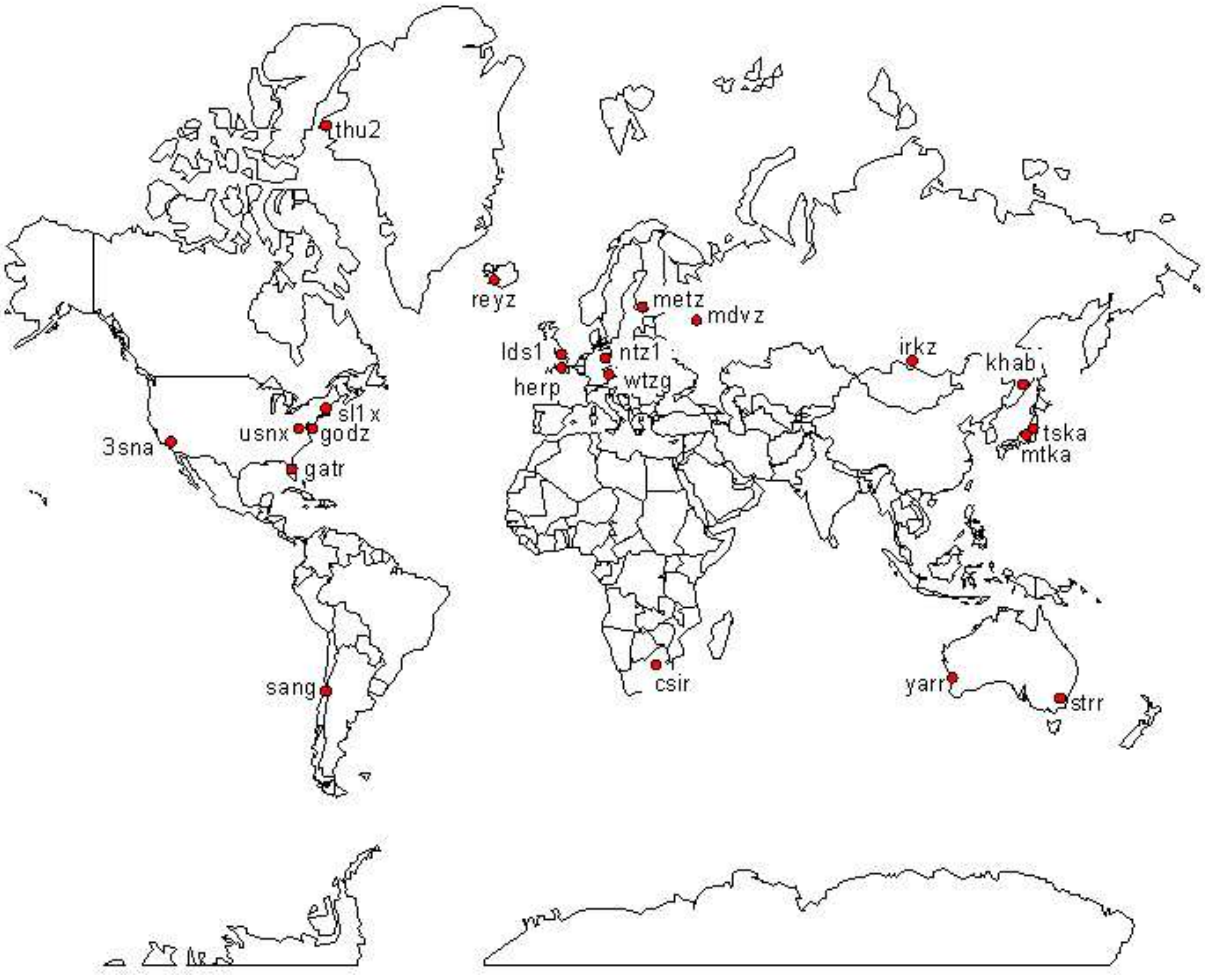

Figure 6.2: Observation sites used for direct estimation of transformation parameters.

the vector of the unknowns, containing the transformation parameters and the receiver clock errors at the observation stations. In these expressions, the abbreviation $\nu = n - 1$ was introduced.

This system of equations can be solved epoch-wise with the conventional means of estimation, e.g. least-squares adjustment or a Kalman filter.

As already stated above, measurement data from the IGEX-98 experiment were used to calculate a set of transformation parameters directly from GLONASS range measurements. Sixteen days of observation data from January 1999, taken from 21 globally distributed observation sites were analyzed. The distribution of observation sites and their coordinates used are given in Figure 6.2 and Table 6.10, respectively. Closely spaced observation sites (e.g. the wtzg/ntz1 pair) were used alternatively in case there were no observations available for the primary site on a particular day. Thus, not all of the stations were used all the time.

Wherever possible, the ionospheric free linear combination of L_1 and L_2 measured pseudoranges were used in the estimation of transformation parameters. Where there were no dual-frequency measurements available, the GPS Klobuchar model, adapted to GLONASS frequencies, was used to reduce the ionospheric path delay.

To reduce the influence of measurement noise and multipath, if present, carrier smoothing of the pseudoranges was applied before the linear combination was formed. To compensate for the tropospheric path delay, a simple model was used that is not depending on actual weather data, but uses empirical weather data, depending on latitude/longitude of the observation site, time of year and time of day. This model is described in (*RTCA, 1998*).

Station	**Name**	x-Coordinate [m]	y-Coordinate [m]	z-Coordinate [m]
3sna	3S Navigation	−2482980.5858	−4696608.3467	3517630.9478
csir	Pretoria	5063683.4628	2723896.1933	−2754444.9755
gatr	Gainesville	738693.0451	−5498293.3041	3136519.5906
godz	Goddard SFC	1130773.8333	−4831253.5816	3994200.4106
herp	Herstmonceux	4033454.7310	23664.4484	4924309.0139
irkz	Irkutsk	−968310.0957	3794414.4427	5018182.1289
khab	Khabarovsk	−2995266.3617	2990444.6917	4755575.9808
lds1	Leeds	3773063.6912	−102444.0029	5124373.4582
mdvz	Mendeleevo	2845461.7803	2160957.5040	5265989.0378
metz	Metsahovi	2892569.9510	1311843.5724	5512634.4596
mtka	Mitaka	−3947762.7194	3364399.8226	3699428.5206
ntz1	Neustrelitz	3718450.4080	863437.7680	5092635.9280
reyz	Reykjavik	2587383.7759	−1043032.7094	5716564.4408
sang	Santiago de Chile	1769719.8283	−5044542.6396	−3468352.4705
sl1x	MIT Lincoln Lab	1513678.5253	−4463031.6196	4283433.5383
strr	Stromlo	−4467102.3957	2683039.4598	−3666949.7020
thu2	Thule	538093.6860	−1389088.0068	6180979.1953
tska	Tsukuba	−3957203.2551	3310203.1701	3737704.4658
usnx	US Naval Observatory	1112158.1709	−4842852.8153	3985491.4382
wtzg	Wettzell	4075580.1058	931855.2874	4801568.3246
yarr	Yarragadee	−2389024.5495	5043315.4590	−3078534.1138

Table 6.10: ITRF-96 coordinates of observation sites used in direct estimation of transformation parameters.

For each of the sixteen days, daily solutions of the transformation parameters were estimated in a Kalman filter. These daily solutions were averaged to obtain a set of transformation parameters:

Parameter	Δx [m]	Δy [m]	Δz [m]	δs [10^{-9}]	$\delta\varepsilon$ [10^{-6}]	$\delta\psi$ [10^{-6}]	$\delta\omega$ [10^{-6}]
Value	0.404	0.357	−0.476	−2.614	0.118	−0.058	−1.664
Std. Dev.	1.039	1.147	0.456	63.860	0.090	0.112	0.170

These results are consistent with previously released transformation parameters (*Misra et al., 1996a*; *Mitrikas et al., 1998*; *Roßbach et al., 1996*) insofar as a rotation around the z-axis in the order of $\delta\omega = -1.6 \cdot 10^{-6} \ldots - 1.9 \cdot 10^{-6}$ can be regarded as the most significant parameter. Average values of the other parameters are in the order of or even less than the standard deviation of the daily solutions.

To verify these transformation parameters, a selection of the observation data was processed again, this time in positioning mode. The station coordinates in WGS84 were computed from the GLONASS measurements, where the estimated set of transformation parameters was applied to convert GLONASS satellite positions from PZ-90 to WGS84 before the computation of station coordinates. Positioning was done in single-point mode, using the ionospheric free linear combination of carrier-smoothed L_1 and L_2 pseudoranges, wherever available. Again, daily solutions (for the station coordinates) were computed and averaged.

Daily solutions using the transformation introduced above were close to the solutions using the transformation given in (*Roßbach et al., 1996*). Distances usually were in the order of 1 m. However, the solutions calculated with the transformation above usually were closer to the known ITRF-96 coordinates of the observation stations. The average deviations from the known position in ITRF-96 using the set of transformation parameters introduced above were smaller than the average deviations resulting from positioning with the set of transformation parameters from (*Roßbach et al., 1996*). The results showed a slight degradation in the x- and y-coordinates, but also a significant improvement in the z-coordinate. Using the transformation introduced above, the average deviation from the known x- and y-coordinates was slightly larger than with the transformation from (*Roßbach et al., 1996*). The average deviation in the x-coordinate was 0.327 m with this transformation, compared to 0.229 m using (*Roßbach et al., 1996*). In the y-component, the deviations were 0.536 m and 0.225 m, respectively. But for the z-coordinate, the average deviation was significantly smaller (0.836 m compared to 1.397 m with (*Roßbach et al., 1996*)). The overall distance to the known coordinates was reduced from 1.433 m using (*Roßbach et al., 1996*) to 1.046 m.

7 Satellite Clock and Orbit Determination

7.1 Satellite Clock Offset

The first step towards the computation of the user's position always is the determination of the time of signal transmission. A GLONASS (or GPS) receiver correlates the incoming satellite signal with an internally created signal, thus determining the signal travel time. The signal travel time, multiplied by the speed of signal propagation (speed of light in vacuum) then yields the measured (pseudo-)range to this satellite, which is output by the receiver as an observable.

Given the time of signal reception in a receiver and the signal travel time (or pseudorange), the time of signal transmission at the satellite can then be determined as

$$t_{TX} = t_{RX} - \Delta t_{tr} = t_{RX} - PR/c \tag{7.1.1}$$

with

t_{TX}	Time of signal transmission at satellite
t_{RX}	Time of signal reception at receiver
Δt_{tr}	Signal travel time
PR	Measured pseudorange
c	Speed of light in vacuum

The time of signal reception is read by the receiver from its own clock and thus is given in the receiver time frame. Signal generation in the satellite is governed by the satellite clock, running in its own time frame. Therefore, the measured signal travel time is only an approximation of the true signal travel time. That's why the range derived from the measurement of the signal travel time is called "pseudo"-range.

To eliminate the effects of different time frames, a unique time frame has to be employed – GLONASS system time. GLONASS ephemerides contain parameters to determine the offset of the time frame of the transmitting satellite to system time (*ICD-GLONASS, 1995*; *ICD-GLONASS, 1998*). These parameters are the time scale offset to system time τ and the relative difference of the frequency to the nominal frequency $\gamma = (f - f_{nom})/f_{nom}$. Applying these parameters, GLONASS system time t_{Sys} can be computed from satellite time t_{Sat} using the relation

$$t_{Sys}(t_{Sat}) = t_{Sat} + \tau(t_b) - \gamma(t_b) \cdot (t - t_b) \tag{7.1.2}$$

with t_b being the reference time of the satellite ephemeris data and t the time, for which GLONASS system time is desired, $t = t_{Sat}$. Reference time t_b is given in system time scale. Thus, in a strict sense t also must be given in system time scale. But when determining the satellite clock offset in a receiver or post-processing software, t is given in satellite time scale. However, differences between clock offsets computed with t in system time scale and t in satellite time scale are negligibly small, in the order of 10^{-40} s. Therefore, it is sufficient to use the time in satellite time scale: $t = t_{Sat}$. Eq. (7.1.2) has to be applied to the observed time of signal transmission.

L_1 and L_2 signals may be transmitted by the satellite at slightly different instances in time due to different hardware delays in the equipment used onboard the satellite. Dual-frequency users therefore must compute different satellite clock offsets for their L_1 and L_2 pseudorange measurements. However, this is not taken care of by the GLONASS ICD (*ICD-GLONASS, 1995*). This definitely is one of the improvements of the GLONASS-M satellites. In their navigation message, they will include the difference $\Delta\tau_n$ between the equipment delays in L_1 and L_2 bands: $\Delta\tau_n = t_{f2} - t_{f1}$, where t_{f1} and t_{f2} are the respective delays (*ICD-GLONASS, 1998*).

For an L_1 pseudorange measurement, GLONASS system time is then still computed according to Eq. (7.1.2), whereas for an L_2 pseudorange measurement this inter-frequency bias must be considered:

$$t_{Sys,L_1}(t_{Sat}) = t_{Sat} + \tau(t_b) - \gamma(t_b) \cdot (t - t_b) \tag{7.1.3}$$

$$t_{Sys,L_2}(t_{Sat}) = t_{Sys,L_1}(t_{Sat}) - \Delta\tau_n \tag{7.1.4}$$

The parameter γ does not only contain the effects of the satellite clock drift, but also all gravitational and relativistic effects. Therefore, a separate compensation for these effects is not necessary, contrary to GPS.

The offset of the receiver clock with respect to GLONASS system time usually is not known a priori. Therefore, this receiver clock error is treated as an additional unknown, which is to be estimated in the course of the position determination. This additional unknown necessitates the observation of a fourth satellite besides the three measurements required for the x-, y- and z-coordinates of the user position.

7.2 Satellite Orbit Determination

7.2.1 Orbital Force Model

Given the time of signal transmission, the next step is to determine the satellite position at that point of time.

GLONASS broadcast ephemerides contain the satellite position in PZ-90 at the reference time t_b, together with the satellite velocity and its acceleration due to luni-solar attraction. These data usually are updated every 30 minutes and refer to the center of this 30 minute interval. To obtain the satellite position at an epoch other than this reference time (within the validity period of data), the satellite's equations of motion have to be integrated, using the given values as initial values.

In compliance with Newton's laws of motion, the motion of a satellite orbiting the Earth is determined by the forces acting on that satellite. The primary force acting is that caused by Earth's gravity field potential. This potential can be expressed as

$$V = \frac{\mu}{r} + U \tag{7.2.1}$$

with

V	Total gravitational potential
μ	Earth's gravitational constant
r	Distance of satellite to center of Earth
U	Non-spherical part of Earth's gravitational potential

The value for μ is adopted from the PZ-90 reference frame (see Table 3.1). Considering only the spherical part of the gravitational potential $V = \mu/r$ and neglecting also all non-gravitational forces on the satellite, its motion would be pure Keplerian. But these other forces cannot be neglected, thus the motion of the satellite deviates from a Kepler ellipse. To compensate for this, GPS ephemerides contain correctional parameters to be applied to an assumed Keplerian orbit. The designers of the GLONASS system chose a different approach by transmitting in the ephemeris data satellite position, velocity and acceleration vectors and having the user integrate the equations of motion with these vectors as initial values, as stated above.

According to (*Heiskanen and Moritz, 1967*), expansion of the non-spherical part U of the gravitational potential into spherical harmonics gives

$$U = \frac{\mu}{r} \sum_{n=2}^{\infty} \sum_{m=0}^{n} \left(\frac{a_E}{r}\right)^n P_{nm}(\cos\theta) \cdot (c_{nm} \cos m\lambda + s_{nm} \sin m\lambda) \tag{7.2.2}$$

with

a_E	Earth's equatorial radius
$r,\ \lambda,\ \theta$	Earth-fixed polar coordinates (radius, longitude, colatitude)
$n,\ m$	Degree and order of spherical harmonic expansion
$P_{nm}(\cos\theta)$	Associated Legendre functions
$c_{nm},\ s_{nm}$	Spherical harmonic coefficients

The value for a_E is adopted from the PZ-90 reference frame (see Table 3.1).

Since Earth's gravitational potential is in first approximation rotationally symmetric, i.e. independent of λ, the zonal harmonics ($m = 0$ in Eq. (7.2.2)), which cause parts of the gravitational potential independent of λ, are much more significant to satellite motion than the tesseral ($0 < m < n$) and the sectorial ($m = n$) harmonics. It can therefore be assumed that the influence of tesseral and sectorial harmonics is insignificant over a short time span of orbit integration. Thus, Eq. (7.2.2) can be simplified to

$$U = \frac{\mu}{a_E} \sum_{n=2}^{\infty} \left(\frac{a_E}{r}\right)^{n+1} c_{n0} \cdot P_{n0}(\cos\theta) \tag{7.2.3}$$

Besides the gravitational force, other forces are acting on a satellite. (*Spilker, 1996*) summarizes the approximate perturbing forces acting on GPS satellites as:

Source	Max. perturbing acceleration $[m/s^2]$	Max. excursion growth in 1h $[m]$
Spherical Earth	$5.65 \cdot 10^{-1}$	—
Second zonal harmonic	$5.3 \cdot 10^{-5}$	300
Fourth zonal harmonic	10^{-7}	0.6
Gravity anomalies	10^{-8}	0.06
Lunar gravity	$5.5 \cdot 10^{-6}$	40
Solar gravity	$3 \cdot 10^{-6}$	20
Solar radiation pressure	10^{-7}	0.6
All other forces	10^{-8}	0.06

In first approximation considering the forces acting on a GLONASS satellite as identical to those acting on GPS satellites, it can be seen that the second zonal harmonic, resulting from Earth's oblateness, dominates the perturbing forces. Effects of lunar and solar gravitation are one order of magnitude less than the second zonal harmonic, all other terms are negligible against these. Thus, it is justifiable to rewrite Eq. (7.2.3) with only the second order term:

$$U = \frac{\mu a_E^2}{r^3} c_{20} \cdot \left(\frac{3}{2}\cos^2\theta - \frac{1}{2}\right) \tag{7.2.4}$$

where the Legendre polynomial $P_{20}(\cos\theta) = 3/2\ \cos^2\theta - 1/2$ was substituted. Therewith the total gravitational potential becomes

$$V = \frac{\mu}{r} + \frac{1}{2}\frac{\mu a_E^2}{r^3} c_{20} \cdot \left(3\cos^2\theta - 1\right) \tag{7.2.5}$$

The satellite acceleration in Cartesian coordinates $\ddot{\vec{x}}$ due to the gravitational potential is defined as

$$\ddot{\vec{x}} = \nabla V \tag{7.2.6}$$

with its components

$$\ddot{\vec{x}}_i = \frac{dV}{dx_i} = \frac{\partial V}{\partial r}\frac{\partial r}{\partial x_i} + \frac{\partial V}{\partial \lambda}\frac{\partial \lambda}{\partial x_i} + \frac{\partial V}{\partial \theta}\frac{\partial \theta}{\partial x_i} \tag{7.2.7}$$

With the partial derivatives

$$\begin{aligned}
\frac{\partial V}{\partial r} &= -\frac{\mu}{r^2} - \frac{3}{2}\frac{\mu a_E^2}{r^4} c_{20} \cdot \left(3\cos^2\theta - 1\right) \\
\frac{\partial V}{\partial \lambda} &= 0 \\
\frac{\partial V}{\partial \theta} &= -3\frac{\mu a_E^2}{r^3} c_{20} \cdot \cos\theta \sin\theta
\end{aligned}$$

and

$$\begin{aligned}
\frac{\partial r}{x} &= \frac{x}{r} & \frac{\partial r}{y} &= \frac{y}{r} & \frac{\partial r}{z} &= \frac{z}{r} \\
\frac{\partial \theta}{x} &= \frac{1}{\sin\theta} \cdot \frac{xz}{r^3} & \frac{\partial \theta}{y} &= \frac{1}{\sin\theta} \cdot \frac{yz}{r^3} & \frac{\partial \theta}{z} &= -\frac{1}{\sin\theta} \cdot \frac{r^2 - z^2}{r^3}
\end{aligned}$$

the satellite acceleration due to the gravitational potential is obtained as

$$\begin{aligned}
\ddot{x} &= -\frac{\mu}{r^3}\cdot x + \frac{3}{2}c_{20}\frac{\mu a_E^2}{r^5}\cdot x\cdot\left(1-5\frac{z^2}{r^2}\right)\\
\ddot{y} &= -\frac{\mu}{r^3}\cdot y + \frac{3}{2}c_{20}\frac{\mu a_E^2}{r^5}\cdot y\cdot\left(1-5\frac{z^2}{r^2}\right)\\
\ddot{z} &= -\frac{\mu}{r^3}\cdot z + \frac{3}{2}c_{20}\frac{\mu a_E^2}{r^5}\cdot z\cdot\left(3-5\frac{z^2}{r^2}\right)
\end{aligned} \tag{7.2.8}$$

Assuming the acceleration of the satellite due to lunar and solar gravitation to be constant over a short time span of integration $\ddot{x}_{LS},\ \ddot{y}_{LS},\ \ddot{z}_{LS}$ and neglecting all other forces, as stated above, the total acceleration of a GLONASS satellite can then be written as

$$\begin{aligned}
\ddot{x} &= -\frac{\mu}{r^3}\cdot x + \frac{3}{2}c_{20}\frac{\mu a_E^2}{r^5}\cdot x\cdot\left(1-5\frac{z^2}{r^2}\right)+\ddot{x}_{LS}\\
\ddot{y} &= -\frac{\mu}{r^3}\cdot y + \frac{3}{2}c_{20}\frac{\mu a_E^2}{r^5}\cdot y\cdot\left(1-5\frac{z^2}{r^2}\right)+\ddot{y}_{LS}\\
\ddot{z} &= -\frac{\mu}{r^3}\cdot z + \frac{3}{2}c_{20}\frac{\mu a_E^2}{r^5}\cdot z\cdot\left(3-5\frac{z^2}{r^2}\right)+\ddot{z}_{LS}
\end{aligned} \tag{7.2.9}$$

Eq. (7.2.9) is valid only in an inertial system, since Newton's laws of motion as addressed above are only valid in inertial systems. The PZ-90 reference frame of GLONASS, however, is an ECEF system, rotating with the Earth. To determine the satellite coordinates in PZ-90, one could integrate the satellite's equations of motion in the inertial system and then transform the obtained coordinates to the PZ-90 coordinate system. But it is also possible to rewrite the equations of motion in the ECEF coordinate system.

The transformation from an inertial system to an Earth-fixed system is performed as a series of rotations (cf. e.g. (*Hofmann-Wellenhof et al., 1993*)):

$$\vec{x}_{EF} = \mathbf{R}^M\cdot\mathbf{R}^R\cdot\mathbf{R}^N\cdot\mathbf{R}^P\cdot\vec{x}_{INS} \tag{7.2.10}$$

with

$\vec{x}_{INS}$	Coordinates in inertial system
$\vec{x}_{EF}$	Coordinates in ECEF system
$\mathbf{R}^M$	Rotation matrix representing polar motion
$\mathbf{R}^R$	Rotation matrix representing Earth rotation
$\mathbf{R}^N$	Rotation matrix representing nutation of Earth
$\mathbf{R}^P$	Rotation matrix representing precession of Earth

Polar motion, nutation and precession of Earth are very slow processes, with large time constants. So over a small integration interval, they will not significantly contribute to the deviation of the Earth-fixed system from the inertial system. Only Earth rotation, which takes place around the z-axis of the ECEF frame (see definition of the PZ-90 frame), will contribute to this. Accounting for the Coriolis forces caused by this rotation, the satellite's equations of motion finally can be written as

$$\begin{aligned}
\frac{dx}{dt} &= \dot{x}\\
\frac{dy}{dt} &= \dot{y}\\
\frac{dz}{dt} &= \dot{z}\\
\frac{d\dot{x}}{dt} &= -\frac{\mu}{r^3}\cdot x + \frac{3}{2}c_{20}\frac{\mu a_E^2}{r^5}\cdot x\cdot\left(1-5\frac{z^2}{r^2}\right)+\ddot{x}_{LS}+\omega_E^2\cdot x+2\omega_E\cdot\dot{y}\\
\frac{d\dot{y}}{dt} &= -\frac{\mu}{r^3}\cdot y + \frac{3}{2}c_{20}\frac{\mu a_E^2}{r^5}\cdot y\cdot\left(1-5\frac{z^2}{r^2}\right)+\ddot{y}_{LS}+\omega_E^2\cdot y-2\omega_E\cdot\dot{x}\\
\frac{d\dot{z}}{dt} &= -\frac{\mu}{r^3}\cdot z + \frac{3}{2}c_{20}\frac{\mu a_E^2}{r^5}\cdot z\cdot\left(3-5\frac{z^2}{r^2}\right)+\ddot{z}_{LS}
\end{aligned} \tag{7.2.11}$$

with

$x,\ y,\ z$	Satellite coordinates
$\dot{x},\ \dot{y},\ \dot{z}$	Satellite velocities
$\ddot{x}_{LS},\ \ddot{y}_{LS},\ \ddot{z}_{LS}$	Luni-solar acceleration
$r = \sqrt{x^2 + y^2 + z^2}$	Distance of satellite to center of Earth
$\mu = 3.9860044 \cdot 10^{14}\ \mathrm{m}^3/\mathrm{s}^2$	Earth's gravitational constant
$c_{20} = -1.08263 \cdot 10^{-3}$	Second zonal coefficient
$a_E = 6378136\ \mathrm{m}$	Earth's equatorial radius
$\omega_E = 7.292115 \cdot 10^{-5}\ \mathrm{s}^{-1}$	Earth's rotation rate

This is also the way the GLONASS ICD (*ICD-GLONASS, 1995*) formulates the equations of motion. To obtain the satellite position at a specified time, these equations have to be integrated. To accomplish this, GLONASS satellites in their ephemeris data transmit the satellite coordinates $x,\ y,\ z$, velocities $\dot{x},\ \dot{y},\ \dot{z}$ and luni-solar acceleration $\ddot{x}_{LS},\ \ddot{y}_{LS},\ \ddot{z}_{LS}$ at the reference time t_b. These values are then used as initial values in the integration of Eq. (7.2.11). The values for $\mu,\ c_{20},\ a_E,\ \omega_E$ are adopted from the PZ-90 reference frame (see Table 3.1).

7.2.2 Orbit Integration

Even after applying all the approximations and simplifications introduced above, equations (7.2.11) are still too complex to solve analytically. Therefore, integration is performed numerically. The GLONASS ICD (*ICD-GLONASS, 1995*) recommends using a four step Runge-Kutta method for the integration. This method can be briefly summarized as the following (*Jeltsch, 1987*):

Given a system of differential equations $\dot{\vec{X}} = \vec{f}(t, \vec{X})$ with the initial values $\vec{X}_0 = \vec{X}(t_0)$, system state $\vec{X}_{n+1} = \vec{X}(t_{n+1})$ can be computed numerically from state $\vec{X}_n = \vec{X}(t_n)$ using the scheme

$$\begin{aligned}
\vec{X}_{n+1} &= \vec{X}_n + \frac{h}{6} \cdot \left[\vec{f}(t_n, \vec{Y}_1) + 2\vec{f}(t_n + \frac{h}{2}, \vec{Y}_2) + 2\vec{f}(t_n + \frac{h}{2}, \vec{Y}_3) + \vec{f}(t_n + h, \vec{Y}_4) \right] \\
\vec{Y}_1 &= \vec{X}_n \\
\vec{Y}_2 &= \vec{X}_n + \frac{h}{2}\vec{f}(t_n, \vec{Y}_1) \\
\vec{Y}_3 &= \vec{X}_n + \frac{h}{2}\vec{f}(t_n + \frac{h}{2}, \vec{Y}_2) \\
\vec{Y}_4 &= \vec{X}_n + h\vec{f}(t_n + \frac{h}{2}, \vec{Y}_3)
\end{aligned} \tag{7.2.12}$$

with $h = t_{n+1} - t_n$ being the step width of the integration.

Denoting the vector of the requested orbit parameters $(x, y, z, \dot{x}, \dot{y}, \dot{z})^T$ as the state vector $\vec{X}$ – and therewith $(\dot{x}, \dot{y}, \dot{z}, \ddot{x}, \ddot{y}, \ddot{z})^T$ as $\dot{\vec{X}}$ –, system (7.2.11) is already given in the form $\dot{\vec{X}} = \vec{f}(t, \vec{X})$ with no explicit dependence on t: $\dot{\vec{X}} = \vec{f}(\vec{X})$. Thus, the scheme of Eq. (7.2.12) simplifies to

$$\begin{aligned}
\vec{X}_{n+1} &= \vec{X}_n + \frac{h}{6} \cdot \left[\vec{f}(\vec{Y}_1) + 2\vec{f}(\vec{Y}_2) + 2\vec{f}(\vec{Y}_3) + \vec{f}(\vec{Y}_4) \right] = \vec{X}_n + \frac{h}{6} \cdot \left[\vec{D}_1 + 2\vec{D}_2 + 2\vec{D}_3 + \vec{D}_4 \right] \\
\vec{Y}_1 &= \vec{X}_n \\
\vec{Y}_2 &= \vec{X}_n + \frac{h}{2}\vec{f}(\vec{Y}_1) = \vec{X}_n + \frac{h}{2}\vec{D}_1 \\
\vec{Y}_3 &= \vec{X}_n + \frac{h}{2}\vec{f}(\vec{Y}_2) = \vec{X}_n + \frac{h}{2}\vec{D}_2 \\
\vec{Y}_4 &= \vec{X}_n + h\vec{f}(\vec{Y}_3) = \vec{X}_n + h\vec{D}_3
\end{aligned} \tag{7.2.13}$$

with $\vec{D}_i = \vec{f}(\vec{Y}_i) = \dot{\vec{Y}}_i$ being the derivatives of the intermediate values. In this form, the scheme of Eq. (7.2.13) can immediately be applied to the equations of motion Eq. (7.2.11):

1. Compute $\vec{D}_1 = \vec{f}(\vec{X}_n)$

2. Compute $\vec{D}_2 = \vec{f}(\vec{X}_n + \frac{h}{2}\vec{D}_1)$
3. Compute $\vec{D}_3 = \vec{f}(\vec{X}_n + \frac{h}{2}\vec{D}_2)$
4. Compute $\vec{D}_4 = \vec{f}(\vec{X}_n + h\vec{D}_3)$
5. Compute $\vec{X}_{n+1} = \vec{X}_n + \frac{h}{6}\left(\vec{D}_1 + 2\vec{D}_2 + 2\vec{D}_3 + \vec{D}_4\right)$

To determine the position of a GLONASS satellite at time t with the position at the reference time $\vec{X}_0 = \vec{X}(t_0 = t_b)$ given, this scheme has to be repeated for $t_1 = t_0 + h$, $t_2 = t_1 + h$, ..., until epoch t_m is reached with $t_m \leq t < t_m + h$ (respectively $t_m + h < t \leq t_m$, if $t < t_b$, in which case h is negative). If $t_m \neq t$, a final step has to be performed from epoch t_m to t with step width $h = t - t_m$.

It should be noted that according to the GLONASS ICD (*ICD-GLONASS, 1995*), the parameters from the navigation message describe the orbital motion of the satellite's antenna phase center. Thus, the resulting position vector also defines the coordinates of the phase center and may directly be used in positioning applications.

According to (*Habrich, 1999*), however, it must be concluded that the parameters from the GLONASS navigation message actually describe the orbital motion of the satellite's center of mass. When being used in positioning applications, the resulting position and velocity vectors must first be reduced to the point of the antenna phase center. Due to the fact that both the center of mass and the phase center are located on the satellite x- (longitudinal) axis, and the transmission antenna always points to the Earth, this reduction is a merely radial one. The distance between the phase center and the center of mass is specified to be 1.62 m. The satellite state vector has to be diminished by that value in radial direction, which is equivalent to a scaling of the vector:

$$\vec{X}_{PC} = \frac{\left|\vec{X}_{CM}\right| - 1.62 \text{ m}}{\left|\vec{X}_{CM}\right|} \cdot \vec{X}_{CM} \tag{7.2.14}$$

with $\vec{X}_{CM}$ being the state (position and velocity) vector of the satellite's center of mass as computed above, and $\vec{X}_{PC}$ that of the phase center.

This uncertainty between center of mass and antenna phase center in the satellite ephemerides may be considered as orbital error, which cancels out in differential operation over short baselines.

7.2.3 Integration Error

When implementing this scheme and determining the satellite position numerically, the obtained satellite position and velocity will be depending on the chosen integration step width h. It can be expected that the smaller the step width the more accurate the obtained positions will be. On the other hand, the smaller the step width the more integration steps are necessary to obtain the satellite position at a specified epoch in time, increasing the computational load in position determination. After all, in each integration step function (7.2.11) has to be evaluated four times. Thus, for practical applications in positioning, a compromise has to be found for the step width h to allow both satellite positions as accurate as possible and acceptable computation time, especially in real-time applications.

To assess the influence of the step width on the accuracy of the calculated satellite position, satellite positions at the midpoint between two validity periods of adjacent ephemeris data were determined using these different data sets and varying step widths. In addition, satellite positions at the reference epoch of one ephemeris data set were calculated using the other data set. This way, only one of the calculated satellite positions was affected by inaccuracies of the numerical integration, while the other position could serve as true reference. These calculations were performed in both forward (satellite position at reference epoch of following ephemerides) and backward (satellite position at reference epoch of preceding ephemerides) direction. Figure 7.1 illustrates this procedure.

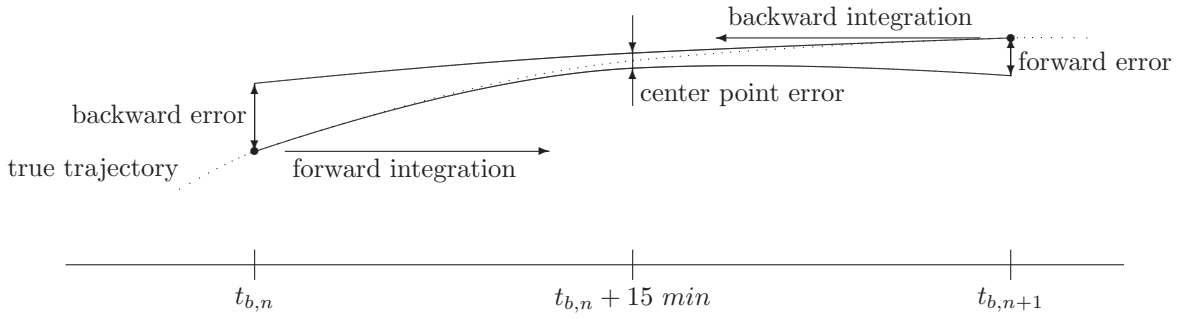

Figure 7.1: Determination of integration error in satellite orbit calculation.

h [s]	$\overline{\lvert\Delta x\rvert}$ [m]	σ_x [m]	$\overline{\lvert\Delta y\rvert}$ [m]	σ_y [m]	$\overline{\lvert\Delta z\rvert}$ [m]	σ_z [m]	r [m]	σ_r [m]
1	0.950	1.089	0.913	0.978	0.812	0.639	1.724	1.406
10	0.950	1.089	0.913	0.978	0.812	0.639	1.724	1.406
30	0.950	1.089	0.914	0.978	0.812	0.639	1.724	1.406
60	0.951	1.089	0.914	0.978	0.812	0.639	1.725	1.406
90	0.953	1.090	0.916	0.979	0.813	0.639	1.728	1.406
120	0.957	1.091	0.920	0.980	0.816	0.640	1.735	1.407
300	1.250	1.183	1.202	1.076	1.015	0.671	2.219	1.456
900	28.294	19.141	28.972	18.501	18.987	7.108	50.760	13.500

Table 7.1: Errors in orbit integration of center epoch between two adjacent ephemerides.

Center point, forward and backward integration was performed for more than 700 pairs of adjacent ephemeris data sets from different satellites and dates and with varying step widths from 1 s to 900 s (15 min, the largest step width to fit into the validity period of ephemeris data). Tables 7.1 to 7.3 show the average errors $\overline{|\Delta x|}$, $\overline{|\Delta y|}$, $\overline{|\Delta z|}$ and standard deviations σ_x, σ_y, σ_z of errors for these step widths in the different components. The tables also show the total error $r = \sqrt{\overline{|\Delta x|}^2 + \overline{|\Delta y|}^2 + \overline{|\Delta z|}^2}$ and its standard deviation σ_r. Figure 7.2 shows a sample behavior of the orbit integration error at the mid point between two adjacent ephemeris data sets.

It can be clearly seen that the error in orbit integration diminishes with decreasing step width, but only to a step width of around 60 - 90 s. Below that step width, further orbit improvement is only in the order of millimeters. Given an orbital period of 11h 15.8 min for a GLONASS satellite, in that time span

h [s]	$\overline{\lvert\Delta x\rvert}$ [m]	σ_x [m]	$\overline{\lvert\Delta y\rvert}$ [m]	σ_y [m]	$\overline{\lvert\Delta z\rvert}$ [m]	σ_z [m]	r [m]	σ_r [m]
1	1.384	1.361	1.368	1.227	1.521	1.231	2.867	1.658
10	1.384	1.361	1.368	1.227	1.521	1.231	2.867	1.658
30	1.384	1.361	1.368	1.227	1.521	1.231	2.867	1.658
60	1.384	1.361	1.368	1.227	1.521	1.231	2.868	1.658
90	1.385	1.361	1.369	1.228	1.522	1.232	2.870	1.658
120	1.387	1.362	1.372	1.230	1.524	1.233	2.874	1.660
300	1.553	1.425	1.553	1.356	1.651	1.314	3.183	1.735
900	27.478	19.239	29.629	18.304	19.873	7.693	50.973	13.898

Table 7.2: Errors in orbit integration to reference epoch of succeeding ephemerides.

h [s]	$\overline{\lvert\Delta x\rvert}$ [m]	σ_x [m]	$\overline{\lvert\Delta y\rvert}$ [m]	σ_y [m]	$\overline{\lvert\Delta z\rvert}$ [m]	σ_z [m]	r [m]	σ_r [m]
1	1.834	1.447	1.411	1.249	1.355	0.997	3.059	1.574
10	1.834	1.447	1.411	1.249	1.355	0.997	3.059	1.574
30	1.834	1.447	1.411	1.249	1.355	0.997	3.059	1.574
60	1.834	1.448	1.411	1.249	1.355	0.997	3.060	1.574
90	1.835	1.448	1.412	1.250	1.356	0.998	3.061	1.574
120	1.839	1.450	1.414	1.251	1.356	0.999	3.066	1.575
300	2.076	1.537	1.581	1.343	1.405	1.049	3.380	1.619
900	29.231	19.309	28.154	18.856	19.090	7.300	51.024	13.746

Table 7.3: Errors in orbit integration to reference epoch of preceding ephemerides.

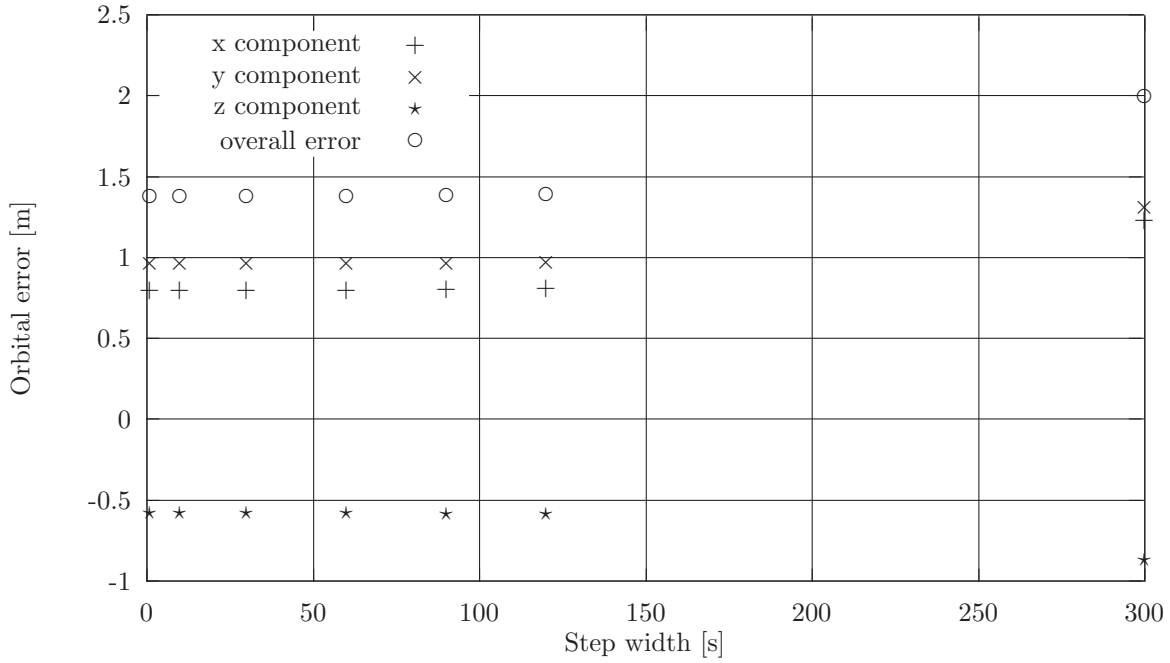

Figure 7.2: Example of orbit errors in dependence of step width (GLONASS satellite 1, ephemeris data of 04/10/97, 1445h and 1515h UTC, center point integration).

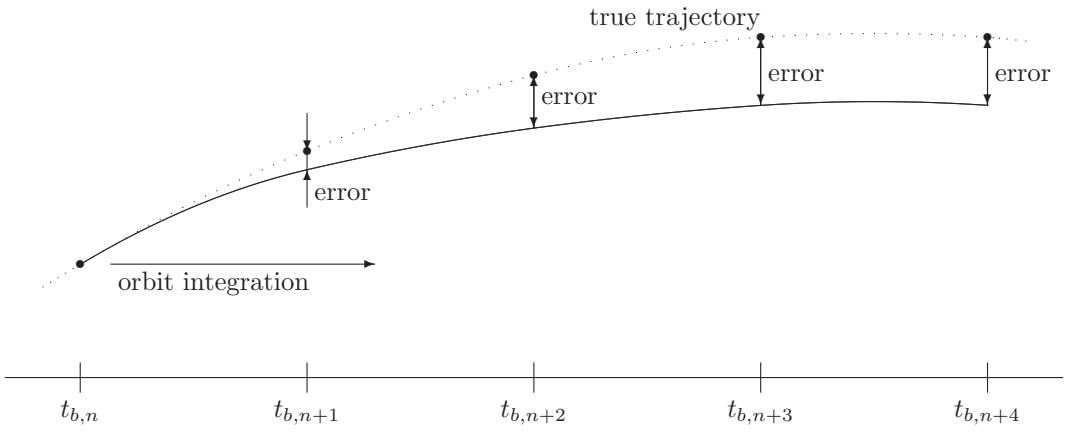

Figure 7.3: Determination of long term integration error.

(60 - 90 s) the satellite travels approximately 2 per mille of one orbit, or approximately 1/100 rad. Over that small angular distance, the satellite orbit can be considered to be nearly linear. Therefore, a smaller step width will not result in a decreased integration error, since all integrated positions will remain on this (nearly) straight line. The remaining error then is caused by the approximations in the orbital force model and the satellite's equations of motion (7.2.11) as well as the simplifications in the Runge-Kutta scheme (7.2.13). So for the purpose of GLONASS satellite orbit determination, an integration step width of 60 s in any case is sufficient.

This stands in contrast to the findings of (*Stewart and Tsakiri, 1998*), who describe a much clearer dependence of the integration error on the step width, even for step widths below 60 s. For a step width of 0.1 s, they note an error in the 15 min midpoint of 0.5 m, 1.2 m and 1.0 m in the x-, y- and z-components; for a step width of 60 s they find errors of 1.0 m, 6.8 m and 4.0 m, respectively. In between, the error behaves nearly linear with the step width.

It should be noted that the errors in satellite velocity determination are much smaller, in the order of millimeters per second in all tests (forward, backward and center point integration) for integration step widths below 120 s.

As can be expected, the errors at the center point between the two reference epochs is smaller than the errors of the forward and backward integration to the reference epoch of the adjacent ephemeris data set, due to the shorter integration time span. The magnitudes of errors of the forward and backward integration are comparable.

Another interesting question is, how long an ephemeris data set could be used in case there were no updates available, i.e. how the integration error behaves with time. To determine this, one ephemeris data set was used to integrate the satellite orbit positions at the reference epochs of subsequent ephemeris data sets. The integrated orbit position can then be compared to the true orbit position as broadcast in the respective ephemeris data. Differences in orbit position are determined and analyzed. Figure 7.3 illustrates this procedure.

Sample results of such a test are shown in Table 7.4 and Figure 7.4. This particular test was carried out with ephemeris data of GLONASS satellite (almanac slot no.) 9 from November 20, 1998, integrating the ephemeris data valid at 1345h UTC up to 5 hours in advance. Table 7.4 shows the errors in the individual components of position and velocity state vector $\Delta\vec{x} = \vec{x}_{true}(t_{b,n+m}) - \vec{x}_{int}(t_b + \Delta t)$ as well as the overall errors, Figure 7.4 depicts only the errors in the position vector. The integration step width was chosen to be 60 s.

As can be seen, for integration up to the reference epoch of the succeeding ephemeris data set (integration time 30 min), the error in orbit determination remains less than 10 m. Even for integration

Δt [min]	Δx [m]	Δy [m]	Δz [m]	r [m]	$\Delta\dot{x}$ [m/s]	$\Delta\dot{y}$ [m/s]	$\Delta\dot{z}$ [m/s]	$\Delta\lvert\dot{\vec{x}}\rvert$ [m/s]
30	2.071	5.884	3.224	7.022	0.001	0.002	-0.002	0.003
60	6.974	10.397	-2.754	12.819	0.002	0.002	-0.005	0.006
90	12.340	14.523	-14.763	24.108	0.002	0.001	-0.009	0.009
120	12.785	17.278	-34.713	40.829	-0.003	0.000	-0.014	0.014
150	2.276	17.929	-64.028	66.530	-0.011	0.000	-0.018	0.021
180	-25.921	19.380	-102.617	107.600	-0.022	-0.000	-0.024	0.033
210	-79.028	21.964	-147.863	169.089	-0.038	0.002	-0.026	0.046
240	-166.242	29.734	-193.979	257.193	-0.059	0.005	-0.024	0.064
270	-295.078	46.562	-230.859	377.537	-0.085	0.013	-0.014	0.087
300	-472.433	77.474	-240.449	535.734	-0.112	0.023	0.006	0.114

Table 7.4: Long-term errors in orbit integration.

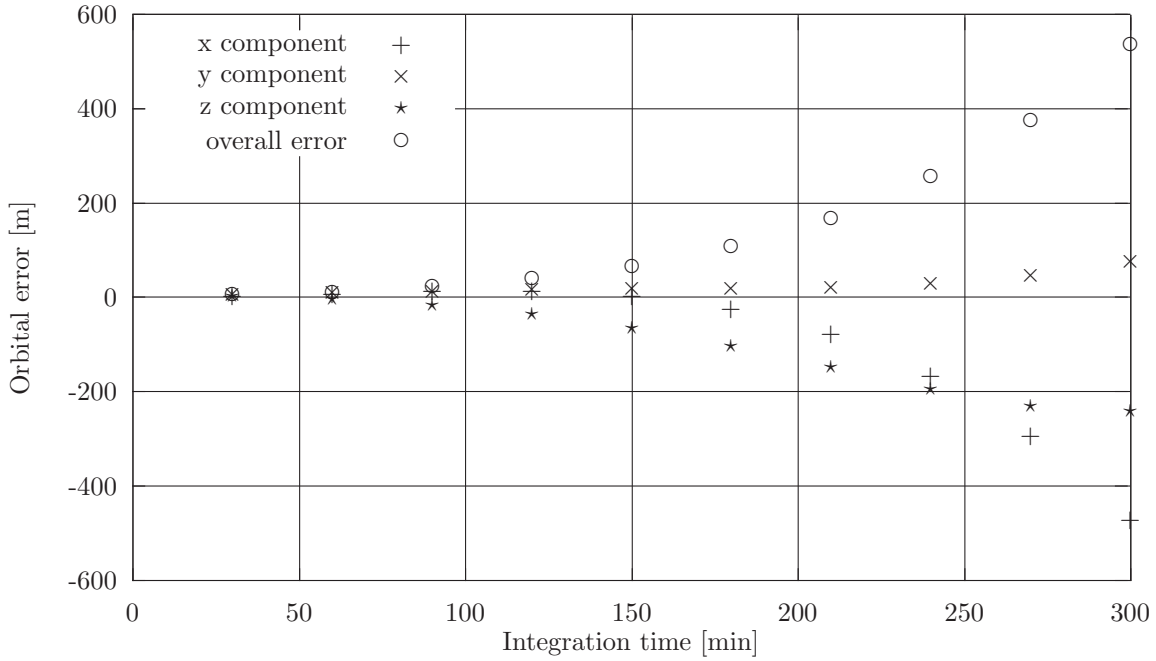

Figure 7.4: Long-term errors in orbit integration.

times of up to 1 h and more, the orbital error can remain less than 20 m. Allowing larger integration errors could be of interest e.g. for differential applications, where the orbital error largely cancels out over short baselines. Nonetheless, it is strongly recommended to use the currently valid set of ephemeris data wherever possible to keep the integration time within the ±15 min interval around the reference epoch.

These results (errors of less than 20 m for 1 h integration time) agree with the findings of (*Stewart and Tsakiri, 1998*).

Again, the orbit integration turns out to be more precise for the satellite velocity. Even after an integration time of 90 min, the error in velocity remains less than 1 cm/s.

7.3 Satellite Positions from Almanac Data

Satellite positions can not only be computed from ephemeris data, but also from almanac data. However, satellite positions computed from almanac data are less accurate than positions computed from ephemeris data. But whereas the accuracy of ephemeris-derived satellite positions decreases rapidly beyond the validity period of the ephemeris data (usually 30 min.), almanac-derived satellite positions keep their accuracy for several days. Therefore, satellite positions derived from almanac data are very useful for purposes such as planning of satellite observations, etc. For purposes of receiver position computation, satellite positions derived from almanac data should only be employed in case there are no ephemeris data available.

Whereas GLONASS ephemeris data contain components of the satellite position, velocity and acceleration vectors in the ECEF PZ-90 system, GLONASS almanac data employ a set of Kepler-like parameters to determine the satellite position. Therefore, the algorithm of computing the satellite position from almanac data is completely different from that of computing the position from ephemeris data. This algorithm, as defined in (*ICD-GLONASS, 1995*), is summarized in the following.

Given the almanac parameters N^A, t_λ^A, λ^A, Δi^A, ΔT^A, $\Delta \dot{T}^A$, ε^A, ω^A and the parameters of the PZ-90 frame μ, a_E and ω_E, the satellite's orbital position at day N and time t can be computed using the following equations:

Compute time difference to reference time: $\Delta t = (N - N^A) \cdot 86400\ \text{s} + t - t_\lambda^A$

Compute the actual inclination: $i = i_{nom} + \Delta i^A$ with $i_{nom} = 63^\circ$

Compute the actual orbital period: $T = T_{nom} + \Delta T^A$ with $T_{nom} = 43200$ s

Compute the mean motion: $n = 2\pi / T$

Compute the semi-major axis: $a = \sqrt[3]{\mu / n^2}$

Compute correction to longitude of ascending node: $\dot{\lambda} = -10 \left(\frac{a_E}{a}\right)^{7/2} \frac{\pi}{180 \cdot 86400\ \text{s}} \cos i$

Compute correction to argument of perigee: $\dot{\omega} = 5 \left(\frac{a_E}{a}\right)^{7/2} \frac{\pi}{180 \cdot 86400\ \text{s}} (5 \cos^2 i - 1)$

Compute corrected longitude of ascending node: $\lambda = \lambda^A + \left(\dot{\lambda} - \omega_E\right) \cdot \Delta t$

Compute corrected argument of perigee: $\omega = \omega^A + \dot{\omega} \cdot \Delta t$

Compute eccentric anomaly at point Π: $E_\Pi = 2 \arctan \left(\tan \frac{\omega}{2} \sqrt{\frac{1 - \varepsilon^A}{1 + \varepsilon^A}} \right)$

Note: Π is that point of the orbit the true anomaly of which is identical to the argument of perigee.

Compute time difference to perigee passing: $\Delta T = \frac{E_\Pi - \varepsilon^A \sin E_\Pi}{n} + \begin{cases} 0 & , \omega < \pi \\ T & , \omega > \pi \end{cases}$

Compute mean anomaly at epoch t: $M = n \cdot (\Delta t - \Delta T)$

Compute eccentric anomaly at epoch t: $E = M + \varepsilon^A \sin E$
Note: Kepler's equation has to be solved iteratively.

Compute position in orbital coordinate system: $\vec{x}^o = a \cdot \begin{pmatrix} \cos E - \varepsilon^A \\ \sqrt{1-(\varepsilon^A)^2}\sin E \\ 0 \end{pmatrix}$

Compute velocity in orbital coordinate system: $\dot{\vec{x}}^o = \frac{a}{1-\varepsilon^A \cos E} \cdot \begin{pmatrix} -n \sin E \\ n\sqrt{1-(\varepsilon^A)^2}\cos E \\ 0 \end{pmatrix}$

Determine orientation vectors of orbital coordinate system in ECEF system:

$$\vec{e}_1 = \begin{pmatrix} \cos\omega\cos\lambda - \sin\omega\sin\lambda\cos i \\ \cos\omega\sin\lambda + \sin\omega\cos\lambda\cos i \\ \sin\omega\sin i \end{pmatrix}, \quad \vec{e}_2 = \begin{pmatrix} -\sin\omega\cos\lambda - \cos\omega\sin\lambda\cos i \\ -\sin\omega\sin\lambda + \cos\omega\cos\lambda\cos i \\ \cos\omega\sin i \end{pmatrix}$$

Convert position from orbital to ECEF system: $\vec{x} = x_1^o \vec{e}_1 + x_2^o \vec{e}_2$

Convert velocity from orbital to ECEF system: $\dot{\vec{x}} = \dot{x}_1^o \vec{e}_1 + \dot{x}_2^o \vec{e}_2 + \omega_E \cdot \begin{pmatrix} x_2 \\ -x_1 \\ 0 \end{pmatrix}$

8 Observations and Position Determination

Determination of satellite clock error, time of signal transmission and satellite position at time of signal transmission according to the algorithms introduced in Chapter 7 are always the first steps to be performed in the calculation of a user's position, independent of which processing mode the user eventually employs to obtain his position.

Analogously to GPS, the computed satellite position at the time of signal transmission has to be corrected for the effects of Earth rotation during the signal travel time, as it is described e.g. in Section 6.3. Signal travel time and the time of signal transmission have to be known with an accuracy below 0.5 ms in order to keep the error in the computed satellite position due to Earth rotation below 1 m.

Just as is the case for GPS, when observing GLONASS satellites, three observables can be measured: code pseudoranges (in the following often denoted only as pseudoranges), carrier phase and Doppler measurements. The following chapters deal with the treatment of these observables and the mathematical models to obtain a user position from these measurements.

8.1 Pseudorange Measurements

8.1.1 Single Point Positioning

Once the signal travel time and the satellite position at the time of signal transmission are known, the receiver position can be computed just as with GPS by linearization of the observation equations and solving for the unknowns. There are four unknowns, namely the x-, y- and z-coordinates of the user's position and the receiver clock offset with respect to GLONASS system time. Thus, to solve for these four unknowns, measurements to at least four satellites are necessary.

Analogously to GPS, the pseudorange observation equation from observer R to satellite S can be written as:

$$PR_R^S = \varrho_R^S + c \cdot \delta t_R - c \cdot \delta t^S + c \cdot \delta t_R^{S,Trop} + c \cdot \delta t_R^{S,Iono} + c \cdot L_R^S + \varepsilon_R^S \tag{8.1.1}$$

Here PR_R^S is the (measured) pseudorange between receiver R and satellite S, ϱ_R^S is the true (geometric) range from receiver to satellite, c is the speed of light in vacuum, δt_R is the receiver clock offset with respect to system time, δt^S is the satellite clock offset with respect to system time, $\delta t_R^{S,Trop}$ is the signal path delay due to the troposphere, $\delta t_R^{S,Iono}$ is the signal path delay due to the ionosphere and ε_R^S stands for the noise and all non-modelled error sources, such as errors in satellite orbit and clock prediction, inaccuracies in ionospheric and tropospheric modelling, multipath and (in the later case of GPS satellites) Selective Availability.

Due to the different frequencies involved, the signals of different GLONASS satellites will take different paths through the HF part of a receiver. These different paths may well lead to different hardware delays for signals from different satellites. These different delays are modelled by the L_R^S term in Eq. (8.1.1). Receiver manufacturers spend a lot of work on avoiding or at least calibrating these biases. Still, these biases cannot be calibrated completely, since they depend on a number of influences, among them receiver temperature. Thus, they must be carefully observed in high-precision applications.

Biases may even occur when tracking the same satellite on different receiver hardware channels. Thus, these delays are dependent on satellite (via its signal frequency) and hardware channel. But since in normal surveying or navigation operation, different receiver channels will track different satellites, these delays are treated as dependent only on the satellite in Eq. (8.1.1).

Splitting this hardware delay into a common (average or specific to one satellite system) term and a satellite (channel) dependent bias:

$$L_R^S = L_{R,GLO} + \delta t_{R,ICB}^S \tag{8.1.2}$$

this common delay $L_{R,GLO}$ can no longer be separated from the clock term δt_R. Eq. (8.1.1) therefore can be re-written as:

$$PR_R^S = \varrho_R^S + c \cdot (\delta t_R + L_{R,GLO}) - c \cdot \delta t^S + c \cdot \delta t_R^{S,Trop} + c \cdot \delta t_R^{S,Iono} + c \cdot \delta t_{R,ICB}^S + \varepsilon_R^S \tag{8.1.3}$$

The satellite dependent bias $\delta t_{R,ICB}^S$ is called inter-channel bias. These biases between individual GLONASS satellites, however, are small, in the order or below the noise level of pseudorange measurements. For Ashtech GG24 receivers e.g., (*Kozlov and Tkachenko, 1998*) shows for different GLONASS satellites code biases of less than ±1.25 m and phase biases of less than ±0.032 cycles, both with respect to mean. The average code and phase biases between GPS and GLONASS are found to be 1.04 m and 0.357 cycles, respectively. (*Zarraoa et al., 1995*) shows for 3S Navigation R-100/R-101 receivers inter-channel biases of up to 28 mm with respect to mean, when the same GLONASS satellite on L_1 and L_2 P-code is tracked on all eight P-channels. Therefore, these inter-channel biases can be neglected in pure pseudorange processing. Eq. (8.1.3) thus rewrites to:

$$PR_R^S = \varrho_R^S + c \cdot (\delta t_R + L_{R,GLO}) - c \cdot \delta t^S + c \cdot \delta t_R^{S,Trop} + c \cdot \delta t_R^{S,Iono} + \varepsilon_R^S \tag{8.1.4}$$

The true range from receiver to satellite can be expressed as

$$\varrho_R^S = \sqrt{(x_R - x^S)^2 + (y_R - y^S)^2 + (z_R - z^S)^2} \tag{8.1.5}$$

Regarding Eqs. (8.1.4) and (8.1.5), x_R, y_R, z_R, δt_R are the unknowns to be solved for, x^S, y^S, z^S, δt^S can be determined from the satellite ephemeris data (see Sections 7.1, 7.2). The tropospheric delay $\delta t_R^{S,Trop}$ has to be determined using a suitable model, e.g. a Modified Hopfield model, if possible supported by measurements of the actual temperature, air pressure and humidity at the time of observation. The ionospheric delay $\delta t_R^{S,Iono}$ also can be modeled using e.g. the GPS Klobuchar model, adapted to GLONASS carrier frequencies. However, in real-time applications this is only possible in a mixed GPS/GLONASS observation scenario, where the parameters of the Klobuchar model have been determined from GPS almanac data. With full access to the GLONASS L_2 frequency and a dual-frequency GLONASS receiver available, however, the ionospheric delay can be determined from the different travel times of the L_1 and L_2 pseudoranges, or one can even form ionospheric-free pseudoranges (see Section 8.5 for more details). In this latter case, the ionospheric delay $\delta t_R^{S,Iono}$ cancels from Eq. (8.1.4) and all further equations derived from that.

Considering Eq. (8.1.5), the observation equation Eq. (8.1.4) is non-linear in the unknowns x_R, y_R, z_R. Therefore, it usually is linearized by means of a Taylor series expansion of the geometric range between observer and satellite:

$$\begin{aligned}
&\varrho_R^S(x_R, y_R, z_R) \\
&= \varrho_R^S(x_0, y_0, z_0) + \left.\frac{\partial \varrho_R^S}{\partial x_R}\right|_{\substack{x_R = x_0 \\ y_R = y_0 \\ z_R = z_0}} \cdot (x_R - x_0) + \left.\frac{\partial \varrho_R^S}{\partial y_R}\right|_{\substack{x_R = x_0 \\ y_R = y_0 \\ z_R = z_0}} \cdot (y_R - y_0) + \\
&\quad \left.\frac{\partial \varrho_R^S}{\partial z_R}\right|_{\substack{x_R = x_0 \\ y_R = y_0 \\ z_R = z_0}} \cdot (z_R - z_0) \\
&= \varrho_0^S + \frac{x_0 - x^S}{\varrho_0^S} \cdot (x_R - x_0) + \frac{y_0 - y^S}{\varrho_0^S} \cdot (y_R - y_0) + \frac{z_0 - z^S}{\varrho_0^S} \cdot (z_R - z_0)
\end{aligned} \tag{8.1.6}$$

with the approximate receiver position $\vec{x}_0$ and $\varrho_0^S = \sqrt{(x_0 - x^S)^2 + (y_0 - y^S)^2 + (z_0 - z^S)^2}$.

In a similar way splitting the receiver clock error (together with the common hardware delay) $\delta t_R + L_{R,GLO}$ into an approximate value $\delta t_{R,0} + L_{R,GLO,0}$ and an amendment to this approximation yields

$$\delta t_R + L_{R,GLO} = (\delta t_{R,0} + L_{R,GLO,0}) + [(\delta t_R + L_{R,GLO}) - (\delta t_{R,0} + L_{R,GLO,0})] \tag{8.1.7}$$

Using Eqs. (8.1.6) and (8.1.7), the observation equation (8.1.4) transforms to:

$$\begin{aligned} &PR_R^S - \varrho_0^S - c \cdot (\delta t_{R,0} + L_{R,GLO,0}) + c \cdot \delta t^S - c \cdot \delta t_R^{S,Trop} - c \cdot \delta t_R^{S,Iono} = \\ &\quad \frac{x_0 - x^S}{\varrho_0^S} \cdot (x_R - x_0) + \frac{y_0 - y^S}{\varrho_0^S} \cdot (y_R - y_0) + \frac{z_0 - z^S}{\varrho_0^S} \cdot (z_R - z_0) + \\ &\quad c \cdot [(\delta t_R + L_{R,GLO}) - (\delta t_0 + L_{R,GLO,0})] + \varepsilon_R^S \end{aligned} \tag{8.1.8}$$

where known and modelled values have been shifted to the left-hand side of the equation.

Having measurements to a number of satellites 1, 2, ..., n, one can summarize the resulting set of observation equations in matrix notation:

$$\vec{l} = \mathbf{A} \cdot \vec{x} + \vec{\varepsilon} \tag{8.1.9}$$

with

$$\vec{l} = \begin{pmatrix} PR_R^1 - \varrho_0^1 - c \cdot (\delta t_{R,0} + L_{R,GLO,0}) + c \cdot \delta t^1 - c \cdot \delta t_R^{1,Trop} - c \cdot \delta t_R^{1,Iono} \\ PR_R^2 - \varrho_0^2 - c \cdot (\delta t_{R,0} + L_{R,GLO,0}) + c \cdot \delta t^2 - c \cdot \delta t_R^{2,Trop} - c \cdot \delta t_R^{2,Iono} \\ \vdots \\ PR_R^n - \varrho_0^n - c \cdot (\delta t_{R,0} + L_{R,GLO,0}) + c \cdot \delta t^n - c \cdot \delta t_R^{n,Trop} - c \cdot \delta t_R^{n,Iono} \end{pmatrix} \tag{8.1.10}$$

the vector of the known values,

$$\mathbf{A} = \begin{pmatrix} \frac{x_0 - x^1}{\varrho_0^1} & \frac{y_0 - y^1}{\varrho_0^1} & \frac{z_0 - z^1}{\varrho_0^1} & 1 \\ \frac{x_0 - x^2}{\varrho_0^2} & \frac{y_0 - y^2}{\varrho_0^2} & \frac{z_0 - z^2}{\varrho_0^2} & 1 \\ \vdots & \vdots & \vdots & \vdots \\ \frac{x_0 - x^n}{\varrho_0^n} & \frac{y_0 - y^n}{\varrho_0^n} & \frac{z_0 - z^n}{\varrho_0^n} & 1 \end{pmatrix} \tag{8.1.11}$$

the design matrix,

$$\vec{x} = \begin{pmatrix} (x_R - x_0) \\ (y_R - y_0) \\ (z_R - z_0) \\ c \cdot [(\delta t_R + L_{R,GLO}) - (\delta t_{R,0} + L_{R,GLO,0})] \end{pmatrix} \tag{8.1.12}$$

the vector of the unknowns, and

$$\vec{\varepsilon} = \begin{pmatrix} \varepsilon_R^1 \\ \varepsilon_R^2 \\ \vdots \\ \varepsilon_R^n \end{pmatrix} \tag{8.1.13}$$

the noise vector.

This system of equations can then be solved using the conventional methods, e.g. a least squares adjustment or Kalman filtering.

Since the satellite positions as computed from GLONASS ephemeris (or almanac) data are expressed in the PZ-90 frame, the resulting receiver position is also given in this coordinate frame. To get the receiver position in a different coordinate frame, the resulting coordinates must be transformed as desired.

In a combined GPS/GLONASS receiver, signals from GPS satellites are also delayed in the HF part of the receiver. But since GPS employs identical frequencies for all satellites, these delays are equal for all satellites and thus form part of the clock term. However, this GPS delay is different from the common GLONASS delay in Eq. (8.1.4), due to the different frequencies. This leads to different realizations of GPS and GLONASS system times in the receiver. In addition, some combined receivers even use different clocks for GPS and GLONASS reception. Thus, in a combined GPS/GLONASS scenario different receiver clock errors with respect to GPS and GLONASS system times must be accounted for.

Thus, rewriting Eq. (8.1.4) for a GPS satellite i and a GLONASS satellite j yields:

$$PR_R^i = \varrho_R^i + c \cdot (t_{R,GPS} - t_{GPS} + L_{R,GPS}) - c \cdot \delta t^i + c \cdot \delta t_R^{i,Trop} + c \cdot \delta t_R^{i,Iono} + \varepsilon_R^i \quad (8.1.14)$$

$$PR_R^j = \varrho_R^j + c \cdot (t_{R,GLO} - t_{GLO} + L_{R,GLO}) - c \cdot \delta t^j + c \cdot \delta t_R^{j,Trop} + c \cdot \delta t_R^{j,Iono} + \varepsilon_R^j \quad (8.1.15)$$

where the receiver clock errors δt_R with respect to GPS and GLONASS system times have been inserted as $t_{R,GPS} - t_{GPS}$ and $t_{R,GLO} - t_{GLO}$, respectively.

Introducing the respective GPS times into Eq. (8.1.15) yields:

$$\begin{aligned} PR_R^j = {} & \varrho_R^j + c \cdot (t_{R,GPS} - t_{GPS} + L_{R,GPS}) + c \cdot (t_{GPS} - t_{GLO}) + c \cdot (L_{R,GLO} - L_{R,GPS}) + \\ & c \cdot (t_{R,GLO} - t_{R,GPS}) - c \cdot \delta t^j + c \cdot \delta t_R^{j,Trop} + c \cdot \delta t_R^{j,Iono} + \varepsilon_R^j \end{aligned} \quad (8.1.16)$$

Denoting $t_{R,GPS} - t_{GPS}$ as the receiver clock error δt_R (with respect to GPS system time), $t_{GPS} - t_{GLO}$ as the difference in system times δt_{Sys} and $(L_{R,GLO} - L_{R,GPS}) + (t_{R,GLO} - t_{R,GPS})$ as the receiver inter-system hardware delay $\delta t_{R,HW}$, Eqs. (8.1.14) and (8.1.16) transform to

$$PR_R^i = \varrho_R^i + c \cdot (\delta t_R + L_{R,GPS}) - c \cdot \delta t^i + c \cdot \delta t_R^{i,Trop} + c \cdot \delta t_R^{i,Iono} + \varepsilon_R^i \quad (8.1.17)$$

$$\begin{aligned} PR_R^j = {} & \varrho_R^j + c \cdot (\delta t_R + L_{R,GPS}) + c \cdot \delta t_{Sys} + c \cdot \delta t_{R,HW} - c \cdot \delta t^j + c \cdot \delta t_R^{j,Trop} + \\ & c \cdot \delta t_R^{j,Iono} + \varepsilon_R^j \end{aligned} \quad (8.1.18)$$

Regarding the pair of Eqs. (8.1.17) and (8.1.18), we notice six unknowns in the combined GPS/GLONASS single point solution: the three coordinates of the receiver position (implicitly contained in ϱ_R^S), the receiver clock offset (including GPS hardware delay) $\delta t_R + L_{R,GPS}$, the time difference between GPS and GLONASS system times δt_{Sys} and the receiver inter-system hardware delay $\delta t_{R,HW}$. However, in a single point solution the latter unknown cannot be separated from the difference in system times, effectively leaving five unknowns to solve for, as already discussed in Section 4. These different receiver hardware delays therefore contribute to the difference in system times as determined by the observer. The estimation of the difference in system times thus yields only an approximation that in addition will be dependent on the receiver.

Thus, for a set of m GPS and n GLONASS satellites, after linearization of the geometric range the observation equations in matrix form read:

$$\vec{l} = \mathbf{A} \cdot \vec{x} + \vec{\varepsilon} \quad (8.1.19)$$

with

$$\vec{l} = \begin{pmatrix} PR_R^1 - \varrho_0^1 - c \cdot (\delta t_{R,0} + L_{R,GPS,0}) + c \cdot \delta t^1 - c \cdot \delta t_R^{1,Trop} - c \cdot \delta t_R^{1,Iono} \\ \vdots \\ PR_R^m - \varrho_0^m - c \cdot (\delta t_{R,0} + L_{R,GPS,0}) + c \cdot \delta t^m - c \cdot \delta t_R^{m,Trop} - c \cdot \delta t_R^{m,Iono} \\ PR_R^{m+1} - \varrho_0^{m+1} - c \cdot (\delta t_{R,0} + L_{R,GPS,0}) - c \cdot (\delta t_{Sys,0} + \delta t_{R,HW,0}) + c \cdot \delta t^{m+1} - \\ c \cdot \delta t_R^{m+1,Trop} - c \cdot \delta t_R^{m+1,Iono} \\ \vdots \\ PR_R^{m+n} - \varrho_0^{m+n} - c \cdot (\delta t_{R,0} + L_{R,GPS,0}) - c \cdot (\delta t_{Sys,0} + \delta t_{R,HW,0}) + c \cdot \delta t^{m+n} - \\ c \cdot \delta t_R^{m+n,Trop} - c \cdot \delta t_R^{m+n,Iono} \end{pmatrix} \quad (8.1.20)$$

the vector of the known values,

$$\mathbf{A} = \begin{pmatrix} \frac{x_0 - x^1}{\varrho_0^1} & \frac{y_0 - y^1}{\varrho_0^1} & \frac{z_0 - z^1}{\varrho_0^1} & 1 & 0 \\ \vdots & \vdots & \vdots & \vdots & \vdots \\ \frac{x_0 - x^m}{\varrho_0^m} & \frac{y_0 - y^m}{\varrho_0^m} & \frac{z_0 - z^m}{\varrho_0^m} & 1 & 0 \\ \frac{x_0 - x^{m+1}}{\varrho_0^{m+1}} & \frac{y_0 - y^{m+1}}{\varrho_0^{m+1}} & \frac{z_0 - z^{m+1}}{\varrho_0^{m+1}} & 1 & 1 \\ \vdots & \vdots & \vdots & \vdots & \vdots \\ \frac{x_0 - x^{m+n}}{\varrho_0^{m+n}} & \frac{y_0 - y^{m+n}}{\varrho_0^{m+n}} & \frac{z_0 - z^{m+n}}{\varrho_0^{m+n}} & 1 & 1 \end{pmatrix} \tag{8.1.21}$$

the design matrix,

$$\vec{x} = \begin{pmatrix} (x_R - x_0) \\ (y_R - y_0) \\ (z_R - z_0) \\ c \cdot [(\delta t_R + L_{R,GPS}) - (\delta t_{R,0} + L_{R,GPS,0})] \\ c \cdot [(\delta t_{Sys} + \delta t_{R,HW}) - (\delta t_{Sys,0} + \delta t_{R,HW,0})] \end{pmatrix} \tag{8.1.22}$$

the vector of the unknowns, and

$$\vec{\varepsilon} = \begin{pmatrix} \varepsilon_R^1 \\ \vdots \\ \varepsilon_R^m \\ \varepsilon_R^{m+1} \\ \vdots \\ \varepsilon_R^{m+n} \end{pmatrix} \tag{8.1.23}$$

the noise vector.

Please note that t_R and δt_R now denote the receiver clock reading and offset with respect to GPS system time, as described above.

Satellite coordinates $\vec{x}^1, \ \ldots, \ \vec{x}^m, \ \vec{x}^{m+1}, \ \ldots, \ \vec{x}^{m+n}$ must be given in the same coordinate frame to obtain a valid receiver position (cf. Section 5). Coordinates of the receiver position are then expressed in the frame used for the satellite positions.

An example of positioning results using GPS and GLONASS absolute positioning with pseudoranges is shown in Figure 8.1. Positions were computed from data logged by a 3S Navigation R-100/R-101 receiver, which was set up at a known location at the Institute of Geodesy and Navigation. Pseudorange and carrier phase measurements were logged every second for approximately one hour. The plot shows the deviation from the known location of the antenna in the horizontal plane. GPS positions were computed from carrier smoothed L_1 C/A-code pseudorange measurements. GLONASS positions were computed from carrier smoothed dual-frequency P-code measurements. Wherever possible, the ionospheric free linear combination was formed. These observables used are not really identical for GPS and GLONASS, but with P-code and dual-frequency measurements readily available on GLONASS, the best possible results for each system are determined. GLONASS satellite positions were converted from PZ-90 to WGS84 using the transformation according to (*Roßbach et al., 1996*).

The large deviations from the true position due to GPS S/A can be clearly seen. Standard deviations of the computed positions are 25.4 m in North/South direction and 10.0 m in East/West direction. Due to the lack of S/A on GLONASS, positions computed only from GLONASS range measurements scatter much less. Here the standard deviations are 4.6 m in North/South direction and 7.5 m in East/West direction. For the combined GPS/GLONASS positioning, all satellite measurements were

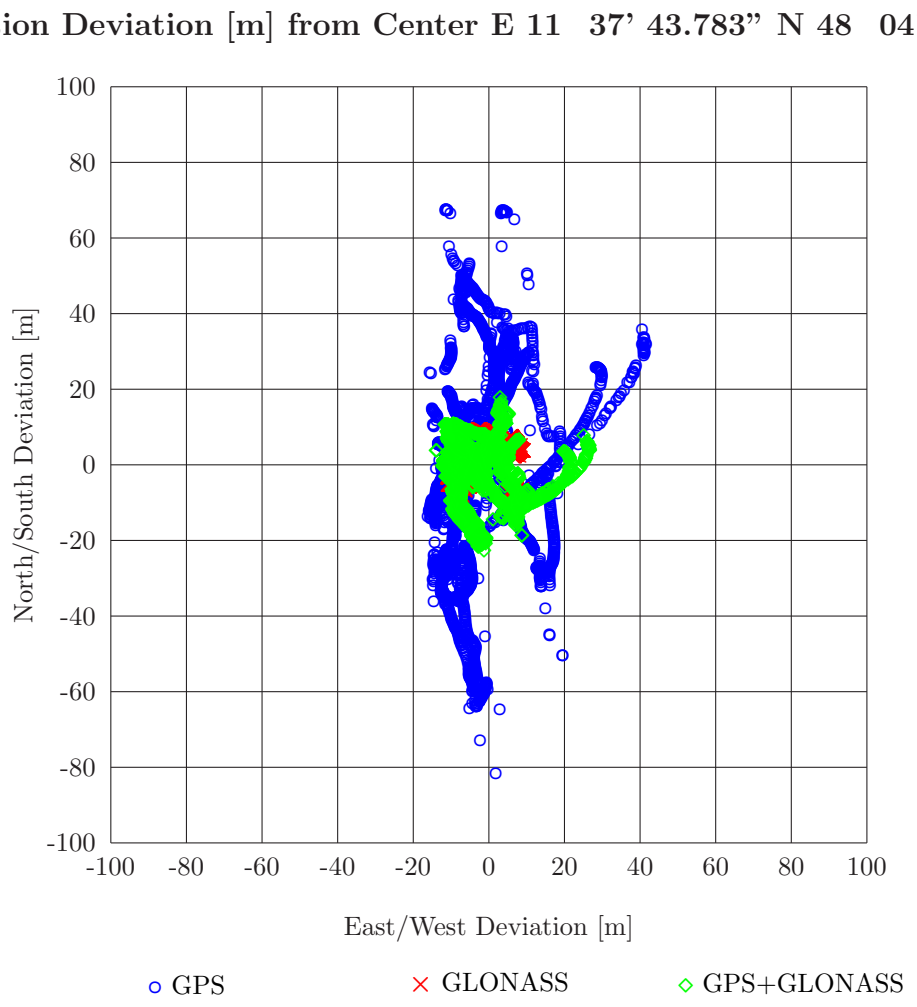

Figure 8.1: GPS, GLONASS and combined GPS/GLONASS absolute positioning.

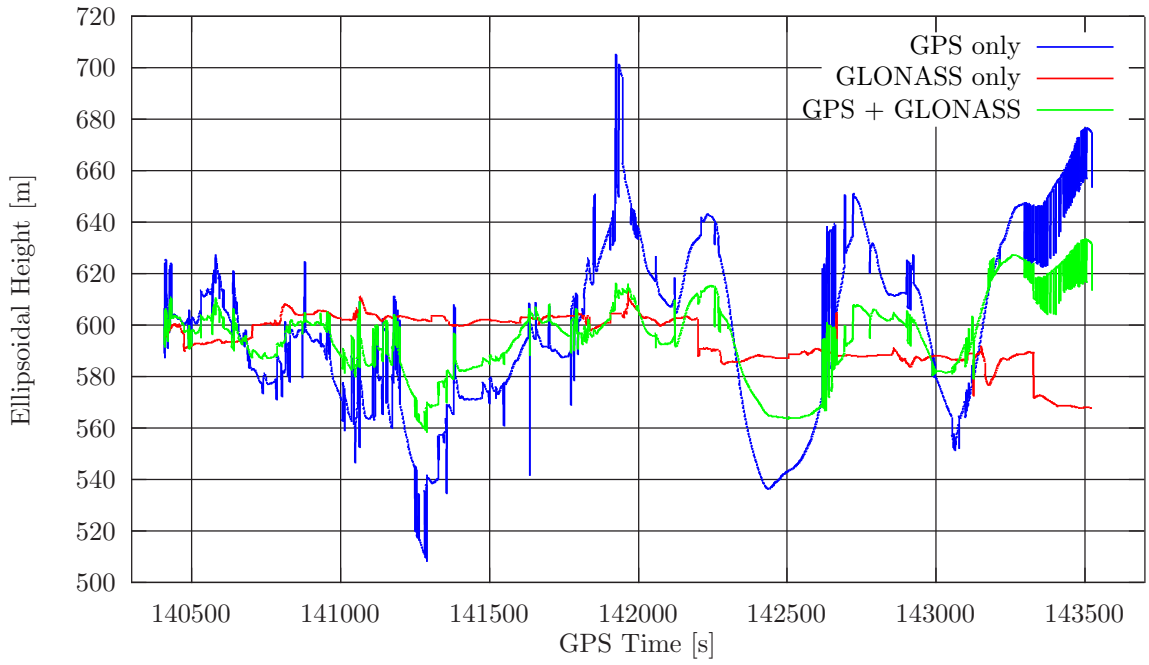

Figure 8.2: GPS, GLONASS and combined GPS/GLONASS absolute positioning, height component.

weighted equally. These results are still affected by GPS S/A, but to a much less extent than the GPS only results. Standard deviations are 8.2 m in North/South direction and 7.7 m in East/West direction.

The height components of the processing results are displayed in Figure 8.2 as a time series. Again it can be seen that the GPS solution deviates far more from the true position, which is 594.5 m, than the GLONASS solution. Oscillations due to S/A are clearly visible. The high frequency oscillations towards the end of the observation session are caused by rapidly changing satellite geometry. Track of one GPS satellite is lost and re-acquired in short time intervals. Mean GPS height is 598.5 m, with a standard deviation of 33.4 m. There are no such oscillations on the GLONASS solutions. These positions are more stable. However, one can notice two major jumps in the GLONASS height component. The first one occurs at 142200 s GPS time and is connected to a change in applicable ephemeris data. The second jump at 143328 s is caused by a change in GLONASS satellite geometry. Mean GLONASS height is 594.4 m. with a standard deviation of 9.7 m. As with the horizontal components, the combined GPS/GLONASS solution also is affected by GPS S/A, but to a less extent than the GPS only results. Here the standard deviation is 15.5 m with a mean value of 595.6 m.

8.1.2 Single Difference Positioning

Single difference positioning using GLONASS can be performed just the way as with GPS. Given two observation sites, the reference station R at a precisely known location and a user U, whose position is to be determined, the pseudorange observation equations to a common satellite S read

$$PR_R^S = \varrho_R^S + c \cdot (\delta t_R + L_{R,GLO}) - c \cdot \delta t^S + c \cdot \delta t_R^{S,Trop} + c \cdot \delta t_R^{S,Iono} + \varepsilon_R^S \quad (8.1.24)$$

$$PR_U^S = \varrho_U^S + c \cdot (\delta t_U + L_{U,GLO}) - c \cdot \delta t^S + c \cdot \delta t_U^{S,Trop} + c \cdot \delta t_U^{S,Iono} + \varepsilon_U^S \quad (8.1.25)$$

Forming a single difference, i.e. subtracting the measurement at the reference station from that at the user, the satellite clock error δt^S will cancel out:

$$PR_U^S - PR_R^S = \varrho_U^S - \varrho_R^S + c \cdot [(\delta t_U - c\delta t_R) + (L_{U,GLO} - L_{R,GLO})] + c \cdot \delta t_U^{S,Trop} - c \cdot \delta t_R^{S,Trop} + c \cdot \delta t_U^{S,Iono} - c \cdot \delta t_R^{S,Iono} + \varepsilon_U^S - \varepsilon_R^S \quad (8.1.26)$$

Supposed the user station is sufficiently close to the reference station, the path of the GLONASS satellite signal through the ionosphere will be almost identical for reference station and user. Thus, the ionospheric delay also will cancel out. This assumption holds true for distances of up to approximately 1000 km.

A similar assumption cannot be made for the tropospheric delay, because the troposphere immediately surrounds the receiver, and the signal travel path through the troposphere can be different even for nearby receivers, especially when the receivers are placed at different altitudes. This may be the case e.g. in mountainous regions or for aircraft approaching an airport. Thus, the tropospheric path delay does not cancel out in single difference positioning.

Denoting the single difference terms $*_U - *_R$ as $\Delta *_{UR}$, Eq. (8.1.26) therefore transforms to

$$\Delta PR^S_{UR} = \Delta\varrho^S_{UR} + c \cdot (\Delta\delta t_{UR} + \Delta L_{UR,GLO}) + c \cdot \Delta\delta t^{S,Trop}_{UR} + \Delta\varepsilon^S_{UR} \tag{8.1.27}$$

Linearizing the geometric range from user to satellite, we obtain

$$\begin{aligned} \Delta PR^S_{UR} \;=\; & \Delta\varrho^S_{UR} + \frac{x_0 - x^S}{\varrho^S_0} \cdot (x_R - x_0) + \frac{y_0 - y^S}{\varrho^S_0} \cdot (y_R - y_0) + \frac{z_0 - z^S}{\varrho^S_0} \cdot (z_R - z_0) + \\ & c \cdot (\Delta\delta t_{UR,0} + \Delta L_{UR,GLO,0}) + \\ & c \cdot [(\Delta\delta t_{UR} + \Delta L_{UR,GLO}) - (\Delta\delta t_{UR,0} + \Delta L_{UR,GLO,0})] + c \cdot \Delta\delta t^{S,Trop}_{UR} + \Delta\varepsilon^S_{UR} \end{aligned} \tag{8.1.28}$$

where $\Delta\varrho^S_{UR}$ now denotes $\varrho^S_0 - \varrho^S_R$, the single difference geometric range from the approximate user position to the satellite.

Again shifting known and modeled terms to the left-hand side of the equation and considering a set of observations to n GLONASS satellites, we obtain a system of observation equations in matrix notation:

$$\vec{l} = \mathbf{A} \cdot \vec{x} + \vec{\varepsilon} \tag{8.1.29}$$

with

$$\vec{l} = \begin{pmatrix} \Delta PR^1_{UR} - \Delta\varrho^1_{UR} - c \cdot (\Delta\delta t_{UR,0} + \Delta L_{UR,GLO,0}) - c \cdot \Delta\delta t^{1,Trop}_{UR} \\ \Delta PR^2_{UR} - \Delta\varrho^2_{UR} - c \cdot (\Delta\delta t_{UR,0} + \Delta L_{UR,GLO,0}) - c \cdot \Delta\delta t^{2,Trop}_{UR} \\ \vdots \\ \Delta PR^n_{UR} - \Delta\varrho^n_{UR} - c \cdot (\Delta\delta t_{UR,0} + \Delta L_{UR,GLO,0}) - c \cdot \Delta\delta t^{n,Trop}_{UR} \end{pmatrix} \tag{8.1.30}$$

the vector of the known values,

$$\mathbf{A} = \begin{pmatrix} \frac{x_0 - x^1}{\varrho^1_0} & \frac{y_0 - y^1}{\varrho^1_0} & \frac{z_0 - z^1}{\varrho^1_0} & 1 \\ \frac{x_0 - x^2}{\varrho^2_0} & \frac{y_0 - y^2}{\varrho^2_0} & \frac{z_0 - z^2}{\varrho^2_0} & 1 \\ \vdots & \vdots & \vdots & \vdots \\ \frac{x_0 - x^n}{\varrho^n_0} & \frac{y_0 - y^n}{\varrho^n_0} & \frac{z_0 - z^n}{\varrho^n_0} & 1 \end{pmatrix} \tag{8.1.31}$$

the design matrix,

$$\vec{x} = \begin{pmatrix} (x_R - x_0) \\ (y_R - y_0) \\ (z_R - z_0) \\ c \cdot [(\Delta\delta t_{UR} + \Delta L_{UR,GLO}) - (\Delta\delta t_{UR,0} + \Delta L_{UR,GLO,0})] \end{pmatrix} \tag{8.1.32}$$

the vector of the unknowns, and

$$\vec{\varepsilon} = \begin{pmatrix} \Delta\varepsilon^1_{UR} \\ \Delta\varepsilon^2_{UR} \\ \vdots \\ \Delta\varepsilon^n_{UR} \end{pmatrix} \tag{8.1.33}$$

the noise vector.

In a combined GPS/GLONASS scenario, single differences from a user station U and a reference station R to a GPS satellite i and a GLONASS satellite j can be formed analogously, starting from Eqs. (8.1.17) and (8.1.18), respectively:

$$PR_R^i = \varrho_R^i + c \cdot (\delta t_R + L_{R,GPS}) - c \cdot \delta t^i + c \cdot \delta t_R^{i,Trop} + c \cdot \delta t_R^{i,Iono} + \varepsilon_R^i \quad (8.1.34)$$

$$PR_U^i = \varrho_U^i + c \cdot (\delta t_U + L_{U,GPS}) - c \cdot \delta t^i + c \cdot \delta t_U^{i,Trop} + c \cdot \delta t_U^{i,Iono} + \varepsilon_U^i \quad (8.1.35)$$

$$PR_R^j = \varrho_R^j + c \cdot (\delta t_R + L_{R,GPS}) + c \cdot \delta t_{Sys} + c \cdot \delta t_{R,HW} - c \cdot \delta t^j + c \cdot \delta t_R^{j,Trop} + c \cdot \delta t_R^{j,Iono} + \varepsilon_R^j \quad (8.1.36)$$

$$PR_U^j = \varrho_U^j + c \cdot (\delta t_U + L_{U,GPS}) + c \cdot \delta t_{Sys} + c \cdot \delta t_{U,HW} - c \cdot \delta t^j + c \cdot \delta t_U^{j,Trop} + c \cdot \delta t_U^{j,Iono} + \varepsilon_U^j \quad (8.1.37)$$

yielding:

$$\Delta PR_{UR}^i = \Delta\varrho_{UR}^i + c \cdot (\Delta\delta t_{UR} + \Delta L_{UR,GPS}) + c \cdot \Delta\delta t_{UR}^{i,Trop} + \Delta\varepsilon_{UR}^i \quad (8.1.38)$$

$$\Delta PR_{UR}^j = \Delta\varrho_{UR}^j + c \cdot (\Delta\delta t_{UR} + \Delta L_{UR,GPS}) + c \cdot \Delta\delta t_{UR,HW} + c \cdot \Delta\delta t_{UR}^{j,Trop} + \Delta\varepsilon_{UR}^j \quad (8.1.39)$$

Besides the satellite clock errors and the ionospheric path delays, now also the time difference between GPS and GLONASS system time δt_{Sys} cancels out, however leaving the difference of the receiver inter-system hardware delays $\Delta\delta t_{UR,HW}$ as a fifth unknown.

Again linearizing the geometric range from observer to satellite, shifting known and modeled terms to the left-hand sides of the equations and considering a set of m GPS and n GLONASS satellites, we obtain for the observation equation in matrix notation:

$$\vec{l} = \mathbf{A} \cdot \vec{x} + \vec{\varepsilon} \quad (8.1.40)$$

with

$$\vec{l} = \begin{pmatrix} \Delta PR_{UR}^1 - \Delta\varrho_{UR}^1 - c \cdot (\Delta\delta t_{UR,0} + \Delta L_{UR,GPS,0}) - c \cdot \Delta\delta t_{UR}^{1,Trop} \\ \vdots \\ \Delta PR_{UR}^m - \Delta\varrho_{UR}^m - c \cdot (\Delta\delta t_{UR,0} + \Delta L_{UR,GPS,0}) - c \cdot \Delta\delta t_{UR}^{m,Trop} \\ \Delta PR_{UR}^{m+1} - \Delta\varrho_{UR}^{m+1} - c \cdot (\Delta\delta t_{UR,0} + \Delta L_{UR,GPS,0}) - c \cdot \Delta\delta t_{UR,HW,0} - c \cdot \Delta\delta t_{UR}^{m+1,Trop} \\ \vdots \\ \Delta PR_{UR}^{m+n} - \Delta\varrho_{UR}^{m+n} - c \cdot (\Delta\delta t_{UR,0} + \Delta L_{UR,GPS,0}) - c \cdot \Delta\delta t_{UR,HW,0} - c \cdot \Delta\delta t_{UR}^{m+n,Trop} \end{pmatrix} \quad (8.1.41)$$

the vector of the known values,

$$\mathbf{A} = \begin{pmatrix} \frac{x_0 - x^1}{\varrho_0^1} & \frac{y_0 - y^1}{\varrho_0^1} & \frac{z_0 - z^1}{\varrho_0^1} & 1 & 0 \\ \vdots & \vdots & \vdots & \vdots & \vdots \\ \frac{x_0 - x^m}{\varrho_0^m} & \frac{y_0 - y^m}{\varrho_0^m} & \frac{z_0 - z^m}{\varrho_0^m} & 1 & 0 \\ \frac{x_0 - x^{m+1}}{\varrho_0^{m+1}} & \frac{y_0 - y^{m+1}}{\varrho_0^{m+1}} & \frac{z_0 - z^{m+1}}{\varrho_0^{m+1}} & 1 & 1 \\ \vdots & \vdots & \vdots & \vdots & \vdots \\ \frac{x_0 - x^{m+n}}{\varrho_0^{m+n}} & \frac{y_0 - y^{m+n}}{\varrho_0^{m+n}} & \frac{z_0 - z^{m+n}}{\varrho_0^{m+n}} & 1 & 1 \end{pmatrix} \quad (8.1.42)$$

the design matrix,

$$\vec{x} = \begin{pmatrix} (x_R - x_0) \\ (y_R - y_0) \\ (z_R - z_0) \\ c \cdot [(\Delta\delta t_{UR} + \Delta L_{UR,GPS}) - (\Delta\delta t_{UR,0} + \Delta L_{UR,GPS,0})] \\ c \cdot (\Delta\delta t_{UR,HW} - \Delta\delta t_{UR,HW,0}) \end{pmatrix} \tag{8.1.43}$$

the vector of the unknowns, and

$$\vec{\varepsilon} = \begin{pmatrix} \Delta\varepsilon_{UR}^{1} \\ \vdots \\ \Delta\varepsilon_{UR}^{m} \\ \Delta\varepsilon_{UR}^{m+1} \\ \vdots \\ \Delta\varepsilon_{UR}^{m+n} \end{pmatrix} \tag{8.1.44}$$

the noise vector.

An example of positioning results using GPS and GLONASS single difference positioning with pseudoranges is shown in Figure 8.3. Positions were computed from data logged by two 3S Navigation R-100/R-101 receivers, which were set up at known locations at the Institute of Geodesy and Navigation. Pseudorange and carrier phase measurements were logged every second for approximately one hour each, of which some forty minutes were common to both receivers. One of these receivers was used as reference station, the other was treated as the user station. Its position was determined in this example. Observation epochs at both receivers were not exactly synchronized. The data of the user station are the same as the data already used for the absolute positioning example. The plot shows the deviation from the known location of the antenna of the user station in the horizontal plane. GPS positions were computed from carrier smoothed L_1 C/A-code pseudorange measurements. GLONASS positions were computed from carrier smoothed dual-frequency P-code measurements. Wherever possible, the ionospheric free linear combination was formed. These observables used are not really identical for GPS and GLONASS, but with P-code and dual-frequency measurements readily available on GLONASS, the best possible results for each system are determined. GLONASS satellite positions were converted from PZ-90 to WGS84 using the transformation according to (*Roßbach et al., 1996*).

The large deviations from the true position due to GPS S/A have been eliminated by the differencing of observations, but not completely. Due to the measurements at reference and user station not being exactly synchronized, the effects of GPS S/A do not cancel entirely. This is most clearly visible in North/South direction, where the S/A effects on the absolute positioning also were most obvious. Standard deviations of the computed positions from GPS only are 3.7 m in North/South direction and 1.3 m in East/West direction. Since there is no S/A on GLONASS, its effects cannot remain in the differenced positioning solution due to imperfect synchronization of measurements. Consequently, positions computed only from GLONASS range measurements scatter much less. Here the standard deviations are 1.4 m in North/South direction and 0.8 m in East/West direction. For the combined GPS/GLONASS positioning, all satellite measurements were weighted equally. These results are still affected by GPS S/A due to imperfect synchronization, but to a much less extent than the GPS only results. Standard deviations are 1.6 m in North/South direction and 0.8 m in East/West direction.

The height components of the processing results are displayed in Figure 8.4 as a time series. Again it can be seen that the GPS solution deviates far more from the true position, which is 594.5 m, than the GLONASS solution. Oscillations due to S/A, caused by the imperfect synchronization, are clearly visible. Standard deviation of the GPS height component is 7.3 m around a mean value of 591.6 m. There are no such oscillations on the GLONASS solutions. These positions are more stable. However, one can notice one extended outlier around 142100 - 142200 s GPS time. The cause of this is not clear.

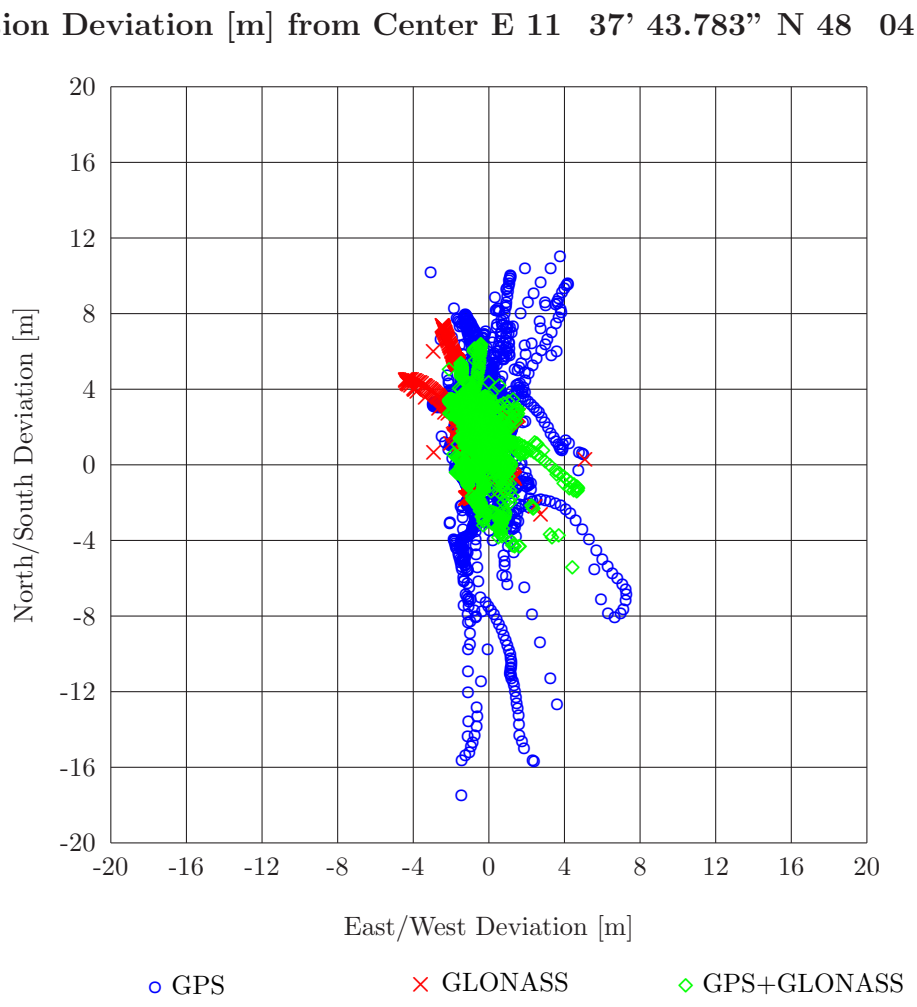

Figure 8.3: GPS, GLONASS and combined GPS/GLONASS single difference positioning.

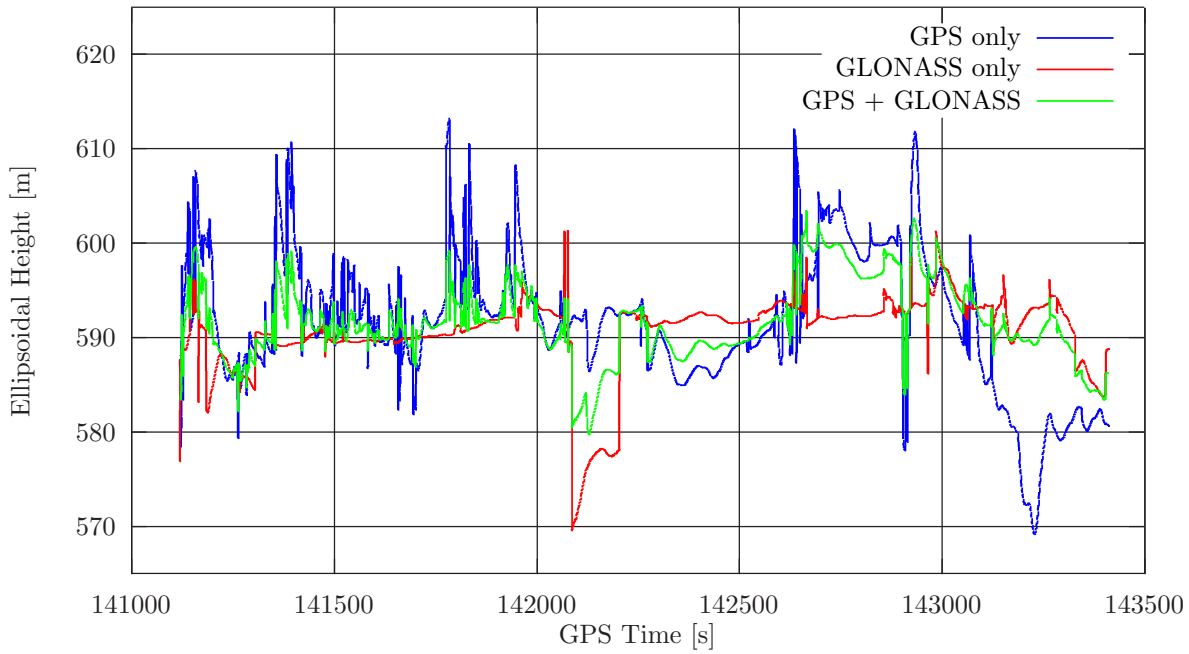

Figure 8.4: GPS, GLONASS and combined GPS/GLONASS single difference positioning, height component.

Contrary to the absolute positioning example, it cannot be caused by the change in applicable GLONASS satellite ephemeris data. New ephemeris data become effective at 142200 s GPS time, which is at the end of the outlier. Satellite geometry neither does change during the period in question. Changing satellite geometry does, however, cause a jump in the height solution at 143328 s like in the cause of the absolute positioning example. Standard deviation of the GLONASS height component is 4.2 m around a mean height of 590.5 m. As with the horizontal components, the combined GPS/GLONASS solution also is affected by remaining GPS S/A, but to a less extent than the GPS only results. The mean GPS/GLONASS height is 591.7 m with a standard deviation of 4.2 m.

8.1.3 Double Difference Positioning

Having available single differences from two observers U and R to two GLONASS satellites S and r,

$$\Delta PR^S_{UR} = \Delta\varrho^S_{UR} + c\cdot(\Delta\delta t_{UR} + \Delta L_{UR,GLO}) + c\cdot\Delta\delta t^{S,Trop}_{UR} + \Delta\varepsilon^S_{UR} \quad (8.1.45)$$

$$\Delta PR^r_{UR} = \Delta\varrho^r_{UR} + c\cdot(\Delta\delta t_{UR} + \Delta L_{UR,GLO}) + c\cdot\Delta\delta t^{r,Trop}_{UR} + \Delta\varepsilon^r_{UR} \quad (8.1.46)$$

one can subtract the single difference measurement to the reference satellite r from the single difference measurement to the other satellite:

$$\Delta PR^S_{UR} - \Delta PR^r_{UR} = \Delta\varrho^S_{UR} - \Delta\varrho^r_{UR} + c\cdot\Delta\delta t^{S,Trop}_{UR} - c\cdot\Delta\delta t^{r,Trop}_{UR} + \Delta\varepsilon^S_{UR} - \Delta\varepsilon^r_{UR} \quad (8.1.47)$$

Now also the relative receiver clock error $\Delta\delta t_{UR}+\Delta L_{UR,GLO}$ (including the relative common hardware delays) cancels out. Denoting the double difference terms $\Delta *^S_{UR} - \Delta *^r_{UR}$ as $\nabla\Delta *^{Sr}_{UR}$, Eq. (8.1.47) transforms to

$$\nabla\Delta PR^{Sr}_{UR} = \nabla\Delta\varrho^{Sr}_{UR} + c\cdot\nabla\Delta\delta t^{Sr,Trop}_{UR} + \nabla\Delta\varepsilon^{Sr}_{UR} \quad (8.1.48)$$

Linearizing the geometric ranges from the user station to the satellites, we obtain

$$\nabla\Delta PR^{Sr}_{UR} = \nabla\Delta\varrho^{Sr}_{UR} + \frac{x_0 - x^S}{\varrho^S_0}\cdot(x_R - x_0) - \frac{x_0 - x^r}{\varrho^r_0}\cdot(x_R - x_0) + \frac{y_0 - y^S}{\varrho^S_0}\cdot(y_R - y_0) -$$

$$\frac{y_0 - y^r}{\varrho_0^r} \cdot (y_R - y_0) + \frac{z_0 - z^S}{\varrho_0^S} \cdot (z_R - z_0) - \frac{z_0 - z^r}{\varrho_0^r} \cdot (z_R - z_0) + c \cdot \nabla\Delta\delta t_{UR}^{Sr,Trop} + \nabla\Delta\varepsilon_{UR}^{Sr} \tag{8.1.49}$$

where $\nabla\Delta\varrho_{UR}^{Sr}$ now denotes $(\varrho_0^S - \varrho_R^S) - (\varrho_0^r - \varrho_R^r)$, the double difference geometric range from the approximate user position to the satellites.

Again shifting known and modeled terms to the left-hand side of the equation and considering a set of observations to n GLONASS satellites (not including the reference satellite r), we obtain a system of observation equations in matrix notation:

$$\vec{l} = \mathbf{A} \cdot \vec{x} + \vec{\varepsilon} \tag{8.1.50}$$

with

$$\vec{l} = \begin{pmatrix} \nabla\Delta PR_{UR}^{1r} - \nabla\Delta\varrho_{UR}^{1r} - c \cdot \nabla\Delta\delta t_{UR}^{1r,Trop} \\ \nabla\Delta PR_{UR}^{2r} - \nabla\Delta\varrho_{UR}^{2r} - c \cdot \nabla\Delta\delta t_{UR}^{2r,Trop} \\ \vdots \\ \nabla\Delta PR_{UR}^{nr} - \nabla\Delta\varrho_{UR}^{nr} - c \cdot \nabla\Delta\delta t_{UR}^{nr,Trop} \end{pmatrix} \tag{8.1.51}$$

the vector of the known values,

$$\mathbf{A} = \begin{pmatrix} \frac{x_0 - x^1}{\varrho_0^1} - \frac{x_0 - x^r}{\varrho_0^r} & \frac{y_0 - y^1}{\varrho_0^1} - \frac{y_0 - y^r}{\varrho_0^r} & \frac{z_0 - z^1}{\varrho_0^1} - \frac{z_0 - z^r}{\varrho_0^r} \\ \frac{x_0 - x^2}{\varrho_0^2} - \frac{x_0 - x^r}{\varrho_0^r} & \frac{y_0 - y^2}{\varrho_0^2} - \frac{y_0 - y^r}{\varrho_0^r} & \frac{z_0 - z^2}{\varrho_0^2} - \frac{z_0 - z^r}{\varrho_0^r} \\ \vdots & \vdots & \vdots \\ \frac{x_0 - x^n}{\varrho_0^n} - \frac{x_0 - x^r}{\varrho_0^r} & \frac{y_0 - y^n}{\varrho_0^n} - \frac{y_0 - y^r}{\varrho_0^r} & \frac{z_0 - z^n}{\varrho_0^n} - \frac{z_0 - z^r}{\varrho_0^r} \end{pmatrix} \tag{8.1.52}$$

the design matrix,

$$\vec{x} = \begin{pmatrix} (x_R - x_0) \\ (y_R - y_0) \\ (z_R - z_0) \end{pmatrix} \tag{8.1.53}$$

the vector of the unknowns, and

$$\vec{\varepsilon} = \begin{pmatrix} \nabla\Delta\varepsilon_{UR}^{1r} \\ \nabla\Delta\varepsilon_{UR}^{2r} \\ \vdots \\ \nabla\Delta\varepsilon_{UR}^{nr} \end{pmatrix} \tag{8.1.54}$$

the noise vector.

In a combined GPS/GLONASS scenario, with a GPS satellite i, a GLONASS satellite j and the reference satellite r, two cases must be distinguished, depending on whether the reference satellite is a GPS or a GLONASS satellite:

1. The reference satellite is a GPS satellite.

   From the single difference observations

$$\Delta PR_{UR}^{i} = \Delta\varrho_{UR}^{i} + c \cdot (\Delta\delta t_{UR} + \Delta L_{UR,GPS}) + c \cdot \Delta\delta t_{UR}^{i,Trop} + \Delta\varepsilon_{UR}^{i} \tag{8.1.55}$$

$$\Delta PR_{UR}^{j} = \Delta\varrho_{UR}^{j} + c \cdot (\Delta\delta t_{UR} + \Delta L_{UR,GPS}) + c \cdot \Delta\delta t_{UR,HW} + c \cdot \Delta\delta t_{UR}^{j,Trop} + \Delta\varepsilon_{UR}^{j} \tag{8.1.56}$$

$$\Delta PR_{UR}^{r} = \Delta\varrho_{UR}^{r} + c \cdot (\Delta\delta t_{UR} + \Delta L_{UR,GPS}) + c \cdot \Delta\delta t_{UR}^{r,Trop} + \Delta\varepsilon_{UR}^{r} \tag{8.1.57}$$

one can form the double differences

$$\nabla\Delta PR_{UR}^{ir} = \nabla\Delta\varrho_{UR}^{ir} + c\cdot\nabla\Delta\delta t_{UR}^{ir,Trop} + \nabla\Delta\varepsilon_{UR}^{ir} \quad (8.1.58)$$

$$\nabla\Delta PR_{UR}^{jr} = \nabla\Delta\varrho_{UR}^{jr} + c\cdot\Delta\delta t_{UR,HW} + c\cdot\nabla\Delta\delta t_{UR}^{jr,Trop} + \nabla\Delta\varepsilon_{UR}^{jr} \quad (8.1.59)$$

The single difference receiver inter-system hardware delay $\Delta\delta t_{UR,HW}$ remains in the mixed GLONASS/GPS double difference.

2. The reference satellite is a GLONASS satellite.

From the single difference observations

$$\Delta PR_{UR}^{i} = \Delta\varrho_{UR}^{i} + c\cdot(\Delta\delta t_{UR} + \Delta L_{UR,GPS}) + c\cdot\Delta\delta t_{UR}^{i,Trop} + \Delta\varepsilon_{UR}^{i} \quad (8.1.60)$$

$$\Delta PR_{UR}^{j} = \Delta\varrho_{UR}^{j} + c\cdot(\Delta\delta t_{UR} + \Delta L_{UR,GPS}) + c\cdot\Delta\delta t_{UR,HW} + c\cdot\Delta\delta t_{UR}^{j,Trop} + \Delta\varepsilon_{UR}^{j} \quad (8.1.61)$$

$$\Delta PR_{UR}^{r} = \Delta\varrho_{UR}^{r} + c\cdot(\Delta\delta t_{UR} + \Delta L_{UR,GPS}) + c\cdot\Delta\delta t_{UR,HW} + c\cdot\Delta\delta t_{UR}^{r,Trop} + \Delta\varepsilon_{UR}^{r} \quad (8.1.62)$$

one can form the double differences

$$\nabla\Delta PR_{UR}^{ir} = \nabla\Delta\varrho_{UR}^{ir} - c\cdot\Delta\delta t_{UR,HW} + c\cdot\nabla\Delta\delta t_{UR}^{ir,Trop} + \nabla\Delta\varepsilon_{UR}^{ir} \quad (8.1.63)$$

$$\nabla\Delta PR_{UR}^{jr} = \nabla\Delta\varrho_{UR}^{jr} + c\cdot\nabla\Delta\delta t_{UR}^{jr,Trop} + \nabla\Delta\varepsilon_{UR}^{jr} \quad (8.1.64)$$

The single difference receiver inter-system hardware delay $\Delta\delta t_{UR,HW}$ now cancels out in the GLONASS/GLONASS double difference, but it shows up in the mixed GPS/GLONASS double difference with the opposite sign instead.

The single difference receiver inter-system hardware delay $\Delta\delta t_{UR,HW}$ remains as a fourth unknown in the double difference observation equations. Depending on whether the reference satellite is a GPS or a GLONASS satellite, it shows up with opposite sign either at the GLONASS or the GPS satellites.

Considering this fact, we obtain for the observation equations of a set of m GPS and n GLONASS satellites (not including the reference satellite r):

$$\vec{l} = \mathbf{A}\cdot\vec{x} + \vec{\varepsilon} \quad (8.1.65)$$

with

$$\vec{l} = \begin{pmatrix} \nabla\Delta PR_{UR}^{1r} - \nabla\Delta\varrho_{UR}^{1r} - k_{GPS}\cdot c\cdot\Delta\delta t_{UR,HW,0} - c\cdot\nabla\Delta\delta t_{UR}^{1r,Trop} \\ \vdots \\ \nabla\Delta PR_{UR}^{mr} - \nabla\Delta\varrho_{UR}^{mr} - k_{GPS}\cdot c\cdot\Delta\delta t_{UR,HW,0} - c\cdot\nabla\Delta\delta t_{UR}^{mr,Trop} \\ \nabla\Delta PR_{UR}^{m+1,r} - \nabla\Delta\varrho_{UR}^{m+1,r} - k_{GLONASS}\cdot c\cdot\Delta\delta t_{UR,HW,0} - c\cdot\nabla\Delta\delta t_{UR}^{m+1,r,Trop} \\ \vdots \\ \nabla\Delta PR_{UR}^{m+n,r} - \nabla\Delta\varrho_{UR}^{m+n,r} - k_{GLONASS}\cdot c\cdot\Delta\delta t_{UR,HW,0} - c\cdot\nabla\Delta\delta t_{UR}^{m+n,r,Trop} \end{pmatrix} \quad (8.1.66)$$

with

$$k_{GPS} = \begin{cases} 0 & , r\in\text{GPS} \\ -1 & , r\in\text{GLONASS} \end{cases}$$

$$k_{GLONASS} = \begin{cases} 1 & , r\in\text{GPS} \\ 0 & , r\in\text{GLONASS} \end{cases}$$

the vector of the known values,

$$\mathbf{A}=\begin{pmatrix} \frac{x_0-x^1}{\varrho_0^1}-\frac{x_0-x^r}{\varrho_0^r} & \frac{y_0-y^1}{\varrho_0^1}-\frac{y_0-y^r}{\varrho_0^r} & \frac{z_0-z^1}{\varrho_0^1}-\frac{z_0-z^r}{\varrho_0^r} & k_{GPS} \\ \vdots & \vdots & \vdots & \vdots \\ \frac{x_0-x^m}{\varrho_0^m}-\frac{x_0-x^r}{\varrho_0^r} & \frac{y_0-y^m}{\varrho_0^m}-\frac{y_0-y^r}{\varrho_0^r} & \frac{z_0-z^m}{\varrho_0^m}-\frac{z_0-z^r}{\varrho_0^r} & k_{GPS} \\ \frac{x_0-x^{m+1}}{\varrho_0^{m+1}}-\frac{x_0-x^r}{\varrho_0^r} & \frac{y_0-y^{m+1}}{\varrho_0^{m+1}}-\frac{y_0-y^r}{\varrho_0^r} & \frac{z_0-z^{m+1}}{\varrho_0^{m+1}}-\frac{z_0-z^r}{\varrho_0^r} & k_{GLONASS} \\ \vdots & \vdots & \vdots & \vdots \\ \frac{x_0-x^{m+n}}{\varrho_0^{m+n}}-\frac{x_0-x^r}{\varrho_0^r} & \frac{y_0-y^{m+n}}{\varrho_0^{m+n}}-\frac{y_0-y^r}{\varrho_0^r} & \frac{z_0-z^{m+n}}{\varrho_0^{m+n}}-\frac{z_0-z^r}{\varrho_0^r} & k_{GLONASS} \end{pmatrix} \tag{8.1.67}$$

the design matrix,

$$\vec{x}=\begin{pmatrix} (x_R-x_0) \\ (y_R-y_0) \\ (z_R-z_0) \\ c\cdot(\Delta\delta t_{UR,HW}-\Delta\delta t_{UR,HW,0}) \end{pmatrix} \tag{8.1.68}$$

the vector of the unknowns, and

$$\vec{\varepsilon}=\begin{pmatrix} \nabla\Delta\varepsilon_{UR}^{1r} \\ \vdots \\ \nabla\Delta\varepsilon_{UR}^{mr} \\ \nabla\Delta\varepsilon_{UR}^{m+1,r} \\ \vdots \\ \nabla\Delta\varepsilon_{UR}^{m+n,r} \end{pmatrix} \tag{8.1.69}$$

the noise vector.

The single difference receiver inter-system hardware delay $\Delta\delta t_{UR,HW}$ will, however, cancel, if two separate reference satellites for GPS and for GLONASS are chosen. In that case, from the single difference observations

$$\Delta PR_{UR}^{i} = \Delta\varrho_{UR}^{i}+c\cdot(\Delta\delta t_{UR}+\Delta L_{UR,GPS})+c\cdot\Delta\delta t_{UR}^{i,Trop}+\Delta\varepsilon_{UR}^{i} \tag{8.1.70}$$

$$\Delta PR_{UR}^{r^{GPS}} = \Delta\varrho_{UR}^{r^{GPS}}+c\cdot(\Delta\delta t_{UR}+\Delta L_{UR,GPS})+c\cdot\Delta\delta t_{UR}^{r^{GPS},Trop}+\Delta\varepsilon_{UR}^{r^{GPS}} \tag{8.1.71}$$

$$\Delta PR_{UR}^{j} = \Delta\varrho_{UR}^{j}+c\cdot(\Delta\delta t_{UR}+\Delta L_{UR,GPS})+c\cdot\Delta\delta t_{UR,HW}+c\cdot\Delta\delta t_{UR}^{j,Trop}+\Delta\varepsilon_{UR}^{j} \tag{8.1.72}$$

$$\Delta PR_{UR}^{r^{GLO}} = \Delta\varrho_{UR}^{r^{GLO}}+c\cdot(\Delta\delta t_{UR}+\Delta L_{UR,GPS})+c\cdot\Delta\delta t_{UR,HW}+c\cdot\Delta\delta t_{UR}^{r^{GPS},Trop}+\Delta\varepsilon_{UR}^{r^{GPS}} \tag{8.1.73}$$

to GPS satellites i and r^{GPS} and GLONASS satellites j and r^{GLO} the double difference observations

$$\nabla\Delta PR_{UR}^{ir^{GPS}} = \nabla\Delta\varrho_{UR}^{ir^{GPS}}+c\cdot\nabla\Delta\delta t_{UR}^{ir^{GPS},Trop}+\nabla\Delta\varepsilon_{UR}^{ir^{GPS}} \tag{8.1.74}$$

$$\nabla\Delta PR_{UR}^{jr^{GLO}} = \nabla\Delta\varrho_{UR}^{jr^{GLO}}+c\cdot\nabla\Delta\delta t_{UR}^{jr^{GLO},Trop}+\nabla\Delta\varepsilon_{UR}^{jr^{GLO}} \tag{8.1.75}$$

can be formed.

Again shifting all known and modeled terms to the left-hand side of the equation and considering a set of observations to m GPS and n GLONASS satellites (not including the respective reference satellites), we obtain a system of observation equations in matrix notation:

$$\vec{l}=\mathbf{A}\cdot\vec{x}+\vec{\varepsilon} \tag{8.1.76}$$

with

$$\vec{l} = \begin{pmatrix} \nabla\Delta PR_{UR}^{1r^{GPS}} - \nabla\Delta\varrho_{UR}^{1r^{GPS}} - c\cdot\nabla\Delta\delta t_{UR}^{1r^{GPS},Trop} \\ \vdots \\ \nabla\Delta PR_{UR}^{mr^{GPS}} - \nabla\Delta\varrho_{UR}^{mr^{GPS}} - c\cdot\nabla\Delta\delta t_{UR}^{mr^{GPS},Trop} \\ \nabla\Delta PR_{UR}^{m+1,r^{GLO}} - \nabla\Delta\varrho_{UR}^{m+1,r^{GLO}} - c\cdot\nabla\Delta\delta t_{UR}^{m+1,r^{GLO},Trop} \\ \vdots \\ \nabla\Delta PR_{UR}^{m+n,r^{GLO}} - \nabla\Delta\varrho_{UR}^{m+n,r^{GLO}} - c\cdot\nabla\Delta\delta t_{UR}^{m+n,r^{GLO},Trop} \end{pmatrix} \tag{8.1.77}$$

the vector of the known values,

$$\mathbf{A} = \begin{pmatrix} \frac{x_0 - x^1}{\varrho_0^1} - \frac{x_0 - x^{r^{GPS}}}{\varrho_0^{r^{GPS}}} & \frac{y_0 - y^1}{\varrho_0^1} - \frac{y_0 - y^{r^{GPS}}}{\varrho_0^{r^{GPS}}} & \frac{z_0 - z^1}{\varrho_0^1} - \frac{z_0 - z^{r^{GPS}}}{\varrho_0^{r^{GPS}}} \\ \vdots & \vdots & \vdots \\ \frac{x_0 - x^m}{\varrho_0^m} - \frac{x_0 - x^{r^{GPS}}}{\varrho_0^{r^{GPS}}} & \frac{y_0 - y^m}{\varrho_0^m} - \frac{y_0 - y^{r^{GPS}}}{\varrho_0^{r^{GPS}}} & \frac{z_0 - z^m}{\varrho_0^m} - \frac{z_0 - z^{r^{GPS}}}{\varrho_0^{r^{GPS}}} \\ \frac{x_0 - x^{m+1}}{\varrho_0^{m+1}} - \frac{x_0 - x^{r^{GLO}}}{\varrho_0^{r^{GLO}}} & \frac{y_0 - y^{m+1}}{\varrho_0^{m+1}} - \frac{y_0 - y^{r^{GLO}}}{\varrho_0^{r^{GLO}}} & \frac{z_0 - z^{m+1}}{\varrho_0^{m+1}} - \frac{z_0 - z^{r^{GLO}}}{\varrho_0^{r^{GLO}}} \\ \vdots & \vdots & \vdots \\ \frac{x_0 - x^{m+n}}{\varrho_0^{m+n}} - \frac{x_0 - x^{r^{GLO}}}{\varrho_0^{r^{GLO}}} & \frac{y_0 - y^{m+n}}{\varrho_0^{m+n}} - \frac{y_0 - y^{r^{GLO}}}{\varrho_0^{r^{GLO}}} & \frac{z_0 - z^{m+n}}{\varrho_0^{m+n}} - \frac{z_0 - z^{r^{GLO}}}{\varrho_0^{r^{GLO}}} \end{pmatrix} \tag{8.1.78}$$

the design matrix,

$$\vec{x} = \begin{pmatrix} (x_R - x_0) \\ (y_R - y_0) \\ (z_R - z_0) \end{pmatrix} \tag{8.1.79}$$

the vector of the unknowns, and

$$\vec{\varepsilon} = \begin{pmatrix} \nabla\Delta\varepsilon_{UR}^{1r^{GPS}} \\ \vdots \\ \nabla\Delta\varepsilon_{UR}^{mr^{GPS}} \\ \nabla\Delta\varepsilon_{UR}^{m+1,r^{GLO}} \\ \vdots \\ \nabla\Delta\varepsilon_{UR}^{m+n,r^{GLO}} \end{pmatrix} \tag{8.1.80}$$

the noise vector.

Compared to the system of Eqs. (8.1.65) to (8.1.69), in system Eqs. (8.1.76) to (8.1.80) one unknown (the single difference receiver inter-system hardware delay $\Delta\delta t_{UR,HW}$) has cancelled. This advantage was obtained by sacrificing one more satellite measurement and using this satellite as reference satellite. In case when there is only one GPS or one GLONASS satellite among the set of observed satellites (the latter seems more likely, if the GLONASS constellation dwindles further), a combined GPS/GLONASS solution therefore cannot be calculated, since there will be no reference satellite for this system. Anyhow, with only one satellite of one system, in the system of Eqs. (8.1.65) to (8.1.69) this one measurement is employed to calculate the single difference receiver inter-system hardware delay. This will cause the calculated combined GPS/GLONASS positioning solution to be identical to the one possible single system positioning solution. Thus, both systems – Eqs. (8.1.65) to (8.1.69) and (8.1.76) to (8.1.80) – are equivalent.

An example of positioning results using GPS and GLONASS double difference positioning with pseudoranges is shown in Figure 8.5. Positions were computed from data logged by two 3S Navigation R-100/R-101 receivers, which were set up on observation pillars at known locations near the Institute

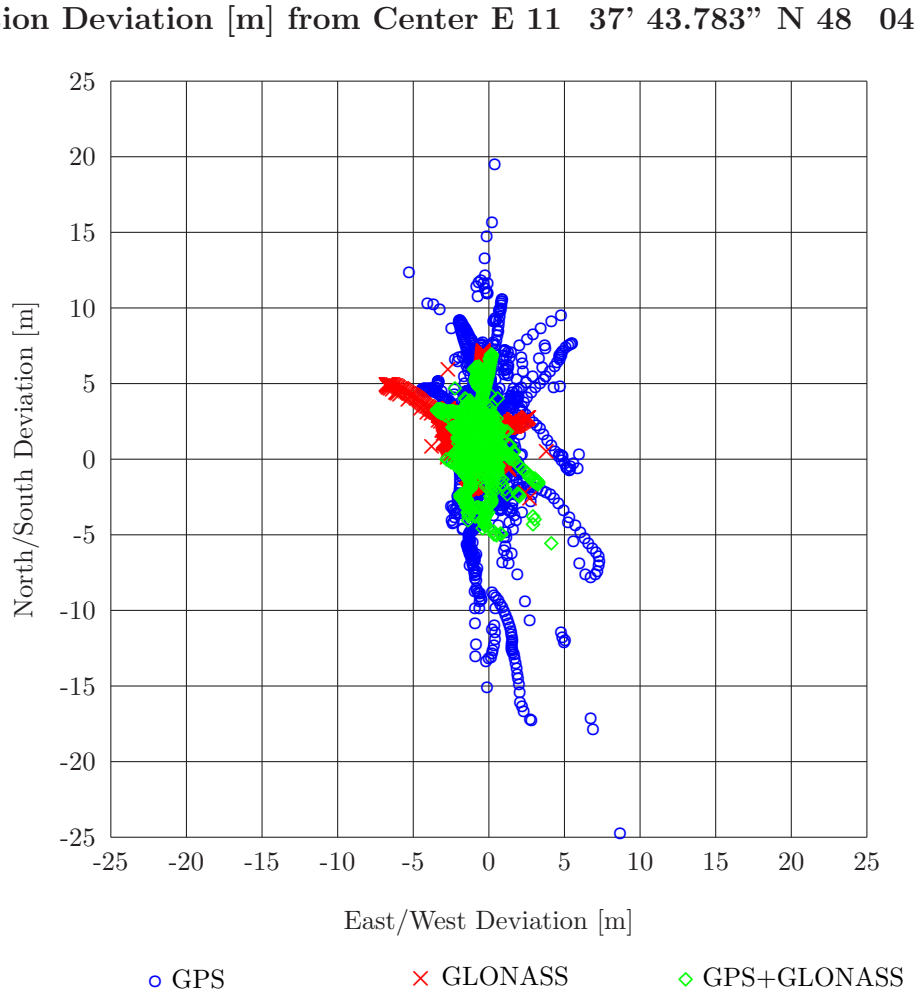

Figure 8.5: GPS, GLONASS and combined GPS/GLONASS double difference positioning.

of Geodesy and Navigation. Pseudorange and carrier phase measurements were logged every second for approximately one hour each, of which some forty minutes were common to both receivers. One of these receivers was used as reference station, the other was treated as the user station. Its position was determined and compared to its known coordinates in this example. Observation epochs at both receivers were not exactly synchronized. The data are the same as already used for the single difference example. The plot shows the deviation from the known location of the antenna of the user station in the horizontal plane. GPS positions were computed from carrier smoothed L_1 C/A-code pseudorange measurements. GLONASS positions were computed from carrier smoothed dual-frequency P-code measurements. Wherever possible, the ionospheric free linear combination was formed. These observables used are not really identical for GPS and GLONASS, but with P-code and dual-frequency measurements readily available on GLONASS, the best possible results for each system are determined. GLONASS satellite positions at the time of signal transmission were converted from PZ-90 to WGS84 using the transformation according to (*Roßbach et al., 1996*). For the combined GPS/GLONASS double difference, the system of Eqs. (8.1.65) to (8.1.69) has been employed.

Like in the single difference case, the large deviations from the true position due to GPS S/A have been eliminated by the differencing of observations, but not completely, due to the imperfect synchronization of measurements at reference and user station. Again, this is most clearly visible in North/South direction, where the S/A effects on the absolute and single difference positioning also were most obvious. Standard deviations of the computed positions from GPS only are 4.1 m in North/South direction and 1.5 m in East/West direction. This is even slightly more than in the single difference case, due to the increased

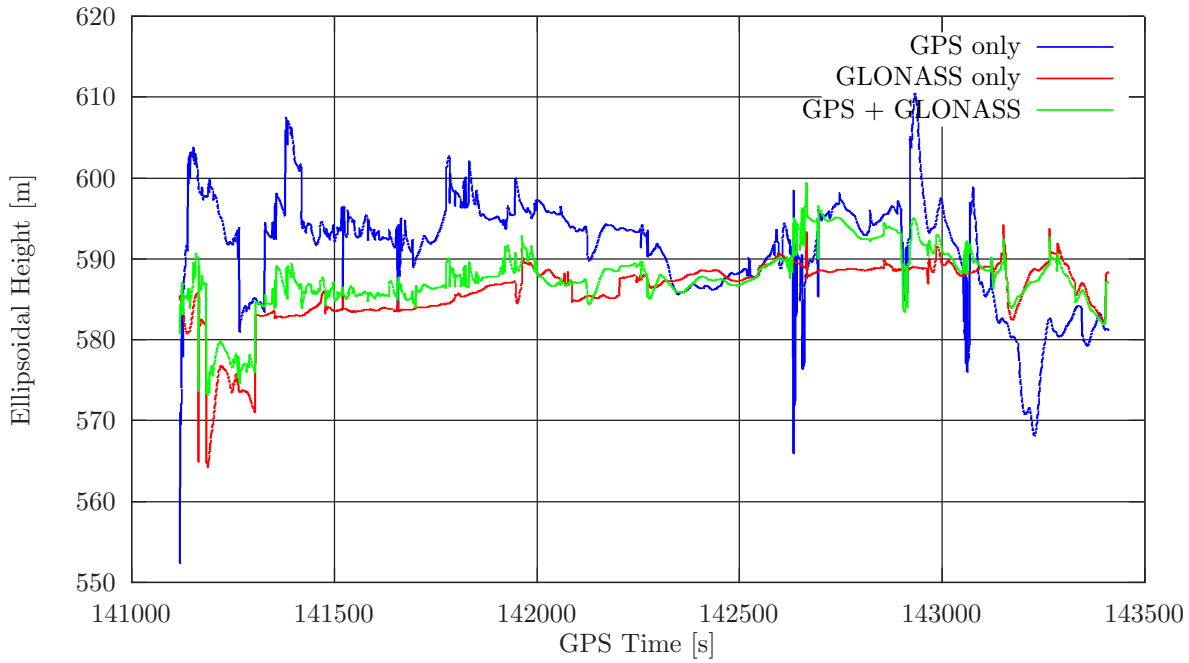

Figure 8.6: GPS, GLONASS and combined GPS/GLONASS double difference positioning, height component.

noise level of the double difference observations. Since there is no S/A on GLONASS, its effects cannot remain in the differenced positioning solution even with imperfect synchronization of measurements. Consequently, positions computed only from GLONASS range measurements scatter much less. Here the standard deviations are 1.4 m in North/South direction and 1.2 m in East/West direction. Again, slightly more than in the single difference example. For the combined GPS/GLONASS positioning, all satellite measurements were weighted equally. These results are still affected by GPS S/A due to imperfect synchronization, but to a much less extent than the GPS only results. Standard deviations are 1.8 m in North/South direction and 0.8 m in East/West direction. This is better than in the single difference case.

The height components of the processing results are displayed as a time series in Figure 8.6. Again it can be seen that the GPS solution oscillates very much due to remaining S/A effects, caused by the imperfect synchronization of measurement epochs. However, the mean GPS height solution of 591.3 m is closest to the true height, which is 594.5 m. Standard deviation of the GPS height component is 6.5 m. Again, there are no oscillations on the GLONASS solutions. These positions are more stable. However, one can notice a clear bias in the GLONASS height solution, especially during the first two thirds of the observation period. The increasing oscillations towards the end of the observation period are most likely caused by multipath effects, together with a change in satellite geometry. Track to one satellite was lost at 143328 s GPS time, leading to an increased VDOP value and thus increased noise of the height solution. Mean GLONASS height is 586.0 m, standard deviation is 3.9 m. Over a large extent of the observation period, the combined GPS/GLONASS height solution is more stable than the GPS or GLONASS only solutions. This definitely is caused by the more favorable VDOP of the extended satellite geometry. However, one can also notice a bias in the combined solution. Mean GPS/GLONASS height is 587.7 m, which is closer to the true height than the GLONASS only solution. Standard deviation of the height component is 3.8 m and thus only slightly better than that of the GLONASS only solution.

Figure 8.7 shows the computed single difference receiver inter-system hardware delay $\Delta\delta t_{UR,HW}$, as used in the system of Eqs. (8.1.65) to (8.1.69). It can be clearly seen that this bias is not constant. Its

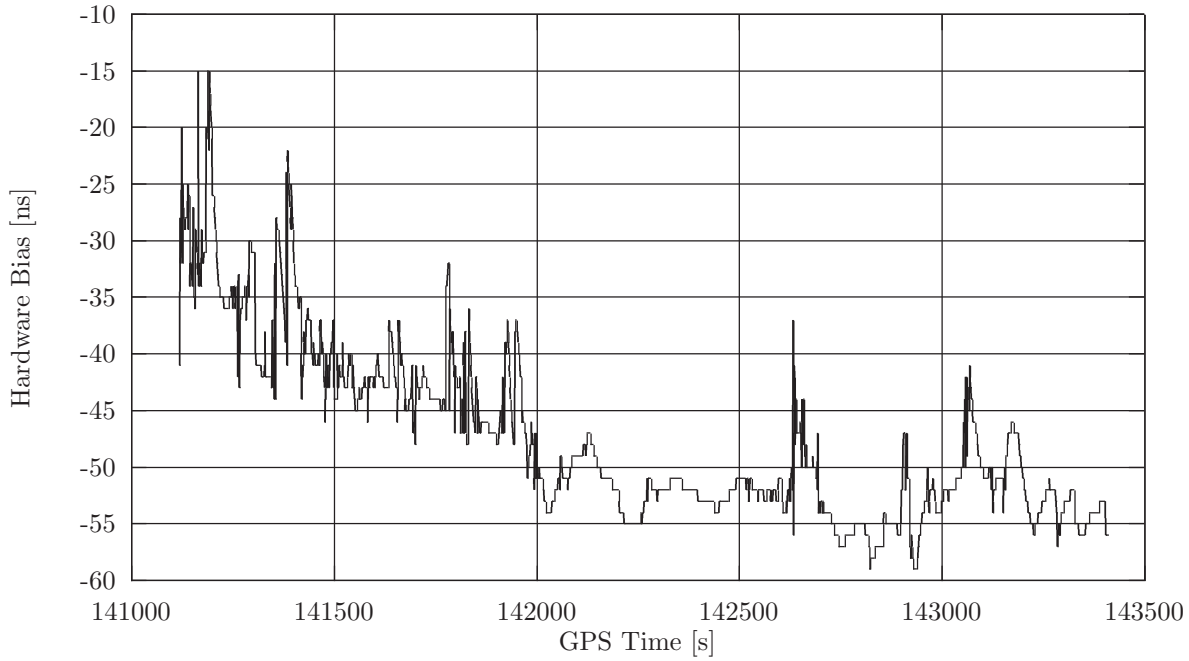

Figure 8.7: GPS/GLONASS double difference inter-system hardware delay.

absolute value increases with time, until it obviously reaches some kind of saturation after approximately fifteen minutes. Even then, it oscillates strongly around this value.

8.2 Carrier Phase Measurements

8.2.1 Single Point Observation Equation

Analogously to GPS, carrier phase measurements to GLONASS satellites can be used to determine user positions even more precisely than by means of pseudorange measurements.

The observation equation for carrier phase measurements from receiver R to satellite S can be written as:

$$\varphi_R^S = \frac{1}{\lambda^S}\varrho_R^S + N_R^S + f^S \cdot (\delta t_R + L_{R,GLO}) - f^S \cdot \delta t^S + f^S \cdot \delta t_R^{S,Trop} - f^S \cdot \delta t_R^{S,Iono} + f^S \cdot \delta t_{R,ICB}^S + \varepsilon_R^S \quad (8.2.1)$$

with $\varrho_R^S = \sqrt{(x_R - x^S)^2 + (y_R - y^S)^2 + (z_R - z^S)^2}$ and

$\vec{x}_R$	Position vector of receiver
$\vec{x}^S$	Position vector of satellite
λ^S	Wavelength of carrier signal of satellite S
Φ_r^S	Carrier phase measurement of receiver R to satellite S
N_R^S	Carrier phase ambiguity of receiver R to satellite S
f^S	Frequency of satellite signal
δt_R	Receiver clock offset with respect to system time
$L_{R,GLO}$	Common frequency-dependent hardware delay for GLONASS satellites
δt^S	Satellite clock offset with respect to system time
$\delta t_R^{S,Trop}$	Tropospheric delay of signal
$\delta t_R^{S,Iono}$	Ionospheric advance of signal
$\delta t_{R,ICB}^S$	Inter channel bias for measurement of receiver R to satellite S
ε_R^S	Measurement noise

It should be noted that, due to the dispersive character of the ionosphere, the carrier signal is accelerated in the ionosphere, contrary to the code signal, which is delayed.

Units in Eq. (8.2.1) are cycles. Scaled to units of length, this equation reads

$$\Phi_R^S = \varrho_R^S + \lambda^S N_R^S + c \cdot (\delta t_R + L_{R,GLO}) - c \cdot \delta t^S + c \cdot \delta t_R^{S,Trop} - c \cdot \delta t_R^{S,Iono} + c \cdot \delta t_{R,ICB}^S + \lambda^S \varepsilon_R^S \quad (8.2.2)$$

where

c	Speed of light in vacuum
$\Phi_R^S = \lambda^S \varphi_R^S$	Carrier phase measurement scaled to distance

Like in the case of the pseudorange observations Eq. (8.1.8), the tropospheric delay $\delta t_R^{S,Trop}$ has to be determined using a suitable model, e.g. a Modified Hopfield model, if possible supported by measurements of the actual temperature, air pressure and humidity at the time of observation. The ionospheric acceleration $\delta t_R^{S,Iono}$ also can be modeled using e.g. the GPS Klobuchar model, adapted to GLONASS carrier frequencies. This model as described in Section 8.5 for the determination of the ionospheric path delay for L_1 pseudorange measurements can likewise be applied to the correction of ionospheric acceleration for L_1 carrier phase measurements, but with negative sign. Or again, the observer can make use of the free availability of the GLONASS L_2 frequency by estimating the ionospheric delay from dual frequency code pseudoranges and applying it with negative sign to correct for the carrier phase acceleration. There are, however, some differences between the ionospheric free linear combinations of code pseudoranges and carrier phase measurements. Section 8.5 will treat the ionosphere in more detail.

In Eq. (8.2.2) the frequency-dependent hardware delays L_R^S are already split into a common part $L_{R,GLO}$ and the inter-channel biases $\delta t_{R,ICD}^S$. Like in the case of the pseudorange observation equation (8.1.8), the common part of the hardware delays contributes to the receiver clock error and cannot be separated from that. But given the low noise of carrier phase observations, the inter-channel biases can no longer be neglected.

In a combined GPS/GLONASS observation scenario, the carrier phase equivalents of Eqs. (8.1.17) and (8.1.18) can be written as

$$\begin{aligned} \varphi_R^i &= \frac{1}{\lambda_{GPS}} \varrho_R^i + N_R^i + f_{GPS} \cdot (\delta t_R + L_{R,GPS}) - f_{GPS} \cdot \delta t^i + f_{GPS} \cdot \delta t_R^{i,Trop} - \\ &\quad f_{GPS} \cdot \delta t_R^{i,Iono} + \varepsilon_R^i \quad (8.2.3) \\ \varphi_R^j &= \frac{1}{\lambda^j} \varrho_R^j + N_R^j + f^j \cdot (\delta t_R + L_{R,GPS}) + f^j \cdot \delta t_{Sys} + f^j \cdot \delta t_{R,HW} - f^j \delta t^j + \\ &\quad f^j \cdot \delta t_R^{j,Trop} - f^j \cdot \delta t_R^{j,Iono} + f^j \cdot \delta t_{R,ICB}^j + \varepsilon_R^j \quad (8.2.4) \end{aligned}$$

in units of cycles or

$$\begin{aligned} \Phi_R^i &= \varrho_R^i + \lambda_{GPS} N_R^i + c \cdot (\delta t_R + L_{R,GPS}) - c \cdot \delta t^i + c \cdot \delta t_R^{i,Trop} - c \cdot \delta t_R^{i,Iono} + \lambda_{GPS} \varepsilon_R^i \quad (8.2.5) \\ \Phi_R^j &= \varrho_R^j + \lambda^j N_R^j + c \cdot (\delta t_R + L_{R,GPS}) + c \cdot \delta t_{Sys} + c \cdot \delta t_{R,HW} - c \cdot \delta t^j + c \cdot \delta t_R^{j,Trop} - \\ &\quad c \cdot \delta t_R^{j,Iono} + c \cdot \delta t_{R,ICB}^j + \lambda^j \varepsilon_R^j \quad (8.2.6) \end{aligned}$$

in units of length. i and j denote a GPS and a GLONASS satellite, respectively.

As already explained in Section 8.1.1, most combined GPS/GLONASS receivers will use different hardware to process HF signals from GPS and from GLONASS satellites, even from different GLONASS satellites to account for the different carrier frequencies. In some cases even different clocks are used for GPS and GLONASS. This may lead to different hardware delays for GPS and GLONASS satellites and even for individual GLONASS satellites. These different hardware delays appear as the hardware offset between GPS and average GLONASS $\delta t_{R,HW}$ and as the inter-channel biases $\delta t_{R,ICB}^j$ in Eq. (8.2.6). In the form as employed in Eq. (8.2.6), these inter-channel biases are zeroed at the average hardware delay for GLONASS satellites. The receiver hardware delay between GPS and average GLONASS in the form as employed in Eq. (8.2.6) cannot be separated from the difference in GPS / GLONASS system times δt_{Sys}.

Single point positioning using carrier phase observations has gained no practical importance. The observation equations are written here for the sake of completeness and as the basis for the derivations in the following sections.

8.2.2 Single Difference Positioning

The differencing techniques as introduced in Section 8.1 for pseudorange measurements can also be applied to carrier phase measurements in order to eliminate error sources from the observations.

Given two observation sites, one reference station R with known coordinates and a user site U, for which the coordinates are to be determined, the single difference GLONASS carrier phase observation equation to satellite S reads:

$$\begin{aligned}\varphi_U^S - \varphi_R^S &= \frac{1}{\lambda^S}\varrho_U^S - \frac{1}{\lambda^S}\varrho_R^S + N_U^S - N_R^S + f^S \cdot (\delta t_U + L_{U,GLO}) - f^S \cdot (\delta t_R + L_{R,GLO}) + \\ &\quad f^S \cdot \delta t_U^{S,Trop} - f^S \cdot \delta t_R^{S,Trop} + f^S \cdot \delta t_{U,ICB} - f^S \cdot \delta t_{R,ICB}^S + \varepsilon_U^S - \varepsilon_R^S\end{aligned} \tag{8.2.7}$$

in units of cycles, and

$$\begin{aligned}\Phi_U^S - \Phi_R^S &= \varrho_U^S - \varrho_R^S + \lambda^S N_U^S - \lambda^S N_R^S + c \cdot (\delta t_U + L_{U,GLO}) - c \cdot (\delta t_R + L_{R,GLO}) + \\ &\quad c \cdot \delta t_U^{S,Trop} - c \cdot \delta t_R^{S,Trop} + c \cdot \delta t_{U,ICB} - c \cdot \delta t_{R,ICB}^S + \lambda^S \varepsilon_U^S - \lambda^S \varepsilon_R^S\end{aligned} \tag{8.2.8}$$

in units of length. The satellite clock error, which is common to both observers, cancels in this single difference. As already discussed in Section 8.1.2, the influence of the ionosphere will be equal at both sites for small and medium baselines and therefore cancels, too. But that does not hold true for the tropospheric path delay, which can be different even for nearby stations.

Using the denotation $*_U - *_R = \Delta *_{UR}$ for the single difference terms, Eqs. (8.2.7) and (8.2.8) transform to

$$\Delta\varphi_{UR}^S = \frac{1}{\lambda^S}\Delta\varrho_{UR}^S + \Delta N_{UR}^S + f^S \cdot (\Delta\delta t_{UR} + \Delta L_{UR,GLO}) + f^S \cdot \Delta\delta t_{UR}^{S,Trop} + f^S \cdot \Delta\delta t_{UR,ICB}^S + \Delta\varepsilon_{UR}^S \tag{8.2.9}$$

$$\Delta\Phi_{UR}^S = \Delta\varrho_{UR}^S + \lambda^S \Delta N_{UR}^S + c \cdot (\Delta\delta t_{UR} + \Delta L_{UR,GLO}) + c \cdot \Delta\delta t_{UR}^{S,Trop} + c \cdot \Delta\delta t_{UR,ICB}^S + \lambda^S \Delta\varepsilon_{UR}^S \tag{8.2.10}$$

Compared to the single difference observation equation for pseudoranges Eq. (8.1.27), Eqs. (8.2.9) and (8.2.10) contain two additional unknowns, the single difference integer ambiguity ΔN_{UR}^S and the single difference inter-channel bias $\Delta\delta t_{UR,ICB}^S$. These are unknowns specific to each tracked satellite. Together with position and single difference receiver clock error, a system of n carrier phase observations features $2n + 4$ unknowns. Even with the addition of pseudorange observations to all the tracked satellite, which would provide n more measurements and no more unknowns, a system of single difference carrier phase observation equations to any number of GLONASS satellites is always underdetermined. The system, however, becomes solvable, if the inter-channel biases are neglected or can be determined in some other way and thus disappear as unknowns in Eqs. (8.2.9) and (8.2.10). In this case, $n + 4$ unknowns remain, leaving the system determined with carrier phase and code pseudorange measurements to at least four satellites.

For combined measurements to a GPS satellite i and a GLONASS satellite j, the single difference observation equations can be written as

$$\begin{aligned}\Delta\varphi_{UR}^i &= \frac{1}{\lambda_{GPS}}\Delta\varrho_{UR}^i + \Delta N_{UR}^i + f_{GPS} \cdot (\Delta\delta t_{UR} + \Delta L_{UR,GPS}) + f_{GPS} \cdot \Delta\delta t_{UR}^{i,Trop} + \\ &\quad \Delta\varepsilon_{UR}^i\end{aligned} \tag{8.2.11}$$

$$\begin{aligned}\Delta\varphi_{UR}^j &= \frac{1}{\lambda^j}\Delta\varrho_{UR}^j + \Delta N_{UR}^j + f^j \cdot (\Delta\delta t_{UR} + L_{UR,GPS}) + f^j \cdot \Delta\delta t_{UR,HW} + \\ &\quad f^j \cdot \Delta\delta t_{UR}^{j,Trop} + f^j \cdot \Delta\delta t_{UR,ICB}^j + \Delta\varepsilon_{UR}^j\end{aligned} \tag{8.2.12}$$

in units of cycles or

$$\Delta\Phi^i_{UR} = \Delta\varrho^i_{UR} + \lambda_{GPS}\Delta N^i_{UR} + c\cdot(\Delta\delta t_{UR}+\Delta L_{UR,GPS}) + c\cdot\Delta\delta t^{i,Trop}_{UR} + \lambda_{GPS}\Delta\varepsilon^i_{UR} \quad (8.2.13)$$

$$\Delta\Phi^j_{UR} = \Delta\varrho^j_{UR} + \lambda^j\Delta N^j_{UR} + c\cdot(\Delta\delta t_{UR}+\Delta L_{UR,GPS}) + c\cdot\Delta\delta t_{UR,HW} + c\cdot\Delta\delta t^{j,Trop}_{UR} + c\cdot\Delta\delta t^j_{UR,ICB} + \lambda^j\Delta\varepsilon^j_{UR} \quad (8.2.14)$$

in units of length.

Along with the common satellite clock error and the ionospheric influence, the GPS/GLONASS system clock offset cancels. As with the GLONASS only case, these equations feature two additional unknowns when compared to the single difference observation equations for pseudorange measurements. Together with position, single difference receiver clock error and single difference receiver hardware delays, a system of observations to m GPS and n GLONASS satellites provides $m + 2n + 5$ unknowns. Adding pseudorange measurements provides another $m + n$ observations, but no further unknowns. Thus, with $2(m + n)$ observations and $m + 2n + 5$ unknowns, the system can be solved for at least 5 observations to GPS satellites.

An example of positioning results using GPS and GLONASS single difference positioning with carrier phases is shown in Figure 8.8. Positions were computed from data logged by two 3S Navigation R-100/R-101 receivers, which were set up at known locations at the Institute of Geodesy and Navigation. Pseudorange and carrier phase measurements were logged every second for approximately one hour each, of which some forty minutes were common to both receivers. One of these receivers was used as reference station, the other was treated as the user station. Its position was determined in this example. Observation epochs at both receivers were not exactly synchronized. The data are the same as the data already used for the pseudorange positioning example. The plot shows the deviation from the known location of the antenna of the user station in the horizontal plane. GPS positions were computed from L_1 carrier phase measurements and raw L_1 C/A-code pseudorange measurements. GLONASS positions were computed from dual-frequency carrier phase measurements and raw dual-frequency P-code measurements. Wherever possible, the ionospheric free linear combinations of the code observables were formed. These observables used are not really identical for GPS and GLONASS, but with dual-frequency measurements readily available on GLONASS, the best possible results for each system are determined. The inter-channel biases $\Delta\delta t^S_{UR,ICB}$ for the GLONASS satellites have been neglected. GLONASS satellite positions were converted from PZ-90 to WGS84 using the transformation according to (*Roßbach et al., 1996*). Carrier phase ambiguities have not been fixed. The pseudorange observations have been included in the positioning to increase the number of observations, even though these observations are much noisier than the carrier phase measurements and thus may adversely affect the accuracy of the results.

Figure 8.8 shows the deviations from the known position in the horizontal plane. The converging of the Kalman filter towards the true position is clearly visible. Figure 8.9 shows the time series of the 3D deviation from the true position. The GPS only solution exhibits some amount of oscillations, probably due to remaining S/A effects, because the observation epochs at reference and user stations were not exactly synchronized. This solution converges towards the true position only very late. The GLONASS only and the combined GPS/GLONASS solutions converge much earlier and then remain steady at a point approximately 60 mm from the true position. The combined solution converges even earlier than the GLONASS solution.

8.2.3 Double Difference Positioning

Using the denotation $\Delta *^S_{UR} - \Delta *^r_{UR} = \nabla\Delta *^{Sr}_{UR}$, differencing two single difference observations at the same sites to two different satellites yields the double difference observation

$$\nabla\Delta\varphi^{Sr}_{UR} = \frac{1}{\lambda^S}\Delta\varrho^S_{UR} - \frac{1}{\lambda^r}\Delta\varrho^r_{UR} + \nabla\Delta N^{Sr}_{UR} + \left(f^S - f^r\right)\cdot(\Delta\delta t_{UR} + \Delta L_{UR,GLO}) + f^S\cdot\Delta\delta t^{S,Trop}_{UR} - f^r\cdot\Delta\delta^{r,Trop}_{UR} + f^S\cdot\Delta\delta t^S_{UR,ICB} - f^r\cdot\Delta\delta t^r_{UR,ICB} + \nabla\Delta\varepsilon^{Sr}_{UR} \quad (8.2.15)$$

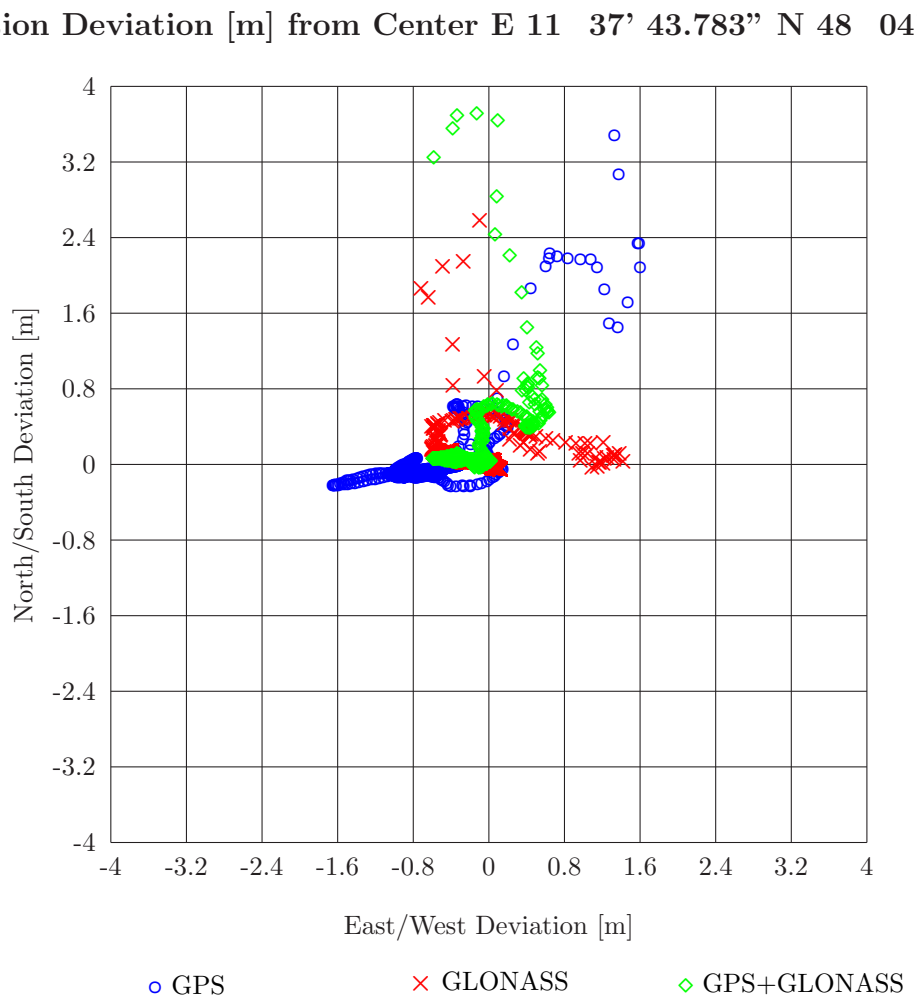

Figure 8.8: GPS, GLONASS and combined GPS/GLONASS single difference positioning using carrier phase observations.

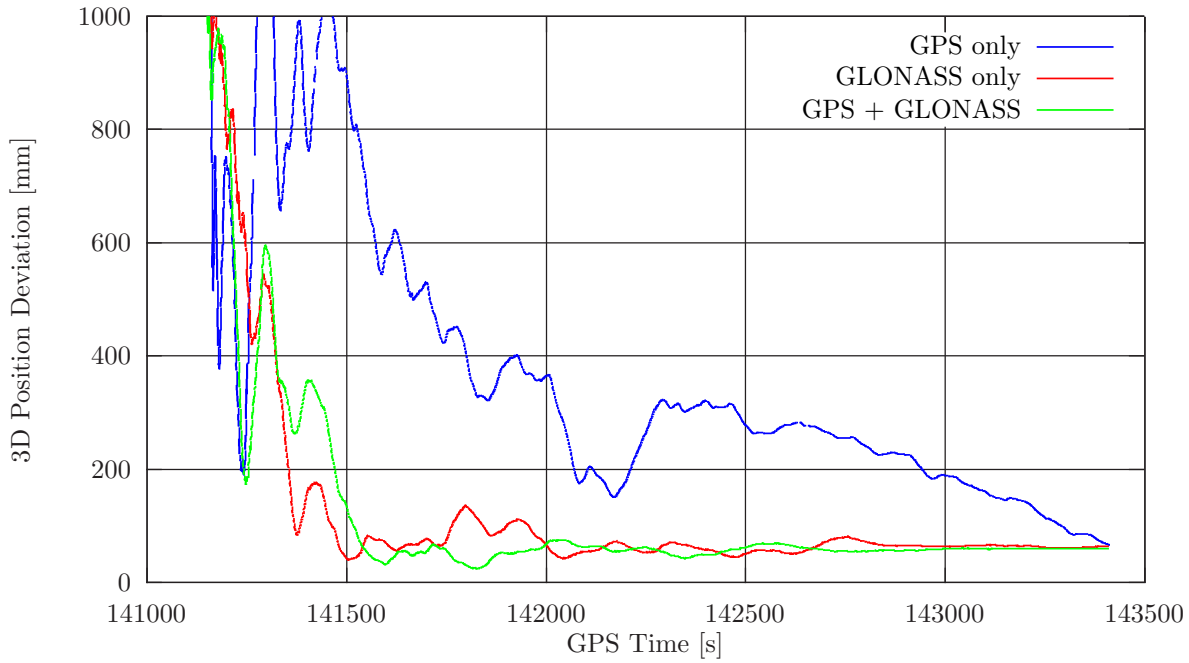

Figure 8.9: GPS, GLONASS and combined GPS/GLONASS single difference positioning using carrier phase observations, position deviation.

$$\lambda^S \Delta\varphi^S_{UR} - \lambda^r \Delta\varphi^r_{UR} = \nabla\Delta\varrho^{Sr}_{UR} + \lambda^S \Delta N^S_{UR} - \lambda^r \Delta N^r_{UR} + c \cdot \nabla\Delta\delta t^{Sr,Trop}_{UR} + c \cdot \nabla\Delta\delta t^{Sr}_{UR,ICB} + \lambda^S \Delta\varepsilon^S_{UR} - \lambda^r \Delta\varepsilon^r_{UR} \quad (8.2.16)$$

in units of cycles and length, respectively. The carrier phase measurement in units of length, $\Phi^S_R = \lambda^S \varphi^S_R$, is now substituted by the long expression in order to demonstrate the frequency-dependency of that term.

Different GLONASS satellites S and r transmit their signals using different carrier frequencies f^S and f^r. Therefore, the single difference receiver clock error does not cancel in the cycles notation of the double difference observation equation, Eq. (8.2.15). It neither can be ignored. For a single difference receiver clock error of 1 ms, which is not unusual, and adjacent GLONASS carrier frequencies on L_1, this term evaluates to 562.5 cycles, or more than 100 m. The single difference receiver clock error does cancel in the notation using units of length, Eq. (8.2.16), where the coefficient in the single difference observation equation was the satellite-independent speed of light c instead of the carrier frequency. In that case, however, the single difference integer ambiguities remain in the equation with different factors. Due to their being scaled with the wavelengths of the satellite signal, they cannot be contracted to one double difference term without losing their integer nature. On the other hand, the single difference inter-channel biases can be combined to a double difference term in the equation using units of length Eq. (8.2.16), but remain as single difference expressions in the equation using units of cycles Eq. (8.2.15). Thus, with the single difference receiver clock offset not cancelling, Eq. (8.2.15) contains one more unknown ($2n+3$ with respect to $2n+2$ for a set of n satellites including the reference satellite) than Eq. (8.2.16). This number of unknowns would be decreased further, if a way was found to either drop the clock error term from Eq. (8.2.15) or to combine the ambiguity terms in (8.2.16) without losing their integer character. A proposed solution to this latter problem is introduced in Section 8.4.

As with the system of single difference observation equations, these are too many unknowns to solve this system, even when code pseudorange observations to the satellites are added. Again, the inter-channel biases must be neglected or determined in some other way to make the system of double difference carrier phase and code pseudorange observations to n GLONASS satellites determined for at least four GLONASS satellites using Eq. (8.2.16) or five satellites in the case of Eq. (8.2.15).

Analogously to the pseudorange observation equations, for the double differenced carrier phase observation equations in a combined GPS/GLONASS scenario with a GPS satellite i and a GLONASS satellite j three different cases must be distinguished, depending on the reference satellite:

1. The reference satellite r^{GPS} is a GPS satellite.

   The double difference observation equations can be written as

$$\nabla\Delta\varphi_{UR}^{ir^{GPS}} = \frac{1}{\lambda_{GPS}}\nabla\Delta\varrho_{UR}^{ir^{GPS}} + \nabla\Delta N_{UR}^{ir^{GPS}} + f_{GPS}\cdot\nabla\Delta\delta t_{UR}^{ir^{GPS},Trop} + \nabla\Delta\varepsilon_{UR}^{ir^{GPS}} \quad (8.2.17)$$

$$\begin{aligned}\nabla\Delta\varphi_{UR}^{jr^{GPS}} = {} & \frac{1}{\lambda^j}\Delta\varrho_{UR}^{j} - \frac{1}{\lambda_{GPS}}\Delta\varrho_{UR}^{r^{GPS}} + \nabla\Delta N_{UR}^{jr^{GPS}} + \left(f^j - f_{GPS}\right)\cdot\left(\Delta\delta t_{UR} + \Delta L_{UR,GPS}\right) + \\ & f^j\cdot\Delta\delta t_{UR,HW} + f^j\cdot\Delta\delta t_{UR}^{j,Trop} - f_{GPS}\cdot\Delta\delta t_{UR}^{r^{GPS},Trop} + \\ & f^j\cdot\Delta\delta t_{UR,ICB}^{j} + \nabla\Delta\varepsilon_{UR}^{j}\end{aligned} \quad (8.2.18)$$

   in units of cycles or

$$\lambda_{GPS}\nabla\Delta\varphi_{UR}^{ir^{GPS}} = \nabla\Delta\varrho_{UR}^{ir^{GPS}} + \lambda_{GPS}\nabla\Delta N_{UR}^{ir^{GPS}} + c\cdot\nabla\Delta\delta t_{UR}^{ir^{GPS},Trop} + \lambda_{GPS}\nabla\Delta\varepsilon_{UR}^{ir^{GPS}} \quad (8.2.19)$$

$$\begin{aligned}\lambda^j\Delta\varphi_{UR}^{j} - \lambda_{GPS}\Delta\varphi_{UR}^{r^{GPS}} = {} & \nabla\Delta\varrho_{UR}^{jr^{GPS}} + \lambda^j\Delta N_{UR}^{j} - \lambda_{GPS}\Delta N_{UR}^{r^{GPS}} + c\cdot\Delta\delta t_{UR,HW} + \\ & c\cdot\nabla\Delta\delta t_{UR}^{jr^{GPS},Trop} + c\cdot\Delta\delta t_{UR,ICB}^{j} + \lambda^j\Delta\varepsilon_{UR}^{j} - \\ & \lambda_{GPS}\Delta\varepsilon_{UR}^{r^{GPS}}\end{aligned} \quad (8.2.20)$$

   in units of length, respectively.

   Of course, the GPS/GPS double difference reads like what one would expect from GPS only processing. The single difference receiver clock offset, common to both satellites, cancels, and all other single difference terms can be combined to double difference expressions. For the GLONASS/GPS double difference, as already observed in the GLONASS only scenario, due to the different frequencies of the participating satellites either the single difference receiver clock offset, combined with the GPS hardware delay, $\Delta\delta t_{UR} + \Delta L_{UR,GPS}$ does not cancel (in the cycles notation) or the two single difference integer ambiguities cannot be contracted to one double difference term (in the length notation). In addition, the single difference receiver inter-system hardware delay $\Delta\delta t_{UR,HW}$ remains in the mixed GLONASS/GPS double difference, as already observed in the pseudorange double difference processing, as well as the single difference receiver inter-channel biases.

   For a scenario with m GPS and n GLONASS satellites, the set of observation equations contains $m + 2n + 4$ unknowns.

2. The reference satellite r^{GLO} is a GLONASS satellite.

   The double difference observation equations can in that case be written as

$$\begin{aligned}\nabla\Delta\varphi_{UR}^{ir^{GLO}} = {} & \frac{1}{\lambda_{GPS}}\Delta\varrho_{UR}^{i} - \frac{1}{\lambda^{r^{GLO}}}\Delta\varrho_{UR}^{r^{GLO}} + \nabla\Delta N_{UR}^{ir^{GLO}} + \\ & \left(f_{GPS} - f^{r^{GLO}}\right)\cdot\left(\Delta\delta t_{UR} + \Delta L_{UR,GPS}\right) - f^{r^{GLO}}\cdot\Delta\delta t_{UR,HW} + \\ & f_{GPS}\cdot\Delta\delta t_{UR}^{i,Trop} - f^{r^{GLO}}\cdot\Delta\delta t_{UR}^{r^{GLO},Trop} - f^{r^{GLO}}\cdot\Delta\delta t_{UR,ICB}^{r^{GLO}} + \nabla\Delta\varepsilon_{UR}^{i}\end{aligned} \quad (8.2.21)$$

$$\begin{aligned}\nabla\Delta\varphi_{UR}^{jr^{GLO}} = {} & \frac{1}{\lambda^j}\Delta\varrho_{UR}^{j} - \frac{1}{\lambda^{r^{GLO}}}\Delta\varrho_{UR}^{r^{GLO}} + \nabla\Delta N_{UR}^{jr^{GLO}} + \\ & \left(f^j - f^{r^{GLO}}\right)\cdot\left(\Delta\delta t_{UR} + \Delta L_{UR,GPS}\right) + \\ & \left(f^j - f^{r^{GLO}}\right)\cdot\Delta\delta t_{UR,HW} + f^j\cdot\Delta\delta t_{UR}^{j,Trop} - f^{r^{GLO}}\cdot\Delta\delta t_{UR}^{r^{GLO},Trop} + \\ & f^j\cdot\Delta\delta t_{UR,ICB}^{j} - f^{r^{GLO}}\cdot\Delta\delta t_{UR,ICB}^{r^{GLO}} + \nabla\Delta\varepsilon_{UR}^{j}\end{aligned} \quad (8.2.22)$$

in units of cycles or

$$\begin{aligned}\lambda_{GPS}\Delta\varphi^{i}_{UR} - \lambda^{r^{GLO}}\Delta\varphi^{r^{GLO}}_{UR} &= \nabla\Delta\varrho^{ir^{GLO}}_{UR} + \lambda_{GPS}\Delta N^{i}_{UR} - \lambda^{r^{GLO}}\Delta N^{r^{GLO}}_{UR} - \\ &\quad c\cdot\Delta\delta t_{UR,HW} + c\cdot\nabla\Delta\delta t^{ir^{GLO},Trop}_{UR} - \\ &\quad c\cdot\Delta\delta t^{r^{GLO}}_{UR,ICB} + \lambda_{GPS}\Delta\varepsilon^{i}_{UR} - \lambda^{r^{GLO}}\Delta\varepsilon^{r^{GLO}}_{UR} \qquad (8.2.23)\\ \lambda^{j}\Delta\varphi^{j}_{UR} - \lambda^{r^{GLO}}\Delta\varphi^{r^{GLO}}_{UR} &= \nabla\Delta\varrho^{jr^{GLO}}_{UR} + \lambda^{j}\Delta N^{j}_{UR} - \lambda^{r^{GLO}}\Delta N^{r^{GLO}}_{UR} + \\ &\quad c\cdot\nabla\Delta\delta t^{jr^{GLO},Trop}_{UR} + c\cdot\nabla\Delta\delta t^{jr^{GLO}}_{UR,ICB} + \\ &\quad \lambda^{j}\Delta\varepsilon^{j}_{UR} - \lambda^{r^{GLO}}\Delta\varepsilon^{r^{GLO}}_{UR} \qquad (8.2.24)\end{aligned}$$

in units of length, respectively

The GPS/GLONASS double difference is equivalent to the GLONASS/GPS double difference from above, but with inverse signs. For the GLONASS/GLONASS double difference, again due to the different frequencies of the participating satellites the single difference receiver clock offset $\Delta\delta t_{UR} + \Delta L_{UR,GPS}$ does not cancel in the cycles notation, nor does the single difference receiver inter-system hardware delay $\Delta\delta t_{UR,HW}$. They both cancel in the notation using units of length. But here again, both single difference integer ambiguities remain in the equation, with different factors. This turns the other way around for the single difference inter-channel biases. They can be combined to one double difference term in the equation using units of length, but remain as single difference terms with different factors in the equation using units of cycles.

For a scenario with m GPS and n GLONASS satellites, the set of observation equations contains $m + 2n + 4$ unknowns.

3. Separate reference satellites r^{GPS} for GPS and r^{GLO} for GLONASS

In that case the double difference observation equations become

$$\begin{aligned}\nabla\Delta\varphi^{ir^{GPS}}_{UR} &= \frac{1}{\lambda_{GPS}}\nabla\Delta\varrho^{ir^{GPS}}_{UR} + \nabla\Delta N^{ir^{GPS}}_{UR} + f_{GPS}\cdot\nabla\Delta\delta t^{ir^{GPS},Trop}_{UR} + \nabla\Delta\varepsilon^{ir^{GPS}}_{UR} \qquad (8.2.25)\\ \nabla\Delta\varphi^{jr^{GLO}}_{UR} &= \frac{1}{\lambda^{j}}\Delta\varrho^{j}_{UR} - \frac{1}{\lambda^{r^{GLO}}}\Delta\varrho^{r^{GLO}}_{UR} + \nabla\Delta N^{jr^{GLO}}_{UR} + \\ &\quad \left(f^{j} - f^{r^{GLO}}\right)\cdot(\Delta\delta t_{UR} + \Delta L_{UR,GPS}) + \left(f^{j} - f^{r^{GLO}}\right)\cdot\Delta\delta t_{UR,HW} + \\ &\quad f^{j}\cdot\Delta\delta t^{j,Trop}_{UR} - f^{r^{GLO}}\cdot\Delta\delta t^{r^{GLO},Trop}_{UR} + \\ &\quad f^{j}\cdot\Delta\delta t^{j}_{UR,ICB} - f^{r^{GLO}}\cdot\Delta\delta t^{r^{GLO}}_{UR,ICB} + \nabla\Delta\varepsilon^{j}_{UR} \qquad (8.2.26)\end{aligned}$$

in units of cycles or

$$\lambda_{GPS}\nabla\Delta\varphi^{ir^{GPS}}_{UR} = \nabla\Delta\varrho^{ir^{GPS}}_{UR} + \lambda_{GPS}\nabla\Delta N^{ir^{GPS}}_{UR} + c\cdot\nabla\Delta\delta t^{ir^{GPS},Trop}_{UR} + \lambda_{GPS}\nabla\Delta\varepsilon^{ir^{GPS}}_{UR} \qquad (8.2.27)$$

$$\begin{aligned}\lambda^{j}\Delta\varphi^{j}_{UR} - \lambda^{r^{GLO}}\Delta\varphi^{r^{GLO}}_{UR} &= \nabla\Delta\varrho^{jr^{GLO}}_{UR} + \lambda^{j}\Delta N^{j}_{UR} - \lambda^{r^{GLO}}\Delta N^{r^{GLO}}_{UR} + \\ &\quad c\cdot\nabla\Delta\delta t^{jr^{GLO},Trop}_{UR} + c\cdot\nabla\Delta\delta t^{jr^{GLO}}_{UR,ICB} + \\ &\quad \lambda^{j}\Delta\varepsilon^{j}_{UR} - \lambda^{r^{GLO}}\Delta\varepsilon^{r^{GLO}}_{UR} \qquad (8.2.28)\end{aligned}$$

in units of length, respectively.

This is the combination of the GPS/GPS and GLONASS/GLONASS double differences of the previous two cases. In the GPS/GPS double difference, the single difference receiver clock offset, common to both satellites, cancels, and all other single difference terms can be combined to double difference expressions. In the GLONASS/GLONASS double difference, again due to the different frequencies of the participating satellites the single difference receiver clock offset $\Delta\delta t_{UR} + \Delta L_{UR,GPS}$ does not cancel in the cycles notation, nor does the single difference receiver inter-system hardware delay

$\Delta\delta t_{UR,HW}$. They both cancel in the notation using units of length. But here again, both single difference integer ambiguities remain in the equation, with different factors. This turns the other way around for the single difference inter-channel biases. They can be combined to one double difference term in the equation using units of length, but remain as single difference terms with different factors in the equation using units of cycles.

For a scenario with m GPS and n GLONASS satellites, the set of observation equations contains $m+2n+3$ unknowns in the formulation in units of cycles and $m+2n+1$ unknowns in the formulation in units of length. Whereas the formulation using cycles is equivalent to the previous two cases (one less unknown, but also one more observation sacrificed in the differencing), the length notation offers a clear advantage with regard to the number of unknowns. Here, both the single difference receiver clock offset $\Delta\delta t_{UR} + \Delta L_{UR,GPS}$ and the single difference receiver inter-system hardware delay $\Delta\delta t_{UR,HW}$ cancel.

8.3 GLONASS and GPS/GLONASS Carrier Phase Positioning

The different carrier frequencies of the GLONASS satellites cause two major problems when using GLONASS carrier phase observations for precise positioning:

- different, frequency-dependent hardware delays in the receiver, and
- either the ambiguities losing their integer nature or the receiver clock errors not cancelling in double difference positioning.

Different groups of scientists proposed different methods to treat GLONASS carrier phase observations in order to tackle these problems, either simultaneously or separately.

8.3.1 Floating GLONASS Ambiguities

Landau et al. (*Landau and Vollath, 1996*) summarize the integer ambiguities and the frequency-dependent delays into one non-integer term per satellite and confines to floating GLONASS ambiguities. In combined GPS/GLONASS scenarios, these GLONASS ambiguities serve only to support fixing of the GPS integer ambiguities. When analyzing GPS/GLONASS data, the solution converges far faster than for GPS data alone. The reliability of the integer fix, quantified in the ratio of the sum of the squared residuals for the best and second best solution, is also improved by a factor of around 3, when GLONASS satellites are included in the position determination. The combined number of GPS and GLONASS satellites may even allow to obtain very precise positioning solutions without any ambiguity fix at all.

8.3.2 Single Difference Positioning and Receiver Calibration

Daly et al. (*Raby and Daly, 1993*; *Walsh and Daly, 1996*) suggest a careful calibration of GLONASS receivers prior to use in order to determine the hardware delays. Since these delays may also depend on receiver temperature, this calibration should be performed at different temperatures. In a combined GPS/GLONASS scenario, it is thinkable to first obtain an accurate position fix from GPS measurements alone for a static receiver. This position fix could then be used to calibrate initial GLONASS hardware delays. As long as lock is maintained to at least four GPS satellites, GLONASS measurement errors can be monitored. If lock is kept to less than four GPS satellites, the most recent calibration values (and perhaps a model for their change in time) will be used. Combined GPS/GLONASS positioning is then possible. This technique is especially useful for surveying in sites with lots of obstructions, e.g. open pit mines. Initialization can be performed outside the mine, with a sufficient number of GPS satellites available, before entering the pit.

Regarding the ambiguities, (*Walsh and Daly, 1996*) avoid the GLONASS double difference carrier phase observations and confine to single differences. This enables fixing the ambiguities to integer values,

at the expense of additionally having to estimate the receiver clock biases. These clock biases can be computed from pseudorange measurements. These are, however, less precise than the carrier phase measurements. After initialization of the GLONASS biases, correct fixing of the integer ambiguities is possible faster than with GPS alone.

8.3.3 Scaling to a Common Frequency

In order to eliminate the receiver clock errors from the double difference carrier phase observation equation in cycles notation, Leick et al. (*Leick et al., 1995*) scale the GLONASS carrier phase observations to a common frequency. They choose the mean frequency in the classical range of frequency numbers $n = 1 \ldots 24$:

$$\overline{f}_i = f_i(n = 12.5)$$

with $i = 1, 2$ for the L_1 and L_2 frequencies, respectively, as this common frequency. This way, for all GLONASS satellites S the inequality

$$0.9959 < \frac{\overline{f}_i}{f^S} < 1.0041$$

holds, at least for the classical range of frequency numbers.

The scaled carrier phase observation equation from receiver R to GLONASS satellite S in units of cycles Eq. (8.2.1) then reads:

$$\begin{aligned}\overline{\varphi}_R^S &= \frac{\overline{f}}{f^S}\varphi_R^S \\ &= \frac{\overline{f}}{c}\varrho_R^S + \frac{\overline{f}}{f^S}N_R^S + \overline{f}\cdot(\delta t_R + L_{R,GLO}) - \overline{f}\cdot\delta t^S + \overline{f}\cdot\delta t_R^{S,Trop} - \overline{f}\cdot\delta t_R^{S,Iono} + \\ &\quad \overline{f}\cdot\delta t_{R,ICB}^S + \frac{\overline{f}}{f^S}\varepsilon_R^S\end{aligned} \tag{8.3.1}$$

Forming a single difference between user receiver U and reference receiver R, the satellite clock error and for short baselines also the ionospheric influence cancel:

$$\begin{aligned}\Delta\overline{\varphi}_{UR}^S &= \frac{\overline{f}}{c}\Delta\varrho_{UR}^S + \frac{\overline{f}}{f^S}\Delta N_{UR}^S + \overline{f}\cdot(\Delta\delta t_{UR} + \Delta L_{UR,GLO}) + \overline{f}\cdot\Delta\delta t_{UR}^{S,Trop} + \\ &\quad \overline{f}\cdot\Delta\delta t_{UR,ICB}^S + \frac{\overline{f}}{f^S}\Delta\varepsilon_{UR}^S\end{aligned} \tag{8.3.2}$$

and the double differenced observation equation between satellite S and reference satellite r then reads:

$$\begin{aligned}\nabla\Delta\overline{\varphi}_{UR}^{Sr} &= \frac{\overline{f}}{f^S}\left(\varphi_U^S - \varphi_R^S\right) - \frac{\overline{f}}{f^r}\left(\varphi_U^r - \varphi_R^r\right) \\ &= \frac{\overline{f}}{c}\nabla\Delta\varrho_{UR}^{Sr} + \frac{\overline{f}}{f^S}\Delta N_{UR}^S - \frac{\overline{f}}{f^r}\Delta N_{UR}^r + \overline{f}\cdot\nabla\Delta\delta t_{UR}^{Sr,Trop} + \overline{f}\cdot\nabla\Delta\delta t_{UR,ICB}^{Sr} + \\ &\quad \frac{\overline{f}}{f^S}\Delta\varepsilon_{UR}^S - \frac{\overline{f}}{f^r}\Delta\varepsilon_{UR}^r\end{aligned} \tag{8.3.3}$$

The single difference receiver clock offsets, combined with the hardware delay, $\Delta\delta t_{UR} + \Delta L_{UR,GLO}$ cancels, as was intended by the scaling of the carrier phase observation equation. However, due to the scaling, the single difference ambiguities now cannot be contracted to a double difference term, without losing their integer nature. In this respect, Eq. (8.3.3) is equivalent to the unscaled double difference observation equation in units of length, Eq. (8.2.16).

To overcome this problem of not being able to contract the single difference ambiguities to a double difference term, (*Leick et al., 1995*) further introduce an approximate value for the single difference carrier phase ambiguity to the reference satellite r such that:

$$\Delta N_{UR}^r = \Delta N_{UR,0}^r + dN_{UR}^r \tag{8.3.4}$$

Substituting Eq. (8.3.4) into Eq. (8.3.3) yields:

$$\begin{aligned}\nabla\Delta\overline{\varphi}^{Sr}_{UR} &= \frac{\overline{f}}{c}\nabla\Delta\varrho^{Sr}_{UR} + \frac{\overline{f}}{f^S}\Delta N^S_{UR} - \frac{\overline{f}}{f^r}\Delta N^r_{UR,0} - \frac{\overline{f}}{f^r}dN^r_{UR} + \overline{f}\cdot\nabla\Delta\delta t^{Sr,Trop}_{UR} + \\ &\quad \overline{f}\cdot\nabla\Delta\delta t^{Sr}_{UR,ICB} + \frac{\overline{f}}{f^S}\Delta\varepsilon^S_{UR} - \frac{\overline{f}}{f^r}\Delta\varepsilon^r_{UR}\end{aligned} \tag{8.3.5}$$

The amendment to this approximate value together with the single difference ambiguity to the reference satellite S can now be contracted to a new double difference term:

$$\begin{aligned}\nabla\Delta\overline{\varphi}^{Sr}_{UR} &= \frac{\overline{f}}{c}\nabla\Delta\varrho^{Sr}_{UR} + \frac{\overline{f}}{f^S}\nabla\Delta N^{Sr}_{UR} - \frac{\overline{f}}{f^r}\Delta N^r_{UR,0} + \overline{f}\cdot\nabla\Delta\delta t^{Sr,Trop}_{UR} + \\ &\quad \overline{f}\cdot\nabla\Delta\delta t^{Sr}_{UR,ICB} + \frac{\overline{f}}{f^S}dN^r_{UR} - \frac{\overline{f}}{f^r}dN^r_{UR} + \frac{\overline{f}}{f^S}\Delta\varepsilon^S_{UR} - \frac{\overline{f}}{f^r}\Delta\varepsilon^r_{UR}\end{aligned} \tag{8.3.6}$$

with

$$\nabla\Delta N^{Sr}_{UR} = \Delta N^S_{UR} - dN^r_{UR}$$

The approximate value for the single difference integer ambiguity $\Delta N^r_{UR,0}$ is determined from pseudorange measurements. The remaining amendment terms

$$\left(\frac{\overline{f}}{f^S} - \frac{\overline{f}}{f^s}\right)\cdot dN^r_{UR}$$

are of small magnitude, since

$$\left|\frac{\overline{f}}{f^S} - \frac{\overline{f}}{f^s}\right| < \frac{1}{124}$$

and the amendment dN^r_{UR} itself is considered small. These terms are regarded as model error and treated as additional noise in Eq. (8.3.6).

Since Eq. (8.3.3) is very similar to the double difference observation equation in units of length, Eq. (8.2.16), splitting of the single difference integer ambiguity to the reference satellite ΔN^r_{UR} can also be applied to this latter equation. The double difference equation in units of length then reads

$$\begin{aligned}\lambda^S\Delta\varphi^S_{UR} - \lambda^r\Delta\varphi^r_{UR} &= \nabla\Delta\varrho^{Sr}_{UR} + \lambda^S\nabla\Delta N^{Sr}_{UR} - \lambda^r\Delta N^r_{UR,0} + c\cdot\nabla\Delta\delta t^{Sr,Trop}_{UR} + \\ &\quad c\cdot\nabla\Delta\delta t^{Sr}_{UR,ICB} + \lambda^S dN^r_{UR} - \lambda^r dN^r_{UR} + \lambda^S\Delta\varepsilon^S_{UR} - \lambda^r\Delta\varepsilon^r_{UR}\end{aligned} \tag{8.3.7}$$

In this case, $|\lambda^S - \lambda^r| < 0.0015$ m

(*Leick et al., 1995*) did not make any attempt to calibrate the inter-channel biases $\delta t^{Sr}_{UR,ICB}$ in Eq. (8.3.6).

8.3.4 Iterative Ambiguity Resolution

(*Habrich et al., 1999*; *Habrich, 1999*) suggest an iterative solution of the GLONASS double difference ambiguities, based on the single difference observation equations:

1. In a first step the normal equation system for single difference phase observations is set up. For observations to n satellites, there are n single difference equations – assuming single frequency observations only.

2. These equations are enhanced by an a priori constraint or by code observations to remove the singularity of the system.

3. The system of single difference equations system is solved, and the single difference ambiguities are estimated as real values.

4. All possible double difference ambiguities $\nabla\Delta N_{kl}^{ij}$ are computed using combinations of the estimated single difference ambiguities ΔN_{kl}^{i}, ΔN_{kl}^{j}. Along with these double difference ambiguities, their formal errors are estimated from the covariance matrix $\mathbf{Q}$ of the single difference solution. These formal errors are computed as $e_{ij} = \varsigma_0\sqrt{Q_{ii} - 2Q_{ij} + Q_{jj}}$, with the a posteriori variance factor ς_0^2. The formal errors are highly correlated with the difference in wavelength $\Delta\lambda^{ij}$ of the satellites involved in the double difference. The smaller the wavelength difference, the smaller the formal error.

5. The double difference combination with the smallest formal error is then fixed to an integer number.

6. With one double difference fixed, one of the two single difference ambiguities involved in forming this double difference combination may then be eliminated from the normal equation system. The observation system of single difference equations is now regular, even without constraints or code observations.

   The iterative ambiguity resolution is then continued with step 3, the solution of the single difference observation equations. This way, $n-1$ single difference ambiguities may be eliminated from the observation equation.

7. Finally, the remaining single difference ambiguity is fixed to an integer number on the single difference level.

This method of GLONASS ambiguity resolution is applicable for short and long baselines. But it may only be used in post processing mode, evaluating data of long observation sessions. Thus, this method is suited for e.g. analysis of IGEX-98 data. But it is not suited for applications that require fast ("rapid static" or "on-the-fly") ambiguity determination. It neither can be applied to any form of navigation.

8.4 A Proposed Solution to the Frequency Problem

The double difference carrier phase observations between stations U and R to satellites S and r in units of length can be written as (cf. Eq. (8.2.16))

$$\lambda^S\Delta\varphi_{UR}^{S} - \lambda^r\Delta\varphi_{UR}^{r} = \nabla\Delta\varrho_{UR}^{Sr} + \lambda^S\Delta N_{UR}^{S} - \lambda^r\Delta N_{UR}^{r} + \lambda^S\Delta\varepsilon_{UR}^{S} - \lambda^r\Delta\varepsilon_{UR}^{r} \tag{8.4.1}$$

Compared to Eq. (8.2.16), the tropospheric path delay and the inter-channel bias have been neglected. These terms do not contribute to the purpose of demonstrating a proposed solution to the problem of having the single difference integer ambiguities in the double difference observation equation.

Given two GPS satellites with identical signal wavelengths $\lambda^S = \lambda^r = \lambda_{GPS}$, Eq. (8.4.1) simplifies to

$$\lambda_{GPS}\nabla\Delta\varphi_{UR}^{Sr} = \nabla\Delta\varrho_{UR}^{Sr} + \lambda_{GPS}\nabla\Delta N_{UR}^{Sr} + \nabla\Delta\varepsilon_{UR}^{Sr} \tag{8.4.2}$$

But as soon as at least one GLONASS satellite is participating in the double difference observation, the wavelengths are no longer identical, and Eq. (8.4.1) can no longer be simplified in this way without losing the integer character of the ambiguity terms. Therefore, single difference terms remain in the double difference observation equation Eq. (8.4.1).

Performing a hybrid single/double difference adjustment using Eq. (8.4.1) means the disadvantage of either having one additional unknown (with respect to a single frequency double difference adjustment) or having one observation missing (with respect to a frequency-independent single difference adjustment). Therefore, a suitable expression of the double difference observation equation with no single difference terms in it, but with integer ambiguities must be found.

This goal can be reached by introducing an auxiliary wavelength λ^*, of which both λ^S and λ^r are integer multiples:

$$\lambda^* = \frac{\lambda^S}{k^S} = \frac{\lambda^r}{k^r} = \frac{c}{k^S f^S}, \quad \text{with } k^S, k^r \in \mathbb{N} \tag{8.4.3}$$

Inserting this definition into Eq. (8.4.1) yields a modified double difference observation equation:

$$\lambda^* \left(k^S \Delta\varphi_{UR}^S - k^r \Delta\varphi_{UR}^r\right) = \nabla\Delta\varrho_{UR}^{Sr} + \lambda^* \left(k^S \Delta N_{UR}^S - k^r \Delta N_{UR}^r\right) + \lambda^* \left(k^S \Delta\varepsilon_{UR}^S - k^r \Delta\varepsilon_{UR}^r\right) \quad (8.4.4)$$

Using the abbreviation

$$\nabla^{a,b}\Delta *_{UR}^{Sr} = a\Delta *_{UR}^{S} - b\Delta *_{UR}^{r}$$

and the special case

$$\nabla\Delta *_{UR}^{Sr} = \nabla^{1,1}\Delta *_{UR}^{Sr}$$

Eq. (8.4.4) can be rewritten:

$$\lambda^* \nabla^{k^S,k^r}\Delta\varphi_{UR}^{Sr} = \nabla^{1,1}\Delta\varrho_{UR}^{Sr} + \lambda^* \nabla^{k^S,k^r}\Delta N_{UR}^{Sr} + \lambda^* \nabla^{k^S,k^r}\Delta\varepsilon_{UR}^{Sr} \quad (8.4.5)$$

where the modified double difference ambiguities $\nabla^{k^S,k^r}\Delta N_{UR}^{Sr}$ are still of integer type. They refer to the auxiliary signal with the wavelength λ^*.

The coefficients k^S, k^r must be chosen depending on the signal frequencies involved. For two GPS satellites, both k^S and k^r are chosen to be 1, resulting in Eq. (8.4.2).

With GLONASS satellites being involved, the coefficients k^S, k^r depend on the frequency letters of those satellites. GLONASS satellite i transmits its signals on the frequencies

$$\begin{aligned} f_{L_1}^i &= 1602 + n^i \cdot 0.5625 \text{ [MHz]} \\ &= \left(2848 + n^i\right) \cdot \Delta f_{L_1} \\ f_{L_2}^i &= \left(2848 + n^i\right) \cdot \Delta f_{L_2} \end{aligned}$$

with $\Delta f_{L_1} = 0.5625$ MHz and $\Delta f_{L_2} = 0.4375$ MHz and n^i being the frequency number of satellite i.

In case of two GLONASS satellites, according to the definition (8.4.3), λ^* must be

$$\lambda^* = \frac{c}{k^S \left(2848 + n^S\right) \Delta f} = \frac{c}{k^r \left(2848 + n^r\right) \Delta f} \quad (8.4.6)$$

This condition is fulfilled for the pair of coefficients $k^S = 2848 + n^r$, $k^r = 2848 + n^S$. Therefore, we obtain for the GLONASS/GLONASS double differences:

$$\lambda^* \nabla^{2848+n^r,2848+n^S}\Delta\varphi_{UR}^{Sr} = \nabla^{1,1}\Delta\varrho_{UR}^{Sr} + \lambda^* \nabla^{2848+n^r,2848+n^S}\Delta N_{UR}^{Sr} + \lambda^* \nabla^{2848+n^r,2848+n^S}\Delta\varepsilon_{UR}^{Sr} \quad (8.4.7)$$

with the auxiliary wavelength

$$\lambda^* = \frac{c}{\Delta f} \frac{1}{\left(2848 + n^S\right)\left(2848 + n^r\right)} \quad (8.4.8)$$

Eqs. (8.4.6) through (8.4.8) hold for both L_1 and L_2. Therefore, the respective indices were omitted.

Considering the case of one GPS and one GLONASS satellite transmitting on L_1 and the GLONASS satellite being the reference satellite r, λ^* must be, according to the definition (8.4.3):

$$\lambda^* = \frac{c}{k^S f_{L_1,GPS}} = \frac{c}{k^r \left(2848 + n^r\right) \Delta f_{L_1}} \quad (8.4.9)$$

This condition is fulfilled for the pair of coefficients $k^S = \left(2848 + n^r\right) \cdot \Delta f_{L_1}/\text{Hz}$, $k^r = f_{L_1,GPS}/\text{Hz}$. Inserting the frequency values, we get $k^S = \left(2848 + n^r\right) \cdot 562500$, $k^r = 1575420000$. Reducing the values to prime numbers and canceling common factors yields $k^S = 75 \cdot \left(2848 + n^r\right)$, $k^r = 210056$. So for the GPS/GLONASS double difference

$$\begin{aligned} \lambda^* \nabla^{75\cdot(2848+n^r),210056}\Delta\varphi_{UR}^{Sr} &= \nabla^{1,1}\Delta\varrho_{UR}^{Sr} + \lambda^* \nabla^{75\cdot(2848+n^r),210056}\Delta N_{UR}^{Sr} + \\ &\quad \lambda^* \nabla^{75\cdot(2848+n^r),210056}\Delta\varepsilon_{UR}^{Sr} \end{aligned} \quad (8.4.10)$$

is obtained with the auxiliary wavelength being

$$\lambda^* = \frac{c}{f_{L_1,GPS}} \frac{1}{75 \cdot \left(2848 + n^r\right)} = \frac{\lambda_{L_1,GPS}}{75 \cdot \left(2848 + n^r\right)} \quad (8.4.11)$$

For L_2 observations the coefficients become $k^S = 35 \cdot (2848 + n^r)$, $k^r = 98208$ (GPS at full wavelength), respectively $k^S = 35 \cdot (2848 + n^r)$, $k^r = 196416$ (GPS at half wavelength). If the GPS satellite is the reference satellite r, the values of the coefficients k^S, k^r must be exchanged.

Adjusting observations using this method eliminates the drawback of the hybrid single/double difference adjustment of having one observation missing or one additional unknown. This method, however, might give rise to numerical problems on adjustment. Even though the modified double difference ambiguities are now still of integer type, their values usually will be very large, due to the small auxiliary wavelengths. For GLONASS/GLONASS double differences on L_1 this wavelength is about 65 μm, for GPS/GLONASS double differences it is even in the range of 880 - 890 nm, which already corresponds to the wavelength of infra-red light. For L_2 the respective wavelengths are about 84 μm and 2.4 μm (GPS at full wavelength) or 1.2 μm (half wavelength).

These small wavelengths also might make the ambiguities difficult to fix. Depending on the participating frequency letters, further canceling of common prime factors in the coefficients k^S, k^r can increase the auxiliary wavelength and thus reduce the ambiguities, but not significantly. Tables 8.1 and 8.2 show the largest common denominators for any combination of the GLONASS/GLONASS double difference coefficients in the traditional GLONASS frequency range from frequency number 0 ... 24 and the planned range -7 ... +6 beyond 2005. The coefficients can be reduced by these values and thus the wavelengths increased accordingly. The diagonal (which would correspond to the combinations $k^r = k^S$) are marked with dashes, since these combinations should not occur in practice due to the antipodal orbit positions of satellites transmitting on identical frequencies.

As can be seen from the tables, the largest common denominator of any two double difference coefficients is 19, which can be found for the pair of frequency numbers 2 and 21. This would increase the 65 μm wavelength of the GLONASS/GLONASS L_1 double difference to approximately 1.2 mm. This wavelength is still in the order or below the noise level of carrier phase measurements and thus too short for fixing the integer ambiguities. Frequency number 19 will only be used until 2005. see Section 3.4. Beyond 2005, the largest common denominator will be 9 for the pair of frequency numbers -4 and 5. This would correspond to a wavelength of approximately 0.6 mm. Generally, it can be stated that the traditional range of GLONASS frequency numbers is better suited to form such pairs, due to the wider range of frequencies.

Some frequency numbers, however, are not suited to form such pairs with common denominators, e.g. numbers -5 and 3. Added to 2848, these numbers are either prime numbers themselves or all their smallest prime factors is so large that the nearest multiple of that prime factor is outside the GLONASS frequency range.

Given a mixed GPS/GLONASS double difference, the largest common denominator of any pair of the coefficients 210056, $75 \cdot (2848 + n)$ is 62 for GLONASS frequency number. This would increase the wavelength from some 880 nm to around 55 μm. But here, again, for some of the pairs common denominators do not exist.

On the other hand, with such small wavelengths, ambiguity fixing to integers will not be necessary, but fixing to thousands (GLONASS/GLONASS) or even hundreds of thousands (GPS/GLONASS) of cycles might be sufficient.

The noise σ_λ of a carrier phase measurement can be written as $\sigma_\lambda = \lambda \cdot \sigma_\varphi$ with σ_φ being the noise of the phase measurement at cycle level. The noise of a linear combination can then be expressed as

$$\sigma_{\lambda_{k^S,k^r}} = \lambda_{k^S,k^r} \sqrt{k^{S2} + k^{r2}} \cdot \sigma_\varphi$$

Considering σ_φ to be constant for all GPS and GLONASS carrier phase measurements, and with $\lambda_{k^S,k^r} = \lambda^*$ from above, the ratio of

$$\frac{\sigma_{\lambda_{k^S,k^r}}}{\sigma_{\lambda_L}} = \frac{\lambda_{k^S,k^r}}{\lambda_L} \sqrt{k^{S2} + k^{r2}}$$

n		0	1	2	3	4	5	6	7	8	9	10	11	12
	$2848+n$	2848	2849	2850	2851	2852	2853	2854	2855	2856	2857	2858	2859	2860
0	2848	–	1	2	1	4	1	2	1	8	1	2	1	4
1	2849	1	–	1	1	1	1	1	1	7	1	1	1	11
2	2850	2	1	–	1	2	3	2	5	6	1	2	3	10
3	2851	1	1	1	–	1	1	1	1	1	1	1	1	1
4	2852	4	1	2	1	–	1	2	1	4	1	2	1	4
5	2853	1	1	3	1	1	–	1	1	3	1	1	3	1
6	2854	2	1	2	1	2	1	–	1	2	1	2	1	2
7	2855	1	1	5	1	1	1	1	–	1	1	1	1	5
8	2856	8	7	6	1	4	3	2	1	–	1	2	3	4
9	2857	1	1	1	1	1	1	1	1	1	–	1	1	1
10	2858	2	1	2	1	2	1	2	1	2	1	–	1	2
11	2859	1	1	3	1	1	3	1	1	3	1	1	–	1
12	2860	4	11	10	1	4	1	2	5	4	1	2	1	–
13	2861	1	1	1	1	1	1	1	1	1	1	1	1	1
14	2862	2	1	6	1	2	9	2	1	6	1	2	3	2
15	2863	1	7	1	1	1	1	1	1	7	1	1	1	1
16	2864	16	1	2	1	4	1	2	1	8	1	2	1	4
17	2865	1	1	15	1	1	3	1	5	3	1	1	3	5
18	2866	2	1	2	1	2	1	2	1	2	1	2	1	2
19	2867	1	1	1	1	1	1	1	1	1	1	1	1	1
20	2868	4	1	6	1	4	3	2	1	12	1	2	3	4
21	2869	1	1	19	1	1	1	1	1	1	1	1	1	1
22	2870	2	7	10	1	2	1	2	5	14	1	2	1	10
23	2871	1	11	3	1	1	9	1	1	3	1	1	3	11
24	2872	8	1	2	1	4	1	2	1	8	1	2	1	4

n		13	14	15	16	17	18	19	20	21	22	23	24	
	$2848+n$	2861	2862	2863	2864	2865	2866	2867	2868	2869	2870	2871	2872	
0	2848	1	2	1	16	1	2	1	4	1	2	1	8	
1	2849	1	1	7	1	1	1	1	1	1	7	11	1	
2	2850	1	6	1	2	15	2	1	6	19	10	3	2	
3	2851	1	1	1	1	1	1	1	1	1	1	1	1	
4	2852	1	2	1	4	1	2	1	4	1	2	1	4	
5	2853	1	9	1	1	3	1	1	3	1	1	9	1	
6	2854	1	2	1	2	1	2	1	2	1	2	1	2	
7	2855	1	1	1	1	5	1	1	1	1	5	1	1	
8	2856	1	6	7	8	3	2	1	12	1	14	3	8	
9	2857	1	1	1	1	1	1	1	1	1	1	1	1	
10	2858	1	2	1	2	1	2	1	2	1	2	1	2	
11	2859	1	3	1	1	3	1	1	3	1	1	3	1	
12	2860	1	2	1	4	5	2	1	4	1	10	11	4	
13	2861	–	1	1	1	1	1	1	1	1	1	1	1	
14	2862	1	–	1	2	3	2	1	6	1	2	9	2	
15	2863	1	1	–	1	1	1	1	1	1	7	1	1	
16	2864	1	2	1	–	1	1	1	4	1	2	1	8	
17	2865	1	3	1	1	–	1	1	3	1	5	3	1	
18	2866	1	2	1	2	1	–	1	2	1	2	1	2	
19	2867	1	1	1	1	1	1	–	1	1	1	1	1	
20	2868	1	6	1	4	3	2	1	–	1	1	3	4	
21	2869	1	1	1	1	1	1	1	1	–	1	1	1	
22	2870	1	2	7	2	5	2	1	2	1	–	1	2	
23	2871	1	9	1	1	3	1	1	3	1	1	–	1	
24	2872	1	2	1	8	1	2	1	4	1	2	1	–	

Table 8.1: Largest common denominators of GLONASS/GLONASS double difference coefficients, frequency range until 2005.

n		-7	-6	-5	-4	-3	-2	-1	0	1	2	3	4	5	6
	$2848+n$	2841	2842	2843	2844	2845	2846	2847	2848	2849	2850	2851	2852	2853	2854
-7	2841	–	1	1	3	1	1	3	1	1	3	1	1	3	1
-6	2842	1	–	1	2	1	2	1	2	7	2	1	2	1	2
-5	2843	1	1	–	1	1	1	1	1	1	1	1	1	1	1
-4	2844	3	2	1	–	1	2	3	4	1	6	1	4	9	2
-3	2845	1	1	1	1	–	1	1	1	1	5	1	1	1	1
-2	2846	1	2	1	2	1	–	1	2	1	2	1	2	1	2
-1	2847	3	1	1	3	1	1	–	1	1	3	1	1	3	1
0	2848	1	2	1	4	1	2	1	–	1	2	1	4	1	2
1	2849	1	7	1	1	1	1	1	1	–	1	1	1	1	1
2	2850	3	2	1	6	5	2	3	2	1	–	1	2	3	2
3	2851	1	1	1	1	1	1	1	1	1	1	–	1	1	1
4	2852	1	2	1	4	1	2	1	4	1	2	1	–	1	2
5	2853	3	1	1	9	1	1	3	1	1	3	1	1	–	1
6	2854	1	2	1	2	1	2	1	2	1	2	1	2	1	–

Table 8.2: Largest common denominators of GLONASS/GLONASS double difference coefficients, frequency range beyond 2005.

will become about 1.4 for both L_1 ($\lambda_L \approx 19$ cm) and L_2 ($\lambda_L \approx 24$ cm), GPS/GLONASS and GLONASS/GLONASS carrier phase measurements (L_2 GPS at full wavelength) and 2.2 for L_2 GPS/GLONASS carrier phase measurements with GPS at half wavelength. This means, the noise of a double difference carrier phase measurement formed in this way is about 1.4 (respectively 2.2 for L_2 with GPS at half wavelength) times higher than the noise of the original measurements.

An example of positioning results using GPS and GLONASS double difference positioning with carrier phases is shown in Figure 8.10. Positions were computed from data logged by two 3S Navigation R-100/R-101 receivers, which were set up at known locations at the Institute of Geodesy and Navigation. Pseudorange and carrier phase measurements were logged every second for approximately one hour each, of which some forty minutes were common to both receivers. One of these receivers was used as reference station, the other was treated as the user station. Its position was determined in this example. Observation epochs at both receivers were not exactly synchronized. The data are the same as the data already used for the pseudorange positioning example. The plot shows the deviation from the known location of the antenna of the user station in the horizontal plane. GPS positions were computed from L_1 carrier phase measurements and raw L_1 C/A-code pseudorange measurements. GLONASS positions were computed from dual-frequency carrier phase measurements and raw dual-frequency P-code measurements. Wherever possible, the ionospheric free linear combinations of the code observables were formed. These observables used are not really identical for GPS and GLONASS, but with dual-frequency measurements readily available on GLONASS, the best possible results for each system are determined. The inter-channel biases $\nabla\Delta\delta t^{Sr}_{UR,ICB}$ for the GLONASS satellites have been neglected. GLONASS satellite positions were converted from PZ-90 to WGS84 using the transformation according to (*Roßbach et al., 1996*). Carrier phase ambiguities have not been fixed. The pseudorange observations have been included in the positioning to increase the number of observations, even though these observations are much noisier than the carrier phase measurements and thus may adversely affect the accuracy of the results.

For the combined GPS/GLONASS processing, mixed GPS/GLONASS double differences – i.e. GPS satellite and GLONASS reference satellite or vice versa – have been allowed. GLONASS/GLONASS and GPS/GLONASS double differences were formed using the algorithm described above. Auxiliary wavelengths were left at their original values, i.e. they were not enlarged by applying common denominators of the double difference coefficients.

Figure 8.10 shows the deviations from the known position in the horizontal plane. The converging of the Kalman filter towards the true position is clearly visible. Figure 8.11 shows the time series of the 3D deviation from the true position. The GPS only solution exhibits some amount of oscillations, probably due to remaining S/A effects, because the observation epochs at reference and user stations were not exactly synchronized. This solution converges towards the true position only very late. The GLONASS

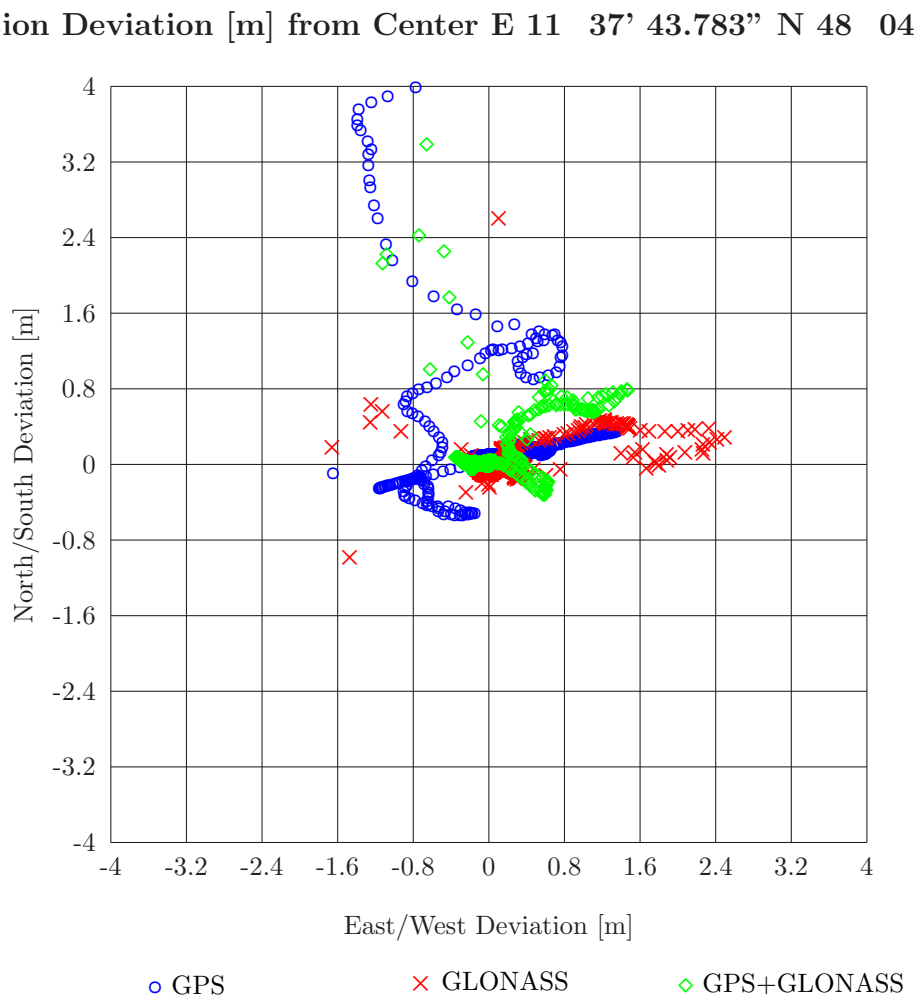

Figure 8.10: GPS, GLONASS and combined GPS/GLONASS double difference positioning using carrier phase observations.

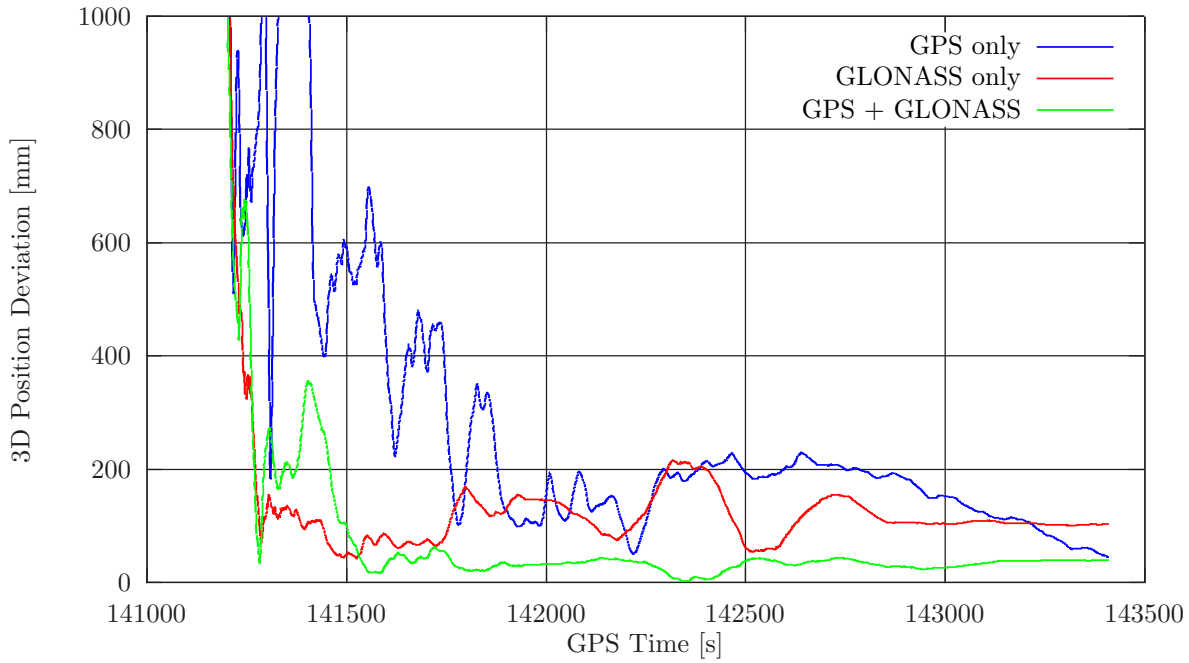

Figure 8.11: GPS, GLONASS and combined GPS/GLONASS double difference positioning using carrier phase observations, position deviation.

solution only converges much earlier and then remains relatively steady at a point approximately 100 mm from the true position. The combined solution converges even earlier than the GLONASS solution and remains approximately 40 mm from the true position.

So even with neglecting the GLONASS inter-channel biases and floating ambiguities, in combined GPS/GLONASS carrier phase processing sub-decimeter accuracy can be achieved.

Figure 8.12 shows the computed single difference receiver inter-system hardware delay $\Delta\delta t_{UR,HW}$. It can be clearly seen that this bias is not constant. Its absolute value increases with time, until it obviously reaches some kind of saturation after approximately fifteen minutes.

Figure 8.13 and 8.14 show the computed double difference floating ambiguities for some of the participating satellites in the GPS only and the GLONASS only solutions. To display the ambiguities, a constant value has been added to them such that the resulting ambiguities take values near zero. Once the filter has converged, the ambiguities vary only slightly. In the GPS only solution, this variation is in the range of a cycle or less. This corresponds to one wavelength of approximately 190 mm or less. In the GLONASS only solution, this variation is in the range of 2000 cycles or less. With a wavelength of approximate 65 μm of the common frequency, these 2000 cycles correspond to a variation of around 130 mm, which is comparable to the variation of the floating ambiguities in the GPS only processing.

8.5 Ionospheric Correction

8.5.1 Single Frequency Ionospheric Correction

The observation equation for pseudorange observations from an observer R to a GPS or GLONASS satellite S (8.1.4) contains the delay of the satellite signal in the ionosphere $\delta t_R^{S,Iono}$. Strictly spoken, this ionospheric delay is unknown. It varies with satellite and may vary with time. Therefore, the ionospheric delay yields one unknown per satellite and epoch in addition to the unknowns that are already to be solved for, i.e. user position and receiver clock offset. With single frequency observations, having exactly

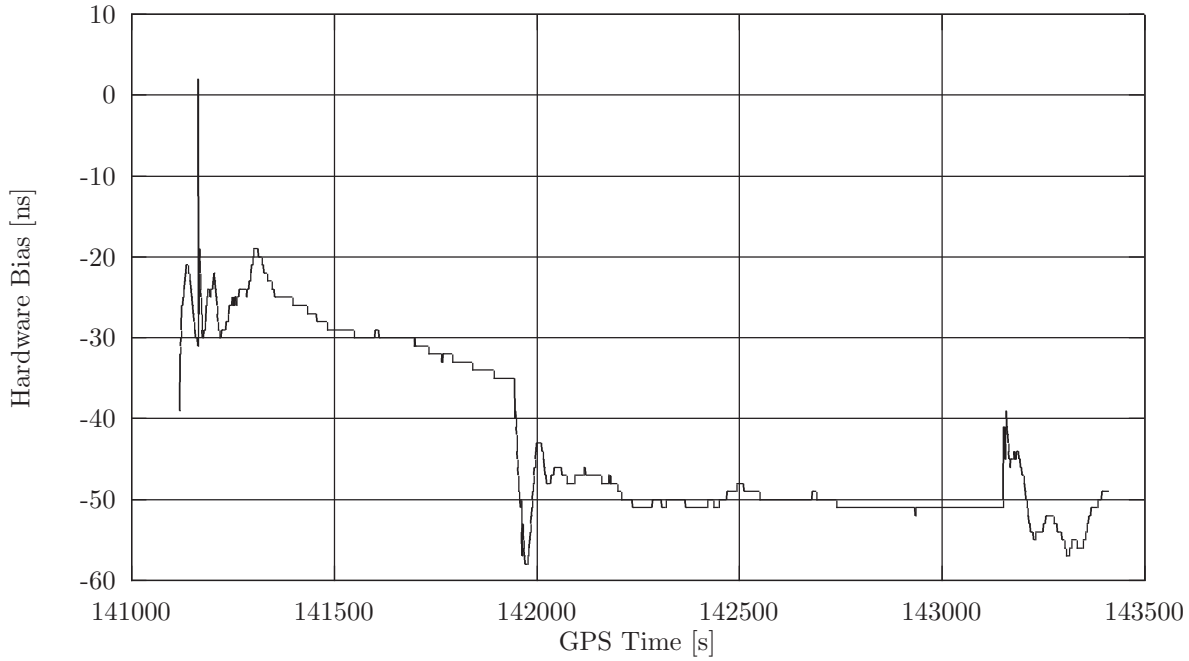

Figure 8.12: GPS/GLONASS double difference carrier phase inter-system hardware delay.

one observation per satellite and epoch, the number of unknowns then is greater than the number of observations, rendering the system of observation equations unsolvable.

To avoid this, GPS introduced a model to estimate the ionospheric path delay for single frequency users. Having determined the ionospheric delay employing this so-called Klobuchar model, the delay now is known and can be shifted to the left hand side of Eq. (8.1.8). Of course, with some minor modifications regarding the signal carrier frequency, this model may as well be applied to single frequency GLONASS pseudorange measurements. However, since GLONASS grants full access to the L_2 frequency, it enables the properly equipped user to deal with the ionosphere problem in a better way, by using dual-frequency ionospheric corrections. These will be treated in Section 8.5.2.

The Klobuchar model is an empirical approach, known to eliminate only about half the actual ionospheric path delay. Still it is used as the recommended model for computation of ionospheric delays for single frequency GPS users. The way this model is to be applied is defined in the GPS Interface Control Document (*ICD-GPS, 1991*). It is briefly described in the following.

Given the geodetic coordinates of the user position λ_R, φ_R (in half circles), the elevation and azimuth E^S, A^S (in half circles) of the observed satellite and the broadcast coefficients α_j, β_j of the ionospheric correction model, the ionospheric time delay at the receiver computed GPS system time t_R is obtained following the algorithm:

Compute Earth's central angle: $\psi = \dfrac{0.0137}{E^S + 0.11} - 0.022$

Compute latitude of ionospheric intersection point: $\varphi^I = \varphi_R + \psi \cos A^S$
Note: Absolute value of φ^I is to be limited to 0.416.

Compute longitude of ionospheric intersection point: $\lambda^I = \lambda_R + \dfrac{\psi \sin A^S}{\cos \varphi^I}$

Compute geomagnetic latitude of ionospheric intersection point:
$\varphi^I_m = \varphi^I + 0.064 \cos(\lambda^I - 1.617)$

Compute local time at ionospheric intersection point: $t^I = t_R + \lambda^I \cdot 43200$ s
Note: t^I is to be limited to the range of 1 day: $0 \le t^I < 86400$ s.

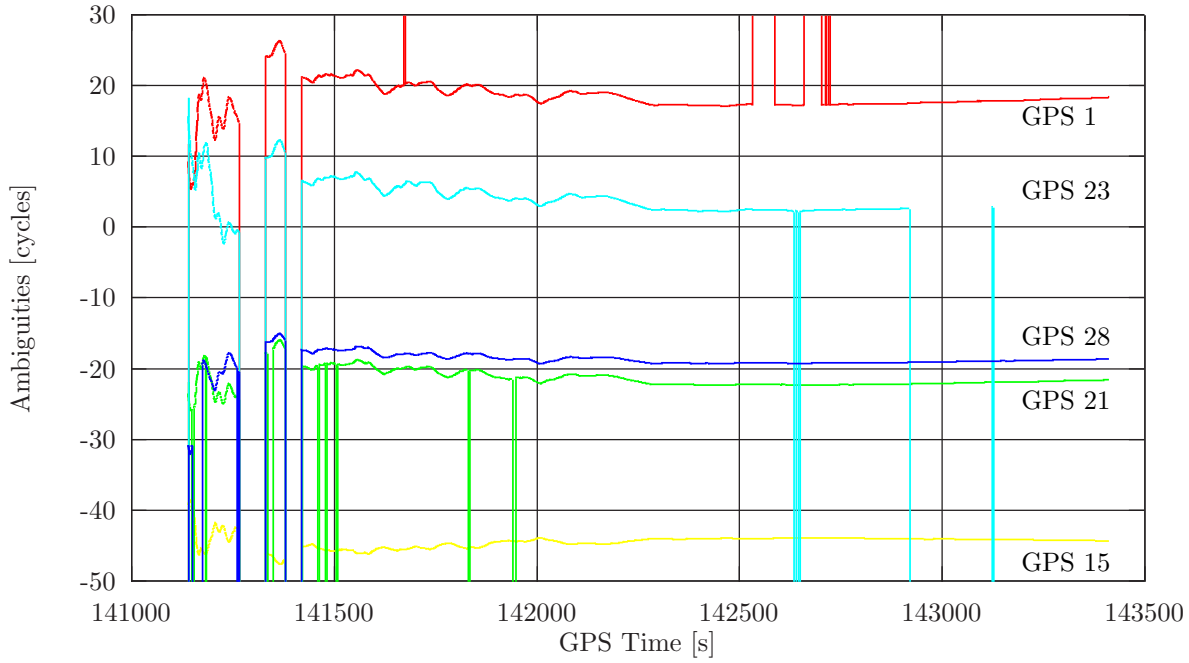

Figure 8.13: GPS double difference carrier phase floating ambiguities.

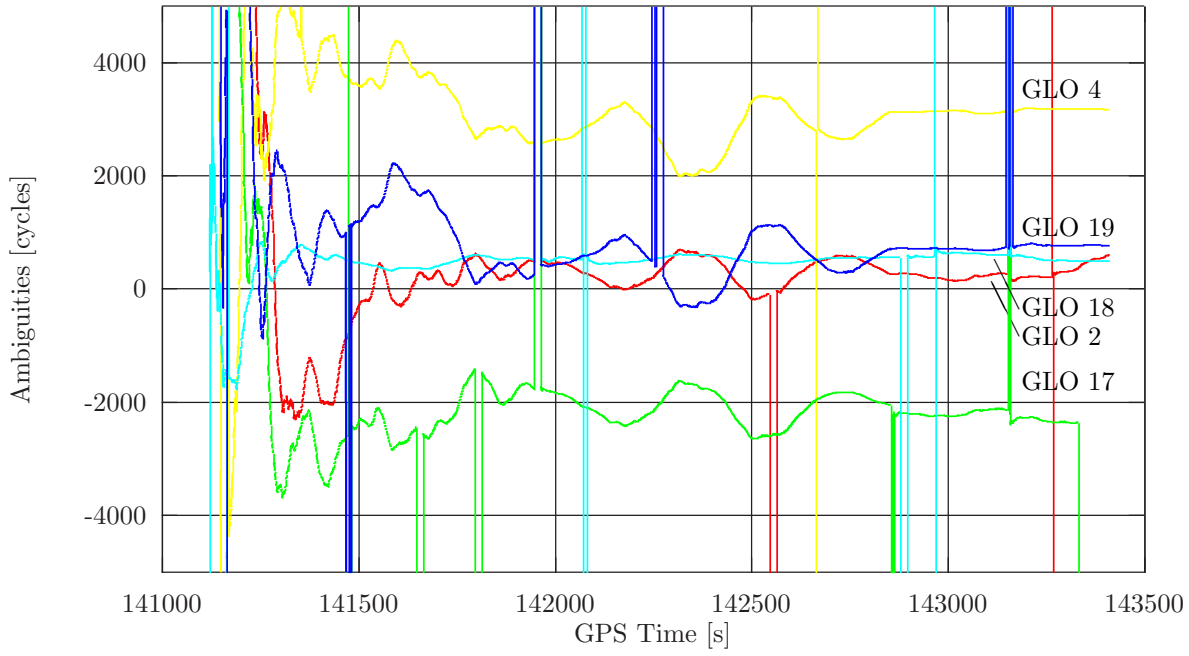

Figure 8.14: GLONASS double difference carrier phase floating ambiguities.

Compute amplitude of ionospheric delay: $A_I = \sum_{j=0}^{3} \alpha_j (\varphi_m^I)^j$

Note: Amplitude is to be limited to values ≥ 0.

Compute period of ionospheric delay: $P_I = \sum_{j=0}^{3} \beta_j (\varphi_m^I)^j$

Note: Period is to be limited to values ≥ 72000.

Compute phase of ionospheric delay: $X_I = \dfrac{2\pi \cdot (t^I - 50400\ \mathrm{s})}{P_I}$ [rad]

Compute obliquity factor: $F = 1 + 16 \cdot (0.53 - E^S)^3$

Compute ionospheric time delay:

$$\delta t^{S,Iono}_{R,\ f_{L_1,\ GPS}} = \begin{cases} \left[5 \cdot 10^{-9} + A_I \cdot \left(1 - \frac{X_I^2}{2} + \frac{X_I^4}{24}\right)\right] \cdot F & ,\ |X_I| < 1.57 \\ 5 \cdot 10^{-9} \cdot F & ,\ |X_I| \geq 1.57 \end{cases} \tag{8.5.1}$$

The ionospheric path delay is dependent on the frequency of the signal; it is inversely proportional to the square of the carrier frequency, cf. e.g. (*Hofmann-Wellenhof et al., 1993*). The algorithm introduced above is designed to compute an estimate of the ionospheric delay of a signal at GPS L_1 frequency (1575.42 MHz). Therefore, for a GLONASS satellite S transmitting on frequency f^S, an additional frequency factor is required to compensate for this:

$$\delta t^{S,Iono}_{R,\ f^S} = \left(\frac{f_{L_1,\ GPS}}{f^S}\right)^2 \delta t^{S,Iono}_{R,\ f_{L_1,\ GPS}} \tag{8.5.2}$$

with $\delta t^{S,Iono}_{R,\ f_{L_1,\ GPS}}$ the ionospheric path delay as calculated for satellite S according to Eq. (8.5.1). The ionospheric path delay from Eq. (8.5.2) for each single satellite is to be inserted in the system of observation equations Eq. (8.1.8) on computation of the receiver position.

8.5.2 Dual Frequency Ionospheric Correction

The ionospheric path delay of a GPS or GLONASS satellite signal depends on the electron content of the ionosphere, the frequency of the signal and the distance that the signal travels through the ionosphere, which in turn depends on the satellite elevation. (*Hofmann-Wellenhof et al., 1993*) e.g. gives the equation

$$c \cdot \delta t^{S,Iono}_R = \frac{1}{\cos z'} \frac{40.3\ \frac{\mathrm{m}^3}{\mathrm{s}^2}}{f^2} TEC \tag{8.5.3}$$

with

z'	Zenith distance of signal at ionospheric piercing point
f	Frequency of carrier signal
TEC	Total electron content of ionosphere

The total electron content in this equation is measured in units of electrons per m^2.

Determination of the Ionospheric Group Delay

Having dual frequency measurements to a satellite available, one can make use of this frequency dependence of the ionospheric path delay to estimate the actual delay without having to rely on a model that may be inaccurate. Denoting the measured pseudorange from receiver R to satellite S on L_1 with PR^S_{R,L_1} and that on L_2 with PR^S_{R,L_2}, we can rewrite Eq. (8.1.4) as:

$$\begin{aligned} PR^S_{R,L_1} &= \varrho^S_R + c \cdot \delta t_R - c \cdot \delta t^S + c \cdot \delta t^{S,Trop}_R + c \cdot \delta t^{S,Iono}_R(f_{L_1}) + \varepsilon^S_{R,L_1} \qquad (8.5.4) \\ &= PR^S_{R,0} + c \cdot \delta t^{S,Iono}_R(f_{L_1}) + \varepsilon^S_{R,L_1} \\ PR^S_{R,L_2} &= \varrho^S_R + c \cdot \delta t_R - c \cdot \delta t^S + c \cdot \delta t^{S,Trop}_R + c \cdot \delta t^{S,Iono}_R(f_{L_2}) + \varepsilon^S_{R,L_2} \qquad (8.5.5) \\ &= PR^S_{R,0} + c \cdot \delta t^{S,Iono}_R(f_{L_2}) + \varepsilon^S_{R,L_2} \end{aligned}$$

where the frequency independent parts of the pseudorange are summarized in $PR^S_{R,0}$. Differencing these two measurements yields

$$PR^S_{R,L_2} - PR^S_{R,L_1} = c \cdot \delta t^{S,Iono}_R(f_{L_2}) - c \cdot \delta t^{S,Iono}_R(f_{L_1}) + \varepsilon^S_{R,L_2} - \varepsilon^S_{R,L_1} \tag{8.5.6}$$

By inserting Eq. (8.5.3) we obtain

$$\begin{aligned} PR^S_{R,L_2} - PR^S_{R,L_1} &= \frac{1}{\cos z'} 40.3 \ \frac{\mathrm{m}^3}{\mathrm{s}^2} \cdot TEC \cdot \left(\frac{1}{f^2_{L_2}} - \frac{1}{f^2_{L_1}} \right) + \varepsilon^S_{R,L_2} - \varepsilon^S_{R,L_1} \\ &= \frac{1}{\cos z'} 40.3 \ \frac{\mathrm{m}^3}{\mathrm{s}^2} \cdot TEC \cdot \frac{1}{f^2_{L_1}} \cdot (\gamma - 1) + \varepsilon^S_{R,L_2} - \varepsilon^S_{R,L_1} \\ &= c \cdot \delta t^{S,Iono}_R(f_{L_1}) \cdot (\gamma - 1) + \varepsilon^S_{R,L_2} - \varepsilon^S_{R,L_1} \qquad (8.5.7) \\ &= c \cdot \delta t^{S,Iono}_R(f_{L_2}) \cdot \frac{\gamma - 1}{\gamma} + \varepsilon^S_{R,L_2} - \varepsilon^S_{R,L_1} \qquad (8.5.8) \end{aligned}$$

with the squared frequency ratio $\gamma = (f_{L_1}/f_{L_2})^2$. Inserting the actual value of $\gamma = 81/49$ for GLONASS and neglecting the measurement noise, the ionospheric path delays become

$$c \cdot \delta t^{S,Iono}_R(f_{L_1}) = \frac{49}{32}(PR^S_{R,L_2} - PR^S_{R,L_1}) \tag{8.5.9}$$

$$c \cdot \delta t^{S,Iono}_R(f_{L_2}) = \frac{81}{32}(PR^S_{R,L_2} - PR^S_{R,L_1}) \tag{8.5.10}$$

for the pseudorange measurements on L_1 and L_2, respectively. These ionospheric delays for each satellite and one measurement is to be inserted in the system of observation equations Eq. (8.1.8) on computation of the receiver position. The second measurement to that satellite now is to be discarded, because it is no longer linearly independent.

Ionospheric Free Pseudorange

A different way of making use of the frequency dependence of the ionospheric path delay to eliminate the influence of the ionosphere in position computation is the forming of an ionospheric-free linear combination of the measured L_1 and L_2 pseudoranges.

Given two pseudorange measurements on L_1 and L_2 from receiver R to satellite S

$$PR^S_{R,L_1} = PR^S_{R,0} + c \cdot \delta t^{S,Iono}_R(f_{L_1}) + \varepsilon^S_{R,L_1} \tag{8.5.11}$$

$$PR^S_{R,L_2} = PR^S_{R,0} + c \cdot \delta t^{S,Iono}_R(f_{L_2}) + \varepsilon^S_{R,L_2} \tag{8.5.12}$$

where the frequency independent parts of the pseudorange are summarized in $PR^S_{R,0}$ (cf. Eq. (8.5.6)), a linear combination can be formed by

$$PR^S_{R,IF} = k_1 \cdot PR^S_{R,L_1} + k_2 \cdot PR^S_{R,L_2} \tag{8.5.13}$$

where k_1 and k_2 are arbitrary factors to be determined in such a way that $PR^S_{R,IF}$ does no longer contain any influence of the ionosphere. Measurement noise again is neglected. However, such a combination is likely to result in an ionospheric free pseudorange that is no longer in the order of magnitude of the measured pseudoranges (including all clock and other errors). When trying to compute a positioning solution from e.g. Eq. (8.1.8) with these "measured" values, one may obtain unlikely large residuals and therewith inaccurate positions. To avoid this, the linear combination from Eq. (8.5.13) is scaled back to the order of magnitude of the measured pseudoranges. This is accomplished by ensuring that the sum of the linear factors is equal to 1:

$$PR^S_{R,IF} = \frac{k_1}{k_1 + k_2} \cdot PR^S_{R,L_1} + \frac{k_2}{k_1 + k_2} \cdot PR^S_{R,L_2} \tag{8.5.14}$$

To match the condition that the ionospheric free pseudorange no longer contain any influence of the ionosphere, it is necessary that the linear combination of the ionospheric delays on both measurements disappears:

$$k_1 \cdot c \cdot \delta t^{S,Iono}_R(f_{L_1}) + k_2 \cdot c \cdot \delta t^{S,Iono}_R(f_{L_2}) \stackrel{!}{=} 0 \tag{8.5.15}$$

Eq. (8.5.15) contains two unknowns, k_1 and k_2. Therefore, one unknown may be chosen arbitrarily to enable solution of the equation. Choosing $k_1 = 1$, we obtain

$$k_2 = -\frac{c \cdot \delta t_R^{S,Iono}(f_{L_1})}{c \cdot \delta t_R^{S,Iono}(f_{L_2})} \tag{8.5.16}$$

and by inserting Eq. (8.5.3)

$$k_2 = -\frac{1}{\gamma} \tag{8.5.17}$$

Inserting these factors k_1 and k_2 into Eq. (8.5.14) yields the ionospheric free pseudorange

$$PR_{R,IF}^S = \frac{\gamma}{\gamma - 1}\left(PR_{R,L_1}^S - \frac{1}{\gamma} PR_{R,L_2}^S\right) \tag{8.5.18}$$

Using this ionospheric free pseudorange from observer R to satellite S in the positioning solution, e.g. according to Eq. (8.1.8), the ionospheric path delay $c \cdot \delta t_R^{S,Iono}$ is equal to zero.

However, the noise of the ionospheric free pseudorange is increased with respect to the original pseudorange measurements. Applying the laws of error propagation, one obtains for the noise of the ionospheric free pseudorange:

$$\sigma_{PR_{IF}}^2 = \left(\frac{\gamma}{\gamma - 1}\right)^2 \sigma_{PR_{L_1}}^2 + \left(\frac{1}{\gamma - 1}\right)^2 \sigma_{PR_{L_2}}^2 \tag{8.5.19}$$

Assuming the noise of the original pseudorange measurements on L_1 and L_2 to be equal, $\sigma_{PR_{L_1}} = \sigma_{PR_{L_2}} = \sigma_{PR}$, this yields

$$\sigma_{PR_{IF}}^2 = \frac{\gamma^2 + 1}{(\gamma - 1)^2} \cdot \sigma_{PR}^2 \tag{8.5.20}$$

or

$$\sigma_{PR_{IF}} = \frac{\sqrt{\gamma^2 + 1}}{\gamma - 1} \cdot \sigma_{PR} \tag{8.5.21}$$

With the actual value of $\gamma = 81/49$, this becomes $\sigma_{PR_{IF}} \approx 2.96 \cdot \sigma_{PR}$.

Ionospheric Free Carrier Phases

Analogously to the pseudoranges, an ionospheric free linear combination of carrier phase measurements can be formed, too. Starting from the observation equation for carrier phase measurements scaled in cycles Eq. (8.2.1), analogously to Eq. (8.5.14), the ionospheric free linear combination of carrier phase measurements can then be written as

$$\varphi_{R,IF}^S = \frac{k_1}{k_1 + k_2} \cdot \varphi_{R,L_1}^S + \frac{k_2}{k_1 + k_2} \cdot \varphi_{R,L_2}^S \tag{8.5.22}$$

Again postulating that the ionospheric influence on this linear combination disappear:

$$k_1 \cdot f_{L_1} \cdot \delta t_R^{S,Iono}(f_{L_1}) + k_2 \cdot f_{L_2} \cdot \delta t_R^{S,Iono}(f_{L_2}) \stackrel{!}{=} 0 \tag{8.5.23}$$

Choosing $k_1 = 1$, we obtain for k_2:

$$k_2 = -\frac{f_{L_1}}{f_{L_2}} \cdot \frac{\delta t_R^{S,Iono}(f_{L_1})}{\delta t_R^{S,Iono}(f_{L_2})} \tag{8.5.24}$$

and by inserting Eq. (8.5.3)

$$k_2 = -\frac{1}{\sqrt{\gamma}} \tag{8.5.25}$$

With these factors, the ionospheric free linear combination of carrier phase measurements becomes

$$\varphi_{R,IF}^S = \frac{\sqrt{\gamma}}{\sqrt{\gamma} - 1}\left(\varphi_{R,L_1}^S - \frac{1}{\sqrt{\gamma}} \varphi_{R,L_2}^S\right) \tag{8.5.26}$$

Under the assumption of the measurement noise of the L_1 carrier phase being identical to that of the L_2 carrier phase, $\sigma_{\varphi_{L_1}} = \sigma_{\varphi_{L_2}} = \sigma_\varphi$ the noise of the ionospheric free carrier phase measurement becomes

$$\sigma_{\varphi_{IF}} = \frac{\sqrt{\gamma+1}}{\sqrt{\gamma}-1} \cdot \sigma_\varphi \tag{8.5.27}$$

Inserting the actual value of $\gamma = (9/7)^2$, the noise of the ionospheric free carrier phase measurement is $\sigma_{\varphi_{IF}} = 5.7 \cdot \sigma_\varphi$.

The wavelength of the ionospheric free carrier signal can be determined by means of the relation

$$\lambda_{IF} = \frac{c}{k_1 f_{L_1} + k_2 f_{L_2}} = \frac{c}{f_{L_1} - \frac{1}{\sqrt{\gamma}} f_{L_2}} = \frac{c}{f_{L_1}} \frac{1}{1-\frac{1}{\gamma}} = \lambda_{L_1} \frac{\gamma}{\gamma-1} \tag{8.5.28}$$

With the actual value of $\gamma = 81/49$, the wavelength of the ionospheric free carrier signal becomes 2.53125 times the wavelength of the L_1 signal. For a GLONASS satellite using frequency number 1 with an L_1 wavelength of approximately 18.707 cm, the wavelength of the ionospheric free signal is approximately 47.35 cm; for frequency number 24 with circa 18.557 cm wavelength on L_1, it is about 46.97 cm. Future frequency number -7 will provide an L_1wavelength of approximately 18.76 cm and thus λ_{IF} will become about 47.49 cm.

The factor $k_2 = -1/\sqrt{\gamma} = -7/9$ is a non-integer value. Therefore, the ionospheric free linear combination of the integer ambiguities $N^S_{R,IF} = N^S_{R,L_1} - (f_{L_2}/f_{L_1}) \cdot N^S_{R,L_2}$ is no longer an integer value. To retain the integer nature of this value, sometimes the so-called L_0 combination $\varphi^S_{L_0} = 9 \cdot \varphi^S_{R,L_1} - 7 \cdot \varphi^S_{R,L_2}$ is suggested as the ionospheric free linear combination. However, the noise of this combination is $\sigma_{\varphi_{L_0}} = \sqrt{9^2+7^2} \cdot \sigma_\varphi \approx 11.4 \cdot \sigma_\varphi$ and thus double the value of $\sigma_{\varphi_{IF}}$. The wavelength of this combination is

$$\lambda_{L_0} = \lambda_{L_1} \cdot \frac{1}{9 - 7\frac{1}{\sqrt{\gamma}}} \tag{8.5.29}$$

or with $\sqrt{\gamma} = 9/7$

$$\lambda_{L_0} = \lambda_{L_1} \cdot \frac{9}{9^2 - 7^2} = 0.28125 \cdot \lambda_{L_1} \tag{8.5.30}$$

This is about 5.26 cm for GLONASS frequency number 1.

GPS with $\gamma = (77/60)^2$ provides an ionospheric free linear combination of the carrier phase measurements with $\sigma_{\varphi_{IF}} = 5.74 \cdot \sigma_\varphi$ and a wavelength of $\lambda_{IF} = 2.546 \cdot \lambda_{L_1}$ or approximately 48.44 cm. While these values are comparable to GLONASS, the noise of the combination φ_{L_0} for GPS becomes $\sigma_{\varphi_{L_0}} = \sqrt{77^2+60^2} \cdot \sigma_\varphi \approx 97.6 \cdot \sigma_\varphi$ at a wavelength of $\lambda_{L_0} = 0.033 \cdot \lambda_{L_1}$, which corresponds to approximately 0.6 cm.

High noise and small wavelength have precluded this combination from having any significant importance for GPS carrier phase positioning. For GLONASS, however, these values are much more favorable. They are still not perfect, but using a low-noise GLONASS receiver one could imagine the L_0 combination gaining importance for carrier phase positioning. Today's GLONASS receivers provide a noise level for carrier phase measurements around 0.5 – 1 mm (1σ). For the L_0 combination, this would mean a noise level of 0.57 – 1.14 cm, well below the 5.26 cm wavelength of the L_0 signal.

8.6 Dilution of Precision

Regarding a set of observations to satellites of one system (either GPS or GLONASS) in matrix notation

$$\vec{l} = \mathbf{A} \cdot \vec{x} + \vec{\varepsilon} \tag{8.6.1}$$

(cf. Eq. (8.1.19)), this equation can be solved according to the scheme

$$\vec{x} = \left(\mathbf{A}^T\mathbf{P}\mathbf{A}\right)^{-1} \mathbf{A}^T\mathbf{P} \cdot \vec{l} \tag{8.6.2}$$

with a weight matrix $\mathbf{P}$ assigning weights to the individual observations, depending on quality of measurement, elevation angle of satellite, or whatever one chooses.

Setting the weight matrix as identity matrix $\mathbf{P} = \mathbf{I}$, i.e. weighting all satellites equally, we obtain the cofactor matrix

$$\mathbf{Q}_X = \left(\mathbf{A}^T\mathbf{A}\right)^{-1} \tag{8.6.3}$$

which depends only on the geometry of the observed satellites relative to the user.

For a set of n observations, the design matrix $\mathbf{A}$ reads

$$\mathbf{A} = \begin{pmatrix} \frac{x_0 - x^1}{\varrho_0^1} & \frac{y_0 - y^1}{\varrho_0^1} & \frac{z_0 - z^1}{\varrho_0^1} & 1 \\ \frac{x_0 - x^2}{\varrho_0^2} & \frac{y_0 - y^2}{\varrho_0^2} & \frac{z_0 - z^2}{\varrho_0^2} & 1 \\ \vdots & \vdots & \vdots & \vdots \\ \frac{x_0 - x^n}{\varrho_0^n} & \frac{y_0 - y^n}{\varrho_0^n} & \frac{z_0 - z^n}{\varrho_0^n} & 1 \end{pmatrix} = \begin{pmatrix} a_{11} & a_{12} & a_{13} & a_{14} \\ a_{21} & a_{22} & a_{23} & a_{24} \\ \vdots & \vdots & \vdots & \vdots \\ a_{n1} & a_{n2} & a_{n3} & a_{n4} \end{pmatrix} \tag{8.6.4}$$

cf. Eq. (8.1.11).

Thus, the cofactor matrix becomes

$$\mathbf{Q}_X = \begin{pmatrix} \sum_{i=1}^{n} a_{i1}^2 & \sum_{i=1}^{n} a_{i1}a_{i2} & \sum_{i=1}^{n} a_{i1}a_{i3} & \sum_{i=1}^{n} a_{i1}a_{i4} \\ \sum_{i=1}^{n} a_{i2}a_{i1} & \sum_{i=1}^{n} a_{i2}^2 & \sum_{i=1}^{n} a_{i2}a_{i3} & \sum_{i=1}^{n} a_{i2}a_{i4} \\ \sum_{i=1}^{n} a_{i3}a_{i1} & \sum_{i=1}^{n} a_{i3}a_{i2} & \sum_{i=1}^{n} a_{i3}^2 & \sum_{i=1}^{n} a_{i3}a_{i4} \\ \sum_{i=1}^{n} a_{i4}a_{i1} & \sum_{i=1}^{n} a_{i4}a_{i2} & \sum_{i=1}^{n} a_{i4}a_{i3} & \sum_{i=1}^{n} a_{i4}^2 \end{pmatrix}^{-1} \tag{8.6.5}$$

which often is denoted as

$$\mathbf{Q}_X = \begin{pmatrix} q_{XX} & q_{XY} & q_{XZ} & q_{Xt} \\ q_{XY} & q_{YY} & q_{YZ} & q_{Yt} \\ q_{XZ} & q_{YZ} & q_{ZZ} & q_{Zt} \\ q_{Xt} & q_{Yt} & q_{Zt} & q_{tt} \end{pmatrix} \tag{8.6.6}$$

The indices in this symmetric matrix depict the origin of the terms by row and column in the design matrix, compare e.g. (*Hofmann-Wellenhof et al., 1993*). It can be shown that the square root of the trace of the cofactor matrix $\sqrt{q_{XX} + q_{YY} + q_{ZZ} + q_{tt}}$ is proportional to the reciprocal value of the volume of a geometric body formed by the intersection points of the site-satellite vectors with the unit sphere centered at the observing site (*Milliken and Zoller, 1996*). The volume of this body is a direct measure of the satellite geometry at the observer. The larger this volume, the better the geometry. And the better the geometry, the more precise the solution for point position and clock offset of the observer. The square root of the trace of the cofactor matrix therefore is called the geometric dilution of precision (GDOP). It is a direct measure of the precision of the combined position and timing solution. Neglecting all error sources other than the influence of satellite geometry, the accuracy of the obtained position and time solution will be the product of the measurement accuracy (standard deviation) σ_0 and the DOP value. The smaller the DOP value, the better the positioning solution.

The GDOP can be split into two further DOPs, representing the satellite geometry with respect to the position and timing solutions separately. These are the position dilution of precision $PDOP = \sqrt{q_{XX} + q_{YY} + q_{ZZ}}$ and the time dilution of precision $TDOP = \sqrt{q_{tt}}$. The PDOP is a measure of how precisely the observer can compute his own position in three-dimensional space given the current satellite geometry. Analogously, the TDOP is a measure of how precisely the observer can compute his own receiver clock offset with respect to system time given the current satellite geometry.

Horizontal (HDOP) and vertical dilution of precision (VDOP) can be computed after splitting the geometrical part of the cofactor matrix and transforming this new matrix into a local cofactor matrix with respect to a topocentric coordinate system (east, north, up) centered at the observation site. The details of this can be found e.g. in (*Hofmann-Wellenhof et al., 1993*).

Thus, for a given measurement accuracy σ_0 the obtainable accuracies for the different kinds of positioning/timing solutions can be expressed as

$$\begin{array}{lcll} \sigma_{Position\ +\ Time} & = & GDOP \cdot \sigma_0 & \text{Accuracy in 3D position and time} \\ \sigma_{Position} & = & PDOP \cdot \sigma_0 & \text{Accuracy in 3D position} \\ \sigma_{Time} & = & TDOP \cdot \sigma_0 & \text{Accuracy in time} \\ \sigma_{Horiz.\ Position} & = & HDOP \cdot \sigma_0 & \text{Accuracy in horizontal position} \\ \sigma_{Vert.\ Position} & = & VDOP \cdot \sigma_0 & \text{Accuracy in vertical position} \end{array} \tag{8.6.7}$$

In case of a combined GPS/GLONASS scenario, there is one more unknown to solve for, and thus the design matrix contains one more column. As noted in Chapter 4, there is the possibility to either introduce a second receiver clock offset or the difference in system time between GPS and GLONASS.

First the case of two different receiver clock offsets with respect to GPS and GLONASS system time as discussed in Section 4.4.1 will be regarded. For a set of m GPS and n GLONASS satellites, the design matrix in this case reads

$$\begin{aligned} \mathbf{A} &= \begin{pmatrix} \frac{x_0 - x^1}{\varrho_0^1} & \frac{y_0 - y^1}{\varrho_0^1} & \frac{z_0 - z^1}{\varrho_0^1} & 1 & 0 \\ \vdots & \vdots & \vdots & \vdots & \vdots \\ \frac{x_0 - x^m}{\varrho_0^m} & \frac{y_0 - y^m}{\varrho_0^m} & \frac{z_0 - z^m}{\varrho_0^m} & 1 & 0 \\ \frac{x_0 - x^{m+1}}{\varrho_0^{m+1}} & \frac{y_0 - y^{m+1}}{\varrho_0^{m+1}} & \frac{z_0 - z^{m+1}}{\varrho_0^{m+1}} & 0 & 1 \\ \vdots & \vdots & \vdots & \vdots & \vdots \\ \frac{x_0 - x^{m+n}}{\varrho_0^{m+n}} & \frac{y_0 - y^{m+n}}{\varrho_0^{m+n}} & \frac{z_0 - z^{m+n}}{\varrho_0^{m+n}} & 0 & 1 \end{pmatrix} \\ &= \begin{pmatrix} a_{11} & a_{12} & a_{13} & a_{14} & a_{15} \\ \vdots & \vdots & \vdots & \vdots & \vdots \\ a_{m1} & a_{m2} & a_{m3} & a_{m4} & a_{m5} \\ a_{m+1,1} & a_{m+1,2} & a_{m+1,3} & a_{m+1,4} & a_{m+1,5} \\ \vdots & \vdots & \vdots & \vdots & \vdots \\ a_{m+n,1} & a_{m+n,2} & a_{m+n,3} & a_{m+n,4} & a_{m+n,5} \end{pmatrix} \end{aligned} \tag{8.6.8}$$

The cofactor matrix becomes

$$\mathbf{Q}_X = \begin{pmatrix} \sum_{i=1}^{m+n} a_{i1}^2 & \sum_{i=1}^{m+n} a_{i1}a_{i2} & \sum_{i=1}^{m+n} a_{i1}a_{i3} & \sum_{i=1}^{m+n} a_{i1}a_{i4} & \sum_{i=m+1}^{m+n} a_{i1}a_{i5} \\ \sum_{i=1}^{m+n} a_{i2}a_{i1} & \sum_{i=1}^{m+n} a_{i2}^2 & \sum_{i=1}^{m+n} a_{i2}a_{i3} & \sum_{i=1}^{m+n} a_{i2}a_{i4} & \sum_{i=m+1}^{m+n} a_{i2}a_{i5} \\ \sum_{i=1}^{m+n} a_{i3}a_{i1} & \sum_{i=1}^{m+n} a_{i3}a_{i2} & \sum_{i=1}^{m+n} a_{i3}^2 & \sum_{i=1}^{m+n} a_{i3}a_{i4} & \sum_{i=m+1}^{m+n} a_{i3}a_{i5} \\ \sum_{i=1}^{m+n} a_{i4}a_{i1} & \sum_{i=1}^{m+n} a_{i4}a_{i2} & \sum_{i=1}^{m+n} a_{i4}a_{i3} & \sum_{i=1}^{m+n} a_{i4}^2 & \sum_{i=m+1}^{m+n} a_{i4}a_{i5} \\ \sum_{i=m+1}^{m+n} a_{i5}a_{i1} & \sum_{i=m+1}^{m+n} a_{i5}a_{i2} & \sum_{i=m+1}^{m+n} a_{i5}a_{i3} & \sum_{i=m+1}^{m+n} a_{i5}a_{i4} & \sum_{i=m+1}^{m+n} a_{i5}^2 \end{pmatrix}^{-1} \tag{8.6.9}$$

Its elements can be denoted as

$$\mathbf{Q}_X = \begin{pmatrix} q_{XX} & q_{XY} & q_{XZ} & q_{Xt} & q_{Xg} \\ q_{XY} & q_{YY} & q_{YZ} & q_{Yt} & q_{Yg} \\ q_{XZ} & q_{YZ} & q_{ZZ} & q_{Zt} & q_{Zg} \\ q_{Xt} & q_{Yt} & q_{Zt} & q_{tt} & q_{tg} \\ q_{Xg} & q_{Yg} & q_{Zg} & q_{tg} & q_{gg} \end{pmatrix} \tag{8.6.10}$$

The PDOP as the influence of the satellite geometry on the precision of the computed position in three-dimensional space can still be computed from the first three elements of the diagonal:

$$PDOP = \sqrt{q_{XX} + q_{YY} + q_{ZZ}}$$

But there are now two separate TDOP values, identifying the influence of satellite geometry on the precision of determination of the two receiver clock offsets. The GPS TDOP is calculated from the fourth element on the diagonal, whereas the GLONASS TDOP is computed from the fifth element on the diagonal:

$$\begin{aligned} TDOP_{GPS} &= \sqrt{q_{tt}} \\ TDOP_{GLONASS} &= \sqrt{q_{gg}} \end{aligned}$$

An overall TDOP could be defined as

$$TDOP = \sqrt{q_{tt} + q_{gg}} = \sqrt{TDOP_{GPS}^2 + TDOP_{GLONASS}^2}$$

Reflecting these two TDOPs, the GDOP as the influence of satellite geometry on the precision of the overall solution (position and time) now becomes

$$GDOP = \sqrt{q_{XX} + q_{YY} + q_{ZZ} + q_{tt} + q_{gg}}$$

For computation of HDOP and VDOP, the geometrical part of the cofactor matrix is split and transformed into a local cofactor matrix with respect to a topocentric coordinate system (east, north, up) centered at the observation site. Thus, the formulation of HDOP and VDOP remain unchanged with respect to the single system case, as does the PDOP.

Focusing instead on the alternative notation with the difference in system times as introduced in Section 4.4.2, the design matrix reads

$$\begin{aligned} \mathbf{A} &= \begin{pmatrix} \frac{x_0 - x^1}{\varrho_0^1} & \frac{y_0 - y^1}{\varrho_0^1} & \frac{z_0 - z^1}{\varrho_0^1} & 1 & 0 \\ \vdots & \vdots & \vdots & \vdots & \vdots \\ \frac{x_0 - x^m}{\varrho_0^m} & \frac{y_0 - y^m}{\varrho_0^m} & \frac{z_0 - z^m}{\varrho_0^m} & 1 & 0 \\ \frac{x_0 - x^{m+1}}{\varrho_0^{m+1}} & \frac{y_0 - y^{m+1}}{\varrho_0^{m+1}} & \frac{z_0 - z^{m+1}}{\varrho_0^{m+1}} & 1 & 1 \\ \vdots & \vdots & \vdots & \vdots & \vdots \\ \frac{x_0 - x^{m+n}}{\varrho_0^{m+n}} & \frac{y_0 - y^{m+n}}{\varrho_0^{m+n}} & \frac{z_0 - z^{m+n}}{\varrho_0^{m+n}} & 1 & 1 \end{pmatrix} \\ &= \begin{pmatrix} a_{11} & a_{12} & a_{13} & a_{14} & a_{15} \\ \vdots & \vdots & \vdots & \vdots & \vdots \\ a_{m1} & a_{m2} & a_{m3} & a_{m4} & a_{m5} \\ a_{m+1,1} & a_{m+1,2} & a_{m+1,3} & a_{m+1,4} & a_{m+1,5} \\ \vdots & \vdots & \vdots & \vdots & \vdots \\ a_{m+n,1} & a_{m+n,2} & a_{m+n,3} & a_{m+n,4} & a_{m+n,5} \end{pmatrix} \end{aligned} \tag{8.6.11}$$

for a set of m GPS and n GLONASS satellites and solving for the receiver clock offset with respect to GPS system time, cf. Eq. (8.1.21).

The cofactor matrix now becomes

$$\mathbf{Q}_X = \begin{pmatrix} \sum_{i=1}^{m+n} a_{i1}^2 & \sum_{i=1}^{m+n} a_{i1}a_{i2} & \sum_{i=1}^{m+n} a_{i1}a_{i3} & \sum_{i=1}^{m+n} a_{i1}a_{i4} & \sum_{i=m+1}^{m+n} a_{i1}a_{i5} \\ \sum_{i=1}^{m+n} a_{i2}a_{i1} & \sum_{i=1}^{m+n} a_{i2}^2 & \sum_{i=1}^{m+n} a_{i2}a_{i3} & \sum_{i=1}^{m+n} a_{i2}a_{i4} & \sum_{i=m+1}^{m+n} a_{i2}a_{i5} \\ \sum_{i=1}^{m+n} a_{i3}a_{i1} & \sum_{i=1}^{m+n} a_{i3}a_{i2} & \sum_{i=1}^{m+n} a_{i3}^2 & \sum_{i=1}^{m+n} a_{i3}a_{i4} & \sum_{i=m+1}^{m+n} a_{i3}a_{i5} \\ \sum_{i=1}^{m+n} a_{i4}a_{i1} & \sum_{i=1}^{m+n} a_{i4}a_{i2} & \sum_{i=1}^{m+n} a_{i4}a_{i3} & \sum_{i=1}^{m+n} a_{i4}^2 & \sum_{i=m+1}^{m+n} a_{i4}a_{i5} \\ \sum_{i=m+1}^{m+n} a_{i5}a_{i1} & \sum_{i=m+1}^{m+n} a_{i5}a_{i2} & \sum_{i=m+1}^{m+n} a_{i5}a_{i3} & \sum_{i=m+1}^{m+n} a_{i5}a_{i4} & \sum_{i=m+1}^{m+n} a_{i5}^2 \end{pmatrix}^{-1} \tag{8.6.12}$$

the elements of which can be denoted as

$$\mathbf{Q}_X = \begin{pmatrix} q_{XX} & q_{XY} & q_{XZ} & q_{Xt} & q_{Xs} \\ q_{XY} & q_{YY} & q_{YZ} & q_{Yt} & q_{Ys} \\ q_{XZ} & q_{YZ} & q_{ZZ} & q_{Zt} & q_{Zs} \\ q_{Xt} & q_{Yt} & q_{Zt} & q_{tt} & q_{ts} \\ q_{Xs} & q_{Ys} & q_{Zs} & q_{ts} & q_{ss} \end{pmatrix} \tag{8.6.13}$$

The PDOP as the influence of the satellite geometry on the precision of the computed position in three-dimensional space again remains unchanged with respect to the single system scenario, $PDOP = \sqrt{q_{XX} + q_{YY} + q_{ZZ}}$. The GDOP as the influence of satellite geometry on the precision of the overall solution (position and time) now becomes $GDOP = \sqrt{q_{XX} + q_{YY} + q_{ZZ} + q_{tt} + q_{ss}}$, caring for the additional unknown to be solved for, the difference between GPS and GLONASS system times. Picking the TDOP as the influence of satellite geometry on the precision of determination of the receiver clock offset to (GPS) system time as $TDOP = \sqrt{q_{tt}}$ as in the single system case, leaves one term not accounted for in the GDOP. $\sqrt{q_{ss}}$ can be interpreted as the influence of the satellite geometry on the precision of the computed offset between GPS and GLONASS system times. For the sake of convenience, it further on will be called SDOP (system time DOP). For a given measurement accuracy σ_0 the obtainable accuracy for the offset between GPS and GLONASS system times therefore can be expressed as

$$\sigma_{System\ Time\ Offset} = SDOP \cdot \sigma_0 \quad \text{Accuracy in GPS / GLONASS system time offset} \tag{8.6.14}$$

The combination of GPS and GLONASS observations, among other advantages of the combination, improves the satellite geometry with respect to GPS or GLONASS observations alone. Figure 8.15 shows actual GDOP values for Munich on February 26, 1999, computed from real GPS and GLONASS almanac data valid at that time. The GLONASS DOP values are affected by the depleted constellation. For a considerable time there are only three or less GLONASS satellites visible; these times are plotted with a GDOP value of zero. At other times, with just enough satellites to compute a GLONASS positioning solution, the satellite geometry is very unfavorable, as can be seen by the high DOP values, beyond the scale of the plot. It can, however, easily be seen that the GDOP values for the combined GPS/GLONASS constellation always is lower than the GDOP values for GPS or GLONASS alone. The combined geometry is much better than the geometry of one system alone.

However, the fact that the satellites belong to different satellite systems is a slight disadvantage, since one satellite measurement must be sacrificed for the determination of the offset between GPS and GLONASS system time. Therefore, the geometry of the combined GPS/GLONASS satellites cannot be as strong as the same geometry of only GPS or only GLONASS satellites.

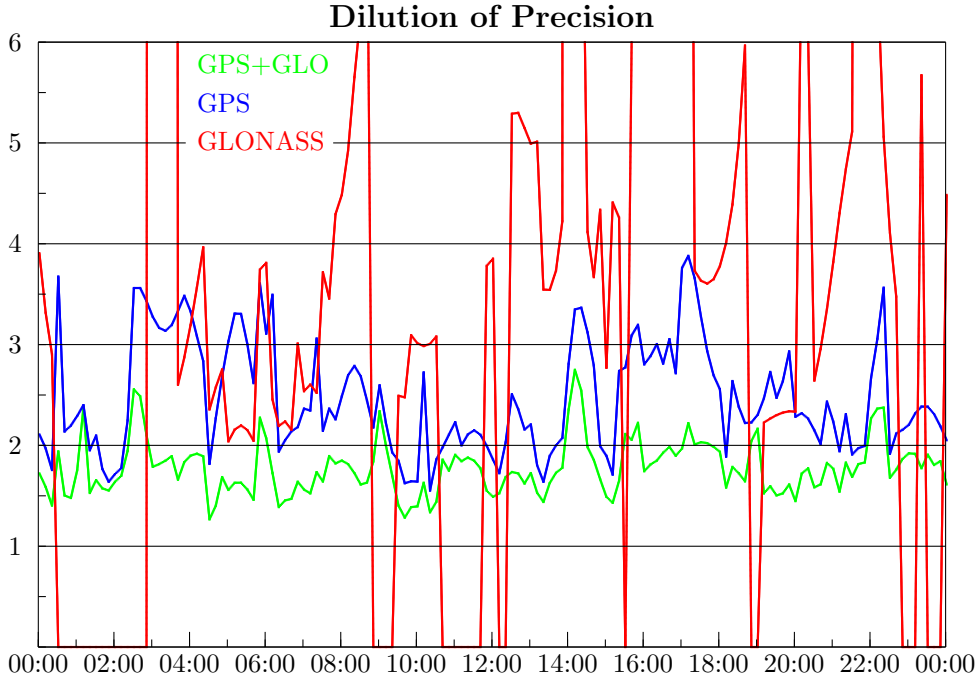

Figure 8.15: GDOP values for 02/26/99.

In a combined constellation of m GPS and n GLONASS satellites, regarding all observed satellites to be belonging to one system and thus having only one receiver clock offset, one would obtain for the design matrix (8.6.11)

$$\mathbf{A} = \begin{pmatrix} \frac{x_0 - x^1}{\varrho_0^1} & \frac{y_0 - y^1}{\varrho_0^1} & \frac{z_0 - z^1}{\varrho_0^1} & 1 \\ \vdots & \vdots & \vdots & \vdots \\ \frac{x_0 - x^m}{\varrho_0^m} & \frac{y_0 - y^m}{\varrho_0^m} & \frac{z_0 - z^m}{\varrho_0^m} & 1 \\ \frac{x_0 - x^{m+1}}{\varrho_0^{m+1}} & \frac{y_0 - y^{m+1}}{\varrho_0^{m+1}} & \frac{z_0 - z^{m+1}}{\varrho_0^{m+1}} & 1 \\ \vdots & \vdots & \vdots & \vdots \\ \frac{x_0 - x^{m+n}}{\varrho_0^{m+n}} & \frac{y_0 - y^{m+n}}{\varrho_0^{m+n}} & \frac{z_0 - z^{m+n}}{\varrho_0^{m+n}} & 1 \end{pmatrix} = \begin{pmatrix} a_{11} & a_{12} & a_{13} & a_{14} \\ \vdots & \vdots & \vdots & \vdots \\ a_{m1} & a_{m2} & a_{m3} & a_{m4} \\ a_{m+1,1} & a_{m+1,2} & a_{m+1,3} & a_{m+1,4} \\ \vdots & \vdots & \vdots & \vdots \\ a_{m+n,1} & a_{m+n,2} & a_{m+n,3} & a_{m+n,4} \end{pmatrix} \tag{8.6.15}$$

The cofactor matrix (8.6.12) would become

$$\mathbf{Q}_X = \begin{pmatrix} \sum_{i=1}^{m+n} a_{i1}^2 & \sum_{i=1}^{m+n} a_{i1}a_{i2} & \sum_{i=1}^{m+n} a_{i1}a_{i3} & \sum_{i=1}^{m+n} a_{i1}a_{i4} \\ \sum_{i=1}^{m+n} a_{i2}a_{i1} & \sum_{i=1}^{m+n} a_{i2}^2 & \sum_{i=1}^{m+n} a_{i2}a_{i3} & \sum_{i=1}^{m+n} a_{i2}a_{i4} \\ \sum_{i=1}^{m+n} a_{i3}a_{i1} & \sum_{i=1}^{m+n} a_{i3}a_{i2} & \sum_{i=1}^{m+n} a_{i3}^2 & \sum_{i=1}^{m+n} a_{i3}a_{i4} \\ \sum_{i=1}^{m+n} a_{i4}a_{i1} & \sum_{i=1}^{m+n} a_{i4}a_{i2} & \sum_{i=1}^{m+n} a_{i4}a_{i3} & \sum_{i=1}^{m+n} a_{i4}^2 \end{pmatrix}^{-1} \tag{8.6.16}$$

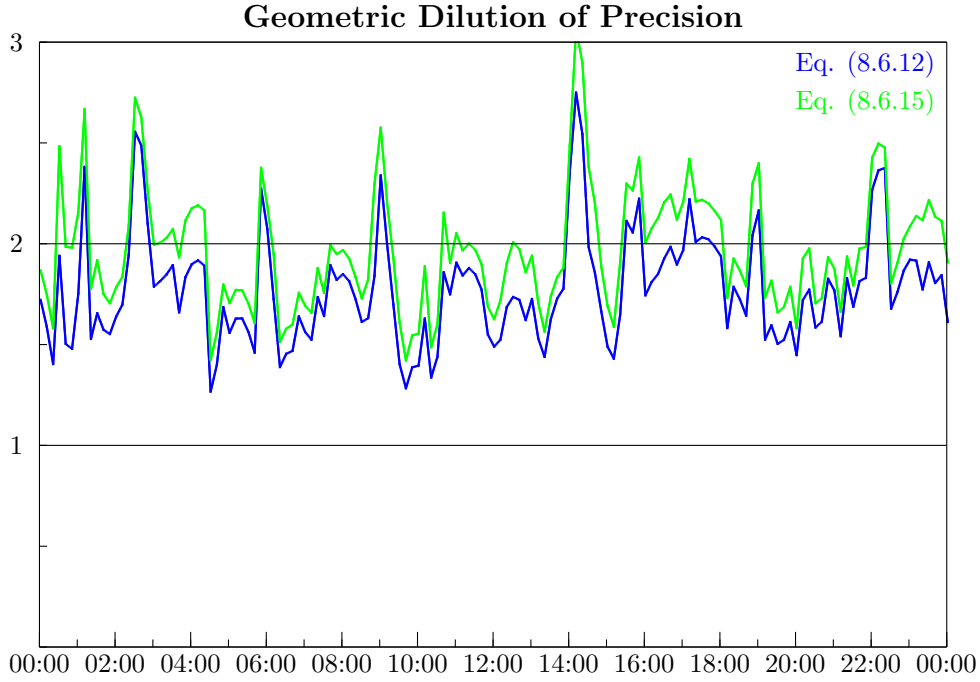

Figure 8.16: Comparison of GDOP values from Eqs. (8.6.12) and (8.6.15).

Of course, apart from the different number of observed satellites, these matrices would be identical to the matrices Eqs. (8.6.4) and (8.6.5). Again denoting the cofactor matrix as

$$\mathbf{Q}_X = \begin{pmatrix} q_{XX} & q_{XY} & q_{XZ} & q_{Xt} \\ q_{XY} & q_{YY} & q_{YZ} & q_{Yt} \\ q_{XZ} & q_{YZ} & q_{ZZ} & q_{Zt} \\ q_{Xt} & q_{Yt} & q_{Zt} & q_{tt} \end{pmatrix} \tag{8.6.17}$$

and forming the DOP values

$$\begin{aligned} GDOP &= \sqrt{q_{XX} + q_{YY} + q_{ZZ} + q_{tt}} \\ PDOP &= \sqrt{q_{XX} + q_{YY} + q_{ZZ}} \\ TDOP &= \sqrt{q_{tt}} \end{aligned} \tag{8.6.18}$$

one would obtain PDOP and TDOP identical in formulation to the values as derived from Eq. (8.6.12). The same holds true to the HDOP and VDOP, which are decompositions of the PDOP. In addition, the numerical values for PDOP, HDOP, VDOP and TDOP are approximately the same as those from Eq. (8.6.12). However, this does not hold true for the GDOP value. The GDOP computed in this way would lack the SDOP component. Due to the quadratic nature of the elements q_{ii} on the diagonal of the cofactor matrix, the GDOP value computed this way would be too small, yielding too optimistic an accuracy of the overall position and time solution.

Figures 8.16 to 8.18 show these different DOP values, computed according to Eqs. (8.6.12) and (8.6.15). Like in Figure 8.15, data were computed for February 26, 1999, in Munich, using GPS and GLONASS almanac data valid at that time.

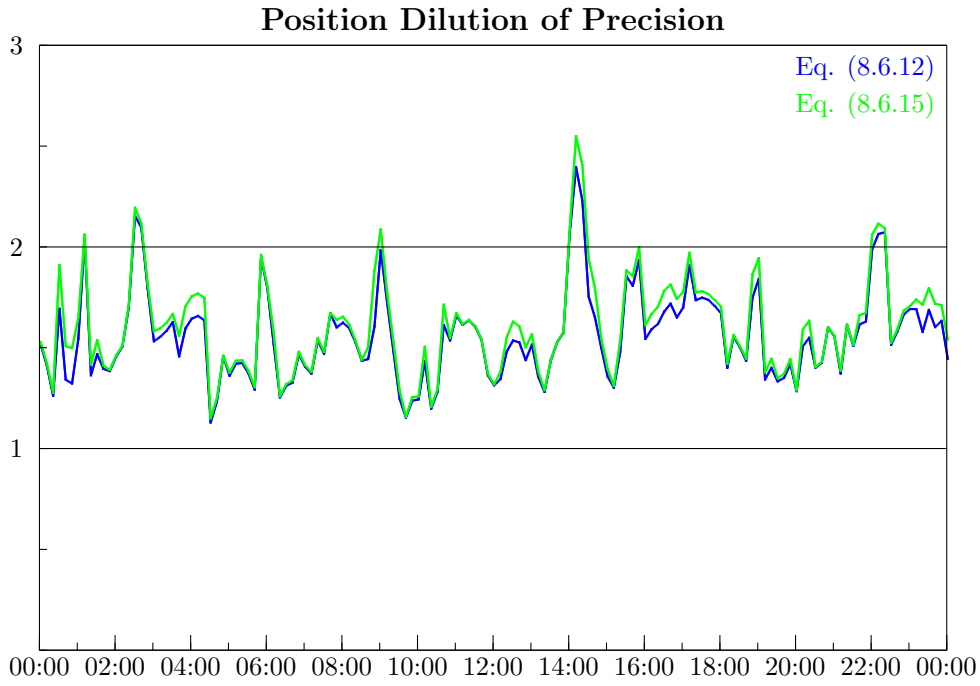

Figure 8.17: Comparison of PDOP values from Eqs. (8.6.12) and (8.6.15).

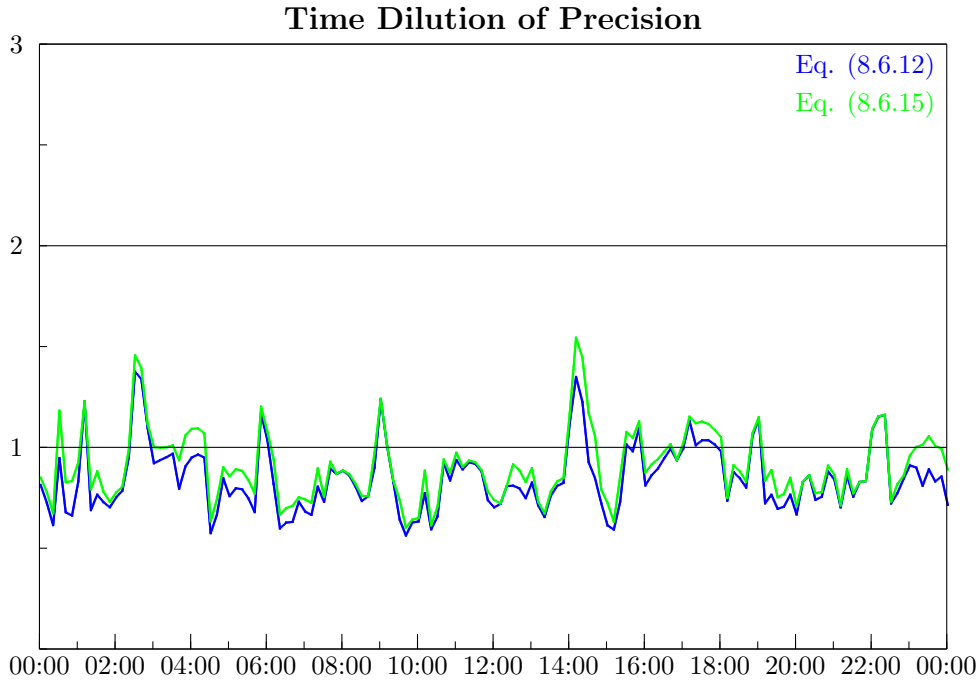

Figure 8.18: Comparison of TDOP values from Eqs. (8.6.12) and (8.6.15).

9 GPS/GLONASS Software Tools

A number of GLONASS and GPS/GLONASS software tools were created during the work on this topic. The purpose of these tools was to test and evaluate the algorithms introduced in the previous chapters. All of the results presented in this work were obtained using this software.

Among the tools created are a GPS/GLONASS planning tool and different tools for processing of GLONASS and GPS/GLONASS measurements. A decoder to convert measurements from different receiver types available at IfEN to RINEX format also belongs to this software. All these tools started out as MS-DOS programs and were later re-written to run under the new 32-bit Windows environments (Windows 95 and Windows NT).

The GPS/GLONASS mission planning tool – as is expressed in its name – is intended to support a GPS/GLONASS user in planning a surveying mission. Prior to 1994, before GPS reached its Initial Operational Capability (IOC) with all 24 satellites operational, similar tools were used to check satellite availability and geometry (DOP values) based on current GPS almanac data before scheduling GPS surveys. With GPS reaching its IOC and later FOC, these tools lost their importance, because the complete satellite constellation now usually provided sufficient satellite coverage and geometry 24 hours a day.

But GLONASS reached its full constellation in 1996 only to see it starting to dwindle again immediately. Today, GLONASS again is far away from a full satellite constellation. Thus, mission planning is still very important for GLONASS. Therefore, the mission planning tool was created. It calculates satellite positions from GPS and GLONASS almanac data for epochs within a specified time span. For a given user location and elevation mask, the number of visible satellites can then be computed, along with the times of visibility, elevations and azimuth angles of the individual satellites. These data can be presented in different graphs, including a polar plot. Of course, the different DOP values can be computed and presented, too.

Figure 9.1 shows a screen shot of this GPS/GLONASS planning tool.

A decoder was written to convert measurement files recorded by IfEN's different GPS/GLONASS receivers to RINEX2 formatted observation and navigation files for purposes of archiving and post-processing. The RINEX (Receiver Independent Exchange) format (*Gurtner, 1998*) was introduced in 1990 for the purpose of archiving and exchanging GPS measurements of different receiver types and institutions within the IGS. Different file formats were defined for observation files (satellite measurements), navigation files (ephemeris data) and meteorological files (weather data). RINEX version 2 as introduced in 1993 provided the possibility to include measurements to GLONASS satellites in the observation files. In 1997, another file format was defined for the exchange of GLONASS ephemeris data, since the parameters used to describe GLONASS broadcast ephemerides differ from those used for GPS satellites. In April 1998, Version 2.01 was introduced for the GLONASS navigation files, correcting a mistaken sign convention for clock parameters.

IfEN has available three different types of combined GPS/GLONASS receivers. In 1994, a couple of 3S Navigation R-100/R-101 receivers were purchased. In 1996, two Ashtech GG24 OEM boards were acquired, which were integrated into full-scale receivers, adding a power supply and a casing. These receivers were joined by one MAN GNSS-200 receiver, which was borrowed from the manufacturer under a long-term testing agreement. The GPS/GLONASS decoder was written to convert measurement data from these receivers to RINEX2.

The decoder creates RINEX observation as well as GPS and GLONASS navigation files from the measurements and ephemeris data contained in the receiver files. Besides that, almanac files can be created as input for the mission planning tool. For testing purposes, satellite measurements can be filtered out using different criteria. It is e.g. possible to decode only measurement data from specified satellites (or from all but some specified satellites). Other criteria include the signal-to-noise ratio of the measurements or the satellite elevation, where this is included in the satellite data (in the Ashtech

GG24). Measurement data can also be filtered by frequency band and/or code. This way, e.g. only P-code measurements can be decoded, or only L_1 C/A-code measurements, or only L_2, or ...

During a decoding run, the assignment of satellites to the different receiver hardware channels can be displayed, together with the number of decoded measurements.

Figure 9.2 shows a screen shot of the GPS/GLONASS decoder.

A real-time version of the decoder reads data online from a receiver connected to a serial port and creates RINEX files in specified intervals.

The GPS/GLONASS processing tools were created to compute user positions from GPS and GLONASS satellite observations, using different algorithms. The single point positioning tool computes positions from observation data recorded at one site, whereas the differential positioning tool employs observations recorded simultaneously at two sites to calculate the position of one receiver, while the other (reference) site is held fixed.

Similar to the RINEX decoder, satellites and measurements to participate in the positioning solution can be selected using a number of criteria, such as satellite number, SNR, elevation mask or frequency band and code. In addition, a DOP threshold can be specified for minimum requirements on the satellite geometry. For evaluating the influence of the coordinate transformation from PZ-90 to WGS84, different coordinate transformations can be applied to GLONASS satellite positions prior to computing the user position.

Either raw pseudoranges, carrier-smoothed pseudoranges or carrier phase ranges (in the differential tool) can be used to compute the receiver position. Computed positions are output epoch-wise in tabular form and in different graphs, e.g. as scatter plots, depicting the distribution of the positioning solutions in the horizontal plane.

For testing different processing algorithms or formulations of the observation equations (e.g. single or double difference processing), these algorithms can easily be implemented in this test software by modifying the source code and re-compiling the software.

Figure 9.3 shows a screen shot of the GPS/GLONASS absolute positioning tool.

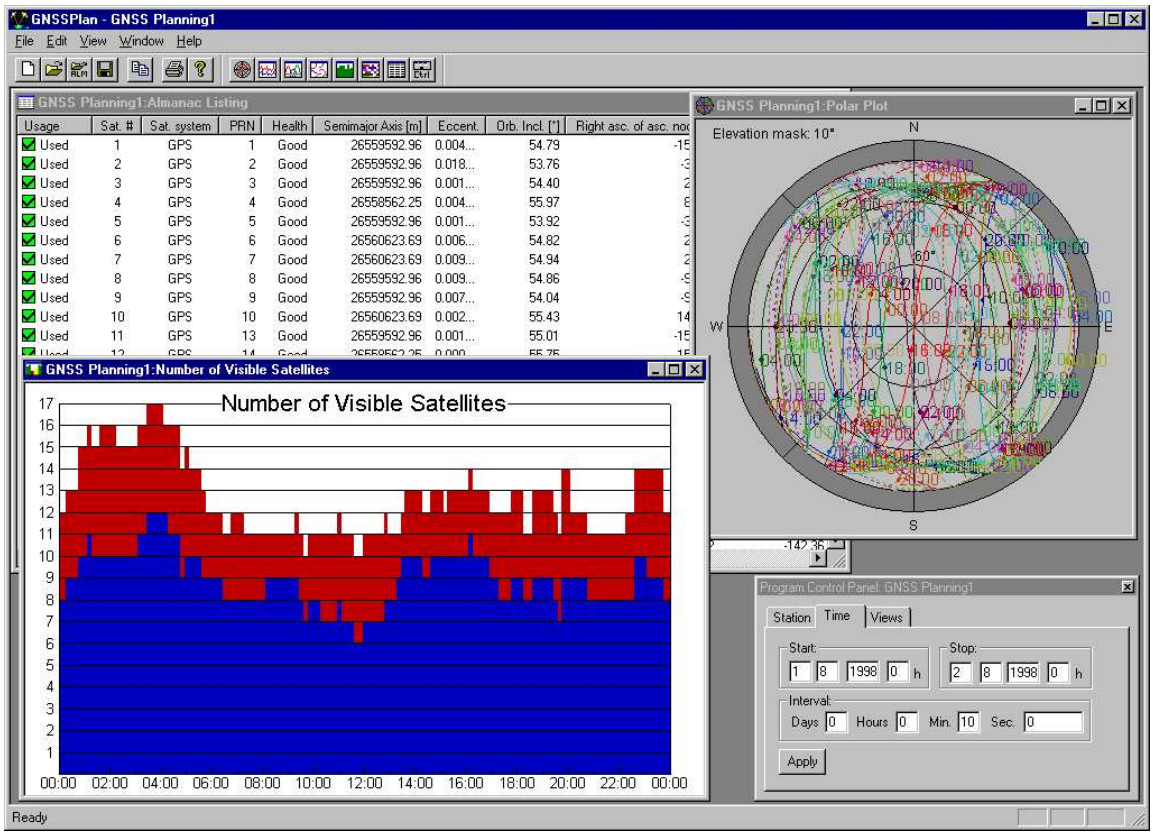

Figure 9.1: Screen shot of the GPS/GLONASS mission planning tool.

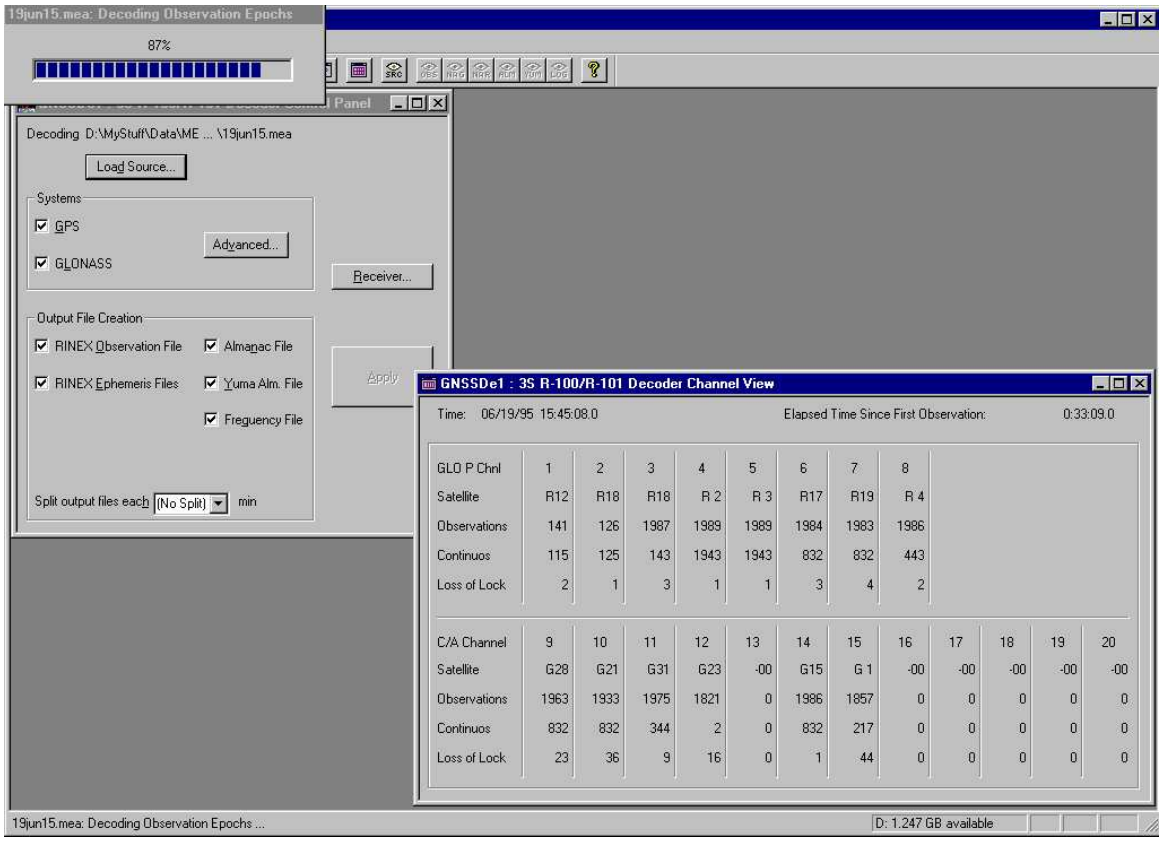

Figure 9.2: Screen shot of the GPS/GLONASS RINEX decoder.

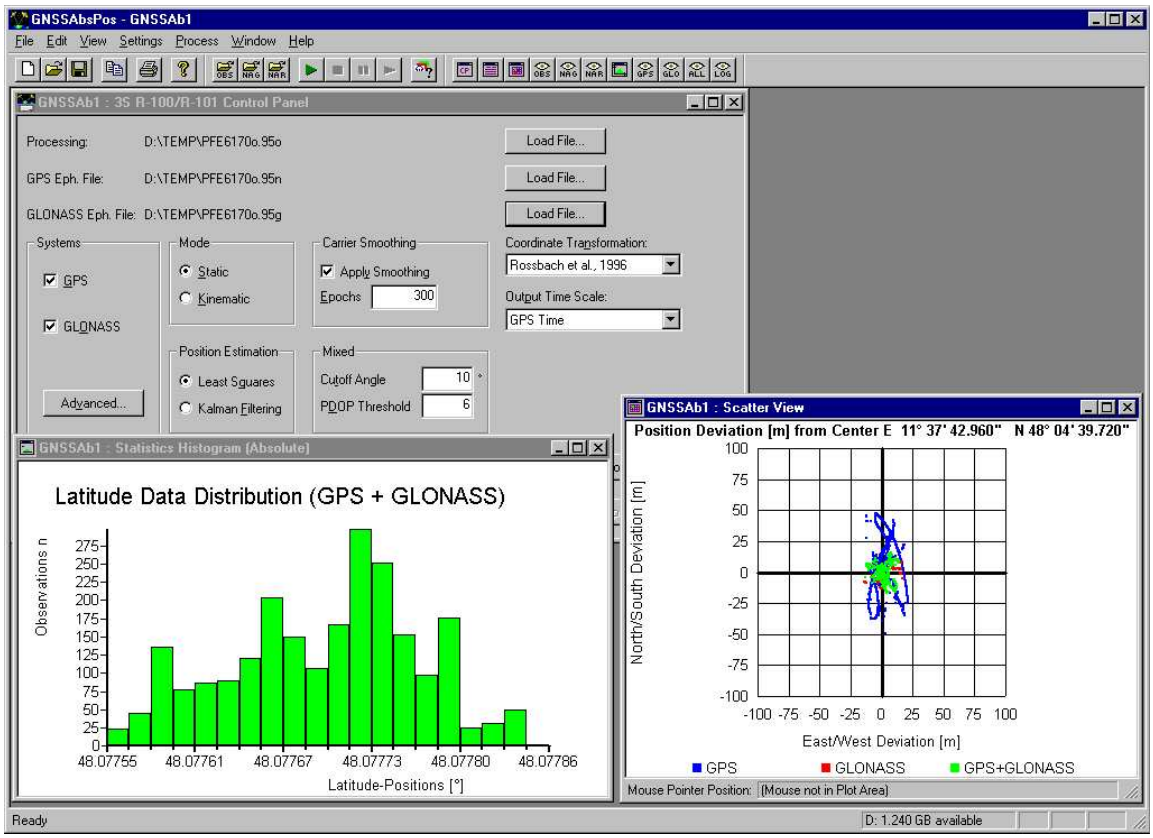

Figure 9.3: Screen shot of the GPS/GLONASS absolute positioning tool.

10 Summary

After a short introduction to the history of GLONASS, the system has been described in detail. It was shown that GPS and GLONASS are very similar systems. However, in all their similarity, there are also differences between these two systems. These differences, and how they affect the combined evaluation of GPS and GLONASS satellite observations, have been worked out.

The first of these differences is the different reference frames for time used by GPS and by GLONASS. Both GPS and GLONASS use their own system time scale. In addition, both system time scales are related to different realizations of UTC. GPS system time is related to $\mathrm{UTC}_{\mathrm{USNO}}$, whereas GLONASS system time is related to $\mathrm{UTC}_{\mathrm{SU}}$. The difference between these two time frames is not known in real-time. However, this problem can be easily overcome by introducing the offset between the system times as an additional unknown in the observation equation. This means sacrificing one observation to solve for that additional parameter. But this is not a problem, as long as the number of additional satellites (compared to observations to one satellite system only) is greater than one. With only one additional satellite, the additional observation will only contribute to the determination of the difference in system times, but not to the computed positions. An actual improvement in positioning solution therefore is only possible with two or more satellites of the additional system.

The next difference is the different coordinate reference frames used by GPS (WGS84) and GLONASS (PZ-90). This difference can be overcome by converting GLONASS satellite positions from the PZ-90 frame to the WGS84 frame before using them in a combined positioning solution. This conversion is done by means of a seven parameter Helmert transformation. A significant part of this work is dedicated to the determination of a suitable set of transformation parameters.

Two different attempts to determine these parameters have been described. In the first method, PZ-90 station coordinates were calculated from GLONASS observations, and transformation parameters were derived from matching these coordinates to the known WGS84 station coordinates. In the second method, the observation equation was modified such that it represents an observation to a GLONASS satellite from a station with given WGS84 coordinates, where the transformation parameters are the unknowns. The results of both methods have been presented, and they show good coincidence.

It was furthermore shown that in differential positioning differences in coordinate frames can be treated as satellite orbital errors, which cancel over short baselines. However, when a suitable coordinate transformation is applied, the baselines, over which any residual errors in coordinate frame can be neglected, are much longer.

The GLONASS navigation message contains satellite coordinates, velocities and accelerations due to the gravitational influences of Sun and Moon, at a specified reference time. To obtain satellite coordinates at a time different from that reference time, the satellite's equations of motion have to be integrated. This can only be done numerically. The four step Runge-Kutta method used for the integration was presented, together with a step width that represents a good compromise between accuracy of the integration and the computational effort.

The second major part of this work is dedicated to the evaluation of GLONASS and combined GPS/GLONASS observations. The observation equations for all cases of single point, single difference and double difference positioning, using code or carrier phase measurements, have been presented.

Whereas the observation equations for GLONASS code range positioning and also carrier phase positioning using single differences are very similar to the respective GPS equations, this is different for double difference carrier phase positioning. Here, the different carrier frequencies of the GLONASS satellites either prevent the single difference clock terms to cancel from the equation, or prevent the single difference integer ambiguities to combine into a double difference integer value. This means the ambiguities can no longer be treated as integers.

After an overview of current attempts to tackle this problem, an own solution attempt was presented. This approach is based on a common signal frequency, of which the frequencies participating in the observation equation are integer multiples. A modified double difference ambiguity on this common

frequency can then be formed. This double difference is still an integer value. However, the draw-back of this solution is the small wavelength of this common frequency, resulting in large ambiguity values that are difficult to fix. But on the other hand, due to that small wavelength it is not required to really fix the ambiguities to integers. A fixing to thousands of integers may be sufficient.

The peculiarities of ionospheric correction and DOP computation for GLONASS and GPS/GLONASS combination are pointed out. The presence of two system time scales in combined GPS/GLONASS positioning brings up an additional DOP value. Depending on the formulation of the observation equations, this can either be interpreted as an additional TDOP value, or as a DOP value associated with the difference in system time scales.

Finally, a bundle of GPS/GLONASS software tools has been described that was designed within the scope of this work. These tools have been used to obtain the results presented herein.

Appendix

A Bibliography

3S Navigation (1994). *R-100 Series GPS/GLONASS Receiver User's Manual.* 3S Navigation, Laguna Hills, CA.

3S Navigation (1996a). *GNSS-200 GPS/GLONASS Receiver User's Manual.* 3S Navigation / MAN Technologie AG, Laguna Hills, CA.

3S Navigation (1996b). *GNSS-300 GPS/GLONASS Receiver User's Manual.* 3S Navigation / MAN Technologie AG, Laguna Hills, CA.

Abusali, P. A. M., Schutz, B. E., Tapley, B. D., and Bevis, M. (1995). Transformation between SLR/VLBI and WGS-84 Reference Frames. *Bulletin Geodesique*, 69:61–72.

Anodina, T. G. (1988). GLONASS System Technical Characteristics and Performance. Working Papers WP/70 and WP/75, Special Committee on Future Air Navigation Systems (FANS/4), International Civil Aviation Organization (ICAO), Montreal.

Ashtech (1996). *GG24 GPS+GLONASS Receiver Reference Manual.* Ashtech Inc., Sunnyvale, CA.

Ashtech (1998a). *WWW Home Page.* Ashtech Inc., Sunnyvale, CA. `http://www.ashtech.com`.

Ashtech (1998b). *Z-18 GPS+GLONASS Receiver Data Sheet.* Ashtech Inc., Sunnyvale, CA.

Balendra, A., Kim, S., and Beser, J. (1994). Fully Integrated GLONASS Dual Frequency P Code and GPS/GLONASS Single Frequency C/A Code Receiver. In *Proceedings of ION Satellite Division GPS-94 International Technical Meeting*, pages 461–470, Salt Lake City, Utah.

Bartenev, V. A. et al. (1994). The GLONASS Global Positioning System.

Bazlov, Y. A., Galazin, V. F., Kaplan, B. L., Maksimov, V. G., and Rogozin, V. P. (1999). GLONASS to GPS: A New Coordinate Transformation. *GPS World Magazine*, 10(1):54–58.

Beser, J. and Danaher, J. (1993). The 3S Navigation R-100 Family of Integrated GPS/GLONASS Receivers: Description and Performance Results. In *Proceedings of ION Satellite Division National Technical Meeting*, San Francisco, California.

Beutler, G., Bauersima, I., Gurtner, W., Rothacher, M., and Schildknecht, T. (1987). Atmospheric Refraction and Other Important Biases in GPS Carrier Phase Observations. Internal Report 22, "Satellitenbeobachtungsstation Zimmerwald", Bern, Switzerland.

BIPM (1995). Annual Report of the BIPM Time Section, Volume 8. Technical report, BIPM, Pavillon de Breteuil.

Boykov, V. V. et al. (1993). Experimental Compiling the Geocentric System of Coordinates PZ-90 (in Russian Language). *Geodezia i Kartografia*, 11:17 – 21.
Бойков, В. В. и др.: Опыт создания геоцентрической системы координат ПЗ-90, в "Геодезия и картографиа", Н 11, ноябрь 1993, стр. 17 - 21.

CCDS (1996). Recommendation S4 (1996) "Coordination of Satellite Systems Providing Timing". Report of the 13th Meeting of the CCDS, Comité Consultatif pour la Définition de la Seconde, BIPM.

CDISS (1998). *WWW Home Page.* Centre for Defence & International Security Studies, Lancaster University, Lancaster, UK. `http://www.cdiss.org/mos_as3.htm`.

Cook, A. H. (1977). *Celestial Masers*. Cambridge University Press, Cambridge.

Cook, G. L. (1997). Critical GPS-GLONASS Interoperability Issues. In *Proceedings of ION Satellite Division National Technical Meeting*, pages 183–193, Santa Monica, California.

CSIC (1994). GLONASS Info, Bulletin 1/94 (1). Coordinational Scientific Information Center Russian Space Forces, Moscow. English Translation of Russian Document.

CSIC (1997). Notice Advisory to GLONASS Users, No. 052-970619. Coordinational Scientific Information Center Russian Space Forces.

CSIC (1998). *GLONASS WWW Home Page*. Coordinational Scientific Information Center Russian Space Forces, Moscow. `http://mx.iki.rssi.ru/SFCSIC/english.html`.

Dale, S. A., Daly, P., and Kitching, I. D. (1989). Understanding Signals From GLONASS Navigation Satellites. *International Journal of Satellite Communications*, 7:11–22.

Dale, S. A., Kitching, I. D., and Daly, P. (1988). Position-Fixing Using the USSR's GLONASS C/A Code. In *Proceedings of IEEE Position Location & Navigation Symposium, PLANS'88*, pages 13–20.

DASA (1996). *ASN-22 GPS/GLONASS Receiver Data Sheet*. DASA–NFS.

Eastwood, R. A. (1990). An Integrated GPS/GLONASS Receiver. *Navigation: Journal of The Institute of Navigation*, 37(2):141–151.

Felhauer, T., Tews, T., Botchkovski, A., Golubev, M., and Vasilyev, M. (1997). ASN-22 Combined GPS/GLONASS Receiver Module – Architecture, Technical Characteristics and Performance Analysis. In *Proceedings of ION Satellite Division GPS-97 International Technical Meeting*, pages 81–87, Kansas City, Missouri.

Ganin, A. (1995). Differential GLONASS in Russia: The Ways of Development. In *Proceedings of ION Satellite Division GPS-95 International Technical Meeting*, pages 1049–1052, Palm Springs, California.

Gourevitch, S. A., Sila-Novitsky, S., and Diggelen, F. v. (1996). The GG24 Combined GPS+GLONASS Receiver. In *Proceedings of ION Satellite Division GPS-96 International Technical Meeting*, pages 141–145, Kansas City, Missouri.

Gouzhva, Y. G., Gevorkyan, A. G., Bogdanov, P. P., Ovchinnikov, V. V., and Pushkina, I. G. (1995). Getting in Sync: GLONASS Clock Synchronization. *GPS World Magazine*, 6(4):48–56.

Government (1995). On executing works in use of the GLONASS global navigation satellite system for the sake of civil users. The Government of the Russian Federation, Decree No. 237.

Government (1997). On Federal aim program of using GLONASS global navigation satellite system for the benefits of civil users. The Government of the Russian Federation, Decree No. 1435.

GPNN (1994). Global Positioning & Navigation News, Vol. 4, No. 16, Phillips Business Information, Washington, D. C.

Graas, Frank, v. and Braasch, M. S. (1996). Selective Availability. In Parkinson, B. W. and Spilker, jr., J. J., editors, *Global Positioning System: Theory and Applications I*, volume 163 of *Progress in Astronautics and Aeronautics*, pages 601–622. American Institute of Aeronautics and Astronautics, Washington, D. C., USA.

Gurtner, W. (1998). RINEX: The Receiver Independent Exchange Format Version 2. Format definition, Astronomical Institute, University of Berne, Berne. Definition file available on IGS WWW Site `ftp://igscb.jpl.nasa.gov/igscb/data/format/rinex2.txt`.

Habrich, H. (1999). *Geodetic Applications of the Global Navigation Satellite System (GLONASS) and of GLONASS/GPS Combinations.* PhD thesis, University of Berne, Department for Philosophy and Natural Sciences, Berne, Switzerland.

Habrich, H., Beutler, G., Gurtner, W., and Rothacher, M. (1999). Double Difference Ambiguity Resolution for GLONASS/GPS Carrier Phase. In *Proceedings of ION Satellite Division GPS-99 International Technical Meeting*, pages 1609–1618, Nashville, Tennessee.

Hartmann, R. (1992). Joint US/USSR Satellite Navigation Studies. *GPS World Magazine*, 3(2):26–36.

Hein, G. W., Pielmeier, J., Zink, T., Eißfeller, B., Perry, M., and Rawlings, R. (1997). GPS and GLONASS RAIM Availability Analysis Over Europe. In *Proceedings of ION Satellite Division GPS-97 International Technical Meeting*, pages 465–475, Kansas City, Missouri.

Heinrichs, G. and Götz, S. (1996). The GNSS-200: Features and Performance of the Fully Integrated Single Frequency, 12 Channel, C/A Code GPS/GLONASS Receiver. In *Proceedings of ION Satellite Division GPS-96 International Technical Meeting*, pages 125–130, Kansas City, Missouri.

Heinrichs, G., Götz, S., and Windl, J. (1997). The NR - Navigation System Family: Features and Performance of the Fully Integrated Single Frequency, 24 Channel, C/A Code GPS/GLONASS Navigation Systems. In *Proceedings of ION Satellite Division GPS-97 International Technical Meeting*, pages 61–67, Kansas City, Missouri.

Heiskanen, W. and Moritz, H. (1967). *Physical Geodesy.* W H Freeman, San Francisco.

Hofmann-Wellenhof, B., Lichtenegger, H., and Collins, J. (1993). *Global Positioning System – Theory and Practice.* Springer Verlag, Wien, New York, 2^{nd} edition.

ICAO (1996). Letter from the President of the ICAO Council to the Russian Minister of Transport, Montreal, July 29.

ICD-GLONASS (1995). *GLONASS Interface Control Document (Rev. 1995).* Coordinational Scientific Information Center Russian Space Forces, Moscow. English Translation of Russian Document.

ICD-GLONASS (1998). *GLONASS Interface Control Document (Version 4.0).* Coordinational Scientific Information Center Russian Space Forces, Moscow. English Translation of Russian Document.

ICD-GPS (1991). *GPS Interface Control Document (ICD-GPS-200).* ARINC Research Corporation.

IGN (1998). *IGEX-98 WWW Home Page.* Institut Géographique Nationale, Paris, France. `http://lareg.ensg.ign.fr/IGEX/`.

ISDE (1991a). *"Gnom" GLONASS Receiver Data Sheet.* Institute of Space Device Engineering, Moscow.

ISDE (1991b). *"Reper" GPS/GLONASS Receiver Data Sheet.* Institute of Space Device Engineering, Moscow.

Ivanov, N. E., Salischev, V., and Vinogradov, A. (1995). Ways of GLONASS System Advancing. In *Proceedings of ION Satellite Division GPS-95 International Technical Meeting*, pages 991–1011, Palm Springs, California.

Jansche, A. M. (1993). GLONASS – A Summary. Technical report, Kayser-Threde GmbH, Munich.

Javad (1998). *WWW Home Page.* Javad Positioning Systems, San Jose, CA, USA. `http://www.javad.com`.

Jeltsch, R. (1987). *Numerische Mathematik I für Ingenieure.* Rheinisch-Westfälische Technische Hochschule Aachen, Aachen. Lecture notes.

Johnson, N. L. (1994). GLONASS Spacecraft. *GPS World Magazine*, 5(11):51–58.

Kayser-Threde (1991a). *ASN-16 GLONASS Receiver Data Sheet*. Kayser-Threde GmbH, Munich.

Kayser-Threde (1991b). *"Skipper" GLONASS Receiver Data Sheet*. Kayser-Threde GmbH, Munich.

Kazantsev, V. (1995). The GLONASS and GLONASS-M Programs. In *Proceedings of ION Satellite Division GPS-95 International Technical Meeting*, pages 985–990, Palm Springs, California.

Kowalski, G. (1995). Plessezk macht zivile Karriere. *Flug Revue 3/95*, page 42.

Kozlov, D. and Tkachenko, M. (1998). Centimeter-Level, Real-Time Kinematic Positioning with GPS + GLONASS C/A Receivers. *Navigation: Journal of The Institute of Navigation*, 45(2):137–147.

Landau, H. and Vollath, U. (1996). Carrier Phase Ambiguity Resolution using GPS and GLONASS Signals. In *Proceedings of ION Satellite Division GPS-96 International Technical Meeting*, pages 917–923, Kansas City, Missouri.

Langley, R. B. (1997). GLONASS Review and Update. *GPS World Magazine*, 8(7):46–51.

Leick, A., Li, J., Beser, J., and Mader, G. (1995). Processing GLONASS Carrier Phase Observations – Theory and First Experience. In *Proceedings of ION Satellite Division GPS-95 International Technical Meeting*, pages 1041–1047, Palm Springs, California.

Leisten, O., Ffoulkes-Jones, G., Whitworth, G., and Belton, D. (1995). Tracking Measurements From a Miniature GLONASS Receiver. In *Proceedings of ION Satellite Division GPS-95 International Technical Meeting*, pages 853–859, Palm Springs, California.

Lennen, G. R. (1989). The USSR's Glonass P-Code – Determination and Initial Results. In *Proceedings of ION Satellite Division GPS-89 International Technical Meeting*, pages 77–83, Colorado Springs, Colorado.

Lewandowski, W. and Azoubib, J. (1998). GPS+GLONASS: Toward Subnanosecond Time Transfer. *GPS World Magazine*, 9(11):30–39.

Lewandowski, W., Azoubib, J., Jong, G. d., Nawrocki, J., and Danaher, J. (1997). A New Approach to International Satellite Time and Frequency Comparisons: 'All-in-View' Multichannel GPS + GLONASS Observations. In *Proceedings of ION Satellite Division GPS-97 International Technical Meeting*, pages 1085–1091, Kansas City, Missouri.

Lewandowski, W., Danaher, J., and Klepczynski, W. J. (1996). Experiment Using GPS/GLONASS Common View Time Transfer Between Europe and North America. In *Proceedings of ION Satellite Division GPS-96 International Technical Meeting*, pages 271–277, Kansas City, Missouri. Institute of Navigation.

Litvak, M. M. (1969). Infra-red pumping of interstellar OH. *Astrophysical Journal*, 156:471–492.

Milliken, R. J. and Zoller, C. J. (1996). Principle of operation of NAVSTAR and system characteristics. In *Global Positioning System*, volume 1, pages 3–14. The Institute of Navigation.

Misra, P. N. and Abbot, R. I. (1994). SGS-85 – WGS84 Transformation. *manuscripta geodaetica*, 19:300–308.

Misra, P. N., Abbot, R. I., and Gaposchkin, E. M. (1996a). Integrated Use of GPS and GLONASS: PZ-90 – WGS84 Transformation. In *Proceedings of ION Satellite Division GPS-96 International Technical Meeting*, pages 307–314, Kansas City, Missouri.

Misra, P. N., Bayliss, E. T., LaFrey, R. R., Pratt, M. M., and Hogaboom, R. A. (1992). GLONASS Data Analysis: Interim Results. *Navigation: Journal of The Institute of Navigation*, 39(1):93–109.

Misra, P. N., Bayliss, E. T., LaFrey, R. R., Pratt, M. M., Hogaboom, R. A., and Muchnik, R. (1993). GLONASS Performance in 1992: A Review. *GPS World Magazine*, 4(5):28–38.

Misra, P. N., Pratt, M. M., Muchnik, R., Burke, B., and Hall, T. (1996b). GLONASS Performance: Measurement Data Quality and System Upkeep. In *Proceedings of ION Satellite Division GPS-96 International Technical Meeting*, pages 261–270, Kansas City, Missouri.

Mitrikas, V. V., Revnivykh, S. G., and Bykhanov, E. V. (1998). WGS84/PZ-90 Transformation Parameters Determination Based on Laser and Ephemeris Long-Term GLONASS Orbital Data Processing. In *Proceedings of ION Satellite Division GPS-98 International Technical Meeting*, pages 1625–1635, Nashville, Tennessee.

MMC (1996). Press Release, Main Metrological Center of the National Time and Frequency Service of the Russian Federation.

NASA (1998). *WWW Home Page on Russian Space Agency launch facilities*. National Aeronautics and Space Administration. `http://liftoff.msfc.nasa.gov/rsa/pads.html`.

NIMA (1997). *Department of Defense World Geodetic System 1984, Its Definition and Relationships with Local Geodetic Systems*. National Imagery and Mapping Agency, Bethesda, Maryland, 3^{rd} edition. Report No. 8350.2.

N.N. (1990a). DoD Turns On Selective Availability. *GPS World Magazine*, 1(3):12 (Global View).

N.N. (1990b). GPS/GLONASS Activity Gains Momentum. *GPS World Magazine*, 1(5):12 (Global View).

N.N. (1990c). GPS/GLONASS Cooperative Effort Moves Forward. *GPS World Magazine*, 1(1):18 (Global View).

N.N. (1990d). Northwest/Honeywell Sign Memorandum with Soviets on GPS/GLONASS. *GPS World Magazine*, 1(4):13 (Global View).

N.N. (1992). WARC Okays 'Shared Use' of GLONASS Frequencies. *GPS World Magazine*, 3(4):22 (Global View).

N.N. (1993a). European Initiatives Press for Civil System. *GPS World Magazine*, 4(3):24 (Global View).

N.N. (1993b). Visit to GLONASS Center is First for Outsiders. *GPS World Magazine*, 4(9):16 (Global View).

NovAtel (1998a). *MiLLenium–GLONASS GPS+GLONASS Receiver Data Sheet*. NovAtel Inc., Calgary, Alberta, Canada.

NovAtel (1998b). *WWW Home Page*. NovAtel Inc., Calgary, Alberta, Canada. `http://www.novatel.com`.

Raby, P. and Daly, P. (1993). Using the GLONASS System for Geodetic Survey. In *Proceedings of ION Satellite Division GPS-93 International Technical Meeting*, pages 1129–1138, Salt Lake City, Utah.

RAG (1998). *WWW Home Page*. Russian Aerospace Guide, Roselle, IL. `http://www.mcs.net/~rusaerog/`.

Revnivykh, S. G. and Mitrikas, V. V. (1998). GLONASS S/C mass and dimension. E-Mail through IGEXMail service.

Riley, S. (1992). An Integrated Multichannel GPS/GLONASS Receiver. In *Proceedings of ION Satellite Division GPS-92 International Technical Meeting*, Albuquerque, New Mexico.

Riley, S. and Daly, P. (1994). Performance of the GLONASS P-code at L1 and L2 Frequencies. *International Journal of Satellite Communication*, 12:453–462.

Riley, S. and Daly, P. (1995). Architecture and Results from the Leeds University 20 Channel GNSS Receiver. In *Proceedings of ION Satellite Division National Technical Meeting*, pages 421–430, Anaheim, California.

Riley, S., Howard, N., Aardom, E., Daly, P., and Silvestrin, P. (1995). A Combined GPS/GLONASS High Precision Receiver for Space Applications. In *Proceedings of ION Satellite Division GPS-95 International Technical Meeting*, pages 835–844, Palm Springs, California.

RNTFS (1996a). Bulletin e-11-96/c. Russian National Time and Frequency Service, National Etalon of Time and Frequency.

RNTFS (1996b). Bulletin: E-12-96/c. Russian National Time and Frequency Service, National Etalon of Time and Frequency.

RNTFS (1997). Bulletin: E-05-97/c. Russian National Time and Frequency Service, National Etalon of Time and Frequency.

Roßbach, U. (1999). PZ-90 / WGS84 Transformation Parameters Directly From GLONASS Range Measurements. In *Proceedings of IGEX-98 Workshop*, Nashville, Tennessee. (to be published).

Roßbach, U., Habrich, H., and Zarraoa, N. (1996). Transformation Parameters Between PZ-90 and WGS84. In *Proceedings of ION Satellite Division GPS-96 International Technical Meeting*, pages 279–285, Kansas City, Missouri.

Roßbach, U. and Hein, G. W. (1996a). DGPS/DGLONASS Carrier Phase Solutions. In *Proceedings of 5^{th} International Conference on Differential Satellite Navigation Systems (DSNS'96)*, St. Petersburg, Russia.

Roßbach, U. and Hein, G. W. (1996b). Treatment of Integer Ambiguities in DGPS/DGLONASS Double Difference Carrier Phase Solutions. In *Proceedings of ION Satellite Division GPS-96 International Technical Meeting*, pages 909–916, Kansas City, Missouri.

Rothacher, M., Beutler, G., Gurtner, W., Bockmann, E., and Mervart, L. (1993). *Bernese GPS software version 3.4, Documentation.* University of Bern.

RTCA (June 1998). *Minimum Operational Performance Standards for Global Positioning System/Wide Area Augmentation System Airborne Equipment.* RTCA, Inc. Document No. RTCA/DO-229A.

RTCM (1994). *RTCM Recommended Standards for Differential Navstar GPS Service, Version 2.1.* Radio Technical Commission For Maritime Services, Special Committee No. 104, Washington, D. C.

RTCM (1996). *RTCM Recommended Standards for Differential GNSS (Global Navigation Satellite Systems) Service, Future Version 2.2, Final Review Draft.* Radio Technical Commission For Maritime Services, Special Committee No. 104, Washington, D. C.

RTCM (1998). *RTCM Recommended Standards for Differential GNSS (Global Navigation Satellite Systems) Service, Version 2.2.* Radio Technical Commission For Maritime Services, Special Committee No. 104, Alexandria, Virginia.

Soler, T. and Hothem, L. D. (1988). Coordinate Systems Used in Geodesy: Basic Definitions and Concepts. *Journal of Surveying Engineering*, 114(2):84–97.

Spectra Precision (1998). *WWW Home Page*. Spectra Precision AB, Danderyd, Sweden. `http://www.geotronics.se`.

Spilker, jr., J. J. (1996). GPS Navigation Data. In Parkinson, B. W. and Spilker, jr., J. J., editors, *Global Positioning System: Theory and Applications I*, volume 163 of *Progress in Astronautics and Aeronautics*, pages 121–176. American Institute of Aeronautics and Astronautics, Washington, D. C., USA.

Stewart, M. and Tsakiri, M. (1998). GLONASS Broadcast Orbit Computation. *GPS Solutions*, 2(2):16–27.

Verschuur, G. L. and Kellermann, K. I., editors (1974). *Galactic and Extra-Galactic Radio Astronomy*. Springer Verlag, Berlin Heidelberg New York.

Walsh, D. and Daly, P. (1996). GPS and GLONASS Carrier Phase Ambiguity Resolution. In *Proceedings of ION Satellite Division GPS-96 International Technical Meeting*, pages 899–907, Kansas City, Missouri.

Werner, W. (1998). *Entwicklung eines hochpräzisen DGPS/DGLONASS Navigationssystems unter besonderer Berücksichtigung von Pseudolites*. PhD thesis, University FAF Munich, Faculty of Civil and Surveying Engineering, Neubiberg, Germany.

Willis, P., Beutler, G., Gurtner, W., Hein, G. W., Neilan, R., and Slater, J. (1998). The International GLONASS Experiment 1998 (IGEX-98), International Call for Participation.

Zarraoa, N., Mai, W., Daedelow, H., and Jungstand, A. (1996). GLONASS Integrity Monitoring by Internet. In *Proceedings of ION Satellite Division National Technical Meeting*, pages 447–451, Santa Monica, California.

Zarraoa, N., Sardón, E., Klähn, D., and Jungstand, A. (1995). Evaluation of GLONASS Performance in Practical Applications: Comparison with GPS-Based Ionospheric TEC Values. In *Proceedings of ION Satellite Division GPS-95 International Technical Meeting*, pages 1031–1039, Palm Springs, California.

Zeglov, Y. I., Denisov, V. I., Zurabov, U. G., Ivanov, N. E., Makoda, V. S., and Kinkulkin, I. E. (1993). Proposals for broadening RTCM recommended standards for differential NAVSTAR GPS service version 2.0 for differential GPS/GLONASS service.

B GLONASS Launch History

Table B.1: Launch history and service lives of GLONASS satellites as of January 31, 2000.

Block	GLONASS No.	COSMOS No.	Launch Date	Commissioned	Status
1	–	1413	10/12/82	11/10/82	Withdrawn 03/30/84
2	–	1490	08/10/83	09/02/83	Withdrawn 10/29/85
2	–	1491	08/10/83	08/31/83	Withdrawn 06/09/88
3	–	1519	12/29/83	01/07/84	Withdrawn 01/28/88
3	–	1520	12/29/83	01/15/84	Withdrawn 09/16/86
4	–	1554	05/19/84	06/05/84	Withdrawn 09/16/86
4	–	1555	05/19/84	06/09/84	Withdrawn 09/17/87
5	–	1593	09/04/84	09/22/84	Withdrawn 11/28/85
5	–	1594	09/04/84	09/28/84	Withdrawn 09/16/86
6	–	1650	05/18/85	06/06/85	Withdrawn 11/28/85
6	–	1651	05/18/85	06/04/85	Withdrawn 09/17/87
7	–	1710	12/25/85	01/17/86	Withdrawn 03/06/89
7	–	1711	12/25/85	01/20/86	Withdrawn 09/17/87
8	–	1778	09/16/86	10/17/86	Withdrawn 07/05/89
8	–	1779	09/16/86	10/17/86	Withdrawn 10/24/88
8	–	1780	09/16/86	10/17/86	Withdrawn 10/12/88
9	–	1838	04/24/87	–	Launch failed
9	–	1839	04/24/87	–	Launch failed
9	–	1840	04/24/87	–	Launch failed
10	–	1883	09/16/87	10/10/87	Withdrawn 06/06/88
10	–	1884	09/16/87	10/09/87	Withdrawn 08/20/88
10	–	1885	09/16/87	10/05/87	Withdrawn 03/07/89
11	–	1917	02/17/88	–	Launch failed
11	–	1918	02/17/88	–	Launch failed
11	–	1919	02/17/88	–	Launch failed
12	–	1946	05/21/88	06/01/88	Withdrawn 05/10/90
12	234	1947	05/21/88	06/03/88	Withdrawn 09/18/91
12	233	1948	05/21/88	06/03/88	Withdrawn 09/18/91
13	–	1970	09/16/88	09/20/88	Withdrawn 05/21/90
13	–	1971	09/16/88	09/28/88	Withdrawn 08/30/89
13	236	1972	09/16/88	10/03/88	Withdrawn 08/12/92
14	239	1987	01/10/89	02/01/89	Withdrawn 02/03/94
14	240	1988	01/10/89	02/01/89	Withdrawn 01/17/92
14	–	1989	01/10/89	–	Etalon Research Satellite
15	–	2022	05/31/89	04/04/89	Withdrawn 01/23/90
15	–	2023	05/31/89	06/15/89	Withdrawn 11/18/89
15	–	2024	05/31/89	–	Etalon Research Satellite
16	242	2079	05/19/90	06/20/90	Withdrawn 08/17/94
16	228	2080	05/19/90	06/17/90	Withdrawn 08/27/94
16	229	2081	05/19/90	06/11/90	Withdrawn 01/20/93
17	247	2109	12/08/90	01/01/91	Withdrawn 06/10/94
17	248	2110	12/08/90	12/29/90	Withdrawn 01/20/94
17	249	2111	12/08/90	12/28/90	Withdrawn 08/15/96
18	750	2139	04/04/91	04/28/91	Withdrawn 11/14/94

Table B.1: Launch history and service lives of GLONASS satellites as of January 31, 2000 (cont'd).

Block	GLONASS No.	COSMOS No.	Launch Date	Commissioned	Status
18	753	2140	04/04/91	04/28/91	Withdrawn 06/04/93
18	754	2141	04/04/91	05/04/91	Withdrawn 06/16/92
19	768	2177	01/30/92	02/24/92	Withdrawn 06/29/93
19	769	2178	01/30/92	02/22/92	Withdrawn 06/25/97
19	771	2179	01/30/92	02/18/92	Withdrawn 12/21/96
20	756	2204	07/30/92	08/19/92	Withdrawn 08/04/97
20	772	2205	07/30/92	08/29/92	Withdrawn 08/27/94
20	774	2206	07/30/92	08/25/92	Withdrawn 08/26/96
21	773	2234	02/17/93	03/14/93	Withdrawn 08/17/94
21	759	2235	02/17/93	08/25/93	Withdrawn 08/04/97
21	757	2236	02/17/93	03/14/93	Withdrawn 08/23/97
22	758	2275	04/11/94	09/04/94	Withdrawn 01/15/00
22	760	2276	04/11/94	05/18/94	Withdrawn 09/09/99
22	761	2277	04/11/94	05/16/94	Withdrawn 08/29/97
23	767	2287	08/11/94	09/07/94	Withdrawn 02/03/99
23	770	2288	08/11/94	09/04/94	Withdrawn 01/15/00
23	775	2289	08/11/94	09/07/94	Operational
24	762	2294	11/20/94	12/11/94	Withdrawn 11/19/99
24	763	2295	11/20/94	12/15/94	Withdrawn 10/05/99
24	764	2296	11/20/94	12/16/94	Withdrawn 11/30/99
25	765	2307	03/07/95	03/30/95	Withdrawn 11/19/99
25	766	2308	03/07/95	04/05/95	Operational
25	777	2309	03/07/95	04/06/95	Withdrawn 12/24/97
26	780	2316	07/24/95	08/26/95	Withdrawn 04/06/99
26	781	2317	07/24/95	08/22/95	Operational
26	785	2318	07/24/95	08/22/95	Operational
27	776	2323	12/14/95	01/07/96	Operational
27	778	2324	12/14/95	04/26/99	Operational
27	782	2325	12/14/95	01/18/96	Operational
28	779	2364	12/30/98	02/18/99	Operational
28	784	2363	12/30/98	01/29/99	Operational
28	786	2362	12/30/98	01/29/99	Operational

C Symbols

C.1 Symbols Used in Mathematical Formulae

a	Semi-major axis	t	Time
a	Elements of design matrix	T	Orbital period
a_E	Earth's equatorial radius	U	Non-spherical part of the gravitational potential
A	Polynomial coefficients		
A	Amplitude	V	Earth's gravitational potential
c	Speed of light	WN	Week number (used in GPS ICD)
$c_{nm},\ s_{nm}$	Spherical harmonic coefficients	X	Phase (used in Klobuchar model)
c_{20}	Normalized 2^{nd} zonal coefficient	x	Variable in polynomial
d	Substitute for differentiation parameters	x, y, z	Cartesian coordinates
		α	Rotation angle
DN	Day number (used in GPS ICD)	γ	Frequency offset
e	Error (in observation equations)	γ	Squared L_1/L_2 frequency ratio
E	Eccentric anomaly	δs	Differential scale change
f	Flattening of Earth	$\delta\varepsilon, \delta\psi, \delta\omega$	Differential rotations
f	Frequency	ε	Eccentricity
h	Ellipsoidal coordinate: Height	ε	Measurement noise
h	Step width	θ	Ellipsoidal coordinate: Colatitude
i	Inclination	λ	Ellipsoidal coordinate: Longitude
J_2	2^{nd} zonal coefficient	λ	Wavelength
k	Constant	μ	Earth's gravitational constant
L	Hardware delay in receiver	ν	Local denotation
m, n	Number of items in a set	ξ, υ, ζ	Coordinate differences
m, n	Order and degree of spherical harmonic expansion	ϱ	Geometric (true) range from observer to satellite
M	Mean anomaly	σ	(Measurement) noise
n	Mean motion	σ	Standard deviation
n	Frequency number of satellite	τ	Clock offset
N	Day in four-year period	φ	Ellipsoidal coordinate: Latitude
N	Integer ambiguity	φ	Carrier phase measurement [cycles]
P	Point		
P	Period	Φ	Carrier phase measurement [distance]
$P(\cos\theta)$	Legendre function		
PR	Measured pseudorange	ψ	Earth's central angle (used in Klobuchar model)
q	Elements of cofactor matrix		
r	Distance (from center of Earth)	ω	Argument of perigee
s, S	Local denotations	ω_E	Earth's rotational velocity

C.2 Vectors and Matrices

$\vec{D}$	Vector of derivatives	$\vec{\varepsilon}$	Noise vector
$\vec{e}$	Orientation vector	$\mathbf{A}$	Design matrix for the observation equations
$\vec{l}$	Left-hand vector with known values in observation equations	$\mathbf{I}$	Identity matrix
		$\mathbf{P}$	Weight matrix
$\vec{x}$	Position vector	$\mathbf{Q}$	Covariance matrix
$\vec{x}$	Vector of unknowns	$\mathbf{Q}_X$	Cofactor matrix
$\vec{X}$	State vector		
$\vec{Y}$	Intermediate state vector		

C.3 Symbols Used as Subscripts

0	Approximate value	m	Geomagnetic coordinates (used in Klobuchar model)
0	Initial value		
CM	Center of mass	nom	Nominal value
E	Earth	ot	Reference time (used in GPS ICD)
EF	Referring to an Earth-fixed coordinate system	PC	Antenna phase center
		PZ	Referring to PZ-90
GLO	Referring to GLONASS system	R	Receiver
$GLONASS$	Referring to GLONASS system	R	Reference station
GPS	Referring to GPS system	RX	Referring to signal reception
HW	Referring to the receiver hardware characteristics	Sat	Referring to a single (specified) satellite
I	Ionospheric delay (used in Klobuchar model)	Sys	Referring to either GPS or GLONASS system
i, n	Arbitrary specimen out of a (time) series	t	Referring to time
		TX	Referring to signal transmission
IF	Ionospheric free linear combination	U	User station
		UTC	Referring to UTC
INS	Referring to an inertial coordinate system	WGS	Referring to WGS84
		λ	Referring to phase measurement at range level
$ITRF$	Referring to ITRF-94		
L_1	Referring to L_1 (measurements)	φ	Referring to phase measurement at cycle level
L_2	Referring to L_2 (measurements)		
LS	Leap seconds (used in GPS ICD)		
LSF	Leap seconds, future (used in GPS ICD)		

C.4 Symbols Used as Superscripts

A	Value from almanac data	o	Orbital coordinate system
I	Ionospheric intersection (piercing) point (used in Klobuchar model)	orb	Referring to orbit determination
		r	Reference satellite
i, j, k	Arbitrary specimen out of a set (of satellites, etc.)	S	Satellite
		$Trop$	Troposphere
$Iono$	Ionosphere		

D Abbreviations and Acronyms

A-S	**A**nti-**S**poofing
BIH	**B**ureau **I**nternational de l'**H**eure
BKG	**B**undesamt für **K**artographie und **G**eodäsie
BPSK	**B**inary **P**hase **S**hift **K**eying
C/A-Code	**C**oarse **A**cquisition **Code**
CCDS	**C**omité **C**onsultatif pour la **D**éfinition de la **S**econde
CCSI	**C**oordination **C**enter of **S**cientific **I**nformation
CDMA	**C**ode **D**ivision **M**ultiple **A**ccess
CHA	**C**hannel of **H**igh **A**ccuracy
CIO	**C**onventional **I**nternational **O**rigin
CIS	**C**ommonwealth of **I**ndependent **S**tates
CRT	**C**athode **R**ay **T**ube
CSA	**C**hannel of **S**tandard **A**ccuracy
CSIC	**C**oordinational **S**cientific **I**nformation **C**enter
DASA	**D**eutsche **A**ero**S**pace **A**G **D**aimler-Benz **A**ero**S**pace **A**G **D**aimlerChrysler **A**ero**S**pace **A**G
DFD	**D**eutsches **F**ernerkundungs-**D**atenzentrum
DGLONASS	**D**ifferential **GLONASS**
DGPS	**D**ifferential **GPS**
DLR	**D**eutsche Gesellschaft für **L**uft- und **R**aumfahrt **D**eutsches Zentrum für **L**uft- und **R**aumfahrt
DMA	**D**efense **M**apping **A**gency
DoD	**D**epartment **o**f **D**efense
DOP	**D**ilution **O**f **P**recision
ECEF	**E**arth-**C**entered, **E**arth-**F**ixed
EGM	**E**arth **G**ravity Field **M**odel
ERP	**E**arth **R**otation **P**arameters
ESA	**E**uropean **S**pace **A**gency
FAA	**F**ederal **A**viation **A**dministration
FAF	**F**ederal **A**rmed **F**orces
FANS	**F**uture **A**ir **N**avigation **S**ystems
FDMA	**F**requency **D**ivision **M**ultiple **A**ccess
FOC	**F**ull **O**perational **C**apability
GDOP	**G**eometric **DOP**
GLONASS	**GLO**bal'naya **NA**vigatsionnaya **S**putnikowaya **S**istema – **GLO**bal **NA**vigation **S**atellite **S**ystem
GNSS	**G**lobal **N**avigation **S**atellite **S**ystem
GPS	**G**lobal **P**ositioning **S**ystem
HDOP	**H**orizontal **DOP**
HEO	**H**igh **E**arth **O**rbit
HF	**H**igh **F**requency
HP	**H**igh **P**recision
IAPG	**I**nstitut für **A**stronomische und **P**hysikalische **G**eodäsie
ICD	**I**nterface **C**ontrol **D**ocument
ICAO	**I**nternational **C**ivil **A**viation **O**rganization
IF	**I**ntermediate **F**requency
IfAG	**I**nstitut **f**ür **A**ngewandte **G**eodäsie

IfEN	**I**nstitut **f**ür **E**rdmessung und **N**avigation
IGEX-98	**I**nternational **G**LONASS **EX**periment 19**98**
IGS	**I**nternational **G**PS **S**ervice for Geodynamics
IMO	**I**nternational **M**aritime **O**rganization
IOC	**I**nitial **O**perational **C**apability
ION	**I**nstitute **O**f **N**avigation
IR	**I**nfra-**R**ed
ISDE	**I**nstitute of **S**pace **D**evice **E**ngineering
ITRF	**I**nternational **T**errestrial **R**eference **F**rame
KNITs	**K**oordinatsionnyj **N**auchno-**I**nformatsionnyj **Ts**entr – Coordinational Scientifc Information Center
LADS	**L**ocal **A**rea **D**ifferential **S**ystem
LCD	**L**iquid **C**rystal **D**isplay
MIT	**M**assachusetts **I**nstitute of **T**echnology
MS-DOS	**M**icro**S**oft **D**isk **O**perating **S**ystem
MSF	**M**ilitary **S**pace **F**orces
NAGU	**N**otice **A**dvisory to **G**LONASS **U**sers
NASA	**N**ational **A**eronautics and **S**pace **A**dministration
NFS	**N**avigations- und **F**lugführungs-**S**ysteme
OEM	**O**riginal **E**quipment **M**anufacturer
PC	**P**ersonal **C**omputer
P-Code	**P**recision **Code**
PDOP	**P**osition **DOP**
PE-90	**P**arameters of the **E**arth 19**90**
ppm	**p**arts **p**er **m**illion
PPS	**P**recise **P**ositioning **S**ervice
PRN	**P**seudo-**R**andom **N**oise
PZ-90	**P**arametry **Z**emli 19**90** Goda – Parameters of the Earth Year 1990
RADS	**R**egional **A**rea **D**ifferential **S**ystem
RAIM	**R**eceiver **A**utonomous **I**ntegrity **M**onitoring
RHCP	**R**ight **H**anded **C**ircularly **P**olarized
RINEX	**R**eceiver **IN**dependent **EX**change Format
RIRT	**R**ussian **I**nstitute of **R**adionavigation and **T**ime
RMS	**R**oot **M**ean **S**quare
RTCM	**R**adio **T**echnical **C**ommission For **M**aritime Services
RTK	**R**eal-**T**ime **K**inematic
S/A	**S**elective **A**vailablity
S/C	**S**pace **C**raft
SDOP	**S**ystem time **DOP**
SGS-85	**S**oviet **G**eodetic **S**ystem 19**85**
SGS-90	**S**oviet **G**eodetic **S**ystem 19**90**
SLR	**S**atellite **L**aser **R**anging
SNR	**S**ignal-to-**N**oise **R**atio
SP	**S**tandard **P**recision
SPS	**S**tandard **P**ositioning **S**ervice
SV	**S**pace **V**ehicle
TDOP	**T**ime **DOP**
TEC	**T**otal **E**lectron **C**ontent
TT&C	**T**elemetry, **T**racking and **C**ontrol
UDS	**U**nited **D**ifferential **S**ystem

URE	**U**ser **R**ange **E**rror
USSR	**U**nion of **S**ocialist **S**oviet **R**epublics
UTC	**U**niversal **T**ime **C**oordinated
UTC_{SU}	**UTC S**oviet **U**nion
UTC_{USNO}	**UTC US N**aval **O**bservatory
VDOP	**V**ertical **DOP**
VGA	**V**ideo **G**raphics **A**dapter
VKS	**V**oenno **K**osmicheski **S**ily – Military Space Forces
VLBI	**V**ery **L**ong **B**aseline **I**nterferometry
WADS	**W**ide **A**rea **D**ifferential **S**ystem
WGS84	**W**orld **G**eodetic **S**ystem 19**84**

Dank

Die vorliegende Dissertation entstand größtenteils während meiner Tätigkeit als wissenschaftlicher Mitarbeiter am Institut für Erdmessung und Navigation der Universität der Bundeswehr München.

Mein besonderer Dank gilt dem Institutsleiter, Herrn Univ.-Prof. Dr.-Ing. G. W. Hein für sein Interesse am Fortgang der Arbeit und die jederzeit vorhandene Diskussionsbereitschaft. Auch möchte ich ihm dafür danken, daß er die Aufgabe des 1. Berichterstatters übernommen hat.

Sehr herzlich möchte ich auch Herrn Univ.-Prof. Dr.-Ing. E. Groten danken für sein Interesse am behandelten Thema und die Übernahme der Aufgabe des 2. Berichterstatters.

Weiter gilt mein Dank Herrn Univ.-Prof. Dr.-Ing. B. Eissfeller, der in seiner Eigenschaft als Laborleiter des Instituts für Erdmessung und Navigation ebenfalls jederzeit offen für Diskussionen war. Er übernahm auch die Aufgabe des 3. Berichterstatters.

Herrn Univ.-Prof. Dr.-Ing. W. Reinhardt danke ich für die bereitwillige Übernahme des Vorsitzes im Promotionsverfahren.

Ferner möchte ich meinen Dank ausdrücken gegenüber den Institutionen, mit denen ich im Rahmen dieser Arbeit zusammenarbeiten durfte:

- Bundesamt für Kartographie und Geodäsie (BKG)
- Deutsches Zentrum für Luft- und Raumfahrt (DLR)

Teile der vorliegenden Arbeit wurden von den folgenden Institutionen im Rahmen von Fördervorhaben finanziell unterstützt:

- Deutsche Forschungsgemeinschaft (DFG)
- Deutsche Agentur für Raumfahrtangelegenheiten (DARA)

Die Ergebnisse in dieser Dissertation wurden teilweise mit Daten erarbeitet, die während des International GLONASS Experiment 1998 (IGEX-98) gesammelt wurden. Ich möchte all den Institutionen und Organisationen danken, die an diesem Experiment teilgenommen haben, sei es bei der Aufzeichnung, Speicherung, Verteilung oder Verarbeitung von Daten.

Mein ganz besonderer Dank geht an meine jetzigen und ehemaligen Kollegen am Institut und bei der IfEN GmbH für ihre Unterstützung.

Last but not least möchte ich auch Frau Betty Jurditsch und Herrn Karl-Franz Müller vom Institut für Erdmessung und Navigation dafür danken, daß sie mich bei meiner Arbeit unterstützt haben durch die Übernahme von Sekretariats-, Verwaltungs- und anderen nicht-wissenschaftlichen aber nichtsdestotrotz wichtigen Aufgaben.

Lebenslauf

Name:	Udo Roßbach
Geburtsdatum:	14. Juli 1965
Geburtsort:	Mayen, Rheinland-Pfalz
Ehestand:	Ledig

Schulbildung:

1971 – 1975	Grundschule in Nickenich, Rheinland-Pfalz
1975 – 1984	Kurfürst-Salentin-Gymnasium in Andernach, Rheinland-Pfalz
Juni 1984	Allgemeine Hochschulreife

Wehrdienst:

Juli 1984 – September 1985	Grundwehrdienst in Homberg/Ohm und Koblenz

Studium:

Oktober 1985 – Juli 1992	Studium des Maschinenbaus mit Spezialisierung in der Luft- und Raumfahrttechnik an der Rheinisch-Westfälischen Technischen Hochschule Aachen, Aachen
1987	Vordiplom
Juli 1992	Abschluß mit dem akademischen Grad eines Dipl.-Ing.

Weiterbildung:

November 1992 – Oktober 1993	Lehrgang als EDV-Fachmann für Computer-Programmierung und CAD am ICT Institut für Computertechnologie-Anwendung in Mainz

Berufserfahrung:

Januar 1994 – Dezember 1998	Beschäftigung als Wissenschaftlicher Mitarbeiter am Institut für Erdmessung und Navigation (früher: Institut für Astronomische und Physikalische Geodäsie) der Universität der Bundeswehr München; Forschungsarbeiten zu GLONASS und GPS/GLONASS Kombination; Machbarkeitsstudie für das GPS-Experiment an Bord des Satelliten EQUATOR-S.
Seit Januar 1999	Beschäftigung als System-Ingenieur bei der Firma IfEN GmbH, Neubiberg; Arbeiten an GPS/GLONASS Software und dem EGNOS CPF Check Set.

Schriftenreihe
des Studiengangs Geodäsie und Geoinformation
der Universität der Bundeswehr München

Bisher erschienene Hefte:

Heft 1 / 1978 *(vergriffen)*

A. Schödlbauer (Bearb.): Curriculum für den wissenschaftlichen Studiengang Vermessungswesen der Hochschule der Bundeswehr München. 53 S.

Heft 2 / 1978

A. Chrzanowski and E. Dorrer (Eds.): Proceedings „Standards and Specifications for Integrated Surveying and Mapping Systems". Workshop held in Munich, Federal Republic of Germany, 1 - 2 June, 1977. Assissted by *J. McLaughlin*. VII, 181 S.

Heft 3 / 1978

W. Caspary und A. Geiger: Untersuchungen zur Leistungsfähigkeit elektronischer Neigungsmesser. 62 S.

Heft 4 / 1979

E. Baumann, W. Caspary, H. Dupraz, W. Niemeier, H. Pelzer, E. Kuntz, G. Schmitt und W. Welsch: Seminar über Deformationsanalysen, gehalten an der Hochschule der Bundeswehr München. 106 S.

Heft 5 / 1981

K. Torlegård: Accuracy Improvement in Close Range Photogrammetry. 68 S.

Heft 6 / 1982

W. Caspary und W. Welsch (Hrsg.): Beiträge zur großräumigen Neutrassierung. 271 S.

Heft 7 / 1982

K. Borre and W. M. Welsch (Eds.): International Federation of Surveyors - FIG. Proceedings „Survey Control Networks". Meeting of Study Group 5B, 7th - 9th July, 1982, Aalborg University Centre, Denmark. 431 S.

Heft 8 / 1982

A. Geiger: Entwicklung und Erprobung eines Präzisionsneigungstisches zur Kalibrierung geodätischer Instrumente. Dissertation. 125 S.

Heft 9 / 1983

W. Welsch (Hrsg.): Deformationsanalysen '83. Geometrische Analyse und Interpretation von Deformationen Geodätischer Netze. Beiträge zum Geodätischen Seminar 22. April 1983. 339 S.

Heft 10 / 1984

W. Caspary, A. Schödlbauer und W. Welsch (Hrsg.): 10 Jahre Hochschule der Bundeswehr München. Beiträge aus dem Institut für Geodäsie. 244 S.

Heft 11 / 1984 *(vergriffen)*

W. Caspary und H. Heister (Hrsg.): Elektrooptische Präzisionsstreckenmessung. Beiträge zum Geodätischen Seminar 23. September 1983. 270 S.

Heft 12 / 1984

P. Schwintzer: Analyse geodätisch gemessener Punktlageänderungen mit gemischten Modellen. Dissertation. 159 S.

Heft 13 / 1984

G. Oberholzer: Landespflege in der Flurbereinigung. 81 S.

Heft 14 / 1984

G. Neukum: Fernerkundung der Planeten und kartographische Ergebnisse. Mit Beiträgen von *G. Neugebauer*. Herausgegeben von *G. Neugebauer*. 102 S.

Heft 15 / 1984

A. Schödlbauer und W. Welsch (Hrsg.): Satelliten-Doppler-Messungen. Beiträge zum Geodätischen Seminar 24./25. September 1984. 396 S.

Heft 16 / 1985 *(vergriffen)*

M. K. Szacherska, W. M. Welsch: Geodetic Education in Europe. 234 S.

Heft 17 / 1986

B. Eissfeller, G. W. Hein: A Contribution to 3d-Operational Geodesy. Part 4: The Observation Equations of Satellite Geodesy in the Model of Integrated Geodesy. 190 S.

Heft 18 / 1985

G. Oberholzer: Landespflege in der Flurbereinigung, Teil II. 116 S.

Heft 19 / 1986 *(vergriffen)*

H. Landau, B. Eissfeller and G. W. Hein: GPS Research 1985 at the Institute of Astronomical and Physical Geodesy. 210 S.

Heft 20 / 1985
Heft 20 - 1
W. Welsch and L. A. Lapine (Eds.): International Federation of Surveyors - FIG. Proceedings „Inertial, Doppler and GPS Measurements for National and Engineering Surveys". Joint Meeting of Study Groups 5B and 5C, July 1 - 3, 1985. Volume 1. 310 S.
Heft 20 - 2
W. Welsch and L. A. Lapine (Eds.): International Federation of Surveyors - FIG. Proceedings „Inertial, Doppler and GPS Measurements for National and Engineering Surveys". Joint Meeting of Study Groups 5B and 5C, July 1 - 3, 1985. Volume 2. S. 311 - 634

Heft 21 / 1986
G. Oberholzer: Landespflege in der Flurbereinigung, Teil III. 100 S.

Heft 22 / 1987
W. Caspary, G. Hein, A. Schödlbauer (Hrsg.): Beiträge zur Inertialgeodäsie. Geodätisches Seminar 25./ 26. September 1986. 386 S.

Heft 23 / 1987
E. Dorrer und J. Peipe (Hrsg.): Motografie. Symposium 11./ 12. März 1986. 285 S.

Heft 24 / 1987
G. Neugebauer (Hrsg.): Brenta - Monographie – Grundlagenforschung auf dem Gebiet der Hochgebirgskartographie. Mit Beiträgen von *D. Beineke, H. C. Berann, W. de Concini, G. Hell, D. Herm, H. Immel, U. Kleim, G. Neugebauer und K.* Ringle. 187 S.

Heft 25 / 1987
A. Perelmuter: Beiträge zur Ausgleichung geodätischer Netze. 75 S.

Heft 26 / 1987
W. Ellmer: Untersuchung temperaturinduzierter Höhenänderungen eines Großturbinentisches. Dissertation. 109 S.

Heft 27 / 1988
H. Heister: Zur automatischen Kalibrierung geodätischer Längenmeßinstrumente. Habilitationsschrift. 213 S.

Heft 28 / 1987
E. H. Paßberger: Systemstudie zur Sicherung ökologischer Vorrangflächen mittels Bodenordnung in Bayern / System study for the protection of ecological priority areas by means of Land rearrangement in Bavaria. Dissertation. 186 S.

Heft 29 / 1987
H. Glasmacher: Die Gaußsche Ellipsoid – Abbildung mit komplexer Arithmetik und numerischen Näherungsverfahren. Dissertation. 131 S.

Heft 30 / 1987
Y. Zhang: Beiträge zum Entwurf von optimalen Beobachtungsplänen für tektonische Überwachungsnetze. Dissertation. 151 S.

Heft 31 / 1988
W. Lechner: Untersuchung einer kreiselorientierten Landfahrzeug - Navigationsanlage im Hinblick auf geodätische Anwendungen und Möglichkeiten der Höhenübertragung. Dissertation. 165 S.

Heft 32 / 1988
R. König: Zur Fehlertheorie und Ausgleichung inertialer Positionsbestimmungen. Dissertation. 143 S.

Heft 33 / 1988
H. Borutta: Robuste Schätzverfahren für geodätische Anwendungen. Dissertation. 161 S.

Heft 34 / 1988
H. Landau, K. Hehl, B. Eissfeller, G. W. Hein and I. W. Reilly: Operational Geodesy Software Packages. 325 S.

Heft 35 / 1988
G. Oberholzer, E. Paßberger: Landespflege in der Flurbereinigung, Teil IV. 153 S.

Heft 36 / 1988
H. Landau: Zur Nutzung des Global Positioning Systems in Geodäsie und Geodynamik: Modellbildung, Softwareentwicklung und Analyse. Dissertation. 287 S.

Heft 37 / 1989
B. Eissfeller: Analyse einer geodätischen raumstabilisierten Inertialplattform und Integration mit GPS. Dissertation. 327 S.

Heft 38 / 1990 *(vergriffen)*
Heft 38 - 1
A. Schödlbauer (Hrsg.): Moderne Verfahren der Landesvermessung. Beiträge zum 22. DVW-Seminar 12.-14. April 1989. Teil I: Global Positioning System. 352 S.
Heft 38 - 2
A. Schödlbauer (Hrsg.): Moderne Verfahren der Landesvermessung. Beiträge zum 22. DVW-Seminar 12.-14. April 1989. Teil II: Nivellement. Teil III: Vermessungskreisel. S. 353 - 551

Heft 39 / 1989
N. Kersting, W. Welsch (Hrsg.): Rezente Krustenbewegungen. Seminar 8./ 9. Juni 1989. 307 S.

Heft 40 / 1989

G. Oberholzer: Ländliche Kulturgeschichte und Landentwicklung. 214 S.

Heft 41 / 1990

G. W. Hein, K. Hehl, B. Eissfeller, M. Ertel, W. Jacoby, D. Czerek: On Gravity Prediction Using Density and Seismic Data. 148 S.

Heft 42 / 1992

N. Kersting: Zur Analyse rezenter Krustenbewegungen bei Vorliegen seismotektonischer Dislokationen. Dissertation. V, 246 S.

Heft 43 / 1992

K. Hehl: Bestimmung von Beschleunigungen auf einem bewegten Träger durch GPS und digitale Filterung. Dissertation. XII, 206 S.

Heft 44 / 1992

W. Oswald: Zur kombinierten Ausgleichung heterogener Beobachtungen in hybriden Netzen. Dissertation. 128 S.

Heft 45 / 1993

Institut für Geodäsie (Hrsg.): Das Global Positioning System im praktischen Einsatz der Landes- und Ingenieurvermessung. Beiträge zum Geo-dätischen Seminar 12.-14. Mai 1993. 314 S.

Heft 46 / 1994

K. Brunner und J. Peipe (Hrsg.): Festschrift für Prof. Dr.-Ing. Egon Dorrer zum 60. Geburtstag. 254 S.

Heft 47 / 1994

Heft 47-1

K.-H. Thiemann: Die Renaturierung strukturarmer Intensivagrargebiete in der Flurbereinigung aus ökologischer und rechtlicher Sicht. Dissertation. Teil I: Renaturierungsleitbild, Naturschutzverfahren. XXXVI, 384 S.

Heft 47-2

K.-H. Thiemann: Die Renaturierung strukturarmer Intensivagrargebiete in der Flurbereinigung aus ökologischer und rechtlicher Sicht. Dissertation. Teil II: Planungsrechtliche Aspekte. XXXVI, S. 385-572

Heft 48 / 1994

C. Schwiertz: Experimente zur GPS-gestützten Aerotriangulation unter besonderer Berücksichtigung systematischer Einflüsse. Dissertation. VIII, 192 S.

Heft 49 / 1995

R. Scheuring: Zur Qualität der Basisdaten von Landinformationssystemen. Dissertation. 126 S.

Heft 50 / 1997

W. M. Welsch, M. Lang, M. M. Miller (Eds.): Geodetic Activities, Juneau Icefield, Alaska, 1981-1996. 268 S.

Heft 51 / 1996

H. Blomenhofer: Untersuchungen zu hochpräzisen kinematischen DGPS-Echtzeitverfahren mit besonderer Berücksichtigung atmosphärischer Fehlereinflüsse. Dissertation. X, 168 S.

Heft 52 / 1997

J. G. Wang: Filtermethoden zur fehlertoleranten kinematischen Positionsbestimmung. Dissertation. XV, 138 S.

Heft 53 / 1996

G. Chen: Robuste Verfahren zur Analyse linearer stochastischer Prozesse im Zeitbereich. Dissertation. III, 128 S.

Heft 54 / 1997

J. Dold: Ein hybrides photogrammetrisches Industriemeßsystem höchster Genauigkeit und seine Überprüfung. Dissertation. 140 S.

Heft 55 / 1997

B. Eissfeller: Ein dynamisches Fehlermodell für GPS Autokorrelationsempfänger. Habilitationsschrift. XII, 182 S.

Heft 56 / 1997

T. Sutor: Robuste Verfahren zur Analyse linearer stochastischer Prozesse im Spektralbereich. Dissertation. 123 S.

Heft 57 / 1997

G. Oberholzer: Ländliche Kulturgeschichte und Landentwicklung, Teil II. 186 S.

Heft 58 / 1997

D. Zhong: Datumsprobleme und stochastische Aspekte beim GPS-Nivellement für lokale Ingenieurnetze. Dissertation. 160 S.

Heft 59 / 1997

T. Jiang: Digitale Bildzuordnung mittels Wavelet-Transformation. Dissertation. II, 136 S.

Heft 60 / 2000

Heft 60-1

W. Caspary, H. Heister, A. Schödlbauer, W. Welsch (Hrsg.): 25 Jahre Institut für Geodäsie. Teil 1: Wissenschaftliche Beiträge und Berichte. 331 S.

Heft 60-2

W. Caspary, H. Heister, A. Schödlbauer, W. Welsch (Hrsg.): 25 Jahre Institut für Geodäsie. Teil 2: Forschungsarbeiten und Veröffentlichungen. 113 S.

Heft 60-3

W. Caspary, H. Heister, A. Schödlbauer, W. Welsch (Hrsg.): 25 Jahre Institut für Geodäsie. Teil 3: Aus dem Leben des Instituts. 149 S.

Heft 61 / 1998

T. Cui: Generierung hochwertiger Digitaler Geländemodelle aus analogen Karten mittels Mathematischer Morphologie. Dissertation. 188 S.

Heft 62 / 1999

K. Brunner, W. M. Welsch (Hrsg.): Hochgebirgs- und Gletscherforschung. Zum 100. Geburtstag von Richard Finsterwalder. 114 S.

Heft 63 / 1999

C. Fosu: Astrogeodetic Levelling by the Combination of GPS and CCD Zenith Camera. Dissertation. 155 S.

Heft 64 / 1999

W. Werner: Entwicklung eines hochpräzisen DGPS-DGLONASS Navigationssystems unter besonderer Berücksichtigung von Pseudolites. Dissertation. 226 S.

Heft 65 / 1999

K. Krack: Dreizehn Aufgaben aus der Landesvermessung im Geographischen Koordinatensystem. 84 S.

Heft 66 / 2000

G. Joos: Zur Qualität von objektstrukturierten Geodaten. Dissertation. 150 S.

Heft 67 / 2000

H. Sternberg: Zur Bestimmung der Trajektorie von Landfahrzeugen mit einem hybriden Meßsystem. Dissertation. 158 S.

Heft 68 / 2000

G. Oberholzer: Die Weiterentwicklung der Kulturlandschaft. Landespflege in der Flurbereinigung, Teil V. 150 S.

Heft 69 / 2000

R. Hollmann: Untersuchung von GPS-Beobachtungen für kleinräumige geodätische Netze. Dissertation. 350 S.

Heft 70 / 2001

U. Roßbach: Positioning and Navigation Using the Russian Satellite System GLONASS. Dissertation. 167 S.